2000:27

LULEÅ UNIVERSITY OF TECHNOLOGY

LICENTIATE THESIS

MARTIN NILSSON - Thermal Cracking of Young Concrete LICENTIATE THESIS 2000:27

Thermal Cracking of Young Concrete

Partial Coefficients, Restraint Effects and Influence of Casting Joints

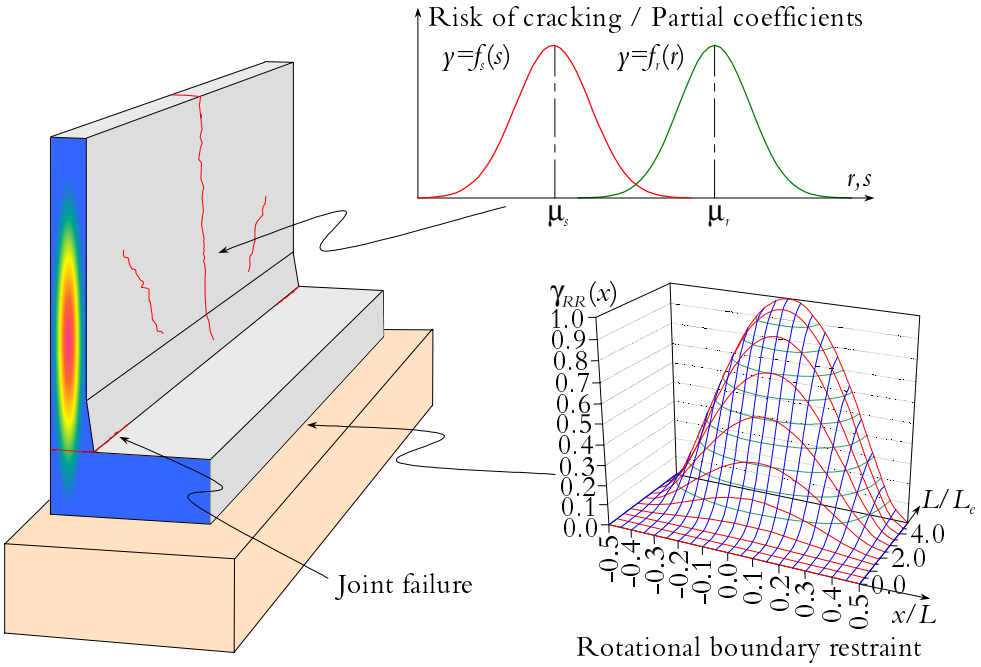

Martin Nilsson

Department of Civil and Mining Engineering
Division of Structural Engineering

2000:27 • ISSN: 1402 - 1757 • ISRN: LTU - LIC -- 00/27 -- SE

LULEÅ UNIVERSITY OF TECHNOLOGY

LICENTIATE THESIS 2000:27

Thermal Cracking of Young Concrete

Partial Coefficients, Restraint Effects and Influence of Casting Joints

Martin Nilsson

Division of Structural Engineering
Department of Civil and Mining Engineering
Luleå University of Technology
SE - 971 87 Luleå
Sweden

Preface

The present thesis is based on work carried out between 1997 and 2000 at the Division of Structural Engineering, the Department of Civil and Mining Engineering at Luleå University of Technology (LTU). The performance of the work has been possible by the participation in a research project under the title Improved Production of Advanced Concrete Structures (IPACS) and in an industrial project called "30 tons on Malmbanan".

The IPACS project is funded by the European Community under the Industrial & Materials Technologies Programme (Brite-EuRam III) and is a joint venture between companies and universities in Germany, Italy, The Netherlands, Norway and Sweden. The project "30 tons on Malmbanan" is supported from the Swedish National Rail Road Administration.

Firstly, I will thank my supervisor Ass Prof. Tech Dr Jan-Erik Jonasson for your never ceasing energy and lack of ideas. Further I thank Prof. Tech Dr Lennart Elfgren, the head of the Division, Ass Prof. Tech Dr Mats Emborg, Tech Lic Hans Hedlund and Tech Dr Ulf Ohlsson for all your advice and support during the work. I will give a special gratitude to Mr Kjell Wallin (LTU and PEAB) for all your guidance and support with the experiments, which never would have been what they become without your help.

Further, I feel thankfulness to the staff at Testlab for all their help with my tests, especially to Mr Håkan Johansson, head of Testlab, Mr Lars Åström and Mr Georg Danielsson. In that context I thank Mr Hans-Olov Johansson for all your help and great ideas in testing the concrete and some of the equipment I have used in the tests. Thank you all.

All the staff at the Division of Structural Engineering should feel my appreciation for being such good colleagues and especially the PhD-students Anders

Carolin, Håkan Thun and Sofia Utsi for all the funny moments and laughter we have shared.

Finally, I would like to express my greatest gratitude to my fiancée Ann for all your support and sacrifice during these first years of my journey towards doctor's degree. Thank you my friend.

Luleå in August 2000

Martin Nilsson

Abstract

Cracks in young concrete can occur due to hindrance of temperature induced movements during the hydration phase of the concrete. Such thermal cracks are not decisive for the load-bearing capacity of structures but cause costs for repair and may reduce the life of the structures.

The risk of thermal cracking can be judged through safety values, (partial coefficients) given in building codes. In the present thesis (Chapter 2), partial coefficients for thermal cracking problems are determined with a probabilistic method.

One crucial parameter influencing the risk of cracking is the restraint. In the report (Chapter 3), methods are derived and presented for the determination of the restraint. Rotational boundary restraint from elastic foundations is treated as well as the restraint in structures. For the determination of the rotational boundary restraint coefficient, applicable and simple graphical tools are presented. The restraint in internal points is based on a so-called plane-section restraint coefficient, a resilience factor for structures with length to height ratios smaller than five, and a factor for slip failures in joints between the young and old parts.

Four experiments of walls cast on slabs are presented in the thesis (Chapter 4). On a precast slab, concrete walls are cast and loaded by restraint stresses induced by the temperature during the hydration. Different boundary restraint situations are used for the structure as well as different amount of reinforcement in the joint between the walls and the slab. The restraint and the amount of reinforcement are investigated regarding the risk of through cracking of the wall. The phenomenon of slip failure in joints has been shown in the tests.

Keywords: Concrete, Young Concrete, Cracking, Thermal Cracking, Restraint, Structural Restraint, Boundary Restraint, Partial Coefficients, Crack Risk Estimation, Joints, Joint Failure, Laboratory Tests.

Sammanfattning

Sprickor i ung betong kan uppstå på grund av förhindrade temperaturinducerade rörelser under betongens hydratationsfas. Termiska sprickor är inte avgörande för en konstruktions bärförmåga men de kan orsaka kostnader för reparationsarbeten och reducera livslängden.

Risken för temperatursprickor kan uppskattas med spricksäkerhetsvärden, dvs. partialkoefficienter, som finns angivna i BRO94 (1999). I den föreliggande uppsatsen, kapitel 2, bestäms partialkoefficienter för temperatursprickriskproblem med en sannolikhetsteoretisk metod.

En avgörande faktor som påverkar risken för sprickbildning är tvånget. I kapitel 3 i rapporten härleds och presenteras metoder för bestämning av tvånget. Rotationstvånget från angränsande elastiska grundmaterial behandlas likväl som tvånget i valda snitt i en konstruktion. För bestämning av rotationstvånget från omgivningen presenteras enkla och tillämpbara grafiska vektyg. Tvånget i långa konstruktioner baseras på analyser under antagande om att plana tvärsnitt förblir plana. En metod för bestämmandet av en reduktionsfaktor för kortare konstruktioner (längd-höjdförhållande mindre än ungefär fem) presenteras. Vidare nyttjas en faktor som tar hänsyn till uppsprickning av gjutfogar mellan ung och gammal betong.

Fyra experiment med väggar gjutna på en platta presenteras i rapporten i kapitel 4. På en prefabricerad betongplatta har betongväggar gjutits och belastats med tvångsspänningar som induceras genom temperaturutvecklingen under hydratationen. Olika tvångssituationer och olika mängder armering genom gjutfogen mellan platta och vägg har studerats. Tvånget och mängden armering har undersökts med avseende på risken för uppkomsten av genomgående sprickor i väggarna. Fenomenet med sprickbildning i gjutfogen har påvisats i försöken.

Nyckelord: Betong, Ung betong, Sprickbildning, Termisk sprickbildning, Tvång, Tvång inom konstruktioner, Tvång från anslutande mark/berg, Partialkoefficienter, Sprickriskuppskattning, Gjutfogar, Brott i gjutfogar, Laboratorieförsök.

Table of Contents

Notations and Abbreviations

Explanations in the text of notations and abbreviations in direct conjunction to their appearance have preference to what is treated here.

Roman upper case letters

A	Area, [m^2]
C	Factor describing uncertainties in design method, [-]
E	Modulus of elasticity, [N/m^2]
F	Load, [N]
G	Gage factor, [-]
H	Height, [m]
I	Moment of inertia, [m^4]
K_j	Modulus of compression, [N/m^2]
L	Length, [m]
L_e	Elastic length, [m]
M_{RO}	Moment distribution, [N/m]
M_{RI}	Bending moment of internal loading, [N/m]
N_{RO}	Outer axial force, [N]
N_{RI}	Axial force of internal loading, [N]
R	Relaxation, [Pa]
T	Temperature, [°C]
V	Coefficient of variation, [-]
	Shear force, [N]
W	Width, [m]

Roman lower case letters

a	Geometric quantity, [depends on the quantity]
b	Weighting coefficient, [-]

c	Weighting coefficient, [-]
e	Eccentricity, [m]
f_{cc}	Concrete compressive strength, [Pa, MPa]
f_{ct}	Concrete tensile strength, [Pa, MPa]
f_d	Design value of strength, [MPa]
f	Strength value, [Pa, MPa]
l_d	Design values of geometry, [m, m^2, …]
k	Variable associated with actual fractile value, [-]
p	Ground pressure, [N/m]
p_f	Probability of failure, [-]
q	Dead weight, [N/m]
r	Resistance parameter, [depends on actual parameter]
s	Load parameter, [depends on actual parameter]
	Space between reinforcement bars, [mm]
	Empirical parameter, [-]
t	Time, [s, h, days]
t_0	Time of loading, [h]
t_e	Equivalent time, [s, h, days]
w	Deflection, [m]
x, y, z	Coordinates, [m]

Greek upper case letters

Θ	Limit State condition, [depends on actual parameter]
Φ	Cumulative distribution function of the standard normal distribution

Greek lower case letters

α	Coefficient of thermal dilatation, [1/°C]
	Sensitivity coefficient, [-]
	Degree of hydration, [-]
β	Safety index, [-]
$\beta_c(\Delta t_{load})$	Time development function for creep deformation, [-]
$\beta_\phi(t_0)$	Relative creep coefficient for loading age less than 28 days, [-]
χ	Ageing function, [-]
δ	Lift factor, [-]
δ_{res}	Resilience factor, [-]
δ_{slip}	Slip reduction factor, [-]
ε	Strain, [-]
ε_T	Non-elastic strain induced by temperature change, [-]
ε_{sh}	Non-elastic strain induced by shrinkage, [-]

ε^0	Strain of imposed volume change, [-]
ε^0_{cen}	Translational strain, [-]
ε^0_{φ}	Rotational strain, [-]
ϕ	Creep coefficient, [-]
γ_m	Partial coefficient for random uncertainty in strength value, [-]
γ_n	Partial coefficient for safety class, [-]
γ_r	Partial coefficient for resistance parameter, [-]
γ_s	Partial coefficient for load parameter, [-]
γ_R	Restraint coefficient, [-]
γ^0_R	Plane-section restraint coefficient, [-]
γ^{0T}_R	Translational plane-section restraint coefficient, [-]
$\gamma^{0\varphi}_R$	Rotational plane-section restraint coefficient, [-]
γ_{RR}	Rotational boundary restraint coefficient, [-]
γ_{RT}	Translational boundary restraint coefficient, [-]
η	Partial coefficient, [-]
φ	Curvature, [1/m] Creep function, [-]
κ	Help values when calculating partial coefficients, [-] Shape factor, [-]
λ	Factor for relation between imposed strain in old and young concrete parts, [-]
μ	Mean value, [depends on the quantity]
ν_{sh}	Relation between mean values of strain of shrinkage and strain of temperature change, [-]
θ	Activation temperature, [K]
ρ	Transferring factor between ultimate strain in specimen and in reality
σ	Stress, [N/m^2] Standard deviation, [depends on the quantity] Relative time, [-]
ω	Location factor, [-]
ξ	Time factor for bending stiffness, [-]
ζ	Time factor for modulus of elasticity, [-]
ψ	Duration of load in time, [-]

Special sub- or superscripts

c	Characteristic Compression

	Concrete
	Contraction
d	Design value
e	Expansion
t	Tension

Abbreviations and acronyms

CDG	Crack Detection Gage
FE(M)	Finite element (method)
FIP	Fédération Internationale de la Précontrainte
IPACS	Improved Production of Advanced Concrete Structures
LDT	Linear Displacement Transducer
OPC	Ordinary Portland Cement
RIM	Relaxation Integral Method
TSTM	Temperature Stress Testing Machine
VSG	Vibrating Strain Gage
vct	Water Cement Ratio

1 Introduction

1.1 Background and Identification of the Problem

Thermal cracking of young concrete in civil engineering structures, such as tunnels, especially beneath the ground water level, and bridges, that is exposed to chlorides, freezing and thawing should be avoided. In this context, young concrete is defined as concrete structures during the hydration phase when the chemical reactions between the cement and the water emit much heat leading to large thermal induced deformations. Any arisen cracks may cause leakage problems. If water may entrain, both freezing and thawing and chlorides, which cause corrosion of reinforcement, lead to increased cracking due to the larger volume of the ice compared to water and the corrosion products compared to the steel.

The understanding of the factors influencing the risks of thermal cracking is of great importance. Enhanced knowledge about the problem and the affecting parameters gain the building processes and lower the final costs. During the last decades, extensive and thorough research has been performed at many universities and companies within this field. At Luleå University of Technology, the Division of Structural Engineering, thermal cracking of young concrete is one of the major research areas.

During the hydration phase of newly cast concrete structures, the temperature varies within the cross sections. Normally, the temperature development is smaller in surface layers than in centre parts leading to larger motions in the centre parts compared to the motions in the surfaces. During the phase of increasing temperature, the expansion in the centre parts is larger than in the surfaces, which induces tensile stresses in the surface layers. If the stresses are larger than the actual tensile strength, surface cracks will occur, see Figure 1.1.

The surface layers in turn counteract the larger expansion in the centre parts, and cause on the opposite compressive stresses in the inner parts. When the temperature in the maturing concrete passes its maximum, the expansion turns into contraction. By the same reason as before, temperature-induced movements in centre parts are larger than in surface layers and consequently the surface cracks tend to close. The surface layers also counteract these motions, but instead they cause tensile stresses in the centre parts. Again, if the stresses are larger than the actual tensile strength, this time, through cracks can occur, see Figure 1.1. The large distinction compared with cracks occurring during the expansion phase is that these cracks are both through and lasting cracks. In Bernander (1973, 1982 & 1993), Emborg & Bernander (1994), Emborg et al. (1997), Jonasson (1994), Jonasson et al. (1994), Larson (1999 & 2000), Nilsson (1998 & 1999), Nilsson et al. (1999) and Wallin et al. (1997), the problem is further described and discussed.

Concrete structural members cast on older ones can be exposed to the corresponding stress situation as described above. When the temperature in the young concrete increases, the volume of the newly cast member also increases. This expansion cause tensile stresses in the adjacent older concrete member, which in turn counteract the expansion and cause compressive stresses in the young concrete. If the tensile stresses in the older concrete are large, cracks may occur. When the temperature in the young concrete starts to decrease, it naturally begins to contract. This contraction causes compressive stresses in the older member, which again counteract the motions and this time cause tensile stresses in the young concrete. These stresses can result in lasting through cracks in the young concrete member, again see Figure 1.1.

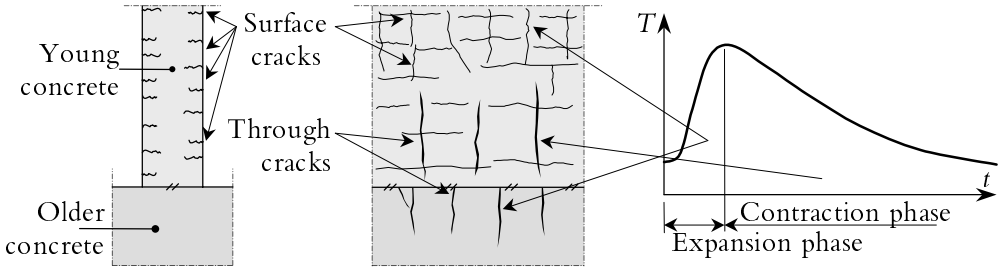

Figure 1.1 *Examples of early age expansion cracks and contraction through cracks in a symmetrical wall cast on older concrete, Bernander (1982).*

All adjacent structures and materials counteract/restrain temperature-induced free movements of young concrete structures and can cause through cracking.

Several parameters are influencing the counteraction/restraint, e.g. the amount of through reinforcement, the strength and surface conditions of casting joints as well as the stiffness of adjacent structures and materials. In addition, the temperature difference between young concrete and adjacent structure, and the length-height ratio of the structure are other parameters of great importance.

The effects caused by different temperature distributions and counteractions are sometimes designated as internal and outer restraint, respectively. However, one must bear in mind what is included in the model or not, otherwise the terms internal and outer restraint may lead to misunderstandings and uncertainties. Therefore, it is instead preferable to classify cracks caused by restraint as, see Emborg & Bernander (1994):

- Early cracking during the expansion phase. These cracks arise during the hydration phase shortly after casting (one or a few days) and tend towards closing by time. Their influence on the static capacity, the function and strength of a structure must be judged from case to case.
- Cracking during the contraction phase. Cracks arising during the cooling phase are usually through cracks. Depending on dimensions and other factors, they do not arise until weeks, months and in extreme cases even years after casting. Cracks formed during the cooling phase are as a rule permanent.

Damages in shape of cracking, due to bad design and building, may reduce the durability and function of structures. The cracking can be very widespread and repairs expansive. Therefore, great resources are put into modern building to predict restraint stresses, the risks of damages due to hindered shrinkage, moist and temperature movements, and in choosing appropriate measures. Today hardly any building contractors overlook the effects of the restraint stresses. Unfortunately cracking can anyhow be observed in many structures in spite of comprehensive quality work and restrictions.

The estimation of the risk of cracking can be performed in beforehand of the building of a structure to determine measures or afterwards for post-analytical purposes. Various models and tools can be used in the crack risk analyses. The types of analyses range from time consuming three-dimensional finite element calculations to certainly simple but accurate methods based on e.g. manual calculations, diagrams or data bases.

Common for all types of analyses is that they are based on a number of steps. Firstly, the type of structure, the material and the measures to avoid cracks have to be chosen. Secondly, the temperature development has to be determined, either by calculations, diagrams/databases or by measurements. Thirdly, the

restraint situation has to be determined, that is both the boundary and the structural restraint. Fourthly, structural calculation of the stress or strain ratios follows, that is, the maximum tensile stress or strain is compared to the tensile strength or the ultimate strain capacity, respectively. Fifthly, the risk of cracking is estimated through so-called crack safety values that the determined stress or strain ratios may not exceed, see Figure 1.2.

The first step in Figure 1.2, choice of structure, material and measures, is the primary base of the design of structures. Properly chosen type of structure and dimensions along with right distribution of the constituents of the concrete is the foundation of the avoidance of cracking. In addition, measures such as cooling and/or heating might be required, e.g. see Wallin et al. (1997). The second step in Figure 1.2 regards the temperature development during the hydration phase, which has to be determined either by calculations, for instance see ConTeSt Pro (1999), from diagrams/database, see Emborg et al. (1997), or from measurements in real structures. From the temperature development, the development of stresses and strength are obtained. As the third step, the restraint situation has to be determined, regarding the restraint within the studied structure, in the interface (joint) between parts of structures, from adjacent structural members and ground/rock. In Emborg et al. (1997), several common cases of internal restraint are presented, and in e.g. Larson (1999 & 2000) the restraint from adjacent structures has been investigated. For the restraint from adjacent elastic ground materials, e.g. Bernander (1993) and Nilsson (1998) give methods for the determination of the restraint coefficients. However, more thorough and wider descriptions and derivations for structures founded on elastic materials as well as on rock with no friction and/or cohesion between the rock and the concrete is presented in Chapter 3 in this thesis. For cases with friction and/or cohesion between rock foundations and concrete structures, more investigations and research work is needed. The determination of the stress/strength or strain/ultimate-strain situation, step four in Figure 1.2, can be done by structural calculations e.g. with ConTeSt Pro (1999), by manual methods, see Larson (2000), or with help from diagrams/databases, e.g. through Emborg et al. (1997). The final crack risk design is performed by comparing the stress/strength or strain/ultimate-strain situations with stated so-called crack safety values, that is partial coefficients, given in design codes, e.g. BRO 94 (1999). One way of determination of crack-safety values will be presented in Chapter 2 below in this thesis.

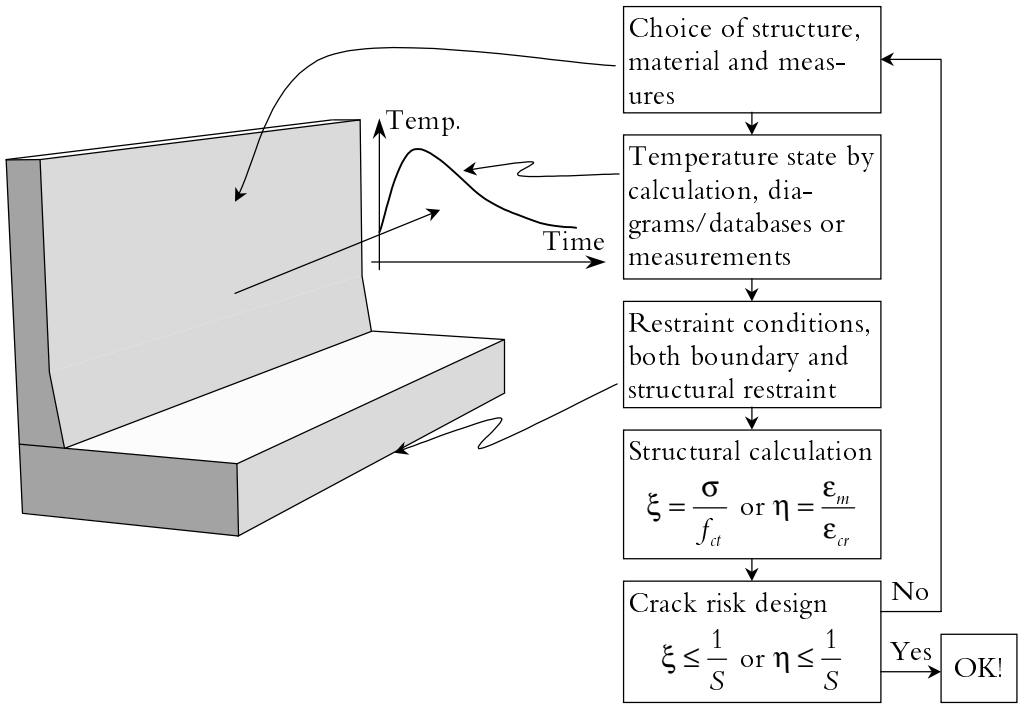

Figure 1.2 *The different steps in the estimation of the risk of cracking when casting concrete structures.*

1.2 Aim and Scope

The scope of this thesis constitutes parts of the steps described above, that is, the restraint conditions, the effects of joints between young and old concrete, and the crack risk design by the means of partial coefficients for thermal cracking.

The first aim of this thesis is to verify the partial coefficients for thermal cracking of young concrete, crack safety values, given in BRO 94 (1999) by use of a probabilistic method. The second aim is partly to derive analytical methods for the determination of restraint coefficients from elastic materials on young deforming concrete structures, partly to derive simple by accurate analytical formulas and graphical application tools for the restraint in decisive points. The third aim is to investigate the effects of joints, but laboratory tests, on young concrete walls, which are cast on slabs and loaded by restraint stresses.

1.3 Acknowledgement

The performance of the four tests presented in this thesis have been possible by the participation in a project funded by the European Community under the

Industrial & Materials Technologies Programme (Brite-EuRam III). The project goes under the title Improved Production of Advanced Concrete Structures (IPACS) and is a joint venture between companies and universities from Germany, Italy, The Netherlands, Norway and Sweden.

1.4 Content

In Chapter 2, safety factors, or more correctly partial coefficients, for thermal cracking of young concrete are presented and derived. The partial coefficients are determined by a probabilistic method and compared to the values stated in the Swedish code BRO 94 (1999).

In Chapter 3, methods for calculation of restraint coefficients are derived and presented. Firstly, equations and diagrams for the determination of the rotational boundary restraint coefficient are derived and described. Secondly, general equations for plane-section restraint coefficients, for structures with length to height ratios larger than or equal to five, in any location of young parts are derived. The equations are then modified for rectangular shaped parts resulting in applicable diagrams. Thirdly, a method for the determination of reduction factors for cases with length to height ratios smaller than about five are presented. Fourthly, the effects of slip failures in joints between young and old parts are being regarded.

In Chapter 4, description and presentation are given of four laboratory tests of walls cast on slab and loaded by restraint stresses. Firstly, the geometry and the test arrangements are described followed by the concrete, the performance and the measurements. Secondly, the results are presented regarding the temperature development, the relative displacements between different parts of the structures, and the cracking (both through cracking of the walls and the cracking of the joints). Finally the strain variations at various locations in the walls are presented and analysed leading to hesitation about the results. Therefore, the restraint developments are not determined and analysed. The first two tests have previously been reported in Nilsson (1999) and Nilsson et al. (1999).

Chapter 5 includes summary and conclusions on the main results from this thesis.

2 Partial Coefficients for Thermal Cracking

2.1 General

In this chapter theories of statistics and the probabilistic method of determination of partial coefficients are presented and applied to thermal cracking. A general background to the methods are given in AK79/81 (1982), Degerman (1981), Nilsson et al. (2000), NKB78 (1978), NKB87 (1987), Schneider (1997), Vännman (1990) and Östlund (1997).

A structure or a structural member should be designed in such a way that safety and serviceability are maintained. This means that no relevant limit state conditions should be exceeded with an in beforehand determined probability. For young concrete structures it is important to prevent surface and through cracks due to e.g. temperature and/or temperature gradients during the hydration phase. Such cracks do not affect the total bearing capacity of a structure, but can influence the aesthetics and cause leakage and durability problems and must be taken care of by e.g. injection.

The risk of thermal cracking in young concrete structures is commonly estimated as the quotient between the calculated maximum tensile stress and the actual tensile strength. Alternatively, the quotient between the calculated maximum tensile strain and the actual ultimate tensile strain is used. If a determined quotient is smaller than a so-called crack safety value, a structure is assumed to fulfil the requirements of no thermal cracking. Depending on the effects of cracking and the accuracy in determining material properties, the Swedish building codes for bridges, BRO94 (1999), states different crack safety values as measures of the risk of cracking.

The crack safety values can be referred to what usually are called partial coefficients. Partial coefficients will generally be discussed below. A presentation

will be given of the probabilistic method, Schneider (1997), AK79/81 (1982), NKB78 (1978), NKB87 (1987), Nilsson et al. (2000) and Östlund (1997), for determination of partial coefficients. The method is then adapted and applied for thermal cracking problems. Further, a determination of partial coefficients, that is crack safety values, for thermal cracking problems will follow as an attempt to indicate the reasonableness in the values given in BRO94 (1999).

2.1.1 Limit state condition and probability of failure

In civil engineering problems, a limit state condition is generally expressed as a function of design values of strengths and loads such as

$$\Theta\left(F_{id}, \psi_i, f_d, l_d\right) \geq 0 \quad i = 1,2,...,n \tag{2.1}$$

where

F_{id} are design values of loads
ψ_i is a factor regarding the duration of loads in time and is used when combining variable loads
f_d are design values of strength
l_d are design values of geometry
n are the number of loads

The safety against failure can be estimated in terms of a resistance parameter r and a stress parameter s. The limit state condition can be expressed as the resistance parameter r reduced by the subtraction of the load (stress) parameter s as

$$\Theta(\cdot) = r - s \geq 0 \tag{2.2}$$

Usually, the resistance parameter r is the material strength and the load parameter s is the stresses caused by acting loads. However, the parameters can also indicate strains, as will be the case in the applications later on in Section 2.4. Depending on their relative size; the limit state condition is not exceeded if the resistance is larger than or equal to the stress, $r \geq s$, and is exceeded if the resistance is smaller than the stress, $r < s$.

The two parameters can be regarded as two normally distributed stochastic variables with given probability density functions, $f_r(r)$ and $f_s(s)$, see Figure 2.1a). Their mean values are denoted μ_r and μ_s and standard deviations σ_r and σ_s. From the presumption that the resistance parameter r and the stress parameter s are stochastic variables, it follows that the limit state condition is a stochastic variable with mean value

$$\mu_\Theta = \mu_r - \mu_s \tag{2.3}$$

and standard deviation

$$\sigma_\Theta = \sqrt{\sigma_r^2 + \sigma_s^2} \tag{2.4}$$

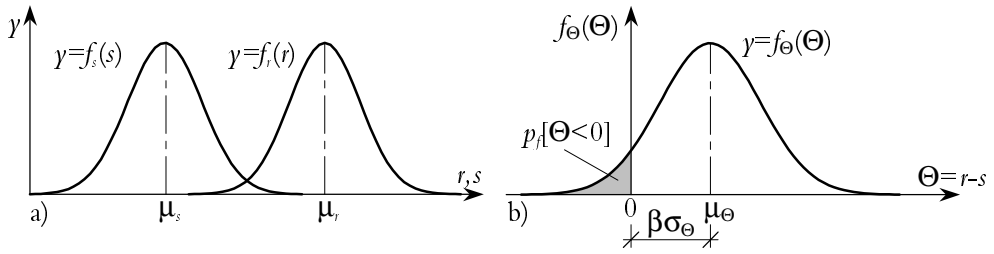

Figure 2.1 *a) Probability density functions for the stress parameter, $f_s(s)$, and the resistance parameter, $f_r(r)$, b) Probability density function for the limit state condition Θ, $f_\Theta(\Theta)$.*

Assuming the resistance parameter *r* and the stress parameter *s* being normally distributed also the limit state condition Θ is normally distributed with probability density function $f_\Theta(\Theta)$, Figure 2.1b), where β is the so-called safety index.

2.1.2 Safety index and safety class

The probability of exceeding a limit state condition, $p_f[\Theta = r\text{-}s < 0]$, is equal to the area of the grey surface in Figure 2.1b). In the figure, the distance, with the standard deviation as unit, from the mean value μ_Θ to the failure limit, $\Theta = 0$, is written as $\beta\sigma_\Theta$. The coefficient β is the so-called safety index and is, according to the figure together with Equations (2.3) and (2.4)

$$\beta = \frac{\mu_\Theta}{\sigma_\Theta} = \frac{\mu_r - \mu_s}{\sqrt{\sigma_r^2 + \sigma_s^2}} \tag{2.5}$$

How much larger the resistance *r* should be than the stress *s* is often specified in building codes in different safety classes and through specified values of the safety index β. The safety index β is defined by a formal probability of failure p_f, as

$$p_f = \Phi(-\beta) \tag{2.6}$$

$\Phi(-\beta)$ denotes the cumulative distribution function of the standard normal distribution, see Figure 2.2.

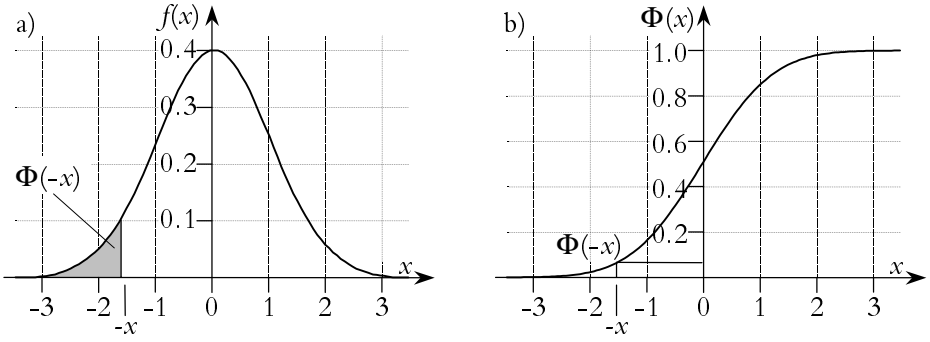

Figure 2.2 *Probability density function a) and cumulative distribution function b) of the standard normal distribution. Schneider (1997).*

The probability of failure is

$$p_f[\Theta < 0] = \Phi\left(\frac{0-\mu_\Theta}{\sigma_\Theta}\right) = \Phi(-\beta) = 1-\Phi(\beta) \tag{2.7}$$

The safety index can then be determined as

$$\Phi(\beta) = 1 - p_f[\Theta = 0] \tag{2.8}$$

which gives the following values of the safety index corresponding to different probabilities of failure, Table 2.1:

Table 2.1 *Relation between the safety index* β*, and the probability of failure* p_f*, for normally distributed* Θ.

β	1.28	1.64	2.33	3.09	3.72	4.26	4.75	5.20	5.61
p_f	10^{-1}	$5\cdot10^{-2}$	10^{-2}	10^{-3}	10^{-4}	10^{-5}	10^{-6}	10^{-7}	10^{-8}

The safety index β is coupled to safety classes, see among others NKB78 (1978), NKB87 (1987) and BBK94 (1995). If the risk of human injuries is low, safety class 1, corresponding probability of failure is $p_f = 10^{-4}$ and the safety index $\beta = 3.72$. The same principle applies to safety classes 2 and 3, Table 2.2. The demand on the safety index β, which is put in relation to the actual limit state, is that it shall be determined on yearly basis.

Table 2.2 *Correspondence between safety class, safety index and probability of failure, BBK94 (1995), BRO94 (1999) etc.*

Safety class	1	2	3
Safety index β	3.72	4.26	4.75
Probability of failure, p_f	10^{-4}	10^{-5}	10^{-6}

2.2 Partial Coefficients

The partial coefficient method is a method based on characteristic values and partial coefficients for verification that prescribed safety requirements are fulfilled. Generally, for the limit state condition with the resistance parameter r and the stress parameter s, partial coefficients are used as follows

$$\Theta = r_d - s_d = \frac{r_c}{\gamma_r} - \gamma_s s_c \geq 0 \tag{2.9}$$

where d indicates design values, c indicates characteristic values and γ_r and γ_s are the partial coefficients for the resistance parameter r and the stress parameter s, respectively.

In Figure 2.3, NKB87 (1987), a geometric interpretation of the principals of the method is shown for the two normally distributed variables r and s, and for the limit state condition $\Theta = r\text{-}s$. The normalised probability density functions $f(r/\sigma_r)$ and $f(s/\sigma_s)$ are called marginal densities as they are represented on the margin as probability density functions. The two-dimensional joint density function $f(r/\sigma_r, s/\sigma_s)$ of the two marginal densities is illustrated with level curves in the figure. For a given value of the safety index β, a limit state line can be drawn from the origin of the axes. For combinations of the resistance and stress parameters larger than zero, $r - s > 0$, the limit state conditions is not exceeded, and consequently, for combinations smaller than zero, $r - s < 0$, the limit state condition is exceeded. The angle, ν, between the limit state line and the stress axis is determined as

$$\tan\nu = \frac{\frac{r_d}{\sigma_r}}{\frac{s_d}{\sigma_s}} = \frac{\kappa_s}{\kappa_r} \tag{2.10}$$

where κ_r and κ_s are help values for the resistance and the stress parameters, respectively. See Appendix A and Section 2.4.3 below.

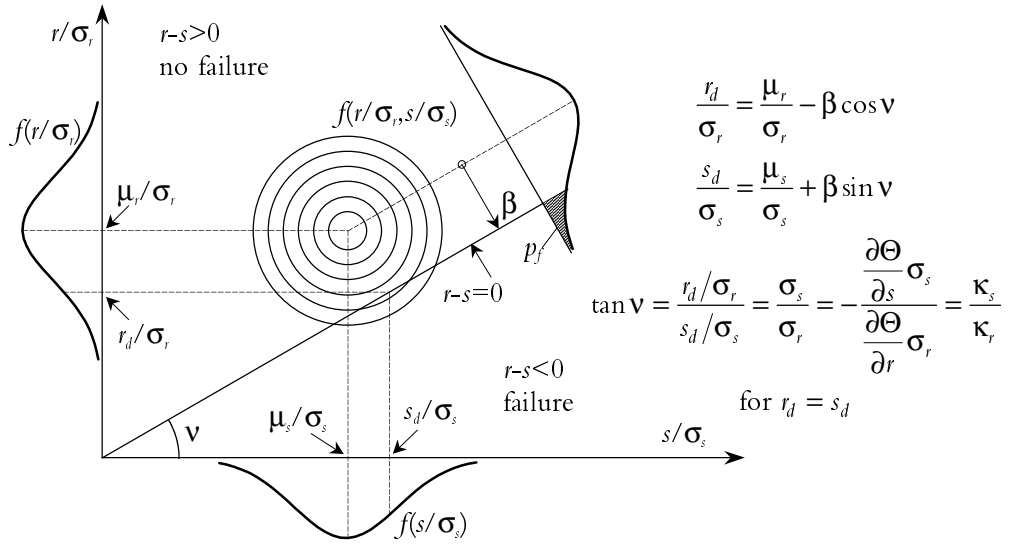

$$\frac{r_d}{\sigma_r} = \frac{\mu_r}{\sigma_r} - \beta\cos\nu$$

$$\frac{s_d}{\sigma_s} = \frac{\mu_s}{\sigma_s} + \beta\sin\nu$$

$$\tan\nu = \frac{r_d/\sigma_r}{s_d/\sigma_s} = \frac{\sigma_s}{\sigma_r} = -\frac{\frac{\partial\Theta}{\partial s}\sigma_s}{\frac{\partial\Theta}{\partial r}\sigma_r} = \frac{\kappa_s}{\kappa_r}$$

Figure 2.3 *The two-dimensional density function $f(r,s) = f(r/\sigma_r)f(s/\sigma_s)$ illustrated with level curves. Modified from AK79/81 (1982).*

The material strength is usually used as the resistance parameter and its design value is calculated as, BBK94 (1995)

$$f_d = \frac{f_c}{\eta\gamma_m\gamma_n} \tag{2.11}$$

where f_d and f_c are the design values of the strength and the characteristic values of the strength, respectively. $\eta\gamma_m\gamma_n$ are the partial coefficients where η takes into account systematic differences between strength values in test specimens and in real structures. γ_m is a partial coefficient for random uncertainties in the strength values while γ_n is the partial coefficient for the actual safety class.

Loads acting on structures cause stresses and strains that are used as the load parameter. The stresses or strains are calculated as a function of the sum of the design values of the acting forces as

$$\sigma_d = \sigma\left(\sum_{i=1}^{n}\gamma_{iF}\psi_i F_{ic}\right) \tag{2.12}$$

where σ_d is the design value of the stresses or strains, γ_{iF} is the partial coefficient for the i:th load F, F_{ic} is the i:th characteristic load value and ψ_i is a factor regarding the duration of the loads in time and is used when combining variable loads.

Equations (2.11) and (2.12) in Equation (2.9) give an expression for the limit state condition expressed in characteristic values and partial coefficients

$$\frac{f_c}{\eta\gamma_m\gamma_n} - \sigma\left(\sum_{i=1}^{n}\gamma_{iF}\psi_i F_{ic}\right) \geq 0 \tag{2.13}$$

This equation is general in design work and is used below in the determination of partial coefficients, but is instead expressed in terms of strains.

2.3 Crack Safety Values According to the Swedish Code

Temperature cracks in concrete are dealt with in BRO94 (1999). The risk of cracking due to temperature and temperature gradients can be estimated according to three different methods.

In Method 1 certain demands are specified such as the casting temperature and the air temperature, the maximum amount of cement content and the minimum value of the water cement ratio. Further, demands are also given on the thickness and height of structure members, the casting lengths, and when form stripping is allowed.

In Method 2 and Method 3, certain values of the crack safety are prescribed depending on the accuracy in the determination of material data. Method 2 implies that requirements in a handbook by Emborg et al. (1997) should be applied. The requirements have been established by numerous thermal stress analyses. Further, material data are given in the code.

In Method 3, the risk of cracking should be estimated very accurately with tried and documented computer software and material properties.

The crack safety values shall not be larger than the values given in Table 2.3. The environmental classes referred to in the legend of the first column are according to BBK94 (1994).

Table 2.3 *Crack safety values for Method 2 and Method 3 given in BRO94 (1999). For Method 2 values from the two right columns are used where C is the cement content [kg/m³].*

Environm. class	Method 3 Complete material data	Method 2 Material data given in the code	
		$360 \leq C \leq 430$kg/m^3	$430 \leq C \leq 460$kg/m^3
A2	1.11	1.25	1.42
A3	1.18	1.33	1.54
A4	1.25	1.42	1.67

For the risk of thermal cracking of young concrete, the crack safety values are the product of the partial coefficients for the resistance parameter r and the stress parameter s, $\gamma_r\gamma_s$, according to

$$\frac{r_c}{s_c} \geq \gamma_r \gamma_s \tag{2.14}$$

r_c is the actual concrete strength and s_c is the actual stress. In this case all partial coefficients have been collected in one coefficient limiting the ratio between the resistance parameter and the load parameter.

In Method 3, the concrete strength is not a 5% fractile value that usually is used in the design process, but a larger value, smaller but close to the true mean value. Cracking of young concrete structures do not mean total collapse but cause flaws and costs for injection work and repair implying that larger fractile values can be used.

2.4 Determination of Partial Coefficients

A method further referred to as the probabilistic method will be used to determine alternative values of the partial coefficients, safety values, for thermal cracking problems, given in Table 2.3. The method has the advantage of being consequent but it also includes many approximations. The results can therefore not be used directly without additional judgements.

The following determination of partial coefficients will be based on strains, alternatively to what was derived in Equation (2.13). As design condition with partial coefficients for thermal cracking problems, Equation (2.9) will be used as the limit state condition.

Some simple and fast forward derivations of many, but not all, equations that are used below can be found in Appendix A.

2.4.1 Resistance parameter

The resistance parameter r is expressed as, Östlund (1997)

$$r = Ca\rho\varepsilon \tag{2.15}$$

where

- C is a factor describing uncertainties in the calculation method. C is a stochastic variable with mean μ_C and coefficient of variation V_C.
- a is a geometric quantity (e.g. cross-section area). a is a stochastic variable with mean μ_a and coefficient of variation V_a.
- ρ is a factor transferring concrete strain from test specimen at failure to concrete strain in real structures. ρ is a stochastic variable with mean μ_ρ and coefficient of variation V_ρ.
- ε is the actual concrete ultimate strain. ε is a stochastic variable with mean μ_ε and coefficient of variation V_ε.

The stochastic variables r, C, a, ρ and ε are assumed to be logarithmic normally distributed.

The mean value of the resistance parameter is

$$\mu_r = \mu_C \mu_a \mu_\rho \mu_\varepsilon \tag{2.16}$$

and the coefficient of variation, according to Appendix A, Equation (A.3), if terms of higher order are neglected

$$V_r \approx \sqrt{V_C^2 + V_a^2 + V_\rho^2 + V_\varepsilon^2} \tag{2.17}$$

Equation (2.15) divided by Equation (2.16) gives for "actual" values (with indices c)

$$\frac{r_c}{\mu_r} = \frac{C_c}{\mu_C}\frac{a_c}{\mu_a}\frac{\rho_c}{\mu_\rho}\frac{\varepsilon_c}{\mu_\varepsilon} \tag{2.18}$$

which will be used further on in the final calculation of the partial coefficients, see Equation (2.33) below.

2.4.2 Load parameter

The load parameter s for thermal cracking problems can in terms of strains, be formulated as

$$s = \gamma_R \left(b\varepsilon_T + c\varepsilon_{sh} \right) \tag{2.19}$$

where

- γ_R is the coefficient of restraint. γ_R is a deterministic coefficient, $0 \leq \gamma_R \leq 1$. For further explanations and the determination of the coefficient of restraint, see Chapter 3.
- ε_T is the non-elastic strain of volume changes from temperature changes. ε_T is a stochastic variable with mean μ_T and coefficient of variation V_T.
- ε_{sh} is the strain of volume changes from shrinkage. ε_{sh} is a stochastic variable with mean μ_{sh} and coefficient of variation V_{sh}.
- b is a deterministic coefficient, $0 \leq b$.
- c is a deterministic coefficient, $0 \leq c$.

The stochastic variables ε_T and ε_{sh} are assumed to be normally distributed. The deterministic coefficients b and c are used when either the temperature induced strain is of greater importance than the shrinkage strain, or the opposite.

The variables are put together so that the mean value of the stress parameter is

$$\mu_s = \gamma_R \left(b\mu_T + c\mu_{sh} \right) \tag{2.20}$$

In the calculation of the partial coefficients for thermal cracking problems of concrete, it is very difficult to give any absolute values of the mean values of the strains of shrinkage and temperature changes. However, the relation between them is easier to estimate. Therefore, a coefficient ν_{sh} is introduced stating the ratio between the mean values of the strains of shrinkage and of the temperature change

$$\nu_{sh} = \frac{c\mu_{sh}}{b\mu_T} \tag{2.21}$$

2.4.3 Design condition

When calculating partial coefficients by the probabilistic method, the following design values are used for the stochastic variables r, ε_T and ε_{sh}, together with their help values κ, see Appendix A, Equations (A.9) to (A.13)

$$r_d = \mu_r \exp(-\alpha_r \beta V_r) \quad \kappa_r = r_d V_r \tag{2.22}$$

$$\varepsilon_{T,d} = \mu_T \left(1 - \alpha_T \beta V_T\right) \quad \kappa_T = -b\gamma_R \mu_T V_T \tag{2.23}$$

$$\varepsilon_{sh,d} = \mu_{sh} \left(1 - \alpha_{sh} \beta V_{sh}\right) \quad \kappa_{sh} = -c\gamma_R \mu_{sh} V_{sh} \tag{2.24}$$

When using design values in Equation (2.9), the equal sign is valid. This gives together with Equation (2.19)

$$r_d - b\gamma_R \varepsilon_{T,d} - c\gamma_R \varepsilon_{sh,d} = 0 \tag{2.25}$$

In the expressions above, α are so-called sensitivity coefficients, see Equation (A.7), which have to fulfil the condition

$$\alpha_r^2 + \alpha_T^2 + \alpha_{sh}^2 = 1 \tag{2.26}$$

where

$$\alpha_i = \frac{\kappa_i}{\sqrt{\Sigma \kappa_i^2}} \tag{2.27}$$

The sensitivity coefficients take values between -1 and 1, $-1 \le \alpha \le 1$, and are positive for favourable factors, the resistance parameters, and negative for unfavourable, the load/stress parameters. The larger the coefficient is, the larger the importance of the uncertainty is in the corresponding variable.

The help variables κ_i are defined according to Appendix A, Equations (A.9) and (A.10).

$c\mu_{sh} = \nu_{sh} b\mu_T$ according to Equation (2.21) and design values according to Equations (2.22) to (2.24) in Equation (2.25) give

$$\frac{\mu_r}{b\gamma_R \mu_T} \exp(-\alpha_r \beta V_r) - \left(1 - \alpha_T \beta V_T\right) - \nu_{sh} \left(1 - \alpha_{sh} \beta V_{sh}\right) = 0 \tag{2.28}$$

By introducing the help variables

$$Z = \frac{\mu_r}{b\gamma_R \mu_T}$$

and

$$\psi_1 = \left(1 - \alpha_T \beta V_T\right) + \nu_{sh} \left(1 - \alpha_{sh} \beta V_{sh}\right) \tag{2.29}$$

Equation (2.28) is simplified to

$$Z \exp(-\alpha_r \beta V_r) - \psi_1 = 0$$

where from

$$Z = \psi_1 \exp(\alpha_r \beta V_r) \tag{2.30}$$

Z can be determined if the values of α_i, β, ν_{sh}, b, c and V_i are known. The steps for calculating Z can be as follows:

(1) A value of α'_{sh} is assumed

(2) $\alpha'_T = \dfrac{\kappa_T}{\sqrt{\Sigma\kappa_T^2}} = \dfrac{-b\gamma_R\mu_T V_T}{-c\gamma_R\mu_{sh}V_{sh}}\alpha'_{sh} = \dfrac{V_T\alpha'_{sh}}{\nu_{sh}V_{sh}}$ is calculated

(3) ψ is calculated with Equation (2.29), α'_{sh} and α'_T

(4) $r_d = \mu_r \exp(-\alpha_r\beta V_{r)} = \mu_r \dfrac{\psi_1}{Z} = b\gamma_R\mu_T\psi_1$ and $\kappa_r = r_d V_r$ are calculated

(5) $N = \dfrac{\sqrt{\Sigma\kappa_i^2}}{b\gamma_R\mu_T} = \sqrt{(V_T)^2 + (\nu_{sh}V_{sh})^2 + (\psi_1 V_r)^2}$

(6) $\alpha_{sh} = \dfrac{\kappa_{sh}}{\sqrt{\Sigma\kappa_i^2}} = \dfrac{-\gamma_R b\mu_T\nu_{sh}V_{sh}}{\sqrt{\Sigma\kappa_i^2}} = \dfrac{-\nu_{sh}V_{sh}}{N}$ is calculated and compared to α'_{sh}

(7) When $\alpha'_{sh} \approx \alpha_{sh}$, $\alpha_T = \dfrac{-V_T}{N}$ and $\alpha_r = \dfrac{\psi_1 V_r}{N}$ are calculated

(8) Check of $\Sigma\alpha_i^2 = 1$

(9) Z is calculated by Equation (2.30).

The value of Z is used below in the calculation of the partial coefficients.

2.4.4 Partial coefficients

The design values in Equations (2.22) through (2.24) can alternatively be expressed with partial coefficients as

$$r_d = \frac{r_c}{\gamma_r} = \frac{\mu_r}{\gamma_r}\exp(-k_r V_r) \tag{2.31}$$

$$\begin{aligned} s_d &= \gamma_s\gamma_R\left(b\varepsilon_{T,c} + c\varepsilon_{sh,c}\right) = \\ &\gamma_s\gamma_R\left(b\mu_T(1+k_T V_T) + c\mu_{sh}(1+k_{sh}V_{sh})\right) \end{aligned} \tag{2.32}$$

which in the limit state condition, Equation (2.9), give

$$\frac{\mu_r}{\gamma_r}\exp(-k_r V_r) - \gamma_s\gamma_R\left(b\mu_T(1+k_T V_T) + c\mu_{sh}(1+k_{sh}V_{sh})\right) \geq 0$$

that with $Z = \mu_r/b\gamma_R\mu_T$, $\nu_{sh} = c\mu_{sh}/b\mu_T$ and $\psi_2 = (1+k_T V_T)+\nu_{sh}(1+k_{sh} V_{sh})$ can be written as

$$\gamma_s\gamma_r \le \frac{Z}{\psi_2}\exp(-k_r V_r) = \frac{Z}{\psi_2}\frac{r_c}{\mu_r} \tag{2.33}$$

giving the partial coefficients $\gamma_r\gamma_s$. Z is calculated according to Section 2.4.3 and r_c/μ_r is calculated from Equation (2.18) with $x_{i,c}/\mu_i = \exp(-\alpha_i\beta V_i) = \exp(-k_i V_i)$. k_i depends on actual fractile value according to Table (A.1) in Appendix A.

2.4.5 Numerical values

Calculations of partial coefficients for thermal cracking problems of young concrete have been done by varying the variables in Table 2.4 and keeping all others constant.

Table 2.4 *Variables varied in the determination of partial coefficients for thermal cracking problems.*

Variable	Values				
ν_{sh}	$0.01\frac{c}{b}$	$0.20\frac{c}{b}$	$0.50\frac{c}{b}$	$1.00\frac{c}{b}$	$2.00\frac{c}{b}$
b	1/3	1	3		
c	1/3	1	3		
V_ε	0.05	0.10	0.15	0.20	0.25
V_C	0.05	0.10	0.15	0.20	0.25
β	3.72	4.75			

ν_{sh} are according to Equation (2.21) and state the ratio between the mean values of the strains of shrinkage and of the strains of temperature change. b and c are varied to simulate situations when one of the two strain components has smaller or larger influence. Especially in high strength concrete the shrinkage is considerable implying larger values of c. V_ε is the coefficient of variation of the actual concrete (actual ultimate strain ε_{cu}). V_C is the coefficient of variation of the methods used for estimating the risk of thermal cracking. Compare V_C with Methods 1 to 3 in Section 2.3 where e.g. $V_C = 0.15$ for Method 1, $V_C = 0.10$ for Method 2 and $V_C = 0.05$ for Method 3. These values are just an attempt of estimation of the accuracy in the methods and should not be seen as what is

right. The safety index β is varied to coincide with safety classes 1 and 3 with probabilities of failure of 10^{-4} and 10^{-6}, see Table 2.2.

The coefficient of variation of the temperature induced strains is given the value $V_T = 0.08$ according to Jonasson et al. (1994). The coefficient of variation of the shrinkage is given the value $V_{sh} = 0.20$. This value is a bit small than what can be determined from Jonasson (1994). The values of k_T and k_{sh} are 1.65 coinciding with 95 % fractile values of the temperature and shrinkage induced strains, respectively, see Table 2.5.

The coefficients of variations of the geometry parameter V_a and of the factor transferring strength in test specimens and in real structures V_ρ are both given the value 0, that is $V_a = 0$ and $V_\rho = 0$. The coefficient of variation of the geometry is assumed being very low since in civil engineering structures, any divergences from the right measures do not affect the risk of thermal cracking. For the concrete ultimate strain, $k_\varepsilon = 0.13$, see Appendix A, Table A.1, assuming 45% fractile value. The high value of the ultimate strain for the concrete is chosen bearing in mind that thermal cracking only causes flaws and costs for repair and reduction of the life of the structure but not total failure. For the accuracy in design method, *C*, for the geometry parameter, *a*, and for the factor transferring the ultimate strain in test specimens and in real structures ρ, the coefficient *k* is chosen $k_C = k_a = k_\rho = 1.65$ assuming 5% fractile values. Further, see Table 2.5.

Table 2.5 *Constant values for the resistance parameters C, a, ρ and ε and the load parameters T and sh used in the determination of the partial coefficients.*

k_C	V_a	k_a	V_ρ	k_ρ	k_ε	V_T	k_T	V_{sh}	k_{sh}
1.65	0	1.65	0	1.65	0.13	0.08	1.65	0.20	1.65

2.4.6 Example 1: Procedures for determination of partial coefficients

The following presumptions and values are used to illustrate the calculation of partial coefficients. Let the influence of the imposed volume changes be equal, $b = c = 1$. The mean value of the volume change due to shrinkage is one hundredth of the mean value of the imposed volume change due to the temperature change, $\nu_{sh} = 0.01 \cdot 1/1 = 0.01$. Further, the variation coefficients of the strength of the concrete and the calculation method are assumed to be five percentage, $V_\varepsilon = V_C = 0.05$ and the safety index $\beta = 3.72$ corresponding to safety class 1

and the probability of failure $p_f = 10^{-4}$. The following values for the resistance parameter, the sensitivity values α and the help values ψ, N and Z are obtained, Table 2.6 and Table 2.7, and see Table B.1a in Appendix B.

Table 2.6 *Calculated values for the resistance parameter.*

V_r	C_c/μ_C	a_c/μ_a	ρ_c/μ_ρ	$\varepsilon_c/\mu_\varepsilon$	r_c/μ_r
0.071	0.921	1.000	1.000	0.994	0.915

Table 2.7 *Calculated sensitivity values α and help-values ψ_1, N and Z.*

α'_{sh}	α_T	ψ_1	N	α_φ	α_T	α_r	Z
-0.017	-0.682	1.213	0.117	-0.017	-0.682	0.731	1.470

The partial coefficient for this case is then calculated as, Equation (2.33)

$$\gamma_r\gamma_s = \frac{Z}{\psi_2}\frac{r_c}{\mu_r} = \frac{1.470}{(1+1.65\cdot 0.08)+0.01(1+1.65\cdot 0.20)}0.915 = 1.174 \quad (2.34)$$

implying that the resistance parameter must be about 1.174 times larger than the load parameter for not exceeding the limit state condition.

2.4.7 Calculations and numerical results

All the partial coefficients calculated with values according to the description and Table 2.4 above are presented in Figure 2.4 to Figure 2.8 below. In all the diagrams, the curves from the lowest to the upper represent V_C = 0.05, 0.10, 0.15, 0.20 and 0.25, respectively. See Appendix B, Table B.1 through Table B.15 for the determination of the partial coefficients. Especially in Table B.11 through Table B.15, a thorough description of the calculations of the partial coefficients for the case of the safety index β = 3.72, and the deterministic coefficients b = 1 and c = 1 is presented.

It can be seen that with increased safety index β, the partial coefficient $\gamma_r\gamma_s$ increases and is varying over a larger range with the values of V_C. When the coefficient b increases also the partial coefficient increases, and when b decreases the partial coefficient decreases. Compare Figure 2.5 and Figure 2.6 with Figure

2.4. For the coefficient *c,* the opposite is valid. When *c* increases, the partial coefficient decreases and when *c* decreases, the partial coefficient increases. Compare Figure 2.7 and Figure 2.8 with Figure 2.4.

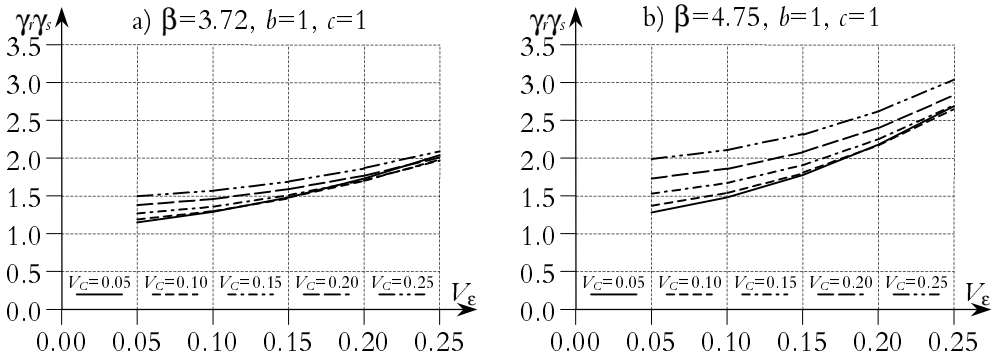

Figure 2.4 *Partial coefficient $\gamma_r\gamma_s$ for a) β=3.72, b=1 and c=1, b) β=4.75, b=1 and c=1.*

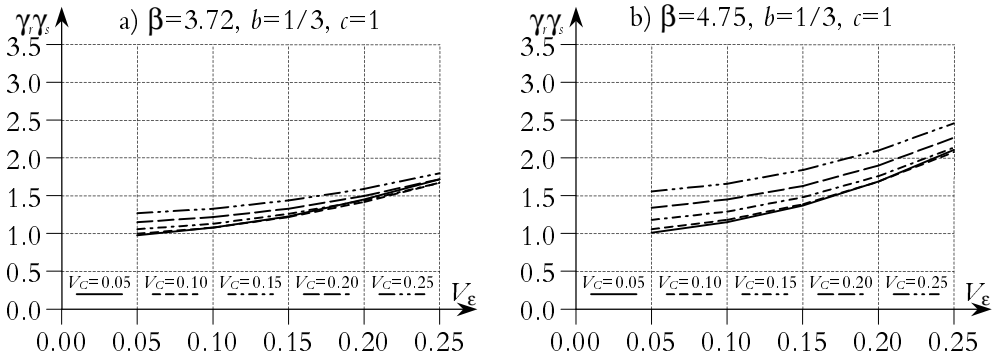

Figure 2.5 *Partial coefficient $\gamma_r\gamma_s$ for a) β=3.72, b=1/3 and c=1, b) β=4.75, b=1/3 and c=1.*

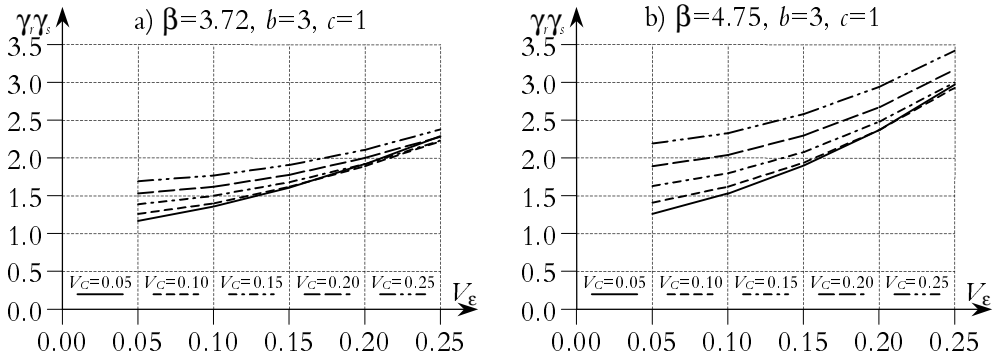

Figure 2.6 *Partial coefficient $\gamma_r\gamma_s$ for a) β=3.72, b=3 and c=1, b) β=4.75, b=3 and c=1.*

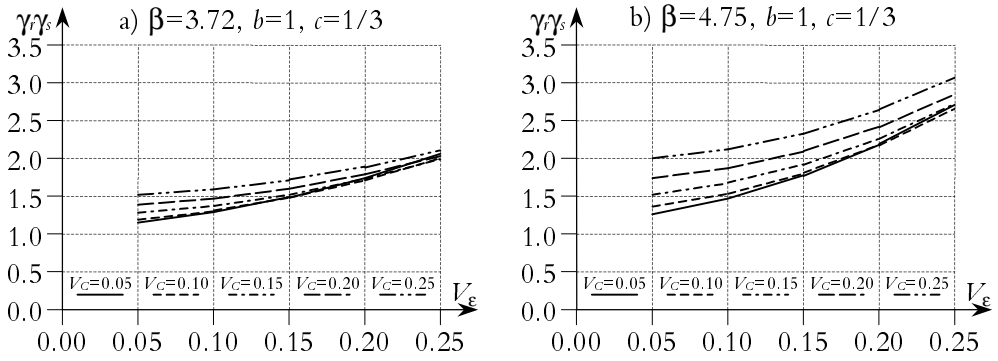

Figure 2.7 *Partial coefficient $\gamma_r\gamma_s$ for a) β=3.72, b=1 and c=1/3, b) β=4.75, b=1 and c=1/3.*

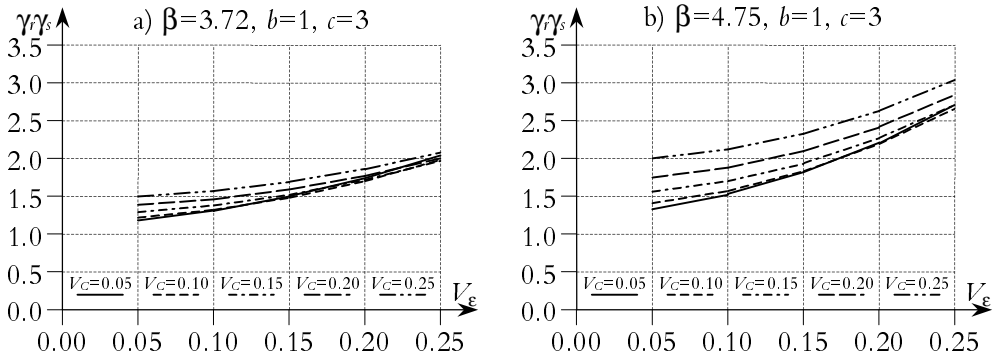

Figure 2.8 *Partial coefficient $\gamma_r\gamma_s$ for a) β=3.72, b=1 and c=3, b) β=4.75, b=1 and c=3.*

2.5 Final Values of Partial Coefficients

Final values of the partial coefficient $\gamma_r\gamma_s$ are determined from the previous calculations with $b = c = 1$, $\beta = 3.72$ (probability of failure, $p_f = 10^{-4}$) and with coefficients of variation, $V_C = 0.05$ and $V_\varepsilon = 0.05$, 0.10 and 0.15. The values are chosen to coincide with the first row in Table 2.3. That is, for Method 3 (the column of complete material data) the models of analysis (computer software) are very well documented and tried and should give results not varying much from reality. Therefore, the coefficient of variation for the method of calculation is chosen small, $V_C = 0.05$. For Method 2, (columns for material data given in BRO94 (1999)) lots of calculations and judgements are behind, Emborg et al. (1997), implying good accuracy of the analyses, again $V_C = 0.05$. The differences in accuracy of material data are taken into account by varying the coefficient of variation of the material V_ε as stated, $V_\varepsilon = 0.05$, 0.10 and 0.15. Again, $k_T = k_{sh} = 1.65$ for 95 % fractile values. Further, as an extension of the final determination of the partial coefficients, 55 % fractile values are assumed for the temperature and the shrinkage induced strains to coincide with the assumed fractile value of the ultimate strain (45 % fractile), see Section 2.4.5.

For environmental class A2 and $V_\varepsilon = 0.05$, 0.10 and 0.15, the partial coefficient $\gamma_r\gamma_s$ are taken as the values of the lowest curve in Figure 2.4a) and Appendix B, Table B.16, see Table 2.8.

Table 2.8 *Partial coefficient $\gamma_r\gamma_s$ from calculation with the probabilistic method for environmental class A2 and $V_\varepsilon = 0.05$, 0.10 and 0.15.*

Environm. class	k_T, k_{sh}	Complete material data V_ε=0.05	Material data given in the code $360 \le C \le 430$kg/m^3 V_ε=0.10	$430 \le C \le 460$kg/m^3 V_ε=0.15
A2	0.13	1.36	1.52	1.75
	1.65	1.15	1.29	1.48

2.5.1 Effects of exceeding the limit state condition

The calculation of partial coefficients above is chosen to be valid for environmental class A2. The effects of exceeding the limit state condition (cracking) in a structural member are smaller in environmental class A2 than in classes A3 and A4. Therefor an extra partial coefficient γ_n is introduced. The values of the extra

partial coefficient γ_n are chosen as the mean ratio between the values in the rows in Table 2.3, see Table 2.9.

Table 2.9 *Partial coefficient γ_n depending on environmental classes.*

	Environmental class		
	A2	A3	A4
γ_n	1.00	1.07	1.14

Final values of the partial coefficient $\gamma_r\gamma_s$ are obtained from Table 2.8 with partial coefficient γ_n in Table 2.9, see Table 2.10.

Table 2.10 *Final values of partial coefficient $\gamma_r\gamma_s$ as determined by probabilistic method.*

Environm. class	k_T, k_{sh}	Complete material data	Material data given in the code	
			$360 \leq C \leq 430$kg/m^3	$430 \leq C \leq 460$kg/m^3
A2	0.13	1.15	1.29	1.48
	1.65	1.36	1.52	1.75
A3	0.13	1.23	1.38	1.58
	1.65	1.45	1.62	1.87
A4	0.13	1.32	1.48	1.70
	1.65	1.56	1.74	2.00

A comparison with the values that is stated in BRO94 (1999) and the values of the partial coefficients obtained by the probabilistic method are depicted in Figure 2.9. As can be seen, the values obtained by the probabilistic method for $k_T = k_{sh} = 1.65$ (95 % fractile values) are somewhat higher than the values stated in BRO94 (1999). The values show good agreement even though the uncertainties in the chosen values of the variables used in the probabilistic method and that the partial coefficients stated in BRO94 (1999) only are based on experiences. For $k_T = k_{sh} = 0.13$ (55 % fractile values), the partial coefficients are much higher than the values in BRO94 (1999). The reason for this is that with

only 55 % fractile values of the temperature and the shrinkage induced strains, there is a increased risk of exceeding these values. This implies an increased risk of exceeding the limit state condition, whereupon higher partial coefficients are needed.

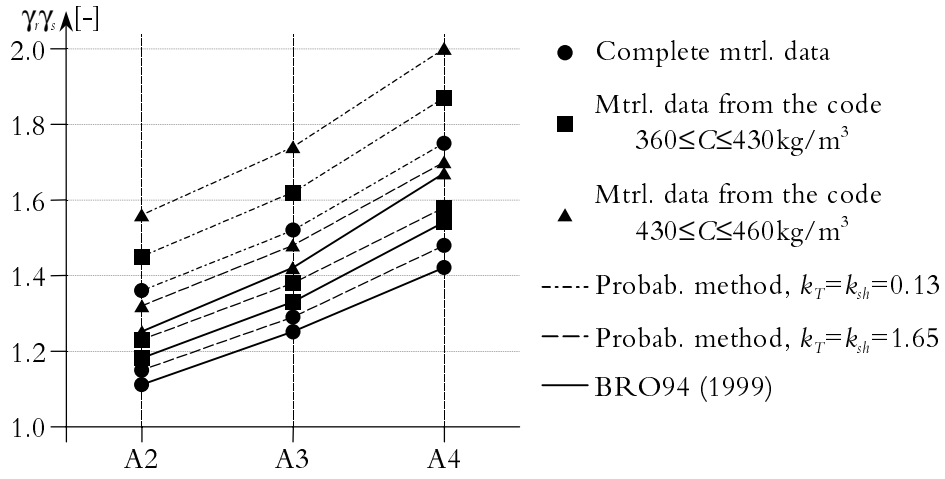

Figure 2.9 *Comparison between partial coefficients stated in BRO94 (1999) and partial coefficients obtained by the probabilistic method.*

2.6 Example 2: Determination of the Risk of Cracking for a Wall in a Rail Road Tunnel Below the Ground Water Level

Consider a concrete wall in a rail road tunnel that is going to be built below the ground water level. The wall is made of concrete that has been well tested regarding thermal cracking properties. The structure should be designed in safety class 1 fulfilling the requirements stated in BRO94 (1999). The importance of the thermal and the shrinkage-induced strains is equal.

According to the Swedish Code BBK94 (1994), the structure is located in environmental class A2. Further, safety class 1 implies that $\beta = 3.72$ corresponding to a probability of failure $p_f = 10^{-4}$. That the importance of the thermal and the shrinkage imposed strains is equal implies that the coefficients b and c equal 1, $b = c = 1$. Well-tested concrete is assumed resulting in a variation coefficient of $V_\varepsilon = 0.05$. With help of Figure 2.4 for $\beta = 3.72$ and $b = c = 1$, the partial coefficients can be found for the actual case presented in Figure 2.10.

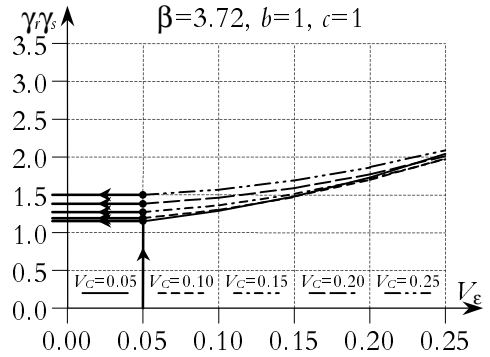

Figure 2.10 *Determination of partial coefficients for thermal cracking design of studied structure in Example 2.*

Depending on the accuracy in the design methods/tools, different partial coefficients are found. Assuming well-documented and tested computer tools for the design, V_C = 0.05, result in $\gamma_r\gamma_s \approx 1.15$. For V_C = 0.25, $\gamma_r\gamma_s \approx 1.51$. Further, again see Figure 2.10 and Appendix B, Table B.1. The results of this example are shown below in Figure 2.11 where the partial coefficient $\gamma_r\gamma_s$ is plotted as function of the variation coefficient V_C for V_ε = 0.05.

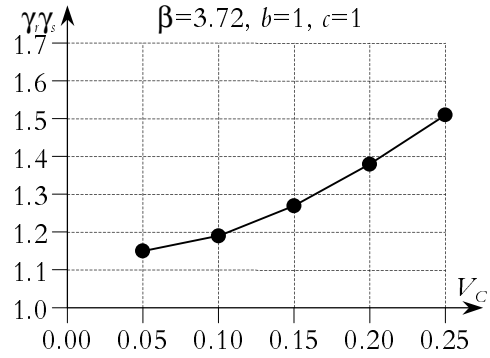

Figure 2.11 *Partial coefficients for different accurate design tools used for the wall in Example 2.*

2.7 Concluding Remarks

It is possible to calculate partial coefficients for thermal cracking problems of young concrete. The values presented above coincide well with the crack safety values stated in BRO94 (1999). However, the calculated values of the partial

coefficient are based on many assumptions and simplifications and they shall not be seen as what are right, further judgements are always necessary.

The used coefficients of variation of the thermal changes and of the shrinkage need further investigation. The values are roughly taken from Jonasson et al. (1994) and are only assumed values not being well verified.

The crack safety values in BRO94 (1999) are all based on experience, so also these values are a bit vague. The calculated partial coefficients presented here can be seen as an attempt of verification of the values in BRO94 (1999). However, all estimations of the risks of thermal cracking of young concrete have to be based on more judgements and analyses of the problems as a whole rather than on the crack safety values given in BRO94 (1999).

The differences in the partial coefficient between the environmental classes need further investigations. The values that are stated in BRO94 (1999) are only based on logical arguments, meaning that higher environmental class needs higher partial coefficients.

3 Coefficients of Restraint

3.1 Introduction

In many cases, it is both interesting and important to find the restraint in a decisive point in a young concrete part that is cast on an older one. In a manual method for calculation of the risk of thermal cracking of young concrete structures, the restraint in decisive points is a vital parameter, see Löfquist (1946), Bernander (1973) and Larson (2000). Further, see for instance Emborg (1989), Emborg & Bernander (1994) and Bernander (1998) for more details and descriptions about the restraint, its origin and effects on concrete structures.

The deformation of young concrete structures, e.g. walls cast on older slabs, depends on, amongst several things, the counteraction/restraint on these deformations from e.g. adjoining structures and materials and from the geometry of the structures. Parts of, or whole structures totally hindered to deform, are subjected to full restraint, and of course, structures totally free to deform, are subjected to no restraint.

The restraint depends on the properties of under-laying, more or less elastic materials, on the height and area ratios of adjoining and young parts of the structures, as well as the length to height ratio of the young concrete. In addition, possible slip failures in the joint between the young and old parts also influence the restraint, see Figure 3.1.

The restraint in decisive points in young concrete parts is a vital parameter in studies of the risk of thermal cracking, and is further referred to as the decisive restraint coefficient, γ_R. For structures with length to height ratios of the newly cast parts being larger than or equal to about five, $L/H \geq 5$, the decisive restraint coefficient is defined as a so-called plane-section restraint coefficient, $0 \leq \gamma^0_R \leq 1$. The plane-section restraint coefficients will be derived under the assumption

of plane sections remaining plane during the deformation, see Section 3.4.1. The decisive restraint coefficient then is

$$\gamma_R = \gamma_R^0$$

The plane-section restraint coefficient, γ^0_R, depends on the geometry of the structure as well as both the rotational and translational boundary restraints from under-laying foundation materials, see Sections 3.2, 3.3 and 3.5.

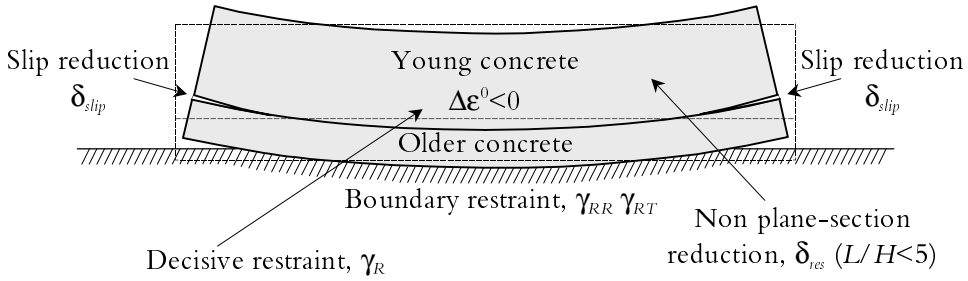

Figure 3.1 *The decisive restraint in structures during the contraction phase of the hydration is effected by boundary restraint from foundation materials, by slip failures in casting joints and by the geometry of the structure itself.*

In structures with $L/H < 5$, plane sections do not remain plane when deforming, implying reduction of the stresses from restrained boundaries to free boundaries of the structures. For these cases, a reduction factor, δ_{res}, is introduced considering the non-linear effects, see Section 3.4.2. This implies the decisive restraint coefficient to be

$$\gamma_R = \gamma_R(\gamma_R^0, \delta_{res})$$

Further, slip failure in casting joints is a phenomenon existing in many situations which reduces the restraint stresses, see Chapter 4. Therefore, a slip factor, $0.5 \le \delta_{slip} \le 1$, is introduced, see Section 3.7. The decisive restraint coefficient for structures with length to height ratio smaller than five then is

$$\gamma_R = \gamma_R(\gamma_R^0, \delta_{res}, \delta_{slip}) \qquad 0 \le \gamma_R \le 1 \tag{3.1}$$

The behaviour, in accordance with a plane-section analysis, during the contraction of a young structural member can schematically be described as in Figure 3.2. First, the actual deformation is divided into one part totally restraining the structure ($\Delta\varepsilon = 0$), and one part allowing the thermal deformation of the young concrete ($\Delta\varepsilon \neq 0$). The deformation is separated into translation

(axial deformation) and rotation (bending). The translation is modelled by an equivalent axial force of internal loading, N_{RI}, which acts in the centroid, $\bar{z}_{tot}$ of the total cross section. The rotation is modelled by an equivalent bending moment of internal loading, M_{RI}. The moment is caused by the equivalent axial force of internal loading and the eccentricity between the thermal centroid of the young concrete and the centroid of the total cross section.

At restrained conditions during the cooling phase, equivalent tensile contraction forces of internal loading N_{RI}, will, as mentioned, rise in young concrete members. The actual axial deformations of cross-sections correspond to outer axial forces $N_{RO}(x)$. Normally, the total sum of the forces of internal loading is not acting in the centroid of cross-sections implying internal eccentricities $e_{\Delta T}$. The forces and the product of forces and eccentricities cause transversal contraction as well as bending moments endeavouring to rotate the whole structure. These bending moments are in the following denoted bending moments of internal loading, M_{RI}. The actual rotations of the cross-sections correspond to outer bending moments, denoted $M_{RO}(x)$.

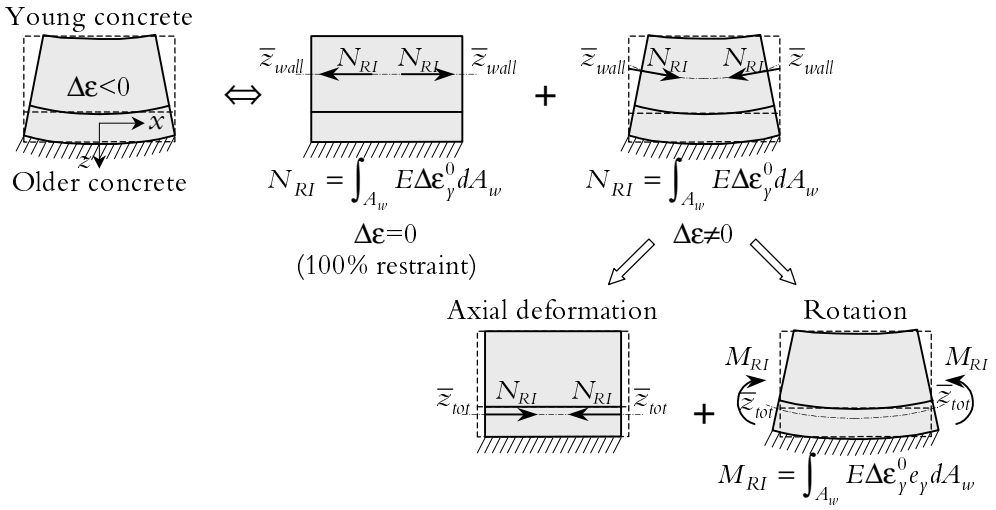

Figure 3.2 *Equivalent internal forces and internal bending moments acting on concrete structures during the contraction phase of young concrete members. Plane-section analysis, modified from Nilsson (1998).*

The outer axial forces, $N_{RO}(x)$, and outer bending moments, $M_{RO}(x)$, are caused by the restraint/counteraction from adjacent older concrete members and/or more or less elastic foundations on the free movements of young con-

crete structures. The amount of translation and/or rotation depends partly on the length of the structures, partly on the friction and cohesion properties and stiffness of the foundation material.

The free translation of a structure is counteracted by the friction and/or cohesion properties of the foundation material. A low friction and/or non-cohesive foundation material gives almost no resistance to the free translation, which means that the translational boundary restraint is almost zero, $\gamma_{RT}(x) \approx 0$. On the contrary, a structure founded on a high friction and/or cohesive foundation material, is subjected to a translational boundary restraint of almost 100%, $\gamma_{RT}(x) \approx 1$. For structures founded on blasted rock, the restraint situation is much more complicated e.g. by means of interlocking between the concrete and the rock and by influence of existing crack zones in the rock.

The bending moment during the cooling, induced by the temperature decreases in the young parts and its eccentricity to the total centroidal axis, tend to rotate the ends of structures upward and the centre parts downward. The stiffness of the foundation material prescribes how much a structure may bend down into the ground. A soft material offers almost no resistance to the free deformation of the structure, implying non-, or very little, restraint, $\gamma_{RR}(x) \approx 0$. On the contrary, a structure founded on a stiff ground, for example rock or dense gravel, can hardly bend at all, that is, the rotational boundary restraint is about 100 percent, $\gamma_{RR}(x) \approx 1$. If the stiffness of the foundation material is high and/or the structure is relatively long, the structure rotates anyhow but lifts at its ends and rests on the ground only at intermediate parts of the structure. The lifting is hindered, naturally, by the dead weight of the concrete.

3.2 Rotational Boundary Restraint

3.2.1 Structures founded on elastic materials

The last two steps in Figure 3.2, regarding axial deformations and rotations, represent all the deformation in plane-section analyses of the studied structural member. Below, the flexural deformation is going to be analysed, wherefore only the rotation of the beam will be studied, i.e. the beam loaded by two opposite bending moments equal to the moment of internal loading, M_{RI}, see Figure 3.3. The distribution of the moment along the beam is denoted $M_{RO}(x)$. This situation is simulating the bending deformation of a young concrete structure with its adjoining structure during the cooling phase.

If the elastic foundation is not giving any noticeable resistance against bending, it is defined not to be subjected to any rotational boundary restraint, $\gamma_{RR}(x) = 0$. The bending moment $M_{RO}(x)$, is then equal to the bending moment of internal loading, $M_{RO}(x) = M_{RI}$. If, on the contrary, a structure is not permitted

to bend at all, the rotational boundary restraint is defined as 100%, $\gamma_{RR}(x) = 1$. The curvature of a construction is then equal to zero, implying the external bending moment also being equal to zero.

The rotational boundary restraint $\gamma_{RR}(x)$ is generally defined as

$$\gamma_{RR}(x) = 1 - \frac{M_{RO}(x)}{M_{RI}} \qquad 0 \le \gamma_{RR}(x) \le 1 \tag{3.2}$$

The bending moment of internal loading, M_{RI}, as shown in Figure 3.2, is calculated in terms of the strain of imposed volume changes in the young concrete $\Delta\varepsilon_\gamma^{\,0} = \Delta\varepsilon_\gamma^{\,0}(t)$, the modulus of elasticity of the young concrete $E_\gamma = E_\gamma(t)$, the eccentricity between the centroidal axes of the total structure and the young part $e_\gamma = e_\gamma(t)$, and the area of the young concrete, A_γ,

$$M_{RI} = \int_{A_\gamma} E_\gamma(t)\varepsilon_\gamma^0(t)e_\gamma(t)dA_\gamma \tag{3.3}$$

where the strain, $\Delta\varepsilon_\gamma^{\,0}$, of imposed volume changes during the contraction phase is

$$\Delta\varepsilon_\gamma^0(t) = \Delta T(t - t_1)\alpha_c + \varepsilon_{sh} \tag{3.4}$$

and

$\Delta T(t\text{-}t_1)$ is the change of temperature from the state of zero stresses, [°C], as this part of the contraction phase is of interest for crack risk estimation

α_c is the thermal contraction coefficient, [1/°C]

ε_{sh} is the strain increment due to shrinkage change

A beam of finite length founded on some elastic material and loaded by two equal and opposite bending moments, M_{RI}, at its ends is drawn in Figure 3.3.

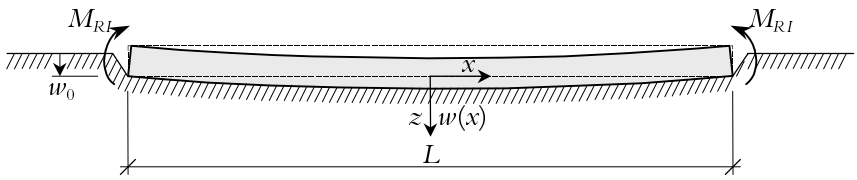

Figure 3.3 *Beam of finite length on elastic foundation loaded by two equal and opposite bending moments at its ends.*

The vertical deflection of the beam is separated into two parts, one rigid body deflection, w_0, and one deflection due to the bending moments, $w(x)$ [m]. The rigid body deflection originates from the immediate settlement after the placing of the concrete, i.e. the self-weight deformation. The deflection due to the bending is, according to Nilsson (1998), Bernander (1993) and Appendix C Equation (C.24), if the ends of the structure are assumed not to lift from the ground, calculated as follows

$$w(x) = -\frac{2\kappa M_{RI}}{K_j L_e^2\left(\sin\frac{L}{L_e}+\sinh\frac{L}{L_e}\right)}\cdot \cdot\left\{\left(\cos\frac{L}{2L_e}\sinh\frac{L}{2L_e}+\sin\frac{L}{2L_e}\cosh\frac{L}{2L_e}\right)\sin\frac{x}{L_e}\sinh\frac{x}{L_e}+ +\left(\cos\frac{L}{2L_e}\sinh\frac{L}{2L_e}-\sin\frac{L}{2L_e}\cosh\frac{L}{2L_e}\right)\cos\frac{x}{L_e}\cosh\frac{x}{L_e}\right\} \tag{3.5}$$

where

L is the length of the structure, [m]

$EI(t)$ is the bending stiffness of the total structure, [Nm^2]

κ is a shape factor depending on the width to length ratio, W/L, of the structural part resting on the ground, see Table 3.2

K_j is the modulus of compression of ground materials, [N/m^2], depending on the type of soil and its grading, see Table 3.1

L_e is the so-called elastic length, [m], calculated as

$$L_e = \sqrt[4]{\frac{2EI(t)\kappa}{K_j}} \tag{3.6}$$

The ground pressure, $p(x)$ [N/m], along the beam is calculated as, see Nilsson (1998), Bernander (1993) and Appendix C Equation (C.25),

$$p(x) = \rho g A_{tot} - \frac{4M_{RI}}{L_e^2\left(\sin\frac{L}{L_e} + \sinh\frac{L}{L_e}\right)} \cdot \left\{\left(\cos\frac{L}{2L_e}\sinh\frac{L}{2L_e} + \sin\frac{L}{2L_e}\cosh\frac{L}{2L_e}\right)\sin\frac{x}{L_e}\sinh\frac{x}{L_e} + \left(\cos\frac{L}{2L_e}\sinh\frac{L}{2L_e} - \sin\frac{L}{2L_e}\cosh\frac{L}{2L_e}\right)\cos\frac{x}{L_e}\cosh\frac{x}{L_e}\right\} \tag{3.7}$$

where $\rho g A_{tot}$ [N/m] is the dead weight of the structure.

The bending moment $M_{RO}(x)$, [Nm], along the beam can be calculated according to, see Nilsson (1998), Bernander (1993) and Appendix C Equation (C.26),

$$M_{RO}(x) = \frac{2M_{RI}}{\left(\sin\frac{L}{L_e} + \sinh\frac{L}{L_e}\right)} \cdot \left\{\left(\cos\frac{L}{2L_e}\sinh\frac{L}{2L_e} + \sin\frac{L}{2L_e}\cosh\frac{L}{2L_e}\right)\cos\frac{x}{L_e}\cosh\frac{x}{L_e} - \left(\cos\frac{L}{2L_e}\sinh\frac{L}{2L_e} - \sin\frac{L}{2L_e}\cosh\frac{L}{2L_e}\right)\sin\frac{x}{L_e}\sinh\frac{x}{L_e}\right\} \tag{3.8}$$

In the mid-span of a structure, $x = 0$, Equation (3.8) is simplified to

$$M_{RO}(x=0) = \frac{2M_{RI}}{\sin\frac{L}{L_e} + \sinh\frac{L}{L_e}}\left(\cos\frac{L}{2L_e}\sinh\frac{L}{2L_e} + \sin\frac{L}{2L_e}\cosh\frac{L}{2L_e}\right) \tag{3.9}$$

Equation (3.8) generally originates from Timoshenko (1958) and is applied for the determination of rotational boundary restraint in Bernander (1993). It is derived for a beam on an elastic material bent by two equal and opposite bending moments at its ends, see Appendix C Equation (C.26).

By substituting Equation (3.8) into Equation (3.2), the rotational boundary restraint coefficient along a structure, $\gamma_{RR}(x)$ [-], can be calculated as

$$\gamma_{RR}(x) = 1 - \frac{2}{\left(\sin\frac{L}{L_e} + \sinh\frac{L}{L_e}\right)} \cdot \cdot \left\{ \left(\cos\frac{L}{2L_e}\sinh\frac{L}{2L_e} + \sin\frac{L}{2L_e}\cosh\frac{L}{2L_e} \right)\cos\frac{x}{L_e}\cosh\frac{x}{L_e} - \left(\cos\frac{L}{2L_e}\sinh\frac{L}{2L_e} - \sin\frac{L}{2L_e}\cosh\frac{L}{2L_e} \right)\sin\frac{x}{L_e}\sinh\frac{x}{L_e} \right\} \quad (3.10)$$

where it can be seen that the restraint only depends on the length to elastic length ratio, which makes the equation very applicable. In the midsection $x = 0$, which in almost all cases is the decisive section, Equation (3.10) is simplified to

$$\gamma_{RR}(x=0) = 1 - \frac{2}{\sin\frac{L}{L_e} + \sinh\frac{L}{L_e}}\left(\cos\frac{L}{2L_e}\sinh\frac{L}{2L_e} + \sin\frac{L}{2L_e}\cosh\frac{L}{2L_e} \right) \quad (3.11)$$

Application tools

Different types of soils give different compression resistance depending on the compaction. Examples of the modulus of compression, according to Nilsson (1998) and Bernander (1993), for different types of foundation materials at different rates of compaction are given in Table 3.1. Higher rate of compaction leads to higher modulus of compression.

Table 3.1 *Modulus of compression, K_j, for different types of foundation materials. From Bernander (1993).*

Type of soil and compaction	K_j [N/m^2]
Clay, soft	$0.5 \cdot 10^6$ - $2 \cdot 10^6$
Clay, semi-solid	$1 \cdot 10^6$ - $3 \cdot 10^6$
Clay, sandy and silty	$2 \cdot 10^6$ - $5 \cdot 10^6$
Sand, soft	$3 \cdot 10^6$ - $10 \cdot 10^6$
Sand, medium dense to dense	$10 \cdot 10^6$ - $60 \cdot 10^6$
Gravel, medium dense to dense	$10 \cdot 10^6$ - $60 \cdot 10^6$

The shape factor κ in Equation (3.6) can be determined e.g. from Löfling (1993) depending on the width to length ratio, W/L, of the structural member resting on the ground, see Table 3.2.

Table 3.2 *The shape factor κ as function of the width to length ratio of the structure member resting on the ground, Löfling (1993).*

W/L	0.2	0.4	0.6	0.8	1.0
κ	0.94	0.83	0.75	0.69	0.65

Equation (3.11) has been used to calculate the length to elastic length ratio of structures that correspond to values of rotational boundary restraint between 0 and 100%. The results are depicted in Figure 3.4 for $x = 0, \pm 0.1L, \pm 0.2L, \pm 0.3L, \pm 0.4L$.

The diagram in Figure 3.4 is very useful e.g. for determining the length of sections being cast corresponding to certain amounts of rotational boundary restraint. From a predetermined value of the rotational boundary restraint $\gamma_{RR}(x)$, the value of L/L_e is given in Figure 3.4. With Equation (3.6), the value of L/L_e is used to calculate the length of the structure. However, the shape factor κ in Equation (3.6) depends on the length of the structure, see Table 3.2, implying iteration is needed to find a final value of the length of a structure.

Conversely, the restraint can be determined for a structure with given geometry that is founded on an elastic material with given modulus of compression. The length to elastic length ratio is first calculated whereupon the rotational boundary restraint coefficient is given from the diagram.

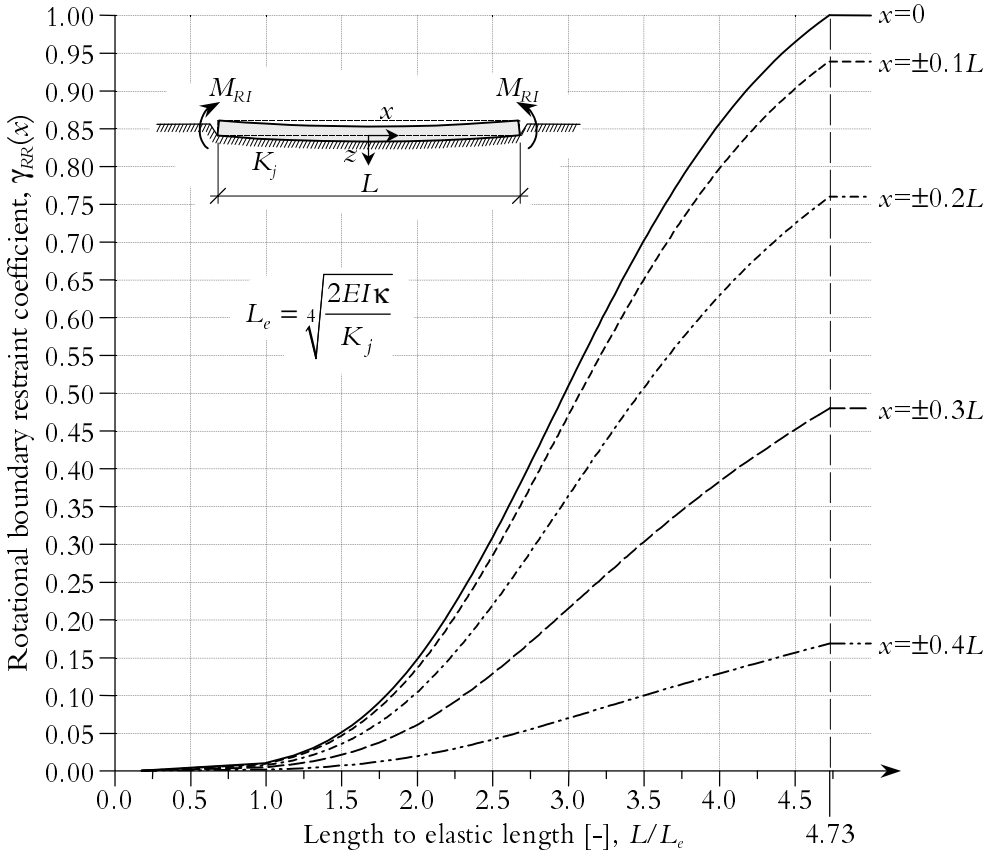

Figure 3.4 *The rotational boundary restraint coefficients $\gamma_{RR}(x)$ as function of the length to elastic length ratio of the structure L/L_e.*

3.2.2 Example 1: The rotational boundary restraint coefficient as function of different lengths and modulus of compression

Study the influence on the rotational boundary restraint coefficient of different lengths and modulus of compression for a structure made of a wall cast on a slab with the cross section depicted in Figure 3.5. The diagram in Figure 3.4 is to be used to solve the problem.

The lengths to study are L = 5, 10, 20 and 40m, the modulus of compression for a semi-solid clay, K_j = 2000kN/m^2, a soft sand, K_j = 7000kN/m^2 and for a medium dense sand, K_j = 25000kN/m^2. The modulus of elasticity in the young wall is assumed being 75 percentage of the final value, $E_y = \zeta E_{28y}$ = 0.75·30000 = 22500MPa and in the older slab E_a = 30000MPa.

Further, the temperature decrease in the wall at the studied stage is ΔT_y = -20°C. This value is an approximated mean value of the temperature decrease over the cross section of the young part. The temperature induced equivalent force is assumed be acting in the centroid of the young part.

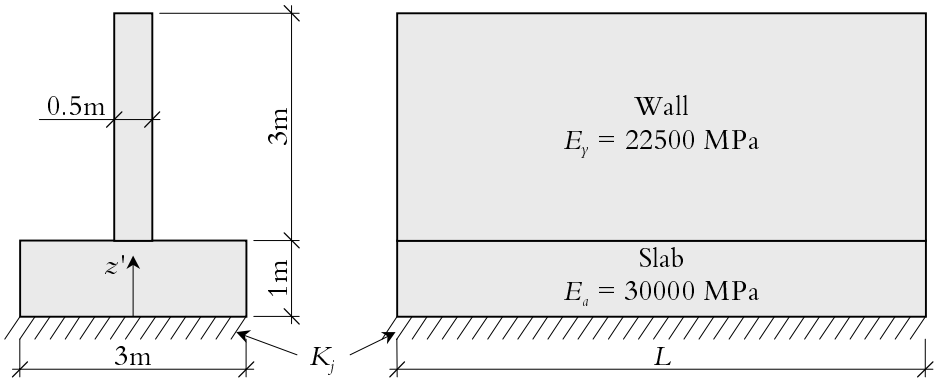

Figure 3.5 *Structure studied in example 1.*

Step 1: Calculation of transformed section properties

With the young concrete as reference the following are computed; the transformed area, A_{trans}, the distance to the centroidal axis of the transformed section, z'_{trans} and the moment of inertia are, I_{trans},

$$A_{trans} = 0.5 \cdot 3 + \frac{30000}{0.75 \cdot 30000} 3 \cdot 1 = 5.500 \text{ m}^2$$

$$z'_{trans} = \frac{0.5 \cdot 3\left(1 + \frac{3}{2}\right) + \frac{30000}{0.75 \cdot 30000} 3 \cdot 1 \cdot \frac{1}{2}}{5.500} = 1.045 \text{ m}$$

$$I_{trans} = \frac{0.5 \cdot 3^3}{12} + 0.5 \cdot 3\left(1.045 - \left(1 + \frac{3}{2}\right)\right)^2 + \\ + \frac{30000}{0.75 \cdot 30000}\left(\frac{3 \cdot 1^3}{12} + 3 \cdot 1\left(1.045 - \frac{1}{2}\right)^2\right) = 5.822 \text{ m}^4$$

Step 2: Calculation of the elastic length and the length to elastic length ratio

By use of Equation (3.6) and Table 3.2 the following values of the length to elastic length ratio will be obtained, see Table 3.3.

Table 3.3 *Length to elastic length ratio for example 1 as function of the modulus of compression and the length of the structure.*

L [m]	L/L_e K_j=2000kN/m^2	K_j=7000kN/m^2	K_j=25000kN/m^2
5	0.282	0.386	0.531
10	0.542	0.742	1.020
20	1.059	1.448	*1.991*
40	2.090	2.858	*3.930*

Step 3: Evaluation of rotational boundary restraint coefficient

The rotational boundary restraint coefficients for the structure are calculated with Equation (3.10) and plotted in Figure 3.6. Further, the values of the length to elastic length ratio are plotted in Figure 3.4 giving the results shown in Figure 3.7.

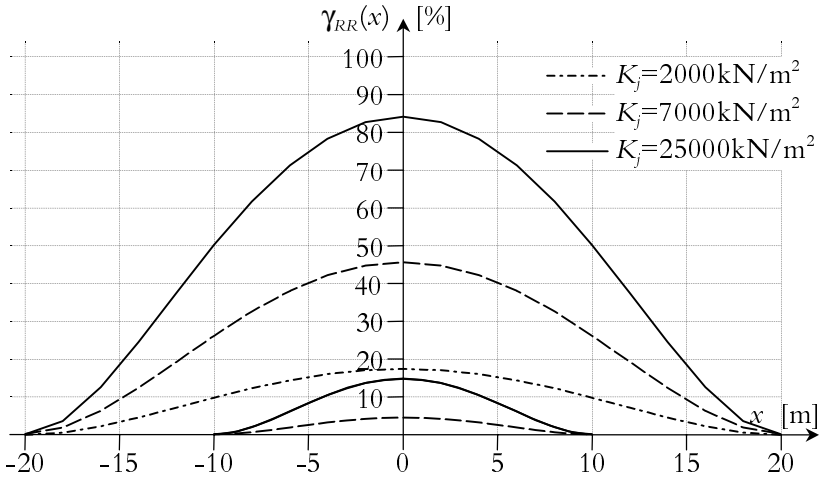

Figure 3.6 *The rotational boundary restraint along the structure in Example 1.*

The general conclusions drawn from this example are that the rotational boundary restraint coefficients increase with increasing lengths of the structure and with increasing values of the modulus of compression.

As can be seen from Figure 3.6 and Figure 3.7, for L = 40m and all the three values of the modulus of compression, and for L = 20m and K_j = 25000kN/m^2,

the rotational boundary coefficient is noticeable. Especially in the midsection, the rotational boundary restraint coefficient varies between about 0.13 for L = 25m and K_j = 7000kN/m^2 to about 0.84 for L = 40m and K_j = 25000kN/m^2. For all other combinations of the length of the structure and the modulus of compression, the rotational boundary restraint coefficient is considerably small, i.e. the structure is more or less free to rotate. In practical applications, $\gamma_{RR} \leq 0.05$ may be regarded as $\gamma_{RR} = 0$.

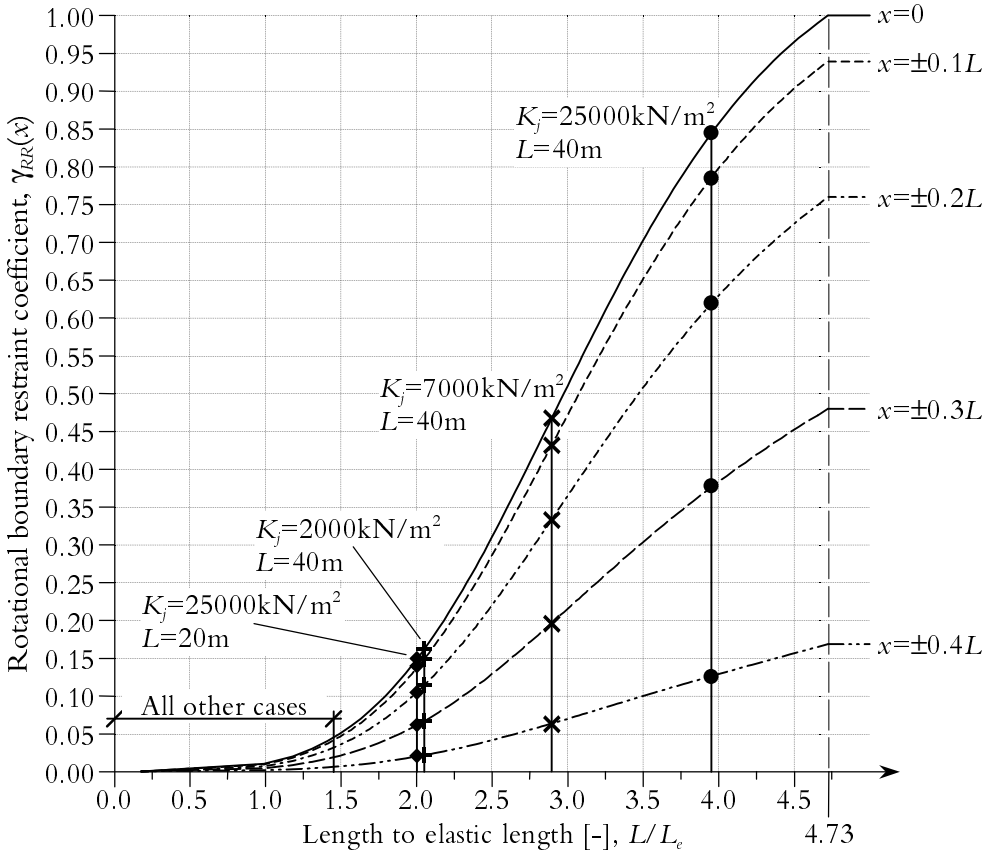

Figure 3.7 *Results of the determination of the rotational boundary restraint coefficient in Example 1.*

It should be pointed out that for K_j = 25000kN/m^2 and L = 20 and 40m, the values of the length to elastic length ratio given in Table 3.3 (in italic letters) are not exact due to lifting of the ends of the structures, see Section 3.2.5 below.

The example indicates that the stiffer foundation material and/or the longer the structure, the possibility that the ends of a structure will lift is increased. For the case of lifting ends, the given model for determination of the rotational boundary restraint coefficient, Equation (3.10) and Figure 3.4, is therefore no longer valid. Structures with lifting ends will be dealt with in Section 3.2.5 and in the continuation of the present example.

3.2.3 Effects of the age of the young concrete

The elastic length of a structure is dependent on time, due to the growth of the modulus of elasticity $E = E(t)$. Therefore, the moment of inertia is also dependent on time. By this, the rotational boundary restraint coefficient depends on both the x-coordinate and the time, $\gamma_{RR} = \gamma_{RR}(x,t)$.

The bending stiffness $EI(t)$ in Equation (3.6) is valid for the total cross-section of a structure. Since the modulus of elasticity and the moment of inertia are not equal in young concrete parts and older parts, all members have to be transformed to one of the members, or to an arbitrary chosen reference material.

For a concrete structure consisting of one young part and one adjoining and older, the transformed moment of inertia will be as follows if the moment of inertia of adjoining parts (subscript a) are transformed to the moment of inertia of younger (subscript y)

$$EI(t) = E_y(t)\left(I_{0,y} + A_y(z'_{cn} - z'_y)^2 + \sum_{i=1}^{n} \frac{E_{ai}}{E_y(t)}\left(I_{0,ai} + A_{ai}(z'_{cn} - z'_{ai})^2\right)\right) \qquad (3.12)$$

where

I_0 is the moment of inertia of the member around its own centroidal axis, [m^4]

A is the area, [m^2]

z' is the distance from a reference axis to the centroidal axis of each member, [m]

z'_{cn} is the distance from a reference axis to the centroidal axis of the transformed cross section, [m]

The modulus of elasticity increases rapidly with age, as is shown in Figure 3.8 where the development over time is depicted for a type of concrete mix at +20°C. In the figure, t_S is the time of setting of the fresh concrete. The development of the modulus of elasticity also depends very much on the actual temperature in the structures. At higher temperatures, the modulus of elasticity develops faster, which may be described by the well-known concept of maturity.

Due to the relatively high temperature in young more massive concrete structures, such as are studied here, the modulus of elasticity growth is very rapid.

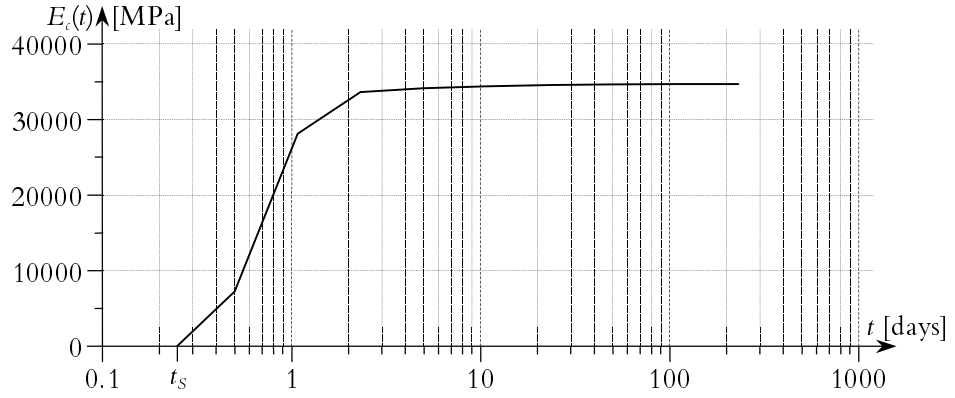

Figure 3.8 *Example of time-dependent development of modulus of elasticity for one type of concrete mix at temperature +20°C.*

The rapid growth can be seen in Figure 3.9, where the modulus of elasticity growth is plotted in relation to a dimensionless relative time $\tau = t/28$. That is, the development of the modulus of elasticity is put in relation to 28days. The modulus of elasticity at 28days at +20°C is put as the reference and final value, $E(t = \infty) = E_{28}$. As can be seen in the figure, for $\tau = 0.1$ ($t = 2.8$days) the modulus of elasticity is already near the final value. This indicates that the effect of time on the rotational boundary restraint is not important for the relatively late problems of through cracking of young concrete.

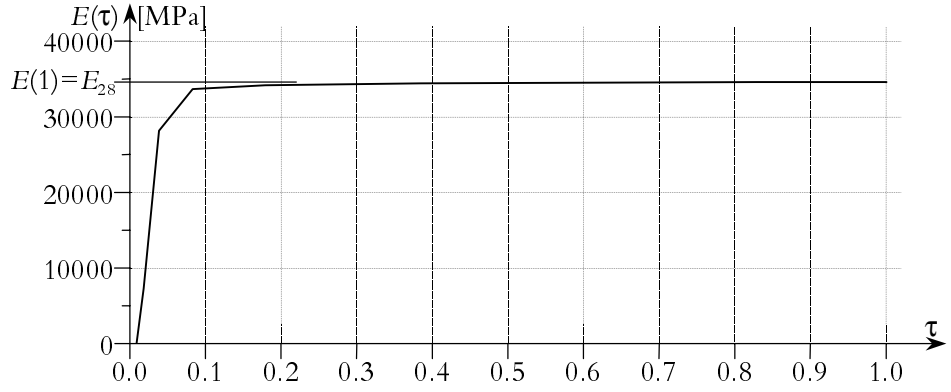

Figure 3.9 *Example of the development of the modulus of elasticity as function of the dimensionless relative time $\tau = t/28$.*

Furthermore, in Larson (2000), an investigation of the ratio between the modulus of elasticity at 28-days and the modulus of elasticity at equivalent actual time is presented for one type of concrete in 81 different cases of casting. The results are depicted in Figure 3.10. It can be seen from the state of zero stresses, t_{e2}, to the state of maximum stresses, t_{e3}, that the ratio of the modulus of elasticity changes from about 1.3 to about 1.03. Again, this indicates that the effect of time is negligible in determination of restraint coefficients for the relatively late problems of through cracking of young concrete structures during the contraction phase.

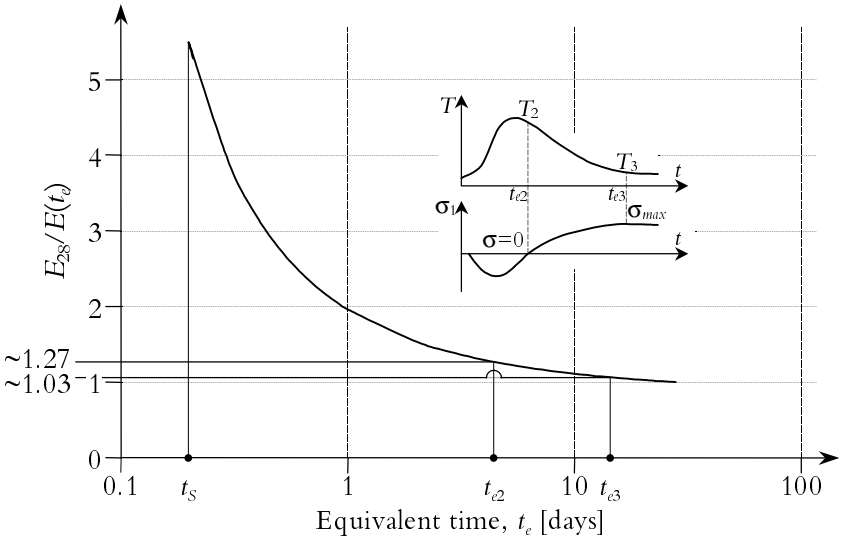

Figure 3.10 *Development of the modulus of elasticity in relation to the value at 28-days indicating occurred time domains at the cooling phase for 81 cases. Modified from Larson (2000).*

As the effect of age could have a large influence on the restraint, it is checked also in this study. This has been performed by determining the influence of different values of the elastic length, read bending stiffness $EI(t)$. The decreases in the elastic length are first calculated for lower values of the bending stiffness. These values are then used to determine increased values of the length to elastic length ratios, which finally give values of the rotational boundary restraint corresponding to the lower values of the bending stiffness.

According to earlier, the elastic length is calculated as, compare Equation (3.6),

$$L_{e,\xi} = \sqrt[4]{\frac{2(\xi EI)\kappa}{K_j}} = \sqrt[4]{\xi} L_e \qquad \xi_0 \le \xi \le 1 \tag{3.13}$$

where ξ is the factor used to take into account the influence of time on the bending stiffness. ξ_0 is the lowest value of factor ξ, that is, the bending stiffness of only the adjoining (older) structural parts at placing of the concrete in the younger member,

$$\xi_0 = \frac{(EI)_{28a}}{EI} \tag{3.14}$$

The increase in the length to elastic length ratio is then given as

$$\frac{L}{L_{e,\xi}} = \frac{1}{\sqrt[4]{\xi}} \frac{L}{L_e} = \xi^{-0.25} \frac{L}{L_e} \tag{3.15}$$

The following values, Table 3.4, of the factor ξ and corresponding increase factors of the length to elastic length ratio are used in the analysis of the influence of time on the rotational boundary restraint.

Table 3.4 *Enlargement values for the length to elastic length, $\xi^{-0.25}$, as function of the reduction factor for the bending stiffness, ξ.*

ξ	0.1	0.2	0.3	0.4	0.5	0.6	0.7	0.8	0.9	1.0
$\xi^{-0.25}$	1.778	1.495	1.351	1.257	1.189	1.136	1.093	1.057	1.027	1.000

The results of the lower values of the bending stiffness are drawn in Figure 3.11 and Figure 3.12. In Figure 3.11, the effects on the rotational boundary restraint in the midsection of a structure (x = 0, Equation (3.11)) of increased time and of increased length to elastic length ratios are depicted. A short time after casting, the rotational boundary restraint is relatively high and decreases with time. In addition, large length to elastic length ratios imply higher values of the rotational boundary restraint.

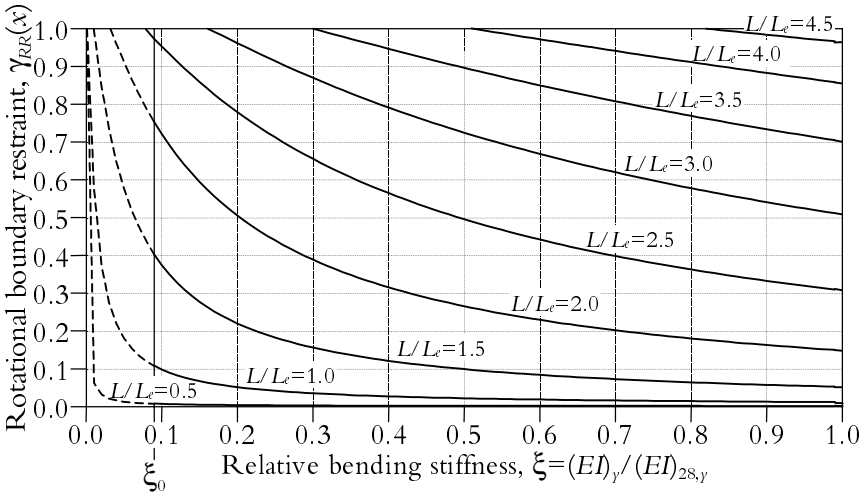

Figure 3.11 *The rotational boundary restraint coefficient as function of the relative bending stiffness* $\xi=(EI)_y/(EI)_{28,y}$*, and the length to elastic length ratio.*

In Figure 3.12 the leftmost curve is for ξ = 0.1, and the rest for increased values of ξ, $\Delta\xi$ = 0.1, to the most right curve where ξ = 1.0. It can be seen that when the bending stiffness is only one tenth of the final value, the rotational boundary restraint is significantly higher than in the late states of the hydration.

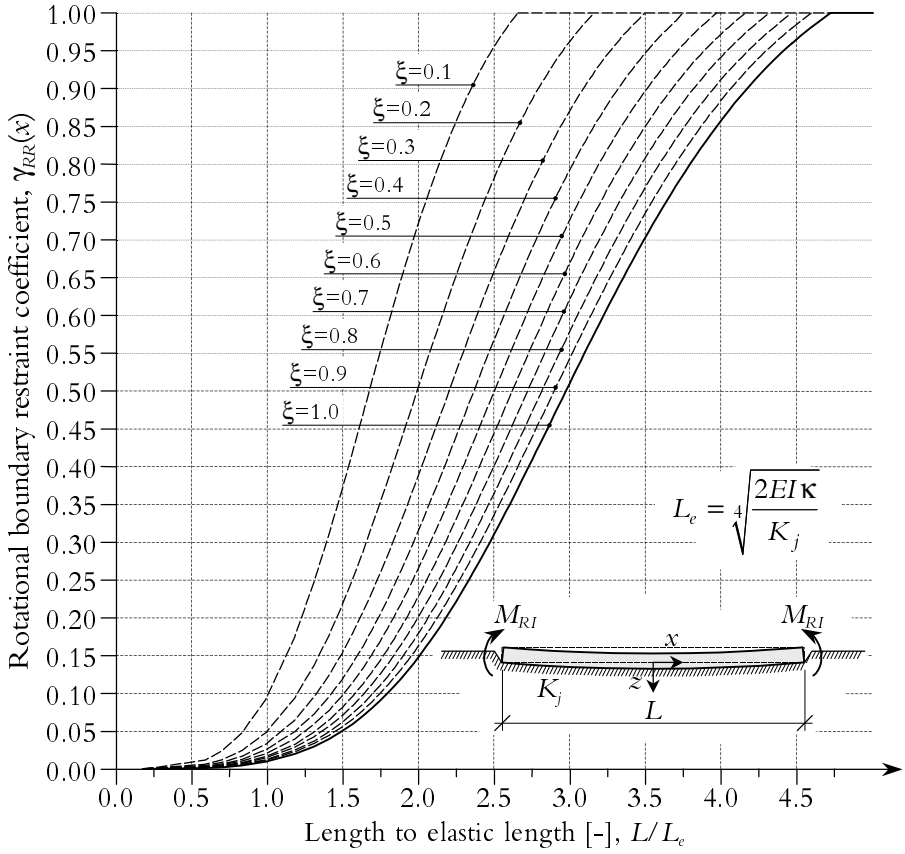

Figure 3.12 *The effect of concrete age on the rotational boundary restraint. The left-most curve is for very low values of the modulus of elasticity* $\xi = 0.1$*, i.e. at very early ages during the heating phase. The most right curve is for final values of the modulus of elasticity, which in most cases can be used at cooling.*

However, since the risks of through (severe) cracking appear a rather long time after casting, as previously stated, the influence of time on the rotational boundary restraint is negligible, Thus, the final value of the modulus of elasticity of the young concrete, $E_{28,y}$, can be used in most cases. Again, see Figure 3.10. A value of $\xi = 0.95$ will however be used in the following to correspond with the results in Figure 3.10.

3.2.4 Structures founded on rock or very stiff materials

For structures founded on rock or very stiff materials, it is also possible to estimate the rotational boundary restraint assuming no cohesion and/or friction between the concrete and the rock. Again, during the contraction phase when

the temperature is decreasing in the young concrete, an equivalent bending moment of internal loading M_{RI} rises, see Figure 3.2 and Equation (3.3). For such a structure, with no joint cohesion and/or friction, the ends tend to lift after the temperature maximum is reached and the cooling phase has progressed a little. Only the bending moment from the dead weight and the length of a structure counteracts the lifting, see Figure 3.13.

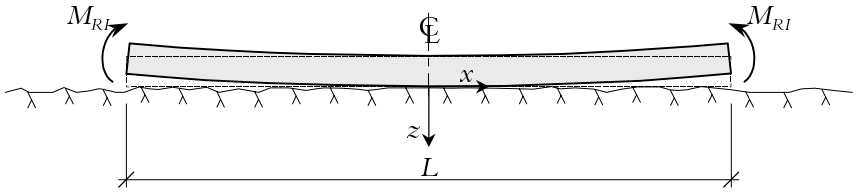

Figure 3.13 *Concrete structure on rock loaded by two equal and opposite bending moments at its ends. No cohesion between the concrete and the rock.*

For structures founded on rock with no cohesion between the concrete and the rock, the restraint depends solely on the lengths of the structures. If a structure is so long that the bending moment corresponding to the rotation, $M_{RO}(x)$, fully counteracts the thermal contraction movements, M_{RI}, the restraint is 100%. This is the fact when the bending moment of internal loading is equal to the outer bending moment corresponding to the rotation, $M_{RI} = M_{RO}(x)$. The rotational boundary restraint is calculated as, see Equation (3.2)

$$\gamma_{RR}(x) = 1 - \frac{M_{RO}(x)}{M_{RI}}$$

The bending moment corresponding to this rotation, $M_{RO}(x)$, can be calculated if the halves of a structure are regarded as two cantilever beams, see Figure 3.13. It is loaded by the dead weight

$$q(x) = \int_{A_{tot}} \rho g dA_{tot} \tag{3.16}$$

and the equivalent bending moment of internal loading M_{RI} giving

$$M_{RO}(x) = M_{RI} - \frac{q}{2}\left(x - \frac{L}{2}\right)^2 \tag{3.17}$$

Equation (3.17) in Equation (3.2) gives a final expression for the rotational boundary restraint for a structure founded on rock with no cohesion between the concrete and the rock as

$$\gamma_{RR}(x) = \frac{q}{2M_{RI}}\left(x - \frac{L}{2}\right)^2 \tag{3.18}$$

3.2.5 Lifting ends of structures founded on elastic materials

Also cases when structures are founded on elastic materials and/or when the structures are relatively long, their ends can lift. When the bending of a structure is large and the lifting of its ends is larger than the rigid body deflection, free spaces will arise between the structure and the ground. Two cantilever beams will so to say arise at the ends of the structure. This will happen when the ground pressure at the ends of the structure is equal to zero, $p(x = \pm L/2) = 0$. Equation (3.7) with $x = \pm L/2$ gives

$$p\left(x = \pm\frac{L}{2}\right) = q\left(1 + \frac{2M_{RI}}{qL_e^2} \cdot \frac{\sin\frac{L}{L_e} - \sinh\frac{L}{L_e}}{\sin\frac{L}{L_e} + \sinh\frac{L}{L_e}}\right) \tag{3.19}$$

To obtain zero ground pressure at the ends of a structure, the expression within the brackets in Equation (3.19) has to equal zero. That will be the case when the second part within the brackets equals negative one.

In Figure 3.14, the quotient $2M_{RI}/qL_e^2$ in Equation (3.19) is drawn as a function of the length to elastic length ratio resulting in zero ground pressure at the ends of structures. From the diagram, it can be determined whether or not the ends of a structure lift. Values of $2M_{RI}/qL_e^2$ above the drawn line result in lifting of the ends and values of $2M_{RI}/qL_e^2$ below the drawn line result in no lifting.

That is, lifting will occur when

$$\frac{2M_{RI}}{qL_e^2} > -\frac{\sin\frac{L}{L_e} + \sinh\frac{L}{L_e}}{\sin\frac{L}{L_e} - \sinh\frac{L}{L_e}} \tag{3.20}$$

and not when

$$\frac{2M_{RI}}{qL_e^2} \le -\frac{\sin\frac{L}{L_e} + \sinh\frac{L}{L_e}}{\sin\frac{L}{L_e} - \sinh\frac{L}{L_e}} \tag{3.21}$$

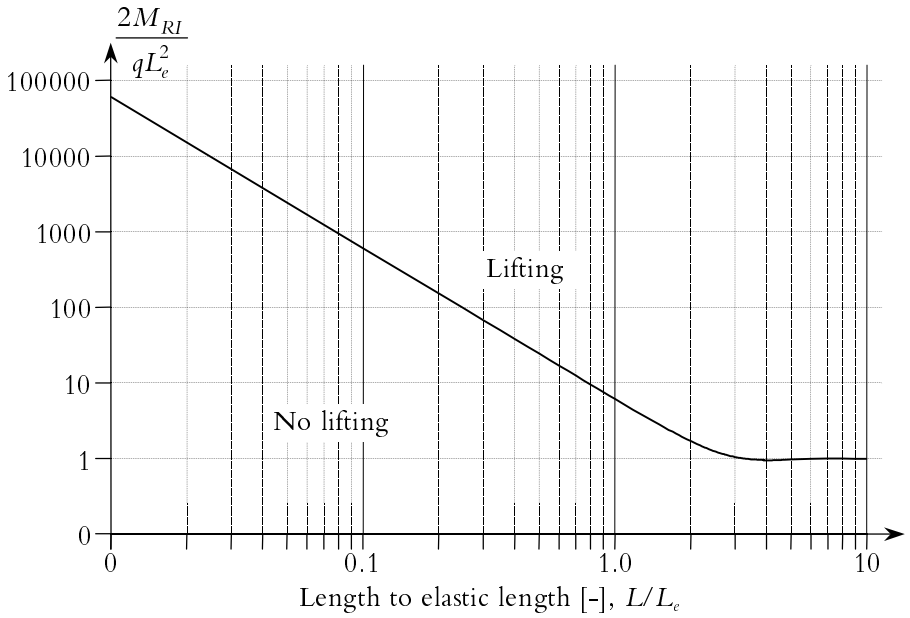

Figure 3.14 *Determination of lifting or not of ends of structures as function of the length to elastic length ratio and the ratio of* $2M_{RI}$ *and* qL_e^2.

As in the previous cases, the structures are bent by the two equals and opposite equivalent bending moments of internal loading M_{RI} tending to rotate the whole structure. The arisen free spaces will be extended a distance δL from the ends towards the centre, implying the length of the intermediate parts of the structures that still are resting on the ground being $L_\delta = L(1-2\delta)$, see Figure 3.15.

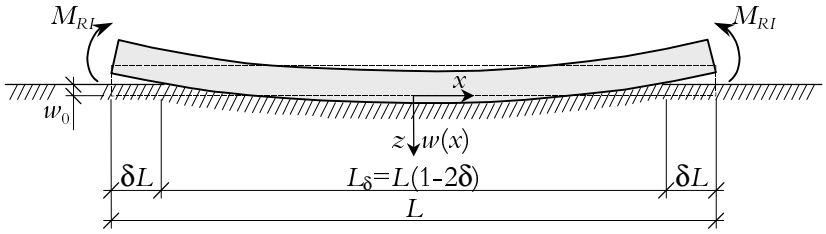

Figure 3.15 *Relatively long structures and/or structures founded on stiff elastic materials imply lifting of the ends of the structures.*

The rotational boundary restraint coefficient for the situation with lifting ends can be solved by combining two cases. The first case, $x = \pm L_\delta/2$, is for structures founded on elastic materials loaded by equal and opposite bending moments and equal vertical forces at the ends of the structures, see Appendix C Section C.3. The second case is for structures founded on rock or very stiff materials, Section 3.2.4, and yields for $L_\delta/2 \le |x| \le L/2$.

The bending moment corresponding to the deflection along the beam, $M_{RO}(x)$, is separated into two parts, one for the intermediate parts, $|x| = L_\delta/2$, and one for the outer parts, $L_\delta/2 \le |x| \le L/2$.

$$M_{RO}(x) = \begin{cases} M_{RO,1}(x) & |x| \le \dfrac{L_\delta}{2} \\ M_{RO,2}(x) & \dfrac{L_\delta}{2} \le |x| \le \dfrac{L}{2} \end{cases} \tag{3.22}$$

For the intermediate parts of a structure resting on the ground, $|x| = L_\delta/2$, the bending moment along the structure is determined according to Appendix C Equation (C.36). In this case, the equivalent bending moments and vertical forces at the ends of the structure equal the bending moments and vertical forces originating from two cantilever beams at the ends of the beam, see Figure 3.16,

$$M_\delta = M_{RI} - \frac{q(\delta L)^2}{2} \tag{3.23}$$

$$V_\delta = q(\delta L) \tag{3.24}$$

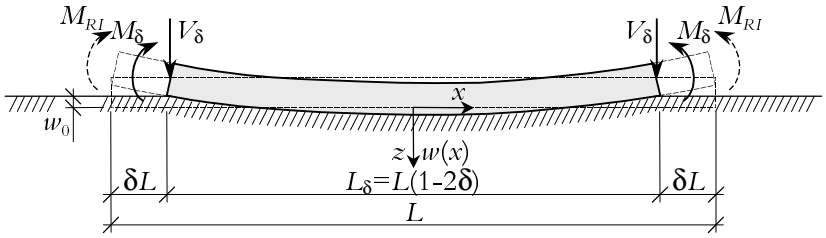

Figure 3.16 *Prismatic beam of finite length on elastic foundation loaded by two equal and opposite bending moments and two vertical forces at its ends.*

The bending moment corresponding to the rotation is

$$M_{RO,1}(x) = -\frac{2V_\delta L_e}{\sin\frac{L_\delta}{L_e}+\sinh\frac{L_\delta}{L_e}}\left(\sin\frac{L_\delta}{2L_e}\sinh\frac{L_\delta}{2L_e}\cos\frac{x}{L_e}\cosh\frac{x}{L_e}-\right.$$
$$\left.-\cos\frac{L_\delta}{2L_e}\cosh\frac{L_\delta}{2L_e}\sin\frac{x}{L_e}\sinh\frac{x}{L_e}\right)+\frac{2M_\delta}{\sin\frac{L_\delta}{L_e}+\sinh\frac{L_\delta}{L_e}}\cdot$$
$$\cdot\left\{\left(\cos\frac{L_\delta}{2L_e}\sinh\frac{L_\delta}{2L_e}+\sin\frac{L_\delta}{2L_e}\cosh\frac{L_\delta}{2L_e}\right)\cos\frac{x}{L_e}\cosh\frac{x}{L_e}-\right.$$
$$\left.-\left(\cos\frac{L_\delta}{2L_e}\sinh\frac{L_\delta}{2L_e}-\sin\frac{L_\delta}{2L_e}\cosh\frac{L_\delta}{2L_e}\right)\sin\frac{x}{L_e}\sinh\frac{x}{L_e}\right\} \tag{3.25}$$

where in these cases κ is determined with W/L_δ when determining the elastic length in Equation (3.6).

For the outer parts of the structure, $L_\delta/2 \le |x| \le L/2$, the outer bending moment corresponding to the deflection, $M_{RO,2}(x)$, is, see Equation (3.17)

$$M_{RO,2}(x) = M_{RI} - \frac{q}{2}\left(x-\frac{L}{2}\right)^2 \tag{3.26}$$

The rotational boundary restraint $\gamma_{RR}(x)$ along the beam is determined as

$$\gamma_{RR}(x) = \begin{cases} \gamma_{RR,1}(x) = 1-\dfrac{M_{RO,1}(x)}{M_{RI}} & |x| \le \dfrac{L_\delta}{2} \\ \gamma_{RR,2}(x) = 1-\dfrac{M_{RO,2}(x)}{M_{RI}} & \dfrac{L_\delta}{2} \le |x| \le \dfrac{L}{2} \end{cases} \tag{3.27}$$

with $M_{RO,1}(x)$ and $M_{RO,2}(x)$ according to Equations (3.25) and (3.26), respectively.

For the intermediate parts of a structure with lifting ends, $|x| = L_\delta/2$, the rotational boundary restraint coefficient along the structure, $\gamma_{RR,1}(x)$, is

$$\gamma_{RR,1}(x) = 1 - \left\{ \frac{2M_\delta}{M_{RI}\left(\sin\frac{L_\delta}{L_e} + \sinh\frac{L_\delta}{L_e} \right)} \cdot \right.$$
$$\cdot \left(\left(\cos\frac{L_\delta}{2L_e}\sinh\frac{L_\delta}{2L_e} + \sin\frac{L_\delta}{2L_e}\cosh\frac{L_\delta}{2L_e} \right)\cos\frac{x}{L_e}\cosh\frac{x}{L_e} - \right.$$
$$\left. - \left(\cos\frac{L_\delta}{2L_e}\sinh\frac{L_\delta}{2L_e} - \sin\frac{L_\delta}{2L_e}\cosh\frac{L_\delta}{2L_e} \right)\sin\frac{x}{L_e}\sinh\frac{x}{L_e} \right) - \qquad (3.28)$$
$$- \frac{2V_\delta L_e}{M_{RI}\left(\sin\frac{L_\delta}{L_e} + \sinh\frac{L_\delta}{L_e} \right)} \left(\sin\frac{L_\delta}{2L_e}\sinh\frac{L_\delta}{2L_e}\cos\frac{x}{L_e}\cosh\frac{x}{L_e} - \right.$$
$$\left. \left. - \cos\frac{L_\delta}{2L_e}\cosh\frac{L_\delta}{2L_e}\sin\frac{x}{L_e}\sinh\frac{x}{L_e} \right) \right.$$

For the outer parts of a structure with lifting ends, $L_\delta/2 \le |x| \le L/2$, the rotational boundary restraint coefficient along the structure, $\gamma_{RR,2}(x)$, is

$$\gamma_{RR,2}(x) = 1 - \frac{M_{RI} - \frac{q}{2}\left(x - \frac{L}{2} \right)^2}{M_{RI}} = \frac{q}{2M_{RI}}\left(x - \frac{L}{2} \right)^2 \qquad (3.29)$$

In the midsection of the structure, $x = 0$ in Equation (3.28), the rotational boundary restraint is

$$\gamma_{RR,1}(x = 0) = 1 - \frac{2}{M_{RI}\left(\sin\frac{L_\delta}{L_e} + \sinh\frac{L_\delta}{L_e} \right)} \cdot$$
$$\cdot \left\{ M_\delta \left(\cos\frac{L_\delta}{2L_e}\sinh\frac{L_\delta}{2L_e} + \sin\frac{L_\delta}{2L_e}\cosh\frac{L_\delta}{2L_e} \right) - V_\delta L_e \sin\frac{L_\delta}{2L_e}\sinh\frac{L_\delta}{2L_e} \right\} \qquad (3.30)$$

Equation (3.30) is very similar to Equation (3.11) except for the M_δ/M_{RI} ratio and the part depending on the moment of the equivalent vertical force and the elastic length in relation to the bending moment of internal loading, $V_\delta L_e/M_{RI}$.

By introducing

$$K_1 = \frac{2}{\left(\sin\frac{L_\delta}{L_e} + \sinh\frac{L_\delta}{L_e}\right)} \cdot \cdot \left\{ \left(\cos\frac{L_\delta}{2L_e}\sinh\frac{L_\delta}{2L_e} + \sin\frac{L_\delta}{2L_e}\cosh\frac{L_\delta}{2L_e} \right)\cos\frac{x}{L_e}\cosh\frac{x}{L_e} - \right. \\ \left. - \left(\cos\frac{L_\delta}{2L_e}\sinh\frac{L_\delta}{2L_e} - \sin\frac{L_\delta}{2L_e}\cosh\frac{L_\delta}{2L_e} \right)\sin\frac{x}{L_e}\sinh\frac{x}{L_e} \right\} \tag{3.31}$$

and

$$K_2 = \frac{2}{\left(\sin\frac{L_\delta}{L_e} + \sinh\frac{L_\delta}{L_e}\right)} \left\{ \sin\frac{L_\delta}{2L_e}\sinh\frac{L_\delta}{2L_e}\cos\frac{x}{L_e}\cosh\frac{x}{L_e} - \right. \\ \left. - \cos\frac{L_\delta}{2L_e}\cosh\frac{L_\delta}{2L_e}\sin\frac{x}{L_e}\sin\frac{x}{L_e} \right\} \tag{3.32}$$

Equation (3.28) can be simplified to

$$\gamma_{RR,1}(x) = 1 - K_1 + \frac{V_\delta}{M_{RI}}\left(\frac{(\delta L)}{2} K_1 - L_e K_2 \right) \tag{3.33}$$

The variation of K_1 and K_2 are depicted in Figure 3.17 as functions of the length to elastic length ratio and for $x = 0$, $\pm 0.1L$, $\pm 0.2L$, $\pm 0.3L$ and $\pm 0.4L$. For various values of the length to elastic length ratio, the restraint in the midsection of a structure can be determined. Equation (3.33) can be used for all cases, both when the ends of a structure are lifting and when they are not. For the case of no lifting, δ equals zero and Equation (3.33) simplifies and equals Equation (3.11).

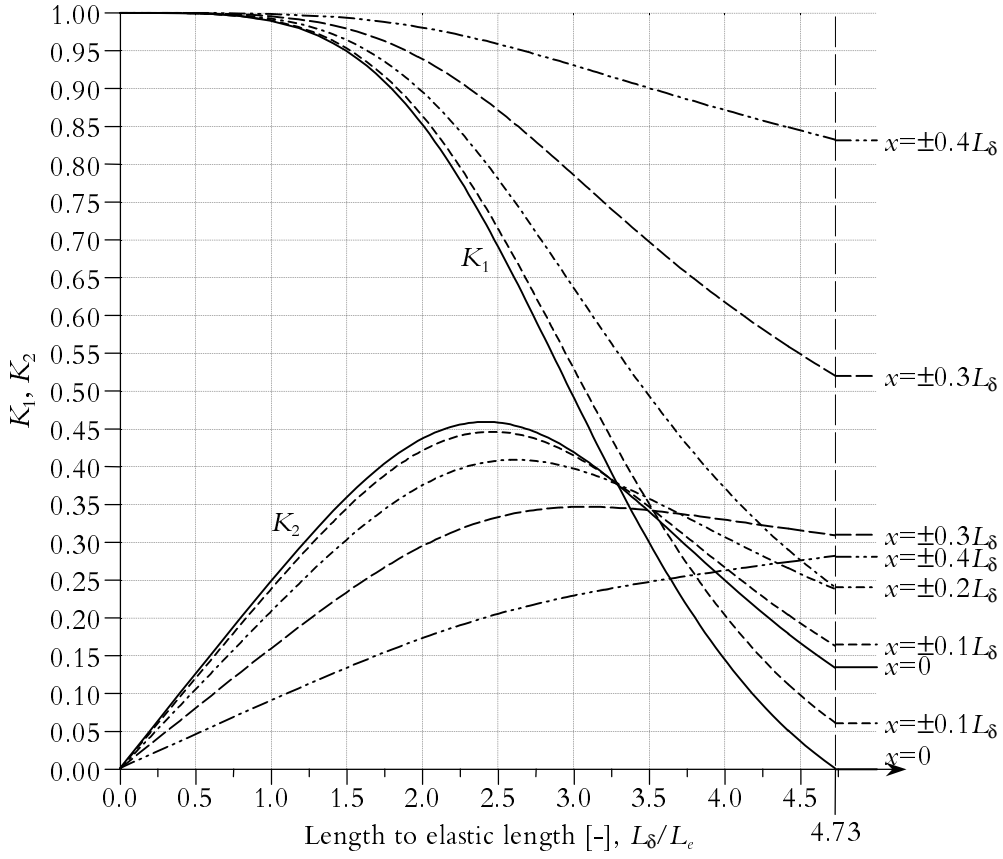

Figure 3.17 *Simplification coefficients K_1 and K_2 as functions of the length to elastic length ratio for the determination of the rotational boundary restraint coefficient in structures which ends are lifting, Equation (3.33).*

3.2.6 Example 2: Lifting ends of a structure

Again, Example 1 in Section 3.2.2 and Figure 3.5 will be considered. The rotational boundary restraint coefficient along the structure should be determined. In this case, the structure is founded on medium dense sand and medium dense gravel with modulus of compression K_j = 25000kN/m^2 and K_j = 60000kN/m^2, respectively. The modulus of elasticity at 28days is equal in both parts, that is $E_{28a} = E_{28y}$ = 30000MPa, but the analysis is performed when $E_y = 0.75E_{28y}$ = 22500MPa. Further, the temperature change in the old parts as well as the shrinkage in the whole structure is assumed to be zero.

Step 1: determination of whether the ends of the structure lift or not.

In the previous calculations, it was only stated that for K_j = 25000kN/m^2 and L = 20 and 40m, the ends of the structures will lift. Therefore, these cases will be re-calculated with the models for lifting ends. Figure 3.14 and Equation (3.20) will be used.

The dead weight of the structure, Equation (3.16),

$$q(x) = \rho g A_{tot} = 24000 \cdot (3 \cdot 1 + 0.5 \cdot 3) = 108000 \text{ N/m}$$

The moment of internal loading, Equation (3.3),

$$M_{RI} = E_y \alpha_c \Delta T (z'_{cen} - z'_y) A_y =$$

$$0.75 \cdot 30000 \cdot 10^6 \cdot 1 \cdot 10^{-5} \cdot (-20) \cdot \left(1.045 - \left(1 + \frac{3}{2} \right) \right) \cdot 0.5 \cdot 3 = 9.82 \text{ MNm}$$

The shape factor κ, Table 3.2, the elastic length, Equation (3.6), and the length to elastic length ratio is calculated, giving the result

L [m]	K_j = 25000kN/m^2 κ [-]	L_e [m]	L/L_e [-]	K_j = 60000kN/m^2 κ [-]	L_e [m]	L/L_e [-]
5	0.749	9.379	0.533	0.749	7.535	0.664
10	0.881	9.768	1.024	0.881	7.848	1.274
20	0.972	10.010	1.998	0.972	8.043	2.487
40	1.025	10.143	3.944	1.025	8.149	4.909

Further, by calculation of both the left and right hand sides of Equation (3.20), it is determined whether the ends of the structure will lift or not, giving

L [m]	K_j = 25000kN/m^2 $\frac{2M_{RI}}{qL_e^2}$	Equ. (3.20)	Lifting	K_j = 60000kN/m^2 $\frac{2M_{RI}}{qL_e^2}$	Equ. (3.20)	Lifting
5	2.067	21.124	no	3.202	13.647	no
10	1.905	5.770	no	2.952	3.765	no
20	1.814	1.672	yes	2.811	1.227	yes
40	1.767	0.946	yes	2.738	0.971	yes

Step 2: finding the lengths, L_δ, of the structures implying no lifting.

By iteration, the length of the structure can be found, that is, the location where the ground pressure equals zero at the ends of the structure. The iteration are performed due to the fact that when changing the length of the structure resting on the ground, the shape factor κ changes and therefore the elastic length also changes.

For the actual example, the following lengths L_δ, elastic lengths L_e and length to elastic length ratios L_δ/L_e of the structure are found after the iteration. The given results imply the ground pressure being zero at the ends of the structures, $p(x=\pm L_\delta/2) = 0$.

L [m]	K_j = 25000kN/m²			K_j = 60000kN/m²		
	L_δ	L_e	L_δ/L_e	L_δ	L_e	L_δ/L_e
20	19.455	10.003	1.945	14.870	7.973	1.865
40	32.703	10.113	3.234	28.536	8.105	3.521

Step 3: calculation of the rotational boundary restraint along the structure.

The rotational boundary restraint along the structure is now found by Equation (3.29) for the outer parts, $L_\delta/2 \le |x| \le L/2$, and either by Equation (3.30) or Equation (3.33) together with Figure 3.17 for the intermediate parts, $|x| \le L_\delta/2$. The results are presented in Figure 3.18, where the small vertical lines at the ends of the curves indicate where the ends of the structures start to lift.

By comparing the correct rotational boundary restraint coefficients obtained here with the wrong values in Example 1, for K_j = 25000kN/m² and L = 40m, the values are lower. It can be seen that in the midspan of the structure, the rotational boundary restraint is about 78 % when taking the lifting into account and about 84 % when not.

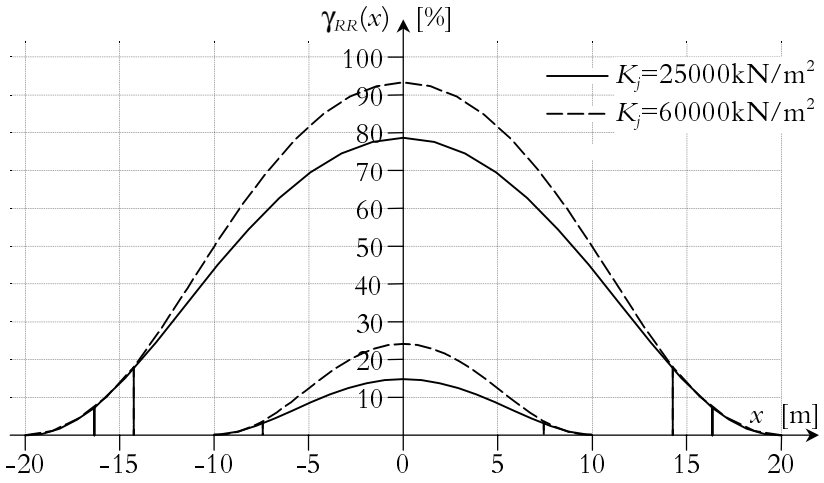

Figure 3.18 *The rotational boundary restraint coefficient along the structure in example 2. The vertical lines indicate when the ground pressure equal zero, i.e. the outer parts are lifting.*

3.2.7 Comments

The determination of the rotational boundary restraint coefficient as stated above is a quite straightforward method and rather simple by use of the application tools. For structures with no lifting ends, see Figure 3.4 and Equation (3.10), whereas for structure with lifting ends, see Figure 3.17 together with Equation (3.33).

In the two examples presented, it was shown that with increasing lengths and with increasing modulus of compression of the foundation materials, the rotational boundary restraint coefficient also increases.

From Example 1, a general three-dimensional presentation of the rotational boundary restraint coefficient can be drawn for any case as function of the length to elastic length ratio and the distance from the midsection of the structure, see Figure 3.19. In the figure it can be seen that the higher length to elastic length ratio in combination with the proximity to the midsection of the structure, the higher the rotational restraint coefficient.

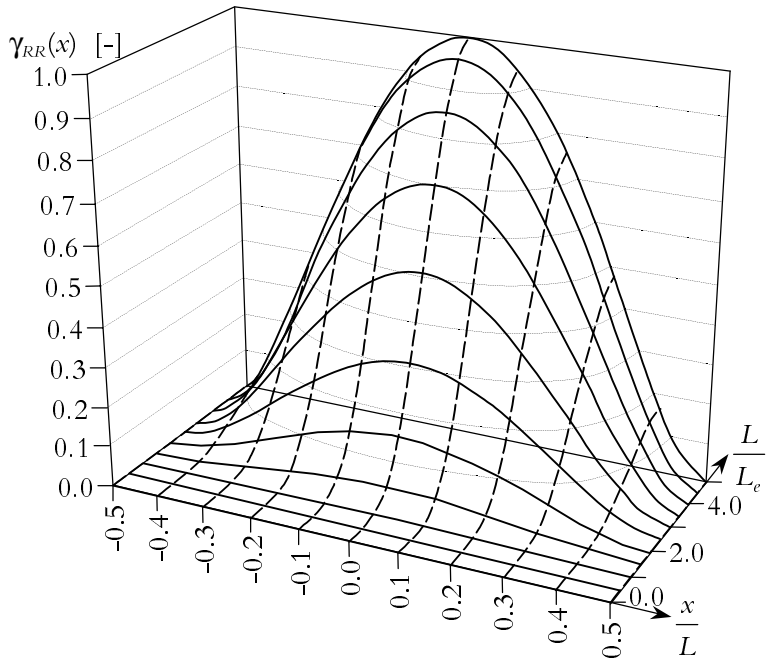

Figure 3.19 *Three-dimensional presentation of the rotational boundary restraint coefficient, $\gamma_{RR}(x)$, as function of the length to elastic length ratio, L/L_e, and the distance from the midsection of the structure, x.*

3.3 Translational Boundary Restraint

Models for the determination of the translational boundary restraint coefficient, $\gamma_{RT}(x,t)$, will not be dealt with in this thesis. However, in Pettersson (1996, 1998) and Rostásy et al. (1999), several models are presented for various situations. Among other things, methods are given for the determination of translational boundary restrain for structures founded on friction materials or cohesive soils, and that slide along parts of or the whole lengths of the base slabs.

For rather short structures founded on non-cohesive materials, the translational boundary restraint is low, and in such situations, $\gamma_{RT}(x,t) \approx 0$ might be a good approximation.

3.4 Structural Restraint Coefficient

3.4.1 Plane-section analysis

For structures with length to height ratios equal to or larger than about five, equations for plane-section restraint coefficient can be derived. In the following,

a young structural member (subscript *y*) cast on an older one (subscript *a*) is studied. The present derivation of plane-section restraint coefficients is based on formulas for prestressed concrete beams, Collins & Mitchell (1991), and a proposed method for calculation of crack widths due to thermal stresses, JCI (1992). Plane sections are assumed remaining plane implying the strains over the height of the structures vary linearly, see Figure 3.21. The application of the formulas, diagrams and expressions is primarily adapted for simple engineering models, as in Larson (2000), and are at the present not adjusted for linear-line or compensation-line calculations. Further, no slip failure between the members is assumed. For the case of slip failure in casting joints, see Section 3.7.

Under the assumption of plane sections remaining plane, the restraint coefficient is in the following being referred to as plane-section restraint coefficient, γ^0_R. The plane-section restraint coefficient in a point in a young concrete part is generally defined as the ratio between actual stresses in the point σ_1 and stresses at fixation ($\varepsilon \equiv 0$) of the volume changes of the young concrete, $-\Delta\varepsilon_y^0 \zeta E_{28y}$, (shrinkage strains and thermal strains). That is

$$\gamma_R^0 = \frac{\sigma_1}{-\Delta\varepsilon_y^0 \zeta E_{28y}} \tag{3.34}$$

The actual stresses in the point is found as

$$\sigma_1 = \zeta E_{28y}(-\Delta\varepsilon_y^0 + \varepsilon_{cen}^0 + \varepsilon_\varphi^0) \tag{3.35}$$

where ε^0_{cen} is the translational strains, ε^0_φ is the rotational strains and $\Delta\varepsilon^0_y$ is the strains due to volume changes, which according to Equation (3.34) give

$$\gamma_R^0 = \frac{-\Delta\varepsilon_y^0 + \varepsilon_{cen}^0 + \varepsilon_\varphi^0}{-\Delta\varepsilon_y^0} \tag{3.36}$$

The plane-section restraint coefficient can be separated in one translational part γ_R^{0T}, and one rotational part $\gamma_R^{0\varphi}$, that is

$$\gamma_R^0 = \frac{\Delta\varepsilon_y^0}{\Delta\varepsilon_y^0} - \frac{\varepsilon_{cen}^0}{\Delta\varepsilon_y^0} - \frac{\varepsilon_\varphi^0}{\Delta\varepsilon_y^0} = 1 - \gamma_R^{0T} - \gamma_R^{0\varphi} \tag{3.37}$$

Depending on the restraint from adjacent materials, e.g. elastic foundations, the translational and rotational plane-section restraint coefficients will vary. If the adjoining material does not give any resistance to the translation and rotation of a studied structure, $\gamma_{RT}(x) = 0$ and $\gamma_{RR}(x) = 0$, the translation and rotation equal the free translation and rotation, $\varepsilon_{cen} = \varepsilon^0_{cen}$ and $\varphi = \varphi^0$ respectively. If,

on the contrary, the adjoining material fully restrains the translation and/or the rotation, $\gamma_{RT}(x) = 1$ and/or $\gamma_{RR}(x) = 1$, the translation and/or the rotation are zero. For intermediate boundary restraint from the adjoining material, the translation and the rotation vary between zero and the actual free deformation for the combined section, see Figure 3.20 and Sections 3.2 and 3.3 for the determination of $\gamma_{RR}(x)$ and $\gamma_{RT}(x)$, respectively.

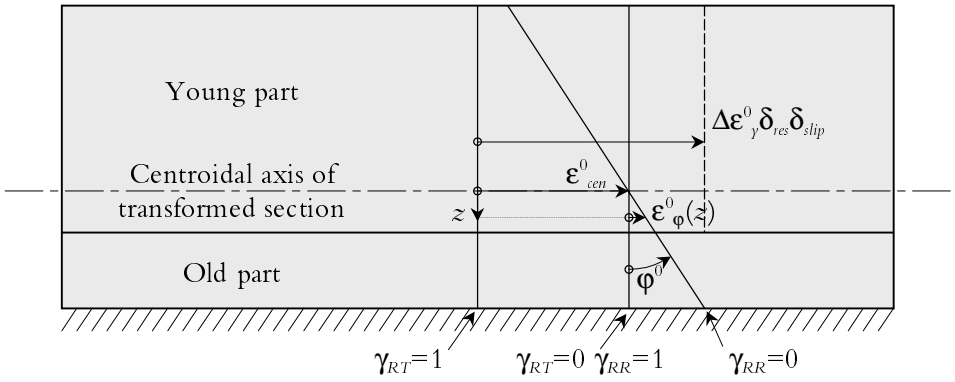

Figure 3.20 *Principal description of plane-section translation and rotation.*

The intermediate restraint situation according to a plane-section analysis is described by

$$\gamma_R^0 = 1 - \gamma_R^{0T}(1 - \gamma_{RT}(x)) - \gamma_R^{0\varphi}(1 - \gamma_{RR}(x)) \tag{3.38}$$

3.4.2 Non plane-section analysis

For non-plane sections (typically length to height ratios below five), the basic approach of plane-section can be maintained in the following three steps:

1. Effect of volume changes in the young concrete structure with the assumption of zero deformation in the adjoining structure; see subfigure a) in Figure 3.21.
2. Formal pure translation of the whole structural section, reflected by the translation at the joint, see Figure 3.21b).
3. Formal pure rotation for the whole structural section, reflected by the rotation at the joint, see Figure 3.21c).

Note that the non-plane-section behaviour without slip in this approach is concentrated to the resilience function δ_{res} in step 1, and that plane-section behaviour corresponds to $\delta_{res} \equiv 1$.

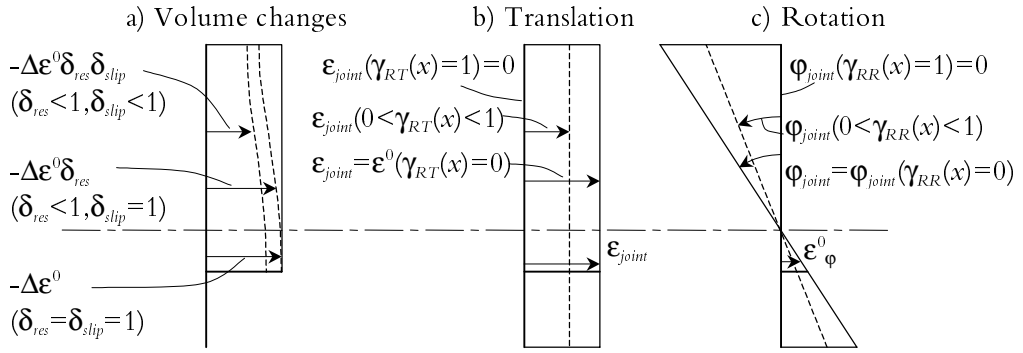

Figure 3.21 *Strains due to volume changes, $-\Delta\varepsilon^0\delta_{res}\delta_{slip}$, normal strains, ε_{joint}, and rotational strains, ε_{φ}, for different amounts of translational and rotational boundary restraint conditions, respectively.*

In Figure 3.21, the variation of the strains due to volume changes, the normal strain and the rotational strains are depicted with resilience factor and the slip failure factor and the translational and rotational boundary restraint conditions from adjoining materials. The strain due to volume is defined as

$$\Delta\varepsilon^0 = \begin{cases} \Delta\varepsilon^0 & \delta_{res} = \delta_{slip} = 1 \\ \Delta\varepsilon^0\delta_{res} & \delta_{res} \le 1, \delta_{slip} = 1 \\ \Delta\varepsilon^0\delta_{slip} & \delta_{res} = 1, \delta_{slip} \le 1 \\ \Delta\varepsilon^0\delta_{res}\delta_{slip} & \delta_{res} \le 1, \delta_{slip} \le 1 \end{cases} \tag{3.39}$$

the translational strain is defined as

$$\varepsilon_{joint} = \begin{cases} \varepsilon_{joint} & \gamma_{RT}(x) = 0 \\ \varepsilon_{joint}(1-\gamma_{RT}(x)) & 0 < \gamma_{RT}(x) < 1 \\ 0 & \gamma_{RT}(x) = 1 \end{cases} \tag{3.40}$$

the rotation as

$$\varphi_{joint} = \begin{cases} \varphi_{joint} & \gamma_{RR}(x) = 0 \\ \varphi_{joint}(1-\gamma_{RR}(x)) & 0 < \gamma_{RR}(x) < 1 \\ 0 & \gamma_{RR}(x) = 1 \end{cases} \tag{3.41}$$

and the rotational strain as

$$\varepsilon_{\varphi} = \begin{cases} \varphi_{joint} z_d & \gamma_{RR} = 0 \\ \varphi_{joint} z_d (1 - \gamma_{RR}) & 0 < \gamma_{RR} < 1 \\ 0 & \gamma_{RR} = 1 \end{cases} \tag{3.42}$$

where z_d is the distance from the centroidal axis of the transformed section to the studied point.

The restraint coefficient for a non-plane-section analysis is now formulated by

$$\gamma_R = \frac{-\Delta\varepsilon_{\gamma}^{0} \delta_{res} \delta_{slip} + \varepsilon_{joint}(1 - \gamma_{RT}(x)) + \varepsilon_{\varphi}(1 - \gamma_{RR}(x))}{-\Delta\varepsilon_{\gamma}^{0}} \tag{3.43}$$

3.4.3 Effective width of adjoining parts

In many cases, the whole area of an adjoining part, A_a, does not influence the deformation of a structure. Instead only a part of the area is effective, implying the introduction of an effective area, $A_{a,eff}$.

The purpose of introducing the effective area of the adjoining part belongs to the curvature of the old part. The derived equations for the restraint coefficients shall result in the same curvature, here chosen at the bottom of the young part, as in reality (or shown to be in finite element (FE) 3-dimensional calculations). The method of using effective area, or rather widths, is further explained and exemplified in Section 3.6.1 below.

3.4.4 Effects of the location of the young parts in relation to adjoining parts

Young parts of a structure are not always placed symmetrically on old and adjoining parts. In these cases with unsymmetrically located young parts, the effect of the adjoining part on the deformation of structures can be different from the effects in symmetrical cases. For this purpose, a factor ω is used to describe the location of the young part on the adjoining part.

For the special case of a rectangular wall cast on a rectangular slab, the location factor ω is determined as

$$\omega = \frac{2u}{W_a - W_{\gamma}} \qquad -1 \le \omega \le 1 \tag{3.44}$$

where u is the distance from the symmetrical location of a young part on an adjoining part to a unsymmetrical location, Figure 3.22. In the figure, three

different locations for a wall on a slab are shown. When the wall is located at the centre of the slab, the location coefficient $\omega = 0$, when it is located at the edges of the slab $\omega = \pm 1$ and for intermediate locations $-1 < \omega < 1$. The effects of unsymmetrical walls cast on slabs are in Section 3.6.2 shown through some examples.

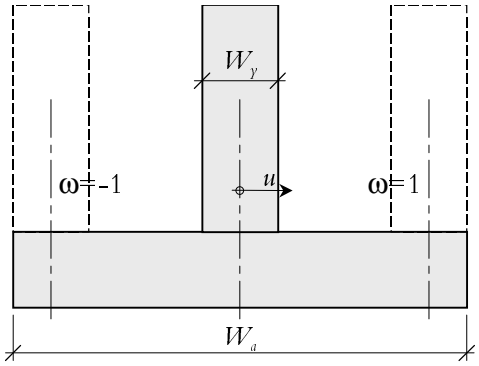

Figure 3.22 *Description of the location of a young part of a structure relative the adjoining and older part.*

3.5 Plane-Section Analysis

3.5.1 Translational restraint

The axial strain is determined from the requirement of translational equilibrium in the section. The integral of stresses over the area of the young part and the effective area of the adjoining part, expressing equilibrium of normal force and flexural moment, implies

$$\int_{A_y} \sigma_y dA_y + \int_{A_{a,eff}} \sigma_a dA_{a,eff} = 0$$

$$\int_{A_y} \zeta E_{28y} (\varepsilon^0_{cen} - \Delta\varepsilon^0_y) dA_y + \int_{A_{a,eff}} E_{28a} (\varepsilon^0_{cen} - \Delta\varepsilon^0_a) dA_{a,eff} = 0$$

The imposed volume changes in the adjoining concrete are expressed as a factor λ times the imposed volume changes in the young concrete, $\Delta\varepsilon_a^{\,0} = \lambda\Delta\varepsilon_y^{\,0}$, giving

$$\int_{A_y} \zeta E_{28y} (\varepsilon^0_{cen} - \Delta\varepsilon^0_y) dA_y + \int_{A_{a,eff}} E_{28a} (\varepsilon^0_{cen} - \lambda\Delta\varepsilon^0_y) dA_{a,eff} = 0$$

Collection of terms

$$\zeta E_{28\gamma}\varepsilon^0_{cen}\left(\int_{A_\gamma} dA_\gamma + \frac{E_{28a}}{\zeta E_{28\gamma}}\int_{A_{a,eff}} dA_{a,eff}\right) - \\ -\Delta\varepsilon^0_\gamma\left(\int_{A_\gamma}\zeta E_{28\gamma}dA_\gamma + \int_{A_{a,eff}} E_{28a}\lambda dA_{a,eff}\right) = 0$$

where from the axial strain is solved

$$\varepsilon^0_{cen} = \frac{N_{RI}}{\zeta E_{28\gamma}A_{trans}} \tag{3.45}$$

A_{trans} is the transformed area

$$A_{trans} = \int_{A_\gamma} dA_\gamma + \frac{E_{28a}}{\zeta E_{28\gamma}}\int_{A_{a,eff}} dA_{a,eff} \tag{3.46}$$

and N_{RI} is the force required to produce zero strain in the concrete

$$N_{RI} = \Delta\varepsilon^0_\gamma\left(\int_{A_\gamma}\zeta E_{28\gamma}dA_\gamma + \int_{A_{a,eff}} E_{28a}\lambda dA_{a,eff}\right) \tag{3.47}$$

The translational part of the plane-section restraint coefficient is then found from Equation (3.37) through Equations (3.40), (3.45) and (3.47) put together

$$\gamma^{0T}_R(x) = \frac{\int_{A_\gamma}\zeta E_{28\gamma}dA_\gamma + E_{28a}\int_{A_{a,eff}}\lambda dA_{a,eff}}{\zeta E_{28\gamma}A_{trans}}(1-\gamma_{RT}(x)) \tag{3.48}$$

where the translational boundary restraint is taken into account.

3.5.2 Rotational restraint

The rotational strain is determined from the requirement of rotational bending equilibrium in the section. The integral of the stresses times the distance from the centroidal axis over the area of the young part and the effective area of the adjoining part imply

$$\int_{A_\gamma}\zeta E_{28\gamma}(\varphi^0 z - \Delta\varepsilon^0_\gamma)zdA_\gamma + \int_{A_{a,eff}} E_{28a}(\varphi^0 z - \lambda\Delta\varepsilon^0_\gamma)zdA_{a,eff} = 0$$

where, once again, the volume changes of the adjoining structure are expressed in relation to the volume changes of the young part.

Collection of terms gives

$$\zeta E_{28\gamma}\varphi^0\left(\int_{A_\gamma} z^2 dA_\gamma + \frac{E_{28a}}{\zeta E_{28\gamma}}\int_{A_{a,eff}} z^2 dA_{a,eff}\right) - \\ -\Delta\varepsilon_\gamma^0\left(\int_{A_\gamma}\zeta E_{28\gamma} z dA_\gamma + \int_{A_{a,eff}} E_{28a}\lambda z dA_{a,eff}\right) = 0$$

from here the rotation is solved

$$\varphi^0 = \frac{M_{RI}}{\zeta E_{28\gamma} I_{trans}} \tag{3.49}$$

I_{trans} is the transformed moment of inertia

$$I_{trans} = \int_{A_\gamma} z^2 dA_\gamma + \frac{E_{28a}}{\zeta E_{28\gamma}}\int_{A_{a,eff}} z^2 dA_{a,eff} \tag{3.50}$$

and M_{RI} is the moment required to produce zero strain in the concrete, that is, the bending moment of internal loading

$$M_{RI} = \Delta\varepsilon_\gamma^0\left(\int_{A_\gamma}\zeta E_{28\gamma} z dA_\gamma + \int_{A_{a,eff}} E_{28a}\lambda z dA_{a,eff}\right) \tag{3.51}$$

The rotational part of the plane-section restraint coefficient is then deduced from Equation (3.37) with Equations (3.42), (3.49) and (3.51)

$$\gamma_R^{0\varphi}(x, z_d) = \frac{\int_{A_\gamma}\zeta E_{28\gamma} z dA_\gamma + \int_{A_{a,eff}} E_{28a}\lambda z dA_{a,eff}}{\zeta E_{28\gamma} I_{trans}} z_d (1 - \gamma_{RR}(x)) \tag{3.52}$$

where the rotational boundary restraint is taken into account.

3.5.3 Application tools for rectangular geometries

For simple situations, application tools can be derived for the plane-section restraint coefficient in the young concrete parts in terms of the translational and the rotational boundary restraint conditions. Both the young and the old concrete parts here are assumed being rectangular shaped. The modulus of elasticity is presumed to be equal over the area of the young part and of the old one, respectively, see Figure 3.23.

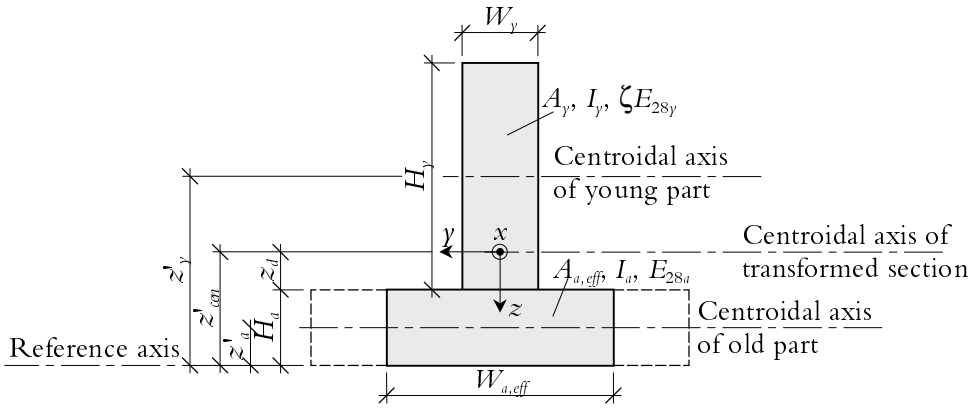

Figure 3.23 *Section properties of a structure built by a young concrete part cast on an older one assuming rectangular shapes and equal properties over the areas of each part.*

Assuming the temperature within the young part is equal over the whole area, theoretically, the maximum restraint is located at the bottom of the young part. However, in reality the temperature varies over a cross-section. The adjoining and older, and thereby colder part, chill the lower parts of the young member, implying the effect of the temperature change and the restraint on the stresses being moved upwards. A good assumption is that the location of the maximum restraint is somewhere between a half and one wall-thickness above the joint, say three quarters of the wall-thickness, $0.75W_y$.

In some cases, the adjoining parts are heated before the casting of the young parts as a measure to avoid thermal cracking, see Wallin et al (1997). If so, the chilling of the lower parts of the young members is considerably reduced, wherefore the location of the maximum restraint may be located closer to the joint.

Below, equations for the plane-section translational and rotational restraint coefficients will be presented for when the maximum restraint is located at the joint and at $0.75W_y$ above the joint. For general purposes, also the variation of restraint for any distance above the joint is presented.

Transformed section properties

For the derivation of the plane-section restraint coefficients for rectangular geometries, transformed section properties are needed if the modulus of elasticity differs between the parts of a structure. Under the stated assumptions, the transformed section properties (according to above) will be as follows if the modulus of elasticity of the young part is chosen as reference. The area of the transformed section is

$$A_{trans} = A_\gamma \left(1 + \frac{E_{28a}}{\zeta E_{28\gamma}} \frac{A_{a,eff}}{A_\gamma} \right) \tag{3.53}$$

The centroid of the transformed section, from a reference axis at the bottom of the structure as depicted in Figure 3.23,

$$z'_{cen} = \frac{z'_\gamma + \frac{E_{28a}}{\zeta E_{28\gamma}} \frac{A_{a,eff}}{A_\gamma} z'_a}{1 + \frac{E_{28a}}{\zeta E_{28\gamma}} \frac{A_{a,eff}}{A_\gamma}} \tag{3.54}$$

The moment of inertia of the transformed section

$$I_{trans} = I_{0\gamma} + A_\gamma (z'_{cen} - z'_\gamma)^2 + \frac{E_{28a}}{\zeta E_{28\gamma}} \left(I_{0a} + A_{a,eff} (z'_{cen} - z'_a)^2 \right) \tag{3.55}$$

Equations for plane-section translational and rotational restraints

Under the given conditions, the plane-section translational restraint coefficient is, see Appendix D Equation (D.13)

$$\gamma_R^{0T}(x) = \frac{1 + \frac{E_{28a}}{\zeta E_{28\gamma}} \lambda \frac{A_{a,eff}}{A_\gamma}}{1 + \frac{E_{28a}}{\zeta E_{28\gamma}} \frac{A_{a,eff}}{A_\gamma}} (1 - \gamma_{RT}(x)) \tag{3.56}$$

depending on the ratios between the modulus of elasticity, areas and imposed volume changes of the adjoining and young parts, λ, and on the translational boundary restraint condition from adjoining materials, see Section 3.3.

The plane-section rotational restraint coefficient at the distance z from the centroidal axis of the transformed cross section is, see Appendix D Equation (D.19)

$$\gamma_R^{0\varphi}(x,z) = (1 - \gamma_{RR}(x))(\lambda - 1) z \cdot \frac{\frac{2}{H_\gamma} \frac{E_{28a}}{\zeta E_{28\gamma}} \frac{A_{a,eff}}{A_\gamma} \left(1 + \frac{H_a}{H_\gamma} \right)}{\frac{1}{3} \left(1 + \frac{E_{28a}}{\zeta E_{28\gamma}} \frac{A_{a,eff}}{A_\gamma} \right) \left(1 + \frac{E_{28a}}{\zeta E_{28\gamma}} \frac{A_{a,eff}}{A_\gamma} \left(\frac{H_a}{H_\gamma} \right)^2 \right) + \frac{E_{28a}}{\zeta E_{28\gamma}} \frac{A_{a,eff}}{A_\gamma} \left(1 + \frac{H_a}{H_\gamma} \right)^2} \tag{3.57}$$

The plane-section rotational restraint coefficient at the bottom of the young concrete $z_1 = z'_{cen}$-H_a is, see Appendix D Equation (D.21)

$$\gamma_R^{0\varphi}(x,z_1) = (\lambda-1)(1-\gamma_{RR}(x))\cdot\frac{\dfrac{E_{28a}}{\zeta E_{28\gamma}}\dfrac{A_{a,eff}}{A_\gamma}}{\left(1+\dfrac{E_{28a}}{\zeta E_{28\gamma}}\dfrac{A_{a,eff}}{A_\gamma}\right)}\cdot \\ \cdot\frac{\left(1+\dfrac{H_a}{H_\gamma}\right)\left(1-\dfrac{E_{28a}}{\zeta E_{28\gamma}}\dfrac{A_{a,eff}}{A_\gamma}\dfrac{H_a}{H_\gamma}\right)}{\dfrac{1}{3}\left(1+\dfrac{E_{28a}}{\zeta E_{28\gamma}}\dfrac{A_{a,eff}}{A_\gamma}\right)\left(1+\dfrac{E_{28a}}{\zeta E_{28\gamma}}\dfrac{A_{a,eff}}{A_\gamma}\left(\dfrac{H_a}{H_\gamma}\right)^2\right)+\dfrac{E_{28a}}{\zeta E_{28\gamma}}\dfrac{A_{a,eff}}{A_\gamma}\left(1+\dfrac{H_a}{H_\gamma}\right)^2} \tag{3.58}$$

depending on the ratios between the modulus of elasticity, areas, heights and imposed volume changes of the adjoining and young parts and on the rotational boundary restraint condition from adjoining materials, see Section 3.2.

Further, at a distance three quarters of the width of the wall above the joint between the young and the old parts, the plane-section rotational restraint coefficient is, see Appendix D Equation (D.23),

$$\gamma_R^{0\varphi}(x,z_1) = (1-\gamma_{RR}(x))(\lambda-1)\cdot\frac{\dfrac{E_{28a}}{\zeta E_{28\gamma}}\dfrac{A_{a,eff}}{A_\gamma}}{\left(1+\dfrac{E_{28a}}{\zeta E_{28\gamma}}\dfrac{A_{a,eff}}{A_\gamma}\right)}\cdot \\ \cdot\frac{\left(1+\dfrac{H_a}{H_\gamma}\right)\left(1-\dfrac{E_{28a}}{\zeta E_{28\gamma}}\dfrac{A_{a,eff}}{A_\gamma}\dfrac{H_a}{H_\gamma}-\dfrac{3}{8}\dfrac{W_\gamma}{H_\gamma}\left(1+\dfrac{E_{28a}}{\zeta E_{28\gamma}}\dfrac{A_{a,eff}}{A_\gamma}\right)\right)}{\left(\dfrac{1}{3}\left(1+\dfrac{E_{28a}}{\zeta E_{28\gamma}}\dfrac{A_{a,eff}}{A_\gamma}\right)\left(1+\dfrac{E_{28a}}{\zeta E_{28\gamma}}\dfrac{A_{a,eff}}{A_\gamma}\left(\dfrac{H_a}{H_\gamma}\right)^2\right)+\dfrac{E_{28a}}{\zeta E_{28\gamma}}\dfrac{A_{a,eff}}{A_\gamma}\left(1+\dfrac{H_a}{H_\gamma}\right)^2\right)} \tag{3.59}$$

From Equations (3.56) to (3.59) it can be seen that the plane-section restraint coefficient $\gamma^0{}_R(x) = \gamma^0{}_R(x,\gamma_{RT}(x))$ when $\gamma_{RR}(x) = 1$ (no rotation) and that $\gamma^0{}_R(x) = \gamma^0{}_R(x,\gamma_{RR}(x))$ when $\gamma_{RT}(x) = 1$ (no translation). That is

$$\gamma_R^0(x) = \begin{cases} 1-\gamma_R^\varphi(x) & \text{for } \gamma_{RT}(x)=1 \\ 1-\gamma_R^T(x) & \text{for } \gamma_{RR}(x)=1 \end{cases} \tag{3.60}$$

Diagrams of the plane-section restraint coefficient in representative points in the young parts of concrete structures, in the bottom of the young part and three fourths of the width of the young part above the joint are drawn with help of Equations (3.56), (3.58) and (3.59).The diagrams are valid for $E_{28a}/\zeta E_{28y}$ = 1.053 (ζ = 0.95), λ = 0 and different values of $A_{a,eff}/A_y$, H_a/H_y. For the plane-section restraint coefficient at the joint and different values of $\gamma_{RT}(x)$ and $\gamma_{RR}(x)$, the results are presented in Appendix E, Figures (E.1) to (E.21). For the case of $\gamma_{RR}(x) = \gamma_{RT}(x) = 0$, which is most common, the plane-section restraint coefficient at three fourths of the width of the wall above the joint is presented in Appendix E, Figures (E.22) to (E.26).

When the rotational boundary restraint is equal to one, $\gamma_{RR}(x) = 1$, the curvature equals zero, $\varphi = 0$, and the plane-section restraint coefficient for a decisive point only depends on the translational boundary restraint condition, Equations (3.60) and (3.56). In Figure 3.24 the plane-section restraint coefficient can be found for various values of the $A_{a,eff}/A_y$ ratio and of the translational boundary restraint condition $\gamma_{RT}(x)$. See Appendix E, Figure E.21.

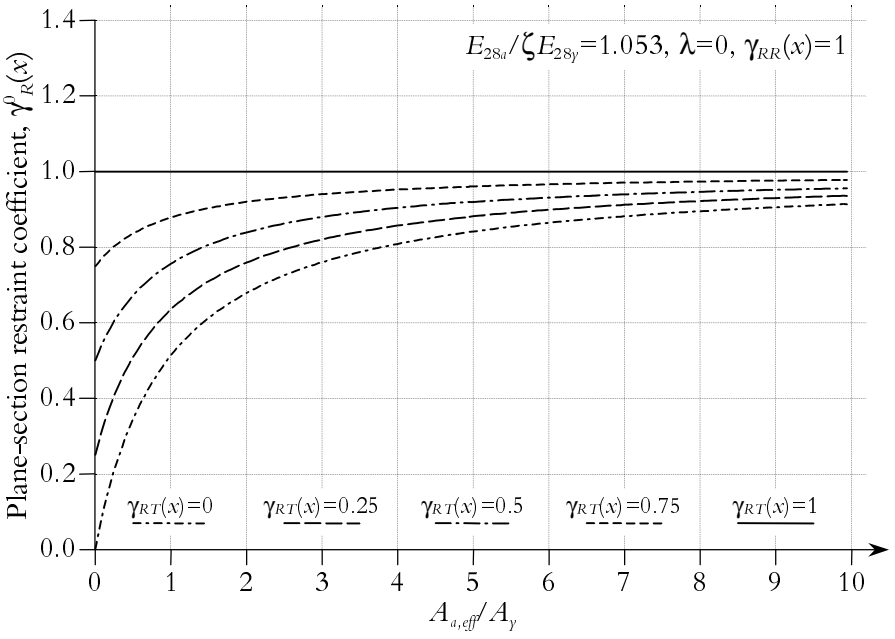

Figure 3.24 *Plane-section restraint coefficient in decisive point in young structural parts when the rotational boundary restraint equals one, $\gamma_{RR}(x) = 1$, i.e. for cases of no (external) bending.*

3.5.4 Example 3: Restraint at the bottom of a wall

As an example, consider a case with a rectangular young concrete wall (H_y = 3m, A_y = 1.5m^2) cast on a rectangular older slab (H_a = 0.75m, $A_{a,eff}$ = 3m^2). In the mid-section, the translational boundary restraint condition from the adjoining foundation material is about 75%, $\gamma_{RT}(x=0)$ = 0.75, and the rotational boundary restraint condition about 25%, $\gamma_{RR}(x=0)$ = 0.25. Figure E.9 in Appendix E is valid for this case and is depicted in Figure 3.25.

From the diagram it is found that for H_a/H_y = 0.75/3 = 0.25 and $A_{a,eff}/A_y$ = 3/1.5 = 2, the plane-section restraint coefficient in the decisive point at the bottom of the wall is, $\gamma^0_R(x=0,z_1=z'_{cen}-H_a)$ = 0.86.

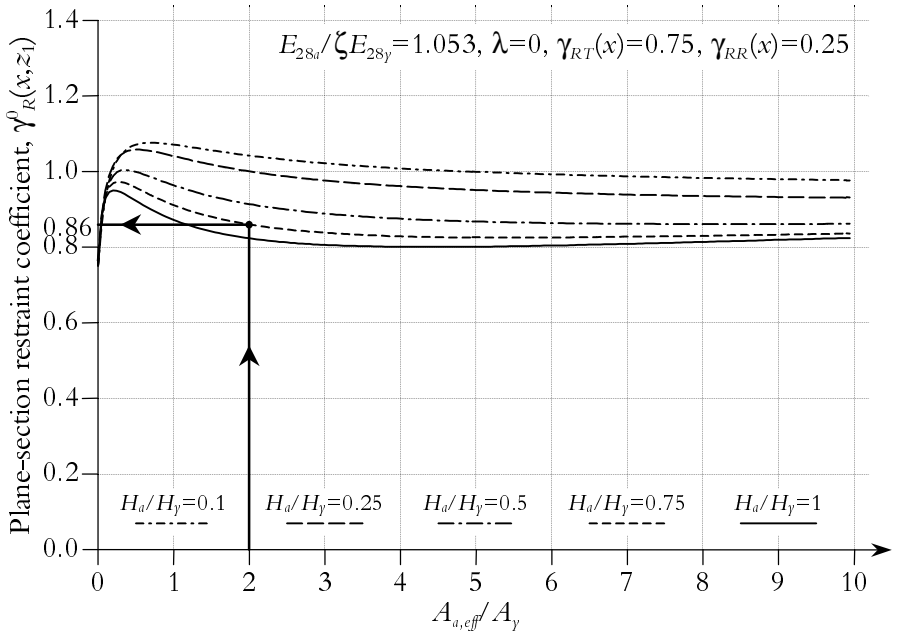

Figure 3.25 *Plane-section restraint coefficient for $A_{a,eff}/A_y$ = 2 and H_a/H_y = 0.25. $E_{28a}/\zeta E_{28y}$ = 1, λ = 0, $\gamma_{RT}(x)$ = 0.75 and $\gamma_{RR}(x)$ = 0.25, giving $\gamma_R(x=0,z_1=z'_{cen}-H_a)$ = 0.86.*

3.5.5 Influence of ratios of modulus of elasticity and imposed volume changes

A study of the effects of the material parameters in Equations (3.56) and (3.58) on the plane-section restraint coefficients in young parts of concrete structures has been performed.

Increased values of $E_{28a}/\zeta E_{28y}$ give higher values of the plane-section restraint coefficients. That is, higher values of the modulus of elasticity at 28days of adjoining parts than young ones, or a short time after casting of young parts, results in higher restraint.

If the volume changes of the adjoining parts are equal to the volume changes of the young ones, $\lambda = 1 \Rightarrow \Delta\varepsilon_a^{\,0} = 1{\cdot}\Delta\varepsilon_y^{\,0}$, the plane-section restraint coefficient is equal to the translational restraint, $\gamma_R(x) = \gamma_{RT}(x)$. For values of λ larger than one, the restraint curves in the diagrams in Appendix E are so to say gradually inverted around the value of $\gamma_{RT}(x)$.

3.6 Non Plane-Section Analysis

All the equations above for determination of the plane-section restraint coefficient are valid for beams, that is, for structures with length to height ratios equal to five or more, implying plane sections remaining plane when deforming. However, in many problems actual for thermal cracking, the length to height ratios are lower. In these cases, the stresses decrease from the restrained boundaries to the free boundaries of the structure. This fact can be dealt with by the resilience factor, δ_{res}, reducing the restraint over the height.

In Figure 3.26, the resilience factor δ_{res}, as a function of the distance from the foundation and the length to height ratio, is freely depicted from Jonasson, Emborg and Bernander (1994), which in turn is based on earlier studies. The resilience factor δ_{res} is derived for structures not allowed translational motions and that are founded on totally stiff foundations not allowing bending.

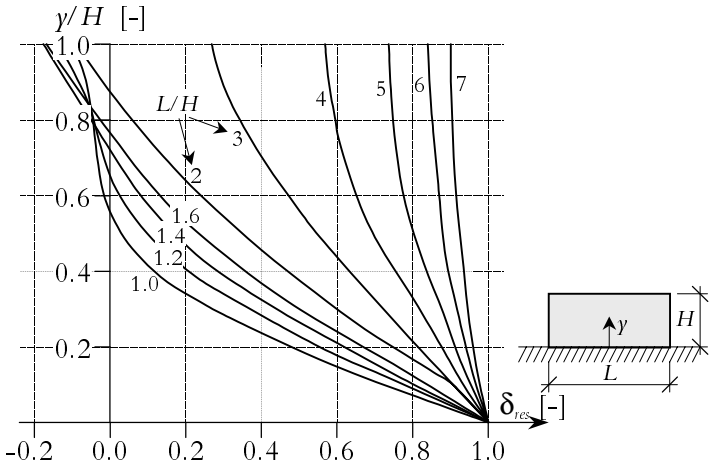

Figure 3.26 *The resilience factor in walls, cast on un-resilient foundations, as function of the height over the foundations for some length to height ratios of the young concrete. Modified from Jonasson, Emborg and Bernander (1994).*

Below, a method for determination of the resilience factor is presented. The method is based on finite element calculations and plane-section analyses. From Equation (3.43) and by introducing the coordinate y directed upward from the joint, as in Figure 3.26, the restraint coefficient is described by

$$\gamma_R = \delta_{res}\delta_{slip} - \frac{\varepsilon_{trans}}{\Delta\varepsilon_\gamma^0}(1-\gamma_{RT}(x)) - \frac{\varphi_{joint}}{\Delta\varepsilon_\gamma^0}(y_{cen}-y)(1-\gamma_{RR}(x)) \qquad (3.61)$$

The method presented here to determine the necessary parameters of Equation (3.61) starts with a FE-calculation for a long structure (length to height ratio equals ten) and an associated plane-section analysis that fulfils the demand

$$\varphi^0 = \varphi_{joint}(L/H = 10) \qquad (3.62)$$

This result in an effective width, $W_{a,eff}$, which leads to the possibility for plane-section analyses for similar structures. From the associated plane-section analysis, the value of the coordinate to the centroidal axis, y^0_{cen}, is chosen to be a representative value for the type of structure studied, expressed by

$$y_{cen} = y^0_{cen} \qquad (3.63)$$

In general, the basic formulation of the method presented here uses FE-calculations for an external free situation ($\gamma_{RT} = \gamma_{RR} = 0$) and elastic materials without any slip at the joint ($\delta_{slip} = 1$). For any length to height ratio, the FE-result is characterised by the following parameters

$$\begin{cases} \varphi_{joint} = \text{ curvature at the joint} \\ \gamma_R(y) = \dfrac{\sigma(y)}{(-\Delta\varepsilon_\gamma^0)\zeta E_{28\gamma}} \end{cases}$$

The evaluation of the parameters in equation (3.61) proceeds by studying the situation at the joint, $y = 0$, as

$$\delta_{res}(y=0) \equiv 1$$

by definition and

$$\gamma_R = \gamma_R(y=0)$$

from the FE-calculation, which gives

$$\frac{\varepsilon_{joint}}{\Delta\varepsilon_\gamma^0} = 1 - \gamma_R(y=0) - \frac{\varphi_{joint}y_{cen}}{\Delta\varepsilon_\gamma^0} \qquad (3.64)$$

and, finally, the resilience function, $\delta_{res}(\gamma)$, is evaluated by

$$\delta_{res}(\gamma) = \gamma_R(\gamma) + \frac{\varepsilon_{joint}}{\Delta\varepsilon_\gamma^0} - \frac{\varphi_{joint}}{\Delta\varepsilon_\gamma^0}\gamma \tag{3.65}$$

New resilience factors have been determined through finite element calculations performed in DIANA using solid 3-dimensional eighth-node brick elements for a 3m high and 0.5m thick wall cast on an older 1m thick slab. The effects of different lengths of the structure, L = 6, 9, 12, 15, 18 and 30m, are studied. Further, two different widths of the base slab, W_a = 3 and 6m, as well as three different locations of the wall relative the 3m wide slab, ω = 0, ±0.5 and ±1, have been analysed, see Figure 3.27. In the calculations, the wall is subjected to momentary decrease of the temperature of ΔT = -10°C. The effects of the temperature change are analysed elastically assuming the modulus of elasticity being $E_\gamma = \zeta E_{28\gamma} = 0.75E_{28\gamma}$ = 22500MPa in the wall and E_a = 30000MPa in the slab. Symmetry is used around the mid-section of the structure. From the finite element analyses, the strain and stress variation over the height of the structure is studied in the middle of the walls at the planes of symmetry.

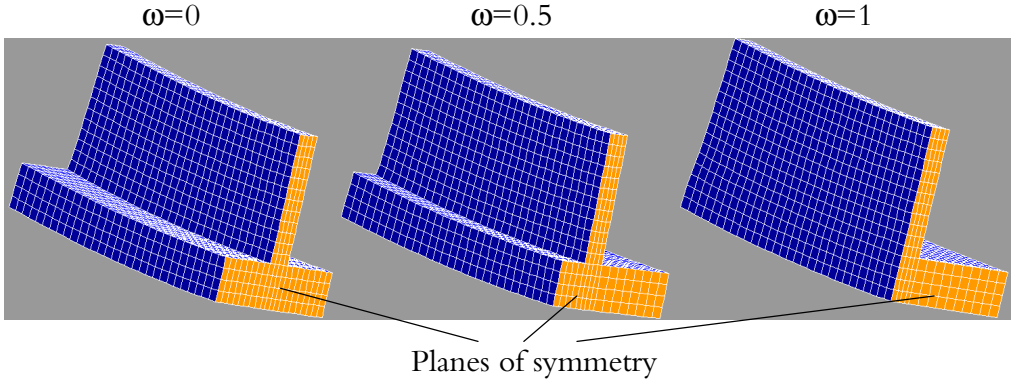

Figure 3.27 *Examples of the finite element models for one of the length to height ratios and the 3m wide slab used in the determination of the resilience factors.* ω *indicates the location of the wall relative the slab, see Section 3.6.2.*

The twelve cases of symmetrically located walls relative the slabs have been studied with the results showed in Figure 3.28. It can be seen that there is a very little difference between the two different widths of the slab.

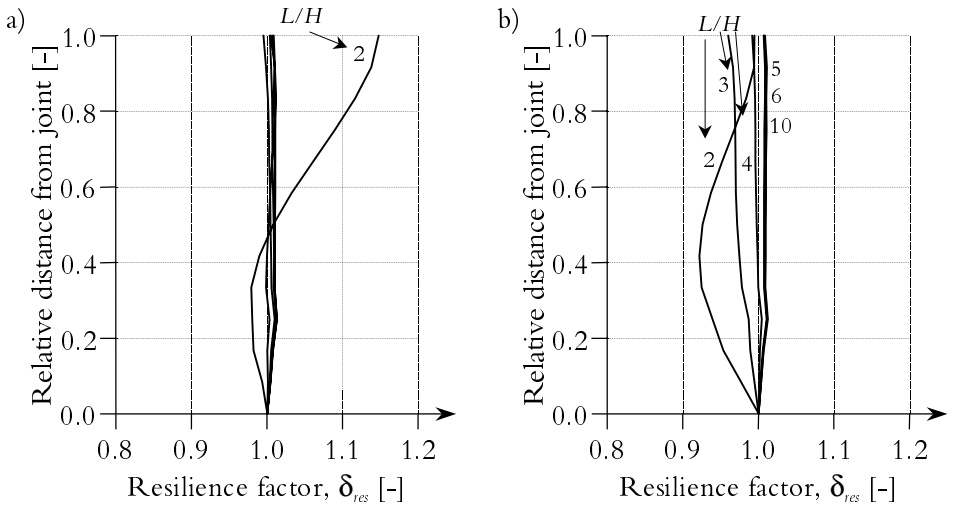

Figure 3.28 *The resilience factor determined according to Equation (3.65). Six different length to height ratios, L/H = 2, 3, 4, 5, 6 and 10, symmetrically located wall in relation to the slab and two different width of the slab, a) W_a = 3m and b) W_a = 6m.*

Notice that the calculated resilience factors are only valid for the mid-section of the studied structures. For other locations along the structures and other geometrical relations between the newly cast and old concrete, new resilience factors have to be determined.

Further, for this particular case, for length to height ratios larger than five no resilience factor seems to be needed implying plane-sections remain plane. This fact is further seen when studying the curvature of each case, see Figure 3.29. In the figure the relative curvature for all structures studied in the analysis are plotted. The relative curvature is defined as the curvature for each length to height ratio and the plane-section curvature. It can be seen that the relative curvature is equal for the 3m wide slab and the 6m wide. The relative curvatures of the structures with non-symmetrically located walls in relation to the 3m wide slab are smaller than of the symmetric structure.

Note that the results so far are only valid for exactly the studied structure. This means that many analyses for varying situations must be performed to get a broad basis for more general application purposes.

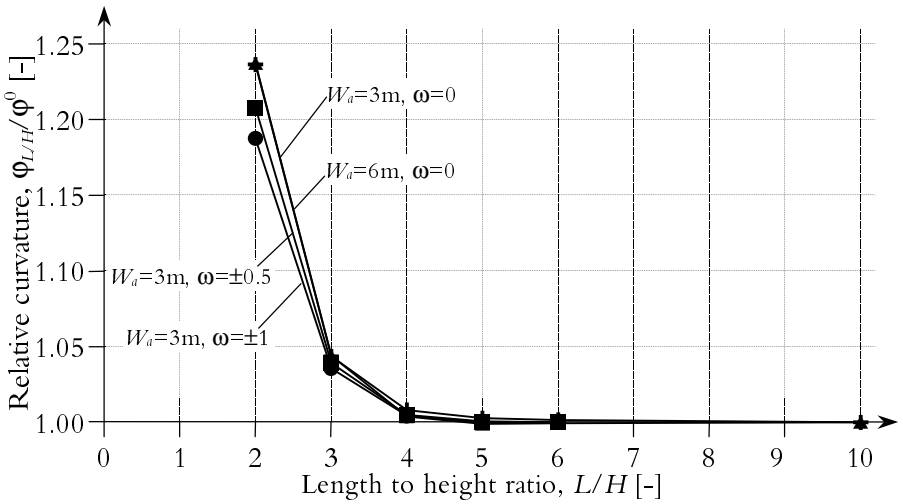

Figure 3.29 *The relative curvature as function of length to height ratio, width of slab and location of wall in relation to slab.*

3.6.1 Effective widths

A plane-section analysis where the width of the slab equals the geometric width ($W_{a,eff} = W_a$) will generally not give agreement with the 3D FE-analysis at the chosen representative point. Therefore, generally, there is a need of an variable effective width ($W_{a,eff} \neq W_a$) in the plane-section analyses. The disagreement between the results belongs to the fact that the equations for the plane-section restraint coefficients do not depend on the length of the structures, more than by way of the translational and rotational boundary restraint coefficients. The same considerations must be taken for unsymmetrically located young parts on older ones.

The use of the effective area in the plane-section analyses is defined by $A_{a,eff} = W_{a,eff}H_a$, see Section 3.4.3. By varying the width of the base slab in Equations (3.56) and (3.57) for $\gamma_{RR} = \gamma_{RT} = 0$ and $\lambda = 0$, the effective width of the base slab is determined resulting in agreement with the curvature obtained in the FE-analyses. In Table 3.5 the resulting curvature, effective width $W_{a,eff}$ and effective width to real width ratios are presented.

For the wider slab, W_a = 6m, the effective width to width ratio is larger than for the more narrow one, W_a = 3m. Further, the effective width to width ratio is larger than one for the wider slab, about 1.07, and smaller than one for the narrow slab, about 0.89. This implies the effective width needed in the analysis has to be larger than the real width for the wide slab and smaller for the narrow

slab. For unsymmetrically located walls in relation to the slab, the effective width to real with decreases rapidly the more unsymmetric the structure is.

Table 3.5 *Effective width and effective width to real width ratios for studied structures attaining the same curvature around the joint by FE-calculations and by the equations for plane-section analyses.*

	ω	0	±0.5	±1
W_a=3m	φ^0	$3.74 \cdot 10^{-5}$	$3.61 \cdot 10^{-5}$	$3.28 \cdot 10^{-5}$
	$W_{a,eff}$ [m]	2.66	1.40	0.69
	$W_{a,eff}/W_a$	0.89	0.47	0.23
W_a=6m	φ^0	$3.68 \cdot 10^{-5}$	-	-
	$W_{a,eff}$ [m]	6.43	-	-
	$W_{a,eff}/W_a$	1.07	-	-

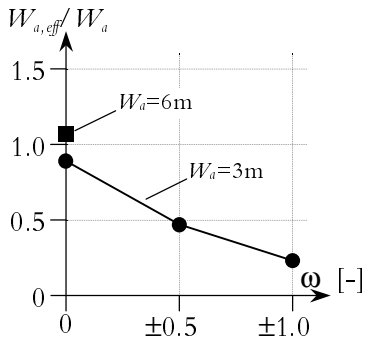

3.6.2 Effects of the location of the young parts in relation to adjoining parts

The effects of the location of the young part on the older and adjoining part on the resilience factor have, as been mentioned, been studied for the structure with the 3m wide slab. The study is performed in FE-calculations by varying the location of the wall according to Figure 3.30, firstly right at the ends of the slab, and secondly half-way between the mid and the outer locations.

The effects on the resilience factor are presented in the diagram in Figure 3.30. For smaller length to height ratios, the effects are noticeable. Larger resilience factors are needed the further out on the slab the wall is located. For larger length to height ratios, $L/H > 4$, the effects of the location of the wall are no longer noticeable and can therefore be neglected. However, further studies are needed for other lengths and widths of the slab before any more precise conclusions can be drawn.

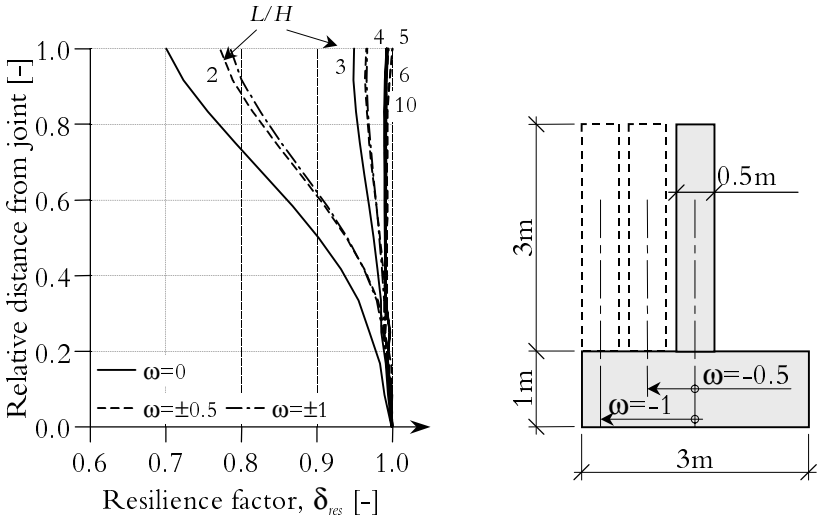

Figure 3.30 *Effects of different locations of the wall on the slab on the resilience factor in Example 4.*

3.7 Restraint Reduction due to Slip

One reason for cracking of young concrete structures cast on older members is the limited knowledge of the conditions and behaviour of casting joints. Today there are no methods for determining how large forces that are transferred across joints and to determine if slipping has occurred between two members. In that connection, decisions about measures, such as heating cables, insulation, concrete temperature at casting etc., are unreliable. In many cases, slip failures in casting joints are supposed to take place, which reduce the restraint stresses. Fewer resources are then put on measures. However, if there is no slipping in reality, the risk of cracking is obvious. In other cases, the stress transferring capacity of casting joints is over-estimated and the measures on cracking are both expensive and unnecessarily comprehensive.

Cracking during the contraction phase of young concrete structures cast on older ones very much depends on the connecting casting joints between the members. If the casting joints are very strong and contain a lot of through reinforcement, they are capable of transferring counteractions/restraint on the free movements from older members to younger ones. On the other hand, if slip failures in casting joints are allowed, the restraint stresses as well as the cracking risks are reduced, see Figure 3.31. A considerable amount of money can thereby be saved during both design and building phase. However, this mechanism has to be proven.

In Figure 3.31, the stress distributions are schematically described for a wall cast on a slab during the cooling phase. Before a slip failure in a casting joint, all stresses are larger than after an eventual cracking. In addition, the area with high restraint effects from the slab is also significantly reduced after a slip failure in a joint.

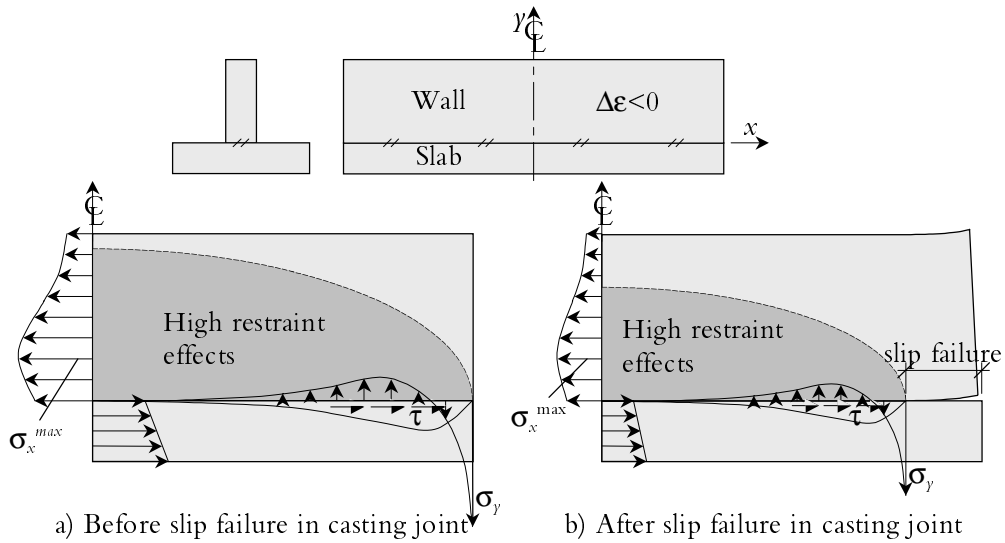

Figure 3.31 *a) Stress distribution a) before and b) after slip failure in a casting joint.*

The phenomenon of slip failure and associate effects in casting joints may be used both in the design and in building phase. A calculated slip failure in a casting joint may be regarded as a controlled form of cracking. In such joints, it is very common to use joint sealers and/or injections hoses. In those cases it is possible to benefit the effects of a slip failure and thereby, reduce the risk of uncontrolled through cracking in young concrete structures.

One method of determination of the slip factor δ_{slip} in Equation (3.1) is shown in Figure 3.32. The method is based on field experiences and is presented in ConTeSt Pro (1999). The coefficient depends on the free length, the width and the height of the casting section.

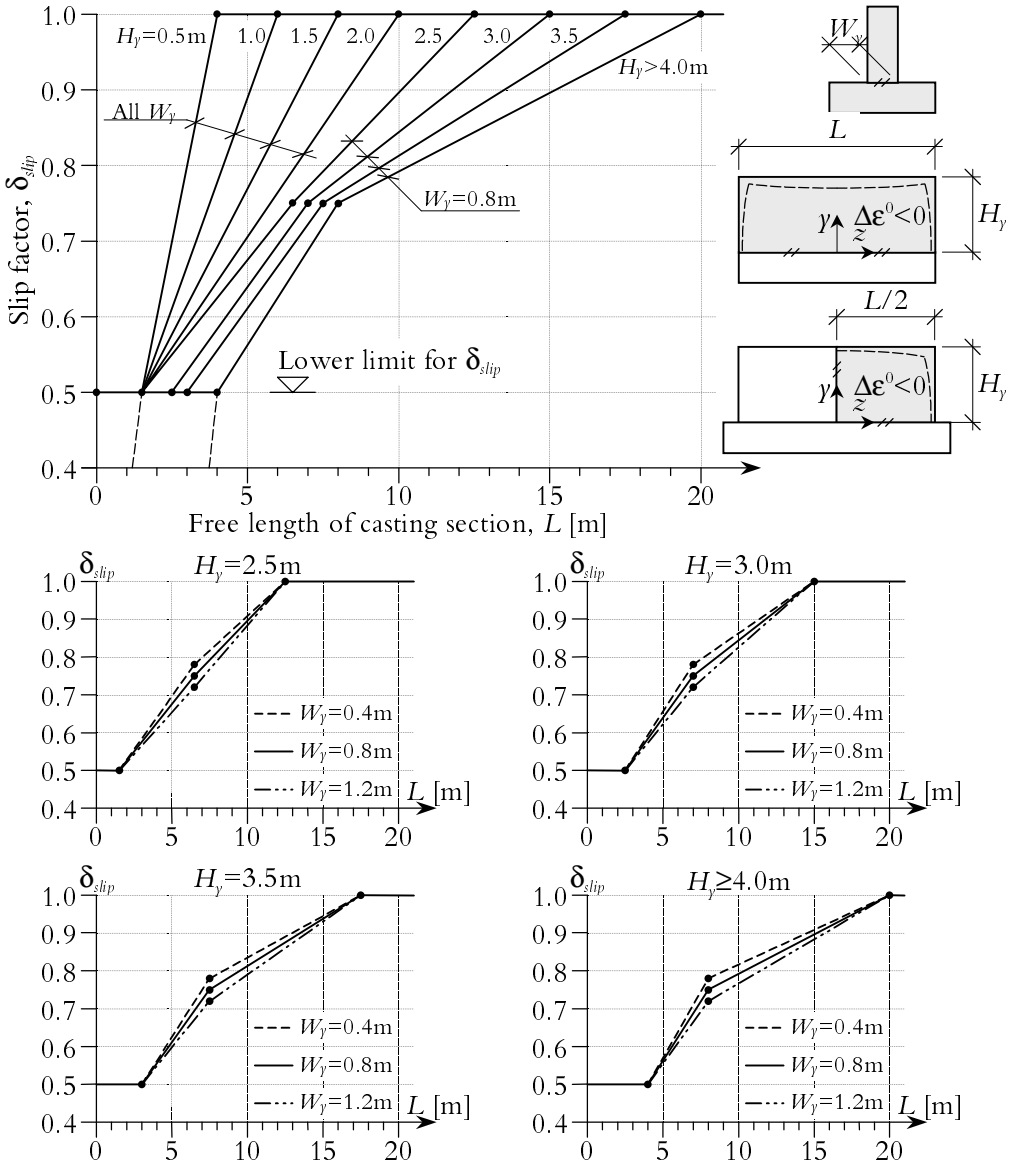

Figure 3.32 *Slip factor δ_{slip} as function of the free length, the height and the width of the casting section. ConStre Pro (1999).*

3.8 Concluding Remarks

Analytical models have been derived and presented for determination of the rotational boundary restraint from elastic materials on deforming concrete structures during the hydration phase. The models are valid both for structures that are totally resting on the foundation and for structures with lifting ends.

The models depends on the stiffness and compaction of the ground material and the bending stiffness and geometric properties of the structures.

The effect of the age of the young concrete on the rotational boundary restraint has been studied and introduced in the models of rotational boundary restraint. The influence is introduced by the time dependent modulus of elasticity and bending stiffness. The modulus of elasticity is temperature dependent. However, the stiffness growth of structures is generally very rapid implying the influence of time on the rotational boundary restraint being negligible.

The restraint in representative points in structures assuming plane sections remaining plane can be determined by the introduced model based on a formulation for prestressed concrete beams, Collins & Mitchel (1991), which is modified for problems of hydrating concrete structures. The model depends on the translational and rotational boundary restraint from foundation materials and on the height, area and modulus of elasticity ratios of adjoining and young parts of structures as well as the volume changes of the parts.

Graphical application tools for simple structures are given for determination of the plane-section restraint in decisive points. The tools are valid for rectangular young concrete parts cast on rectangular older parts. The modulus of elasticity in the young part is 95% of the modulus of elasticity in the older and adjoining part. The volume changes in the adjoining part are equal to zero. The model is dependent on the translational and rotational boundary restraint from adjoining foundation materials. For the case of total rotational boundary restraint, the plane-section restraint in a decisive point is determined from one diagram depending on the translational boundary restraint and the area ratio of the old and young parts. For all other cases, the plane-section restraint in decisive points is given in twenty-five diagrams. The restraint is depending on the height and the area ratios of the old and young parts and on the amounts of translational and rotational boundary restraints from adjoining foundation materials.

For shorter structures, that is, with length to height ratios smaller than about five, plane sections do not remain plane when deforming, which here is expressed by resilience functions. A method is presented for the determination of resilience factors for the cases of walls cast on slabs. The method is based on finite element calculations of stresses and strains, plane-section analysis of curvature and geometrical properties. The requirement for the model is that the curvature obtained by plane-section analysis has to be equal to the curvature in reality (e.g. found in the FE-analysis). Therefore, an effective width is introduced in the analytical model for the condition that the curvature equals the curvature obtained in FE-calculations. From the calculated stresses through the

FE-calculation, the curvature and geometrical properties through the plane-section analysis, the resilience factors are evaluated as a function of the vertical coordinate in the wall.

In many cases, the young part of a structure is not located symmetrically on the adjoining older part. The effects on the resilience factor as well as the effective width have been studied in an example for the structure wall on slab. It has been shown that for more unsymmetrical structures larger resilience factors are needed then for symmetric structures. On the other hand, for the effective width, the location of the young part has great influence. Young parts located at the edges of older parts need smaller effective widths than young part located at the centre of the old part.

For the models of plane-section restraint coefficient, resilience factors and effective areas, further calculations and studies are needed before any general conclusions can be drawn.

4 Medium Scale Experiments of Walls Cast on Slabs and Loaded by Restraint Stresses

4.1 Introduction

Four laboratory tests of medium scale properties have been performed at Testlab, at Luleå University of Technology, studying the risk of through cracking of massive concrete structures during the cooling phase. The phenomenon of through cracking during the cooling phase is most common in massive concrete structures. In civil engineering structures, such cracking is most important to prevent due to for instance problems of leakage and durability. Despite, it was chosen to conduct the tests on structures with medium scale geometrical properties, which behaviour can be transferred into dimensions that are more massive.

The influences of the properties of the joint between the young and old parts and the boundary restraint conditions are the most important parameters of the tests. The properties of the joints regard the texture of the surfaces and the amount of through reinforcement going through the joints. The boundary restraint properties regard zero or full constraint against bending of the structure.

Medium scale experiments in laboratory environment, such as performed in these tests, require a lot of planning. Many different factors have to be taken into consideration and be prepared for. The first and most important task is to define the objectives of the tests and thereby what should be tested. In that context, the kind of structure that shall be tested has to be determined in addition with what shall be measured.

One important aspect of the experiments is that they have to be as authentic as possible. The dimensions of the construction are vital parameters with respect to the needs of the experiment and the available space in the laboratory. The

geometrical relations between different parts of the construction and the temperature development in the young concrete parts have to be as realistic as possible. Further, for these tests, the surface conditions of the casting joints between the young and the old parts of the structure have to be determined. That is, the amount of through reinforcement in the casting joint has to closely coincide with amounts in real structures as well as the texture of the surfaces of the joints. The boundary restraining conditions have to be predetermined, that is, the degree of freedom of the whole system.

Since only four tests were performed, the possibilities of variation were limited regarding the amounts of through reinforcement, texture of the joint-surfaces and the boundary restraint conditions. Therefore, it was determined that at all events the extremes were to be tested when varying the amounts of through reinforcement and the boundary restraint conditions.

The study was conducted in four tests on three different structures. The first two tests, hereinafter referred to as Test I and Test II, were made on a medium scale wall 5.8m long, 0.15m thick and about 2m high cast on a 8m long, 1.4m wide and 0.2m thick slab. Between the wall and the slab, a footing cast prior to the wall was used. The third and four tests, referred to Test III and Test IV, were performed on two different walls 5.8m long, 0.15m thick and about 1.2m high. The walls were cast on similar footings as in Test I and Test II, which in turn were bolted to the same slab as in the previous tests, see Figure 4.1.

Three different amounts of reinforcement, going through the joints between the footings and the walls, were used in the tests: 0, 0.6 and 1 percentage in relation to the surface of the joints. In Test I, one half of the joint contained one percentage of through reinforcement whereas the other half did not contain any reinforcement at all. In Test III and in Test IV, the whole lengths of the joints contained 0.6 percentage of through reinforcement.

The structures in the four tests were subjected to two different boundary restraint conditions: free and full rotational and translational restraint. In Test I, Test II and Test III, the slab was tightly bolted to the floor in the laboratory. In Test IV, instead, the slab was totally free to rotate and translate.

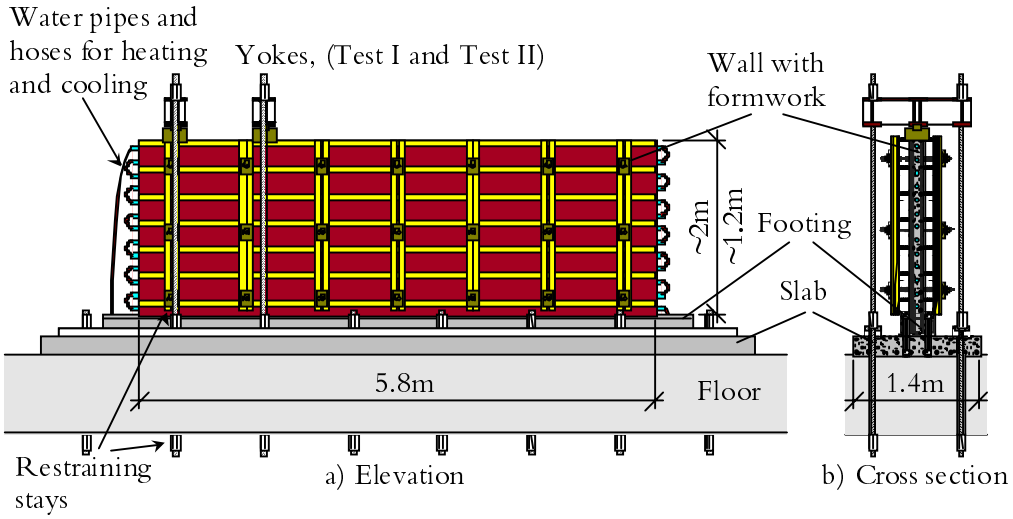

Figure 4.1 *a) Elevation and b) cross section of the walls, footings and the slab of the four tests, Test I - IV. The yokes loading the wall on the top were only used in Test I and Test II. In Test I and Test II, the wall was 2 m high, whereas in Test III and Test IV, the walls were 1.2 m high.*

The four tests were intended to imitate the temperature conditions in massive concrete structures. Therefore, the temperature level in the relatively slender walls used in the tests was increased to better coincide with the temperature development in a reference massive structure. To fulfil these requirements, water pipes of steel were embedded in the walls for regulating the concrete temperature with warm and cold water.

The aim of this report is to present the results from the first test of IPACS sub-task 4.1, Restraint, Laboratory tests L2 - Medium scale studies of behaviour of casting joints loaded by restraint stresses.

Four different aims are set up for the performance of the four tests presented below in this thesis.

- The very first and most important aim is to verify whether the assumed phenomenon of slip failures in casting joints loaded by restraint stresses exist at all.
- The second aim is to investigate the influence of the amount of through reinforcement in the casting joints on the expected slip failures and thereby on the risk of through cracking of the walls.

- The third aim of the experiments is to find the influence of the boundary restraint conditions together with the conditions of the joint on the risk of through cracking of the walls.
- Finally, the fourth aim is to find the development in time of the restraint within the young parts of the structures, that is the restraint variation over time within the walls.

4.2 Description of the Experiments

4.2.1 General

The first two tests, Test I and Test II, were conducted on the same construction. They were performed on a 5.8m long, 1.955m high and 0.15m thick wall on a pre-cast slab, 8m long, 1.4m wide and 0.2m thick. Between the wall and the slab, a footing was used. By using the footings, very well defined properties of the joints were possible to obtain, in addition, money was saved when remounting a wall and a footing after one test was carried through. The footing was cast prior to the wall and was bolted and cast to the slab. In the footing two different amounts of reinforcement were cast pointing upwards into the wall. One half of the joint contained zero percentage reinforcement and the other half one percentage reinforcement ($2\times\varnothing 12\ s150$). The half of the joint containing zero percentage was used in Test I and the other half of the joint in Test II, see Figure 4.1 and Figure 4.2.

The division of the construction into two different tests was done by two yokes on the top of the wall restraining the half of the wall not being used in the actual test. In Test I, testing the half of the wall containing no reinforcement in the casting joint, the yokes were loading the top of the other half of the wall. The yokes were loading the wall with 400kN each. When Test II was conducted, the opposite situation was valid. The yokes were loading the other half of the wall, and thereby examination of the half of the wall with 1 percentage through reinforcement in the casting joint is possible, see Figure 4.2.

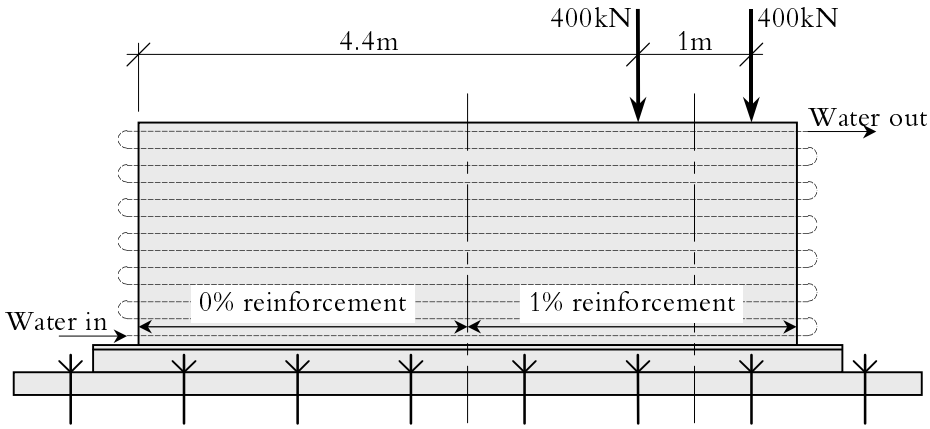

Figure 4.2 *Principal arrangements for Test I when testing the half of the casting joint containing zero percentage through reinforcement. In Test II, the yokes are placed similarly on top of the other half of the wall.*

By using the two yokes, the centre of dilatation is moved from the centre of the wall to somewhere between the two restraining yokes. In this way, the length to height ratio is changed from 5.8/1.955 ≈ 3.0 to about 2(5.8-1)/1.955 ≈ 4.9. The length to height ratio of young concrete members is a very important measure influencing the risk of through cracking.

The concrete slab was bolted to the floor in the laboratory resulting in 100% restraint both for translational and rotational deformation of the young concrete wall, which corresponds to $\gamma_{RT}(x) = \gamma_{RR}(x) = 1$.

The third and fourth tests, Test III and Test IV, were performed on 6m long, 1.155m high and 0.15m thick walls on the same pre-cast slab as in Test I and Test II. As in the previous tests, footings were used between the walls and the slab. The amount of reinforcement aiming upwards from the footings into the walls was 0.6 percentage (2×∅8 *s*110).

In Test III and Test IV, no yokes were used on top of the walls implying the length to height ratios being equal to 5.8/1.155 ≈ 5.0. In addition, steel pipes were cast in also in the second and third walls for regulating the temperature of the young concrete. The water temperature was varied to simulate the temperature development within a reference concrete wall of 0.7m thickness.

In Test III, the concrete slab was bolted to the floor in the laboratory in the same way as in Test I and Test II, implying the translational and rotational boundary restraints being equal or very close to 100 percentage, $\gamma_{RT}(x) = \gamma_{RR}(x) = 1$. On the contrary, in Test IV, the slab was not bolted to the floor and the

structure was free of deforming implying both the translational and the rotational boundary restraints being equal to zero, $\gamma_{RT}(x) = \gamma_{RR}(x) = 0$.

4.2.2 Geometry and test arrangements

Slab

The same pre-cast slab, 8m long, 1.4m thick and 0.2m high, was used in all four experiments. Through the slab, 16 holes were made for restraining the slab to the floor in the laboratory in Test I, II and III. The slab was reinforced by two layers of reinforcement, #∅12 s150, see Figure 4.3 for geometry and Drawing K01 in Appendix I for reinforcement and details.

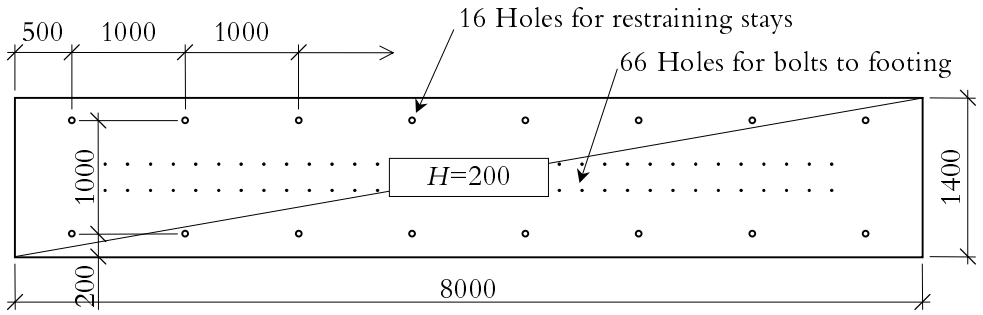

Figure 4.3 *Geometry of pre-cast slab used in all four tests, Test I - IV. Measures in millimetres.*

The slab was cast at a local manufacturer about one month before Test I was started. Through the slab, 66 holes were drilled for bolts to the footings. The bolts to the footings were planned to take vertical forces due to the temperature movements of the walls. The surface of the slab at the location of the footings was chiselled to improve the roughness. Cement layers, which should take horizontal forces, were cast between the slab and the footings. Before bolting and casting the first footing to the slab, the chiselled surface of the slab was sealed by a pore-sealer, type Swenco Tone, to simplify the later removal of the footings and walls.

Footings

The footings used in the tests were 6.6m long and had the dimensions shown in Figure 4.4. They were attached to the slab by a cast cement layer and through-going bolts. The cement layer was made of a fast hydrating grout with high compressive and tensile strength, Finja Betec High-Tech-Grouth 310. The bolting was done with 66 bolts through the holes in the footings and the slab.

The bolts of type M20 8.8 were pre-tensioned with an adjustable moment spanner just before the casting of the walls, moment = 210kNm and then additionally turned 120°.

The technique with a bolted footing has two major advantages. The first one is obvious when one test is finished. The bolts were loosened and the wall together with the footing was easily lifted of the slab, which then was reused in the next test. The second advantage is very important. When casting the footing, its formwork was turned upside-down, so that the bottom of the formwork became the lower part of a future casting joint, see Figure 4.5. The bottom of the formwork was thereby used to create very well defined structures of the casting joints. For that purpose, in all tests, sand of fraction 0.212 - 1mm was glued to the formwork of the footings, in order to fulfil the demand of equal joint properties.

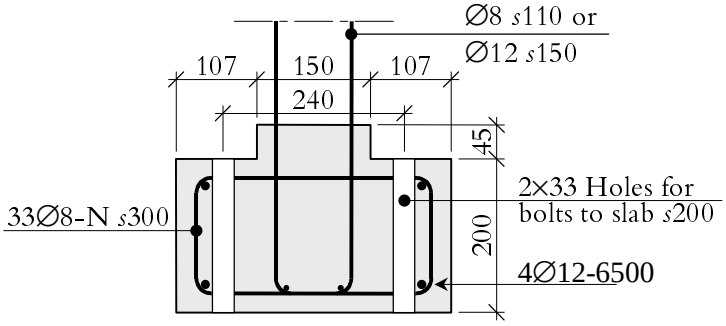

Figure 4.4 *Cross-section of footings: measures and reinforcement. Measures in millimetres.*

The formwork of the footings was made of ordinary 12mm thick plywood for concrete and built on two long and parallel ordinary tables, see Figure 4.5. The tables were placed at an appropriate distance so the bottom of the form, read future casting joints and widths of walls, would be 150mm wide. On the bottom of the formwork, as mentioned above, sand with fraction 0.212 - 1mm was glued. Reinforcement was placed in the form as well as 66 plastic pipes for the bolts from the slab through the footings. Cast-in temperature-gauges were fastened with tape on some reinforcement bars before the casting of the footings, which took place about one week before the casting of the walls.

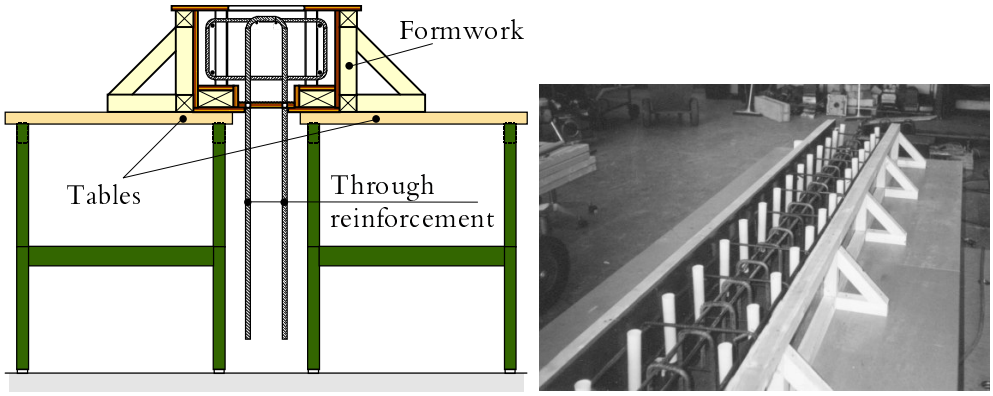

Figure 4.5 *Cross section of the casting situation and photo of the formwork for one of the footings. The footings were placed on two long and parallel tables.*

After the footings were cast and the hydration was more or less finished, the footings were turned right and placed on the slab. Between each footing and the slab, about 10mm of a cementitious material acting like a friction-layer was cast. The layers were made of fast hydrating cement with high tensile strength and modulus of elasticity.

Walls

During the casting of the wall in Test I and Test II, 13 steel pipes, ∅ 25mm, for water were cast in horizontally. In the half of the wall containing one percentage through reinforcement from the casting joint, the wall was reinforced vertically with the same amount, ∅12 *s*150. The other half of the wall contained vertical reinforcement ∅8 *s*300. Horizontally the wall was reinforced with ∅8 *s*300 plus 2+2∅8 extra bars at the bottom, see Figure 4.6 and Appendix I, Drawing K03.

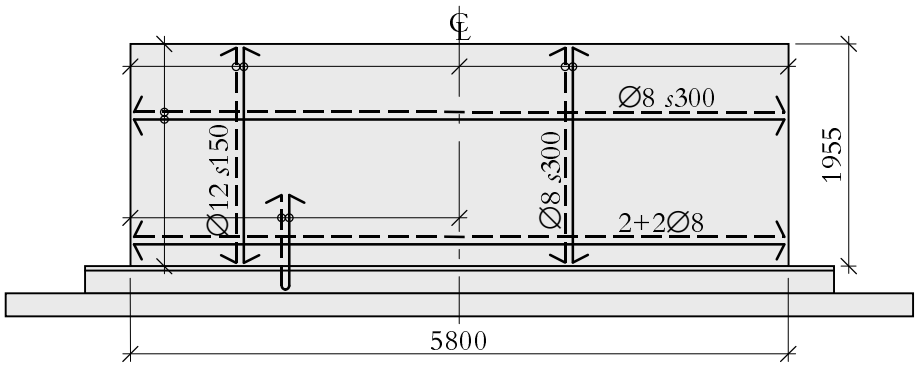

Figure 4.6 *Elevation of wall in Test I and Test II: measures and reinforcement. Measures in millimetres.*

The walls used in Test III and Test IV were lower than the wall used in Test I and Test II. They were 1.155m high, 5.8m long and 0.15m thick. Here seven steel pipes, ∅ 25mm, were cast in. The walls were reinforced vertically with the same amount of reinforcement as through the casting joints between the footings and the walls, that is Ø8 *s*110. Horizontally the walls were reinforced with Ø8 *s*300 plus 2+2Ø8 extra bars at the bottom. The walls were cast of concrete from the same recipe as in Test I and Test II, and the 28-day compressive strength was 44.8MPa in Test III and 62.4MPa in Test IV. Further, see Figure 4.7 and Appendix I, Drawing K03.

The formwork of the walls was made of 12mm thick plywood for concrete between beams and held in place by form ties. During all four tests, the formwork of the walls was attached to the walls during the whole tests and was not removed until the experiments were finished.

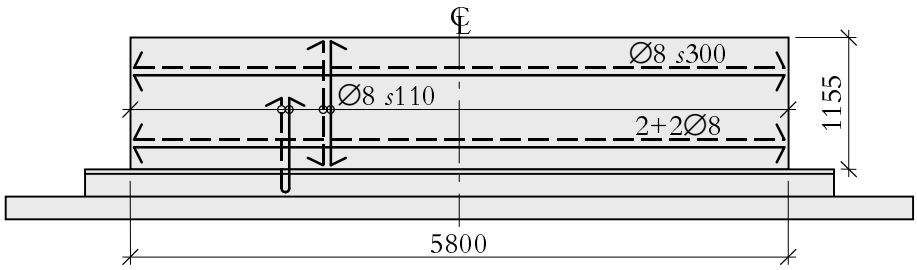

Figure 4.7 *Elevation of walls in Test III and Test IV: measures and reinforcement. Measures in millimetres.*

4.2.3 Restraining

The effects on the risk of through cracking of the walls have been studied in the four tests by two different boundary restraint conditions. With the earlier mentioned 16 through holes for restraining ties, the slab In Test I - III, was tightly bolted to the very well reinforced and 0.9m thick floor in the laboratory. In Test IV, on the opposite, the slab was totally free to deform with the deformation of the wall. The restraining stays were prestressed with a tensional force of about 350kN, holding the slab tightly to the floor. Between the slab and the restraining stays, steel beams were used for better spreading of the force through the slab.

As mentioned in Test I - II, two yokes were used on top of the wall to restrain the half of the wall not being tested. Each yoke loaded the top of the wall with a force of 400kN, see Figure 4.1 and Figure 4.2. By using the two yokes, the centre of dilatation was moved from the geometrical centre of the wall to somewhere between the yokes, approximately halfway between the stays. The tests were thereby simulating a structure with a larger length to height ratio then had been possible without the yokes, from $L/H = 5.8/1.955 \approx 2.9$ to about $L/H = 2(5.8\text{-}1)/1.955 \approx 4.9$. This was done both by economical reasons and due to limited space in the laboratory.

4.2.4 Loading (heating and cooling)

The problem with through cracking is mostly common in massive concrete structures due to the higher temperature within them compared to more slender structures and thereby the larger temperature movements. In spite of the slender structure that was used in the laboratory, it was possible to simulate such a massive structure by using the embedded steel pipes for water. The water was taken from the ordinary water system in the laboratory and the temperature was changed by turning the taps. By using both warm and cold water, the temperature-induced movements of the wall were considerably increased for the thin walls. Consequently, the stresses causing through cracking were also increased.

Thus, only a few hours after casting, warm water was used to increase the temperature within the walls and thereby the rate of hydration. The water temperature was changed in steps of 3-8°C according to the temperature in a reference wall, which consists of concrete type II and has a thickness of 0.7m. In all four tests, the temperature of the water was increased to a maximum of about +43°C at about 48hours after casting and then decreased to about +10-15°C at about 192hours after casting, see Figure 4.8.

The temperature development in the reference wall has been determined by the software Hett2DL on a wall of 0.7m thickness cast with the same type of

concrete as in the performed tests. The temperature presented in Figure 4.8 is the average temperature in the reference wall whose formwork remains during the whole calculation. Further, the temperature at the outside of the wall is about +12°C.

For Test II, the situation was a bit different. It started directly after Test I was finished, at about 120hours after casting, by again increasing the temperature of the water being pumped through the wall, see Figure 4.8.

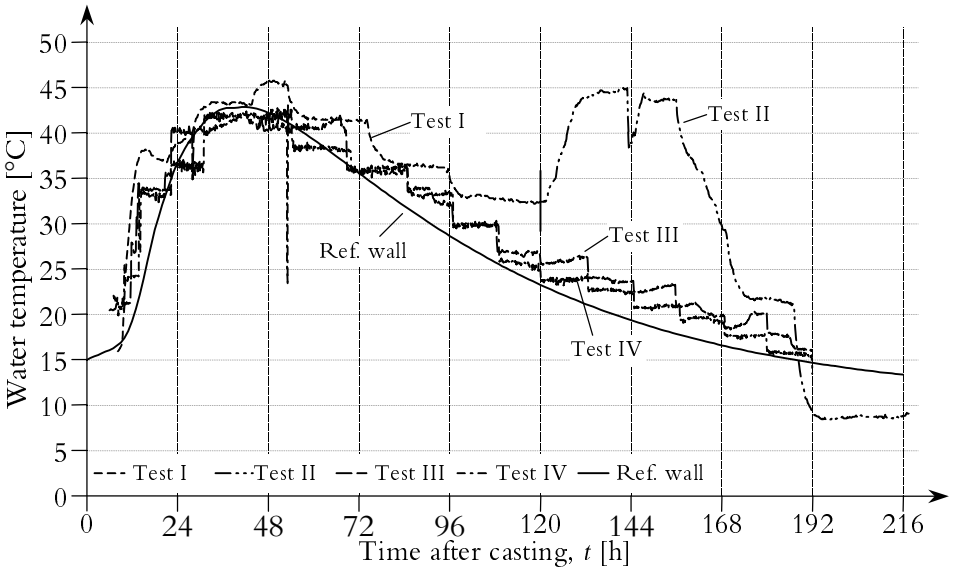

Figure 4.8 *Variation of the mean temperature in the walls of Test I through Test IV in accordance with the temperature in a reference wall by changing the temperature of the water that was pumped through the walls.*

In Figure 4.8 the water temperature as well as the temperature of the reference wall of 0.7m thickness is shown. The water temperatures in the four tests follow each other rather well bearing in mind the temperatures were changed only by turning the taps by hand. In Test II and Test III, the temperatures decreased abruptly at one occasion in each test when the local water supplier only produced cold water for about half an hour. During these drops in water temperature, the water was turned of and turned on again when the warm water returned.

4.3 Concrete

4.3.1 Concrete recipes

Two different concrete recipes were used for the footings and the walls in the four tests. In the first footing, assigned for Test I and Test II, slightly different concrete was used as in the other tests. However, the concrete used in the tests was of type II and was delivered from a local producer, Kallax Betong & Grus in Luleå. For the footing in Test I, recipe KBG416 was used, whereas for all other parts recipe KBG407 was used. The recipe of the concrete was designed to result in concrete suitable for civil engineering purposes in cold climate allowing freezing and thawing. The cement used in the concrete is of a type with lower rate of hydration OPC, Degerhamn. The mixing proportions are given in Table 4.1.

Table 4.1 *Mixing proportions of the concrete used in the tests.*

Content	Recipe	
	KBG407	KBG416
vct	0.40	0.45
Water, [kg/m^3]	181	165
Cement OPC, Degerhamn, [kg/m^3]	390	400
Sand 0-8mm, [kg/m^3]	910	900
Sand 8-16mm, [kg/m^3]	875	-
Sand 16-32mm, [kg/m^3]	-	865
Silica fume, [kg/m^3]	15	15
Air-entraining agent, [kg/m^3]	2.20	1.95
Water reducer agent, [kg/m^3]	2.00	2.15

4.3.2 Properties

Different properties of the concrete used in the tests have been documented. For all parts, except the slab, the development of the compressive strength, f_{α}, has been determined (150×150×150mm cubes). For the fresh concrete of the footings and the walls in Test III and Test IV, the air content as well as the slump were measured, except the air content for the wall in Test IV. The results of the compressive tests, the air contents and the slump are presented in Table 4.2.

In an ongoing Master Thesis at Luleå University of University, the variation of both the tensile and compressive strengths in the wall of Test IV is investi-

gated on drill-cores. In addition, the stress-strain and the stress-crack-opening softening properties of the concrete are determined.

Table 4.2 *Tested compressive strength at 28-days, f_{c28} [MPa], air content, [%], and slump, [mm]. Determined strength classes according to BBK94 (1995) and the used empirical parameter s, [-], see Equation (4.1) for calculation of the development of the concrete strength.*

	Test I and Test II		Test III		Test IV	
	footing	wall	footing	wall	footing	wall
f_{c28} [MPa]	51.2	45.9	53.4	44.8	44.8	62.4
Air content [%]	-	-	5.9	6.6	6.6	-
Slump [mm]	-	-	100	110	110	45
Strength class	K60	K55	K60	K55	K55	K80
s [-]	0.46	0.47	0.38	0.42	0.42	0.35

Compressive strength

The development of the compressive strength has been determined for the concrete used in all the footings and the walls. The compressive strength has been tested by uniaxial compression tests on cast cubes 150×150×150mm at 1, 3, 7, 14 and 28 days after casting of each individual part of the experiments. The cubes were stored in the laboratory at about +20°C under moist conditions. In Figure 4.9 the results from the uniaxial tests of the compressive strength are depicted for the footings and walls in the tests.

In Test I - III, the compressive strength is higher in the footings than in the walls, nevertheless, in Test IV, the opposite situation is valid. For the wall in Test III and the footing in Test IV, which were cast at the same occasion, the compressive strength development had a strength loss at seven days after casting. No rational explanation has been found. Maybe the cubes for testing at seven days were not as good as they should be? Further, bearing in mind that all parts are cast with concrete from the same recipe, except the footing in Test I, there is a wide range in the values of the compressive strength. One reason for this can be the small amounts of concrete in every casting, about 1 to 1.5m^3.

The development of the compressive strength can be modelled by an expression according to the CEB-FIP Model Code 90 (1993), slightly modified to be zero at $t_e = t_s$, as

$$f_{cc}(t_e) = f_{cc,28} \exp\left\{ s\left(1 - \left(\frac{28}{t_e - t_s} \right)^{0.5} \right) \right\} \tag{4.1}$$

where

$f_{cc}(t_e)$	is the compressive strength, [MPa]
$f_{cc,28}$	is the compressive strength at 28days equivalent age, [MPa]
t_s	is the apparent setting time, here chosen to be 10hours, [days]
t_e	is the equivalent time, [days]
s	is an empirical parameter for fitting the development-curve to the tested true values, [-]

From Equation (4.1), the development of the compressive strength is calculated with $f_{cc,28}$ and s according to Table 4.2 to obtain the best fitting of the tested values of the compressive strength. The results are presented in Figure 4.9 below.

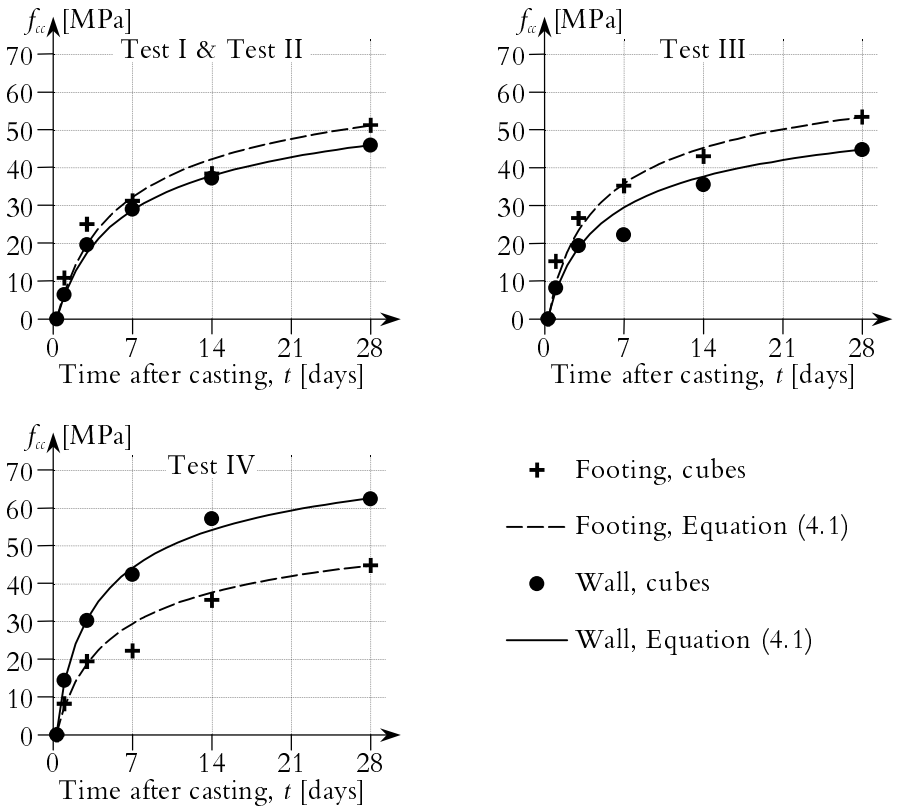

Figure 4.9 *Tested and calculated development of the compressive strength for the footings and walls in Test I through Test IV.*

Tensile strength

From the results of the compressive strength, the tensile strength can be determined through indirect methods. The equation used in the evaluation of the experiments is given in CEB-FIP Model Code 90 (1993) and describes the development of the tensile strength in relation to the compressive strength as

$$f_{ct}(t_e) = f_t^{ref} \left(\frac{f_{cc}(t_e)}{f_c^{ref}} \right)^{\beta_1} \tag{4.2}$$

where

$f_{ct}(t_e)$ is the tensile strength, [MPa]
$f_{cc}(t_e)$ is the compressive strength, [MPa]
f_t^{ref} is a reference tensile strength = 3.3MPa, Larson (2000)
f_c^{ref} is a reference compressive strength = 45MPa, Larson (2000)
β_1 is an exponent expressing the curvature of the development = 0.667, Larson (2000)

The results from the determination of the development of the tensile strength are shown in Figure 4.10. The figures used for the tensile strength according to Larson (2000) are based on testing in a TSTM-equipment (Temperature Stress Testing Machine) at Luleå University of Technology.

Both the developments of the compressive strength and of the tensile strength have, naturally, the same shape. However, there exist some differences between the strengths in the four tests. In Test I, Test II and Test III, the strength in the footings are larger than in the walls. About $f_{cc} \approx 50$MPa in the footings compared to $f_{cc} \approx 45$MPa in the walls and $f_{ct} \approx 3.6$MPa in the footings compared to $f_{ct} \approx 3.3$MPa in the walls. In Test IV, the opposite conditions are found. The strength in the wall is considerably higher than in the footing as well as the strengths in Tests I - III. The compressive strength is $f_{cc} \approx 45$MPa in the footing compared to $f_{cc} \approx 62$MPa in the wall and the tensile strength is $f_{ct} \approx 3.3$MPa in the footing compared to $f_{ct} \approx 4.1$MPa in the wall.

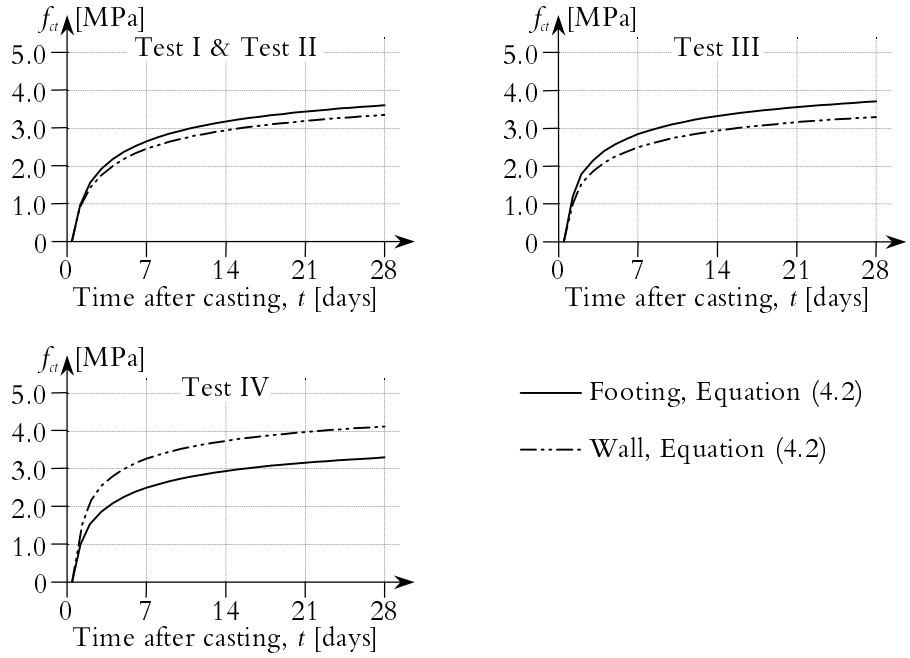

Figure 4.10 *Calculated development of the tensile strength according to Equation (4.2) for the footings and the walls in Test I through Test IV.*

4.4 Performance

The performance of each test will be described below. Each test is supposed being started at the same time as the concrete is placed in the formwork of the walls. The castings of the footings, which took place prior to the castings of the walls, are simulating that the slab is cast 2 á 3 weeks before the casting of the wall.

The performances of the tests will be described with changes of water temperatures and mounting of measuring devices. Further, the applications of yokes (Test I and Test II), slip failures in casting joints and all other things that have influenced the results of the experiments will be presented.

4.4.1 Test I

Test I was performed between the 27 May and 1 June 1998. Three weeks before the casting of the wall, the footing was cast. Much the same concrete that was used in the wall was also used in the footing. The concrete had the same strength but larger maximum aggregate sizes, see Table 4.1.

The casting of the wall started at 12.00 on 27 May 1998. After the casting of the wall, cubes for the testing of the compressive strength were cast. Once the fresh concrete was placed in the form of the wall, the test was started. A few very intensive hours followed, when all the equipment and measuring devices were placed on the construction and then started. The temperature was measured, as well as relative movements between different parts of the structure, the strains in several points, and the crack propagation in the casting joint, see Section 4.5.

When the concrete started to settle, the top of the wall was levelled at its end for the future application of the yokes. After the levelling, the concrete was stiff enough for the application of the vibrating strain gages and the starting of the strain measuring.

About ten hours after casting, warm water was used for the first time to increase the rate of hydration of the wall. Two days after casting, the two yokes were applied on the top of the half of the wall that contained one percentage through reinforcement in the casting joint, see Figure 4.1 and Figure 4.2. The yokes loaded the top of the wall with nearly 400kN each. The load was monitored during the whole test and kept as close as possible to 400kN all the time.

At this stage, the temperature maximum was reached within the wall, about +45°C, and the contraction phase started. The Crack Detection Cages (CDG), see Section 4.5.4 below, were mounted after the formwork was removed at the ends of the casting joint on one side of the wall. A few hours later, the unreinforced casting joint cracked. Due to some mistakes and misunderstandings about the CDG:s, the slip failure was never logged at the right time. However, by continuous visual examination of the joint, from the temperature maximum was reached within the wall, the joint cracking was discovered approximately at the correct time, which was observed to be about 75.75hours after casting. The whole length of the joint cracked, as expected, since it contained zero percentage through reinforcement. During the two next days, the water temperature was decreased twice per day until the temperature of the wall was about +32°C. Then Test I was finished and Test II started.

4.4.2 Test II

Test II was performed between the 1 and 8 June 1998. The water temperature was rapidly increased in a few steps from about +32°C to about +52°C during the first eight hours. Another 16hours later, the yokes were removed from the end of the wall containing one percentage reinforcement in the joint to the footing and applied on top of the other end of the wall.

Eleven hours later the casting joint started to crack. Only small parts of the joint cracked at each time, cracking from reinforcing bar to reinforcing bar. During the following 13hours the joint cracked six times in a total length of about 0.6m. This phenomenon may be regarded as a consequence of a kind of dowel effect in the reinforcement bars.

One and a half-day later, the form was stripped and cracks were searched for on the surface of the wall. One vertical crack in the middle of the wall was found as well as two diagonal cracks in the middle of each half of the wall, see Figure 4.18a) and b).

The bolts fastening the footing in the slab were then loosened and the wall together with the footing was removed from the slab. The slab was then available for the preparation of Test III.

4.4.3 Test III

Test III was performed between 26 May and 3 June 1999. Two week prior the casting of the wall, the footing of Test III was cast. The casting of the wall started at about 12.00 on 26 May 1999. At the casting of the wall, the footing of Test IV was cast. After the casting of the wall, the cubes for the determination of the compressive strength were cast as well as the air content and the slump were determined.

The water temperature was changed accordingly to the temperature in the reference wall.

When Test III was finished, the bolts fastening the footing in the slab were loosened and the wall together with the footing was removed from the slab. The preparation of Test IV was then started by mounting the new footing on the slab.

4.4.4 Test IV

Test IV was performed between 4 and 13 August 1999. After the mounting of the footing and the application of the formwork and reinforcement, the wall was cast at 9.00 on 4 August 1999. After the casting, cubes for compression tests were cast, as well as the slump and the air content were determined for the fresh concrete.

After the fresh concrete was placed in the formwork, the temperature measuring was started. Once the concrete was settled, the strain gages were mounted and the strain measuring was started. The water temperature was then increased accordingly to the temperature development in the reference wall. Some hours later the LDT:s were mounted and started.

4.5 Measuring

In all four tests, lots of measuring has been done to monitor the tests and to save data for future evaluation of the tests and for verification of whether or not the stated aims were fulfilled. Four distinct fields of measuring have been performed. First, the temperature development within the walls and the water temperature are to be measured. Second, the relative movements between the parts of the structures were to be determined. Third, the strains at certain points in the walls, to find the development of the restraint, and fourth the propagation of assumed slip failures in the casting joints between the walls and the footings. A fifth field of measuring was valid for Test I and Test II by the monitoring the loads from the yokes on the wall.

4.5.1 Temperature

The temperature was measured in different locations of the concrete structures as well as in the air and in the incoming and outgoing water. By in-cast temperature gages, the variation was measured, and the storage of data was done with two different systems, ConReg and ACC-2.

The temperature development within the walls was measured both at different heights and at different depths. In the footings, the temperature was measured at three different levels between the slab and the walls. On both the incoming and the outgoing steel pipes for the water, temperature gages were fastened to monitor the differences between the incoming and the outgoing water temperatures. In addition, the temperature was measured at half the length of one of the middle steel pipes.

The purpose of measuring the temperature in the walls was to monitor and to support the changing of the water temperature according to the reference wall, and to map the varying temperature field for the theoretical evaluations. The temperature in the footings was used when evaluating the relative movements between the different parts of the structures. Large temperature changes within the footings and/or in the slab are important factors influencing the relative movements within the structures. Further, see Section 4.6.1 below.

4.5.2 Relative displacements

The relative movements between the different parts of the structures have been measured with Linear Displacement Transducers (LDT). The measuring was performed with at most 16 LDT:s between the floor and the slab, between the slab and the footing, and between the footing and the wall along with the movements of the upper corners of the wall. In Figure 4.11, the general principal of an LDT is depicted. In Figure 4.12 the locations of the LDT:s in the different tests as well as their local orientations are shown.

Figure 4.11 *General description of a Linear Displacement Transducer (LDT). Positive values of the displacement are obtained when the point of the LDT is going inward and negative values when going outwards.*

In Tests I and II, the horizontal relative displacements are measured between the floor in the laboratory and the slab, between the slab and the footing, between the footing and the wall, and between the upper corners of the wall and the floor in the laboratory, see Figure 4.12. Vertical relative displacements were measured between the footing and the wall and between the upper corners of the wall and the floor in the laboratory. In Test III, the same measuring is performed except from the displacement at the upper corners of the wall. In Test IV, no displacements at the upper corners of the wall are measured. In addition, the vertical relative displacement is measured between the floor in the laboratory and the slab.

The LDT:s measure the change in location of their points from a reference value at the beginning of the measuring. They register positive values when the point is moved inwards and negative values when the points are moved outwards.

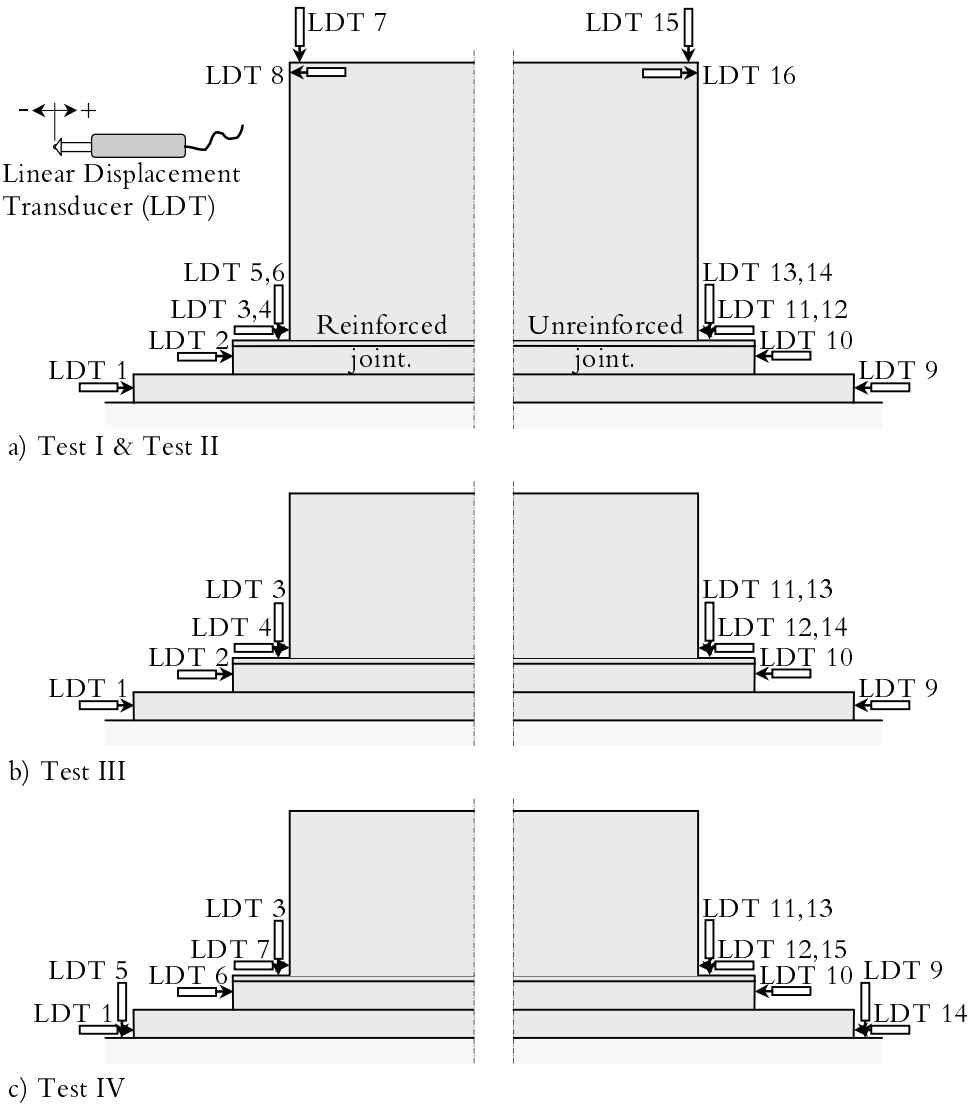

Figure 4.12 *Location of Linear Displacement Transducers (LDT) for measuring of relative movements between the different parts in a) Test I and Test II, b) Test III, and c) Test IV.*

4.5.3 Strains (restraint)

The strain variation in the walls is measured at 16 points with Vibrating Strain Gages (VSG), see Figure 4.13. The gages are of type Geokon model VSM-4000 with an active gage length l_{VSG} = 150mm, Geokon (1996). Data from the gages are stored in a Geokon 8020 MICRO-10 datalogger.

The strains are measured using the vibrating wire principle. A length of steel wire inside a protective steel tube is tensioned between two end blocks that are attached at the concrete surface being studied. Deformations (i.e. strain changes) of the surface will cause the two end blocks to move relative to one another, thus altering the tension in the steel wire. The tension is measured by plucking the wire and measuring the resonant frequency of vibration using an electromagnetic coil.

The gages are attached on the surface of the walls through the formwork with two bolts coming out from the walls and fastened to the end blocks of the VSG:s. The strains are measured between the attachment points over the active gage length, see Figure 4.13. During the casting of the walls, dummy bars are used instead of the real gages to prevent damages. The dummy bars are connected to the end blocks in the same way as the gages and attached to the formwork of the walls. The bolts being screwed to the nuts in the end blocks are going through the formwork in wide holes, which are sealed by tape and plastic. After the concrete is enough settled, the dummy bars are removed and the gages are attached whereupon the strain measuring is started. After the tests are finished, the gages are removed from the end blocks, which in turn are unscrewed from the bolts. Owing to this procedure, the gages can be reused in future tests.

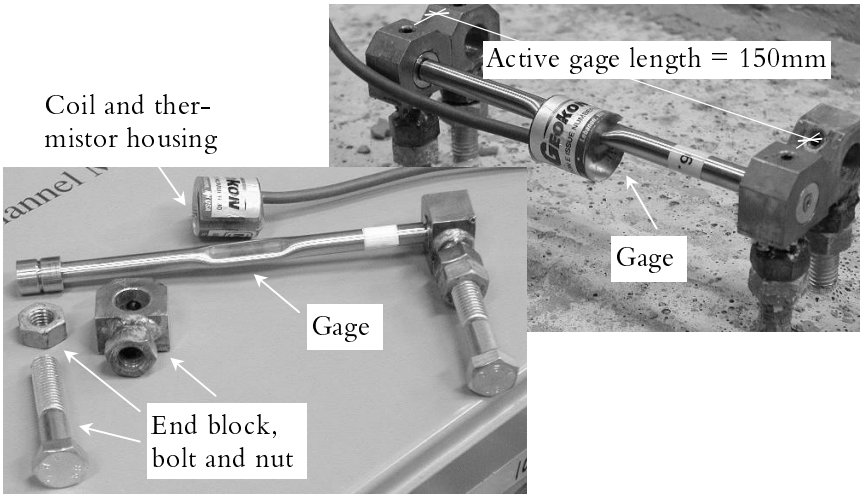

Figure 4.13 *Vibrating Strain Gages (VSG) used in Test I through Test IV.*

In Test I and Test II, five VSG:s were attached at the centre of the wall measuring the horizontal strain variation from the bottom to the top, VSG12-16, see Figure 4.14. The rest of the VSG:s were measuring the strain variations in the wall near the ends of the wall near the casting joint. At the unreinforced joint, six VSG:s were used, were three measured vertically and three measured horizontally, VSG4-6 and VSG1-3, respectively. At the reinforced joint, five VSG:s were used, two measured vertically, VSG10 and 11, and three measured horizontally, VSG7-9, see Figure 4.14.

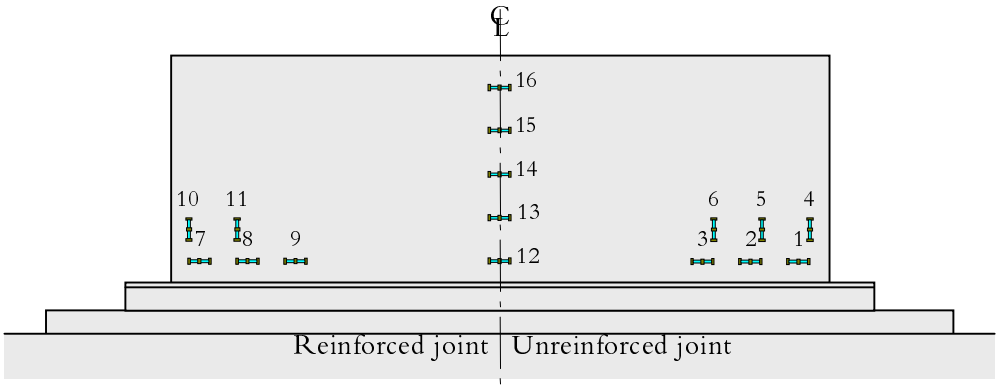

Figure 4.14 *Location of Vibrating Strain Gages (VSG) in Test I and Test II.*

In Test III and Test IV, the VSG:s were rearranged compared to the locations in Test I and Test II. Now the VSG:s were collected closer to the midsection of the walls and all VSG:s measured horizontally, see Figure 4.15. Six of the VSG:s were attached at the third points of the walls, three at each third point at different levels between the bottom and the top of the wall, VSG1-3 and VSG8-10. Four VSG:s were attached at the centre of the wall, measuring the strain variation from the bottom to the top, VSG4-7. Finally, the remaining six VSG:s were measuring the strain variation around the midsection at the middle between the bottom and the top of the wall, VSG11-16.

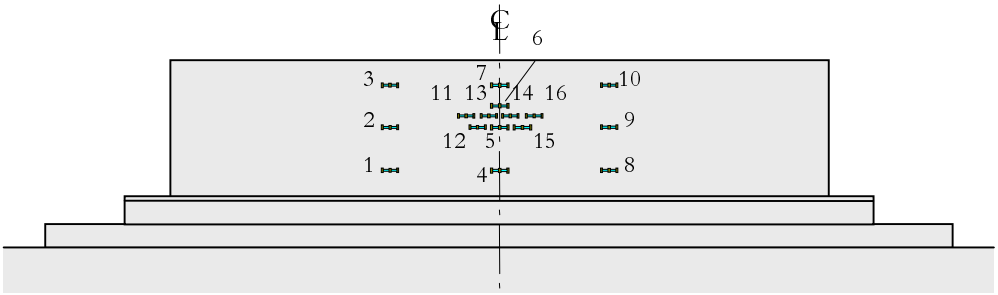

Figure 4.15 *Location of Vibrating Strain Gages (VSG) in Test III and Test IV.*

4.5.4 Slip failures in casting joints

The most important aim of the experiments is to determine whether or not the phenomenon of slip failures in casting joints exist. Therefore, possible propagation of the assumed slip failures in the joints has to be measured. The measuring was done with Crack Detection Gages (CDG) usually utilised to monitor crack opening in rock.

The CDG:s, of type CD-23-50A manufactured by Micro-Measurements, consist of a single strand of high-endurance isoelastic alloy laminated to a strong glass-fibre-reinforced backing. At each joint, several CDG:s are attached perpendicular of the joint being monitored with a conventional strain gage adhesive, see Figure 4.16. Each CDG are connected at both ends to the next CDG making parallel electric circuits. Over the circuits, the electrical resistance is measured. For very, very small tensile or shear stresses, the strands in the CDG:s brake and consequently, the resistance over the electric circuit is increased. The increase of the resistance over the circuit indicates the propagation of a slip failure in the casting joint.

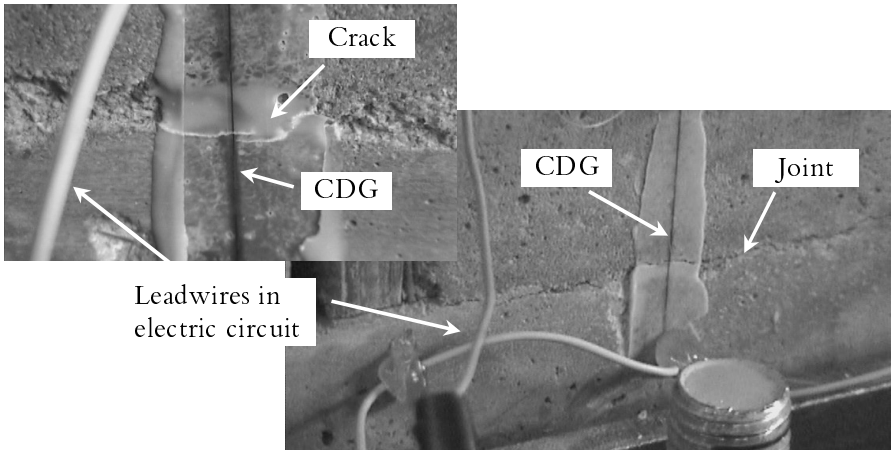

Figure 4.16 *Crack Detection Gages (CDG) as used in Test I trough Test IV, attached perpendicular over a joint with strain gage adhesive and connected to each other at the ends in a parallel electric circuit.*

In Test I, 20 CDG:s were used at the unreinforced joint, see Figure 4.17a. The first CDG was fastened about 50mm from the end of the joint. The rest of the CDG:s were attached about 100mm between each other towards the middle of the wall. In Test II, 10 CDG:s were used to determine the slip failure in the reinforced joint. The CDG:s were attached about 75mm from one another.

In Test III, unfortunately due to problems in removing the formwork at the location of the joints and in attaching the CGD:s across the joint, three CDG:s were used at only one of the joints at the end of the wall. The two first CDG:s were fastened passing the joint about 50 and 160mm from the end of the wall, respectively, whereas the third CDG was fastened about 600mm from the end, see Figure 4.17b.

In Test IV, six CDG:s were attached passing the joint at both ends of the wall. The first CDG:s was attached about 50mm from the ends of the wall, and the rest about 110mm between each, see Figure 4.17c.

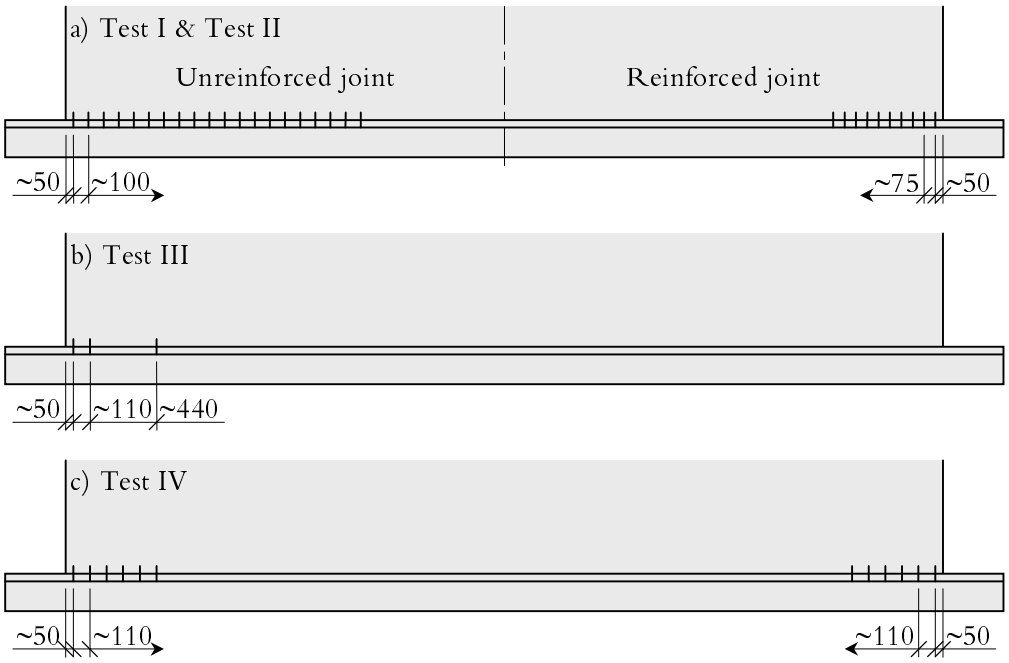

Figure 4.17 *Locations of Crack Detection Cages (CDG) in a) Test I and Test II, b) Test III and c) Test IV.*

4.6 Results

The results from the tests will be separated in three subgroups, relative displacements, cracking of walls and the joints between the walls and the footings (slip failure), and the development of strains. The relative displacements between the parts of the structures, the development of the strains as well as lists of events during the tests are presented in Appendix F, Appendix G and Appendix H, respectively.

4.6.1 Relative displacements

The relative displacements between the different parts of the structures in the tests are shown in Appendix F.

From Test I, the following conclusions can be drawn. Generally, the relative displacements between the parts of the structure coincide in time but not in magnitude with the changing of the water temperature. At the end of the restrained half of the wall, both the horizontal and the vertical relative movements between the different parts are almost zero, except for the upper corner of the wall, see Appendix F, LDT7 and LDT8 in Figures F.2 and F.3. At the upper corner, the movements are larger and follow the changing of the water tem-

perature. Further, at the time of the application of the yokes, the vertical reducing movement of the upper corner of the wall is about 0.35mm, LDT7. Even a small vertical relative movement between the wall and the footing is noticeable, LDT5 and LDT6 in Figures F.3. At the free end of the wall, both the horizontal and the vertical displacements are small during the expansion phase, except for the upper corner of the wall, LDT15 and LDT16 in Figure F.4 and Figure F.5. Right after the water temperature is decreased for the first time, a slip failure in the unreinforced joint took place, implying momentary relative deformations between the parts at the free end of the wall, LDT11 through LDT16. The instantaneous vertical relative lifting displacement between the footing and the wall is about 0.2mm, LDT13 and 14, and about 0.15mm between the upper corner of the wall and the floor in the laboratory, LDT15, see Figures F.4 and F.5. This difference comes from the restraining conditions before the slip failure, that is, the upper corner has previously been free to deform whereas the bottom of the wall has been restrained. The total horizontal and vertical relative displacements between the footing and the wall after the slip failure in the joint are about 0.6mm lifting and 0.4mm shortening. Further, the relative displacement between the upper corner of the wall and the floor in the laboratory is about zero after the slip failure.

Test II was started by again increasing the water temperature going through the wall. Naturally, relative displacements arise between the different parts of the structure, Figure F.6 through Figure F.9. At the still restrained half of the wall, the displacements at the top of the wall is clearly noticeable whereas all other relative movements are small or almost zero. When the yokes are removed from the half of the wall with the reinforced joint, at 144hours after casting, the relative movements at this half of the wall start to coincide with the changing of the water temperature, see Figures F.6 and F.7. At the half of the wall first being free, the horizontal movements clearly follow the changes in water temperature, Figure F.8 and Figure F.9. After the yokes are moved to the top of the wall with no reinforcement in the joint, momentary vertical relative displacements take place at the upper corner of the wall, LDT15, and between the footing and the wall, LDT13 and LDT14. The relative vertical displacement of the upper corner of the wall at the application of the yokes is about 0.6mm pressing up the wall, LDT15. In addition, the upper corner of the wall moves about 0.4mm horizontally in relation to the floor in the laboratory (lengthening the wall), LDT16. This is about the same amount of deformation but in opposite direction as after the slip failure in the unreinforced joint in Test I. After the yokes are applied, the relative movements between all parts are relatively small, about 0.1 to 0.2mm, except between the top corners of the wall and the floor in the laboratory, LDT15 and LDT16.

In Test III, no relative movements were measured between the upper corners of the wall and the floor in the laboratory. The horizontal relative displacements between the floor and the slab and between the slab and the footing are very small during the whole test, LDT1, LDT2, LDT9 and LDT10 in Figures F.11 and F.13. The vertical relative displacements between the footing and the wall show a constant ongoing lifting of the wall in relation to the footing, LDT3, LDT11 and LDT13 in Figures F.12 and F.14. A large difference exists between the results from the vertically measuring between the wall and the footing at one end of the wall, LDT11 and LDT13. LDT13 gives about twice as large values as LDT11. It seems from Figure F.14 that at the beginning of the logging, the results from LDT11 increase rapidly, almost momentary, indicating a possible dislodging of LDT11 at the start of the test.

In Test IV, the slab was lifted and a 10mm thick plastic material was placed between the floor and the slab. When the slab was placed on the plastic material, the slab remained bent upwards at its ends. During Test IV, the horizontal relative displacements between the different parts of the structure are close to zero and even smaller than in the previous tests. The same conditions hold for the vertical relative displacements between the slab and the footing and between the footing and the wall, but not for the relative displacement between the floor and the slab, see Appendix F, Figures F.16 to F.19. Since the slab is totally free to deform, the vertical relative displacement between the floor and the slab is considerable large, LDT5 and LDT9. For one end of the slab, the vertical lifting was about 2mm at the end of the test, LDT5. The results from LDT5 and LDT9 are at the first evaluation contradictory. One end of the slab bends upward and one end bends downwards. At a first thought, both ends should bend upwards. However, the slab contained many transversal cracks before the test and was maybe not in the right condition for being used in the fourth test. Anyhow, as a general conclusion, the fact that only vertical relative displacements were registered for Test IV is perfectly right bearing in mind the boundary restraint condition allowing the structure to freely bend.

4.6.2 Cracking

When the tests are finished and the water was turned off and the measuring was stopped, the formwork of the walls is stripped off. Cracks, and especially through cracks, were then searched for on the surfaces of the walls. In all four experiments, both surface-cracks and through-cracks were found in the walls and in the casting joints between the footings and the walls, except for Test IV, where no slip failure in the joint was found.

Three through cracks were observed in the wall of Test I and Test II, see Figure 4.18a) and b). It is very difficult to tell whether they arise before, during

or after the slip failure in the unreinforced joint. The slip failure in the unreinforced joint occurred immediately after cold water was used for the first time in Test I. The failure in the joint was indicated by the CDG:s. The slip failure in the reinforced joint started about 158hours after casting, that is about 38hours after the start of Test II and about ten hours after the water temperature was first decreased. The slip failures took place step-by-step from reinforcement bars to reinforcement bars. That is, the crack started at the end of the joint and propagated towards the first pair of reinforcement bars. Then after a few hours the cracking propagated further towards the next two bars, and so on. The slip failures were clearly visible by eye, see Figure 4.16. The suggested division of the cracking between Test I and Test II, in accordance with the subfigures a and b of Figure 4.18, are the most probable situation, but at this stage, it has not been proven. Anyhow, this result indicates that through cracks will form very likely if the restraint from adjacent structures is high and/or the restraint-transferring joint is heavily reinforced.

In Test III, five through cracks were found in the wall, see Figure 4.18c). Two of the cracks went all the way from near the joint at the bottom to the top of the wall. One of the through cracks was clearly visible at the top of the wall about 110hours after casting, that is about 54hours after the water temperature first was decreased. The second through crack reaching the top of the wall was found at the end of the test when the water was turned off. Further, the casting joints at both ends of the wall cracked about 0.6m towards the centre of the wall. As in Test I and Test II, the failure propagated from reinforcement bars to reinforcement bars.

In Test IV, only one short through crack was found in the wall after the formwork was removed. The crack was located near the centre of the wall and was about 0.7m long, see Figure 4.18d). No slip failures were determined neither by the CDG:s nor by visual inspection.

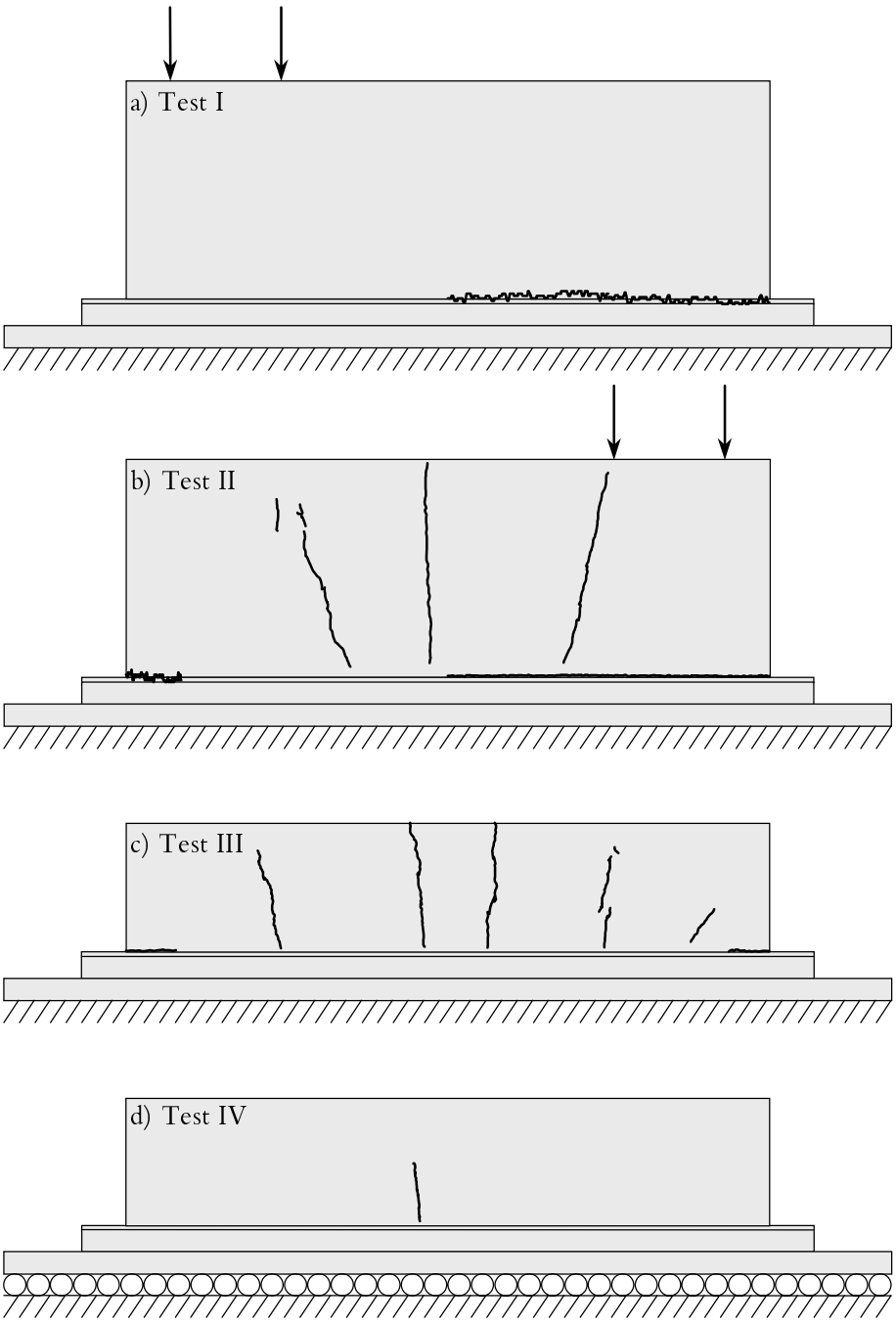

Figure 4.18 *Cracking in joints and walls in Test I through Test IV. The depicted difference between Test I and Test II is the most probable case but is not yet proven.*

The patterns of the through cracks in Test I, Test II and Test III follow the perpendicular directions of the maximum principal stresses in the walls. That is, at the centre of the wall, the maximum principal stresses are oriented horizontally, which results in a vertical decisive crack of the studied structure. Other through cracks are occurring later, and they are therefore not decisive for the structure.

The effect of the different boundary restraint conditions between Test III and Test IV is clearly seen in the amounts of through cracks in the walls and in the slip failures of the casting joints. In Test III, five through cracks arose compared to only one through crack in Test IV. No slip failure was detected in Tests IV but both ends of the joint in Test III cracked. These results originate from the fact that in Test IV, the structure as whole was both free to translate and to rotate whereas in Test III the structure was highly restrained.

4.6.3 Strains and restraint variation

Strains

The results of measuring the strain variation in Test I through Test IV are shown in Appendix G. The results of the strain measuring are started about 10.5hours after casting when the concrete was solid enough to replace the dummy bars with the real gages in the end blocks of the VSG:s. The strain values and the temperature within the gages at this stage are set as the initial values being used when determining the variation of the strain and the restraint in the concrete.

The strains presented are the deformations due to the applied thermal load and shall therefore be corrected for thermal dilatations in the gages and in the concrete. The derivation of the corrected strain is according to the manual for the VSG:s and the logger supplied by the manufacturer, Geokon (1996).

The apparent concrete strain, ε_{app}, is given by

$$\varepsilon_{app} = (\varepsilon_{Gi} - \varepsilon_{G0})G \tag{4.3}$$

where ε_{G0} is the zero reading at temperature T_{G0}, ε_{Gi} is a subsequent reading at temperature T_{Gi} and G = 0.9531 is the calibration factor for the used type of gages, which was supplied by the manufacturer.

To correct for thermal expansion and contraction of the gage itself, the effect is given as

$$\varepsilon_{\Delta T,G} = (T_{Gi} - T_{G0})\alpha_G \tag{4.4}$$

where α_G is the thermal dilatation coefficient of the steel wire in the gage, α_G = $1.22 \cdot 10^{-5}$ 1/°C. The total strain in the concrete corrected for thermal effects on the gage is then given as

$$\varepsilon_{tot} = \varepsilon_{app} + \varepsilon_{\Delta T,G} = (\varepsilon_{Gi} - \varepsilon_{G0})G + (T_{Gi} - T_{G0})\alpha_G \tag{4.5}$$

The total strains, ε_{tot}, include both thermally induced strains in the concrete and those induced by stress, i.e.

$$\varepsilon_{tot} = \varepsilon_{stress} + \varepsilon_{\Delta T,c}$$

giving the searched strains associated with stress as

$$\varepsilon_{stress} = \varepsilon_{tot} - \varepsilon_{\Delta T,c} \tag{4.6}$$

To correct for thermal expansion and contraction of the concrete itself, the effect is given as

$$\varepsilon_{\Delta T,c} = (T_{ci} - T_{c0})\alpha_{\Delta T,c} \tag{4.7}$$

where $\alpha_{\Delta T,c}$ is the formal thermal dilatation coefficient in expansion and contraction phases, respectively, of the concrete. For the actual concrete, the thermal dilatation coefficients have been determined in three thermal dilatation tests giving the values

$$\alpha_{\Delta T,i} = \begin{cases} \alpha_e = 9.5 \cdot 10^{-6} \ ^\circ\mathrm{C}^{-1} & \text{at expansion} \\ \alpha_c = 10.8 \cdot 10^{-6} \ ^\circ\mathrm{C}^{-1} & \text{at contraction} \end{cases} \tag{4.8}$$

Equation (4.5) and Equation (4.7) in Equation (4.6) finally give the stress induced strain, ε_{stress}, according to

$$\varepsilon_{stress} = (\varepsilon_i - \varepsilon_0)G + (T_{Gi} - T_{G0})\alpha_G - (T_{ci} - T_{c0})\alpha_{\Delta T,c} \tag{4.9}$$

In addition, the effects of shrinkage have to be considered to achieve the right results regarding the strains, that is

$$\varepsilon_{stress} = (\varepsilon_i - \varepsilon_0)G + (T_{Gi} - T_{G0})\alpha_G - (T_{ci} - T_{c0})\alpha_{\Delta T,c} - \varepsilon_{sh} \tag{4.10}$$

where ε_{sh} is the shrinkage induced strain. Equation (4.10) is the formula used for calculation of the strains presented in Appendix G.

The variation of the strains associated with stress according to Equation (4.9) in the walls in Test I through Test IV, are shown in Appendix G. The use of strain associated with stress, assuming Equation (4.9) is quite correct, means that if no crack is passing between the bolts of an individual VSG, the word strain can qualitatively be interchanged by the word stress.

The variation of the strains should coincide with the changing of the water temperature. During the increase of the water temperature, the strains should decrease; that is, compressive strains should be registered. After the water temperature has passed the maximum, and started to decrease, the strains should in turn start to increase and after some time, tensile strains should be registered. Due to the different restraint conditions at the locations of the VSG:s, the measured strains differ. With increased distance from the centre of the wall and from the casting joint, the stress-induced strains should be lower due to the lower restraint.

In Test I, the applications of the yokes are clearly noticeable, see Figures G.4 and G.5, especially the vertical strains measured through VSG10 and VSG11. Before the yokes are applied, the variation of the strain at both the ends of the wall varies equally. After the application of the yokes, the vertical variation of the strains is roughly equal, Figures G.3 and G.5. The horizontal variation of the strains are small or almost zero at the free half of the wall compared to the restrained half, see Figures G.2 and G.4. After the slip failure, the strains at the centre of the wall are larger at the bottom of the wall, VSG12, and smaller at the top, VSG16, see Figure G.6. Any effects of the slip failure in the unreinforced joint are not easily seen in the diagrams. Large restraint stresses may not yet been arisen at the time for the slip failure, implying no large strain changes could take place.

In Test II, the effects of the moving and the application of the yokes are clearly noticeable. At the moving of the yokes from the firstly restrained half of the wall, the strains increased noticeably compared with the values before the moving of the yokes, see Appendix G, Figure G.10. After the moving of the yokes and the slip failures in the reinforced joint, the absolute strain values in VSG:s close to one another differ more, VSG4 - VSG6, VSG7 - VSG9 and VSG10 - VSG11. The changing of the water temperature is clearly visible in all VSG:s.

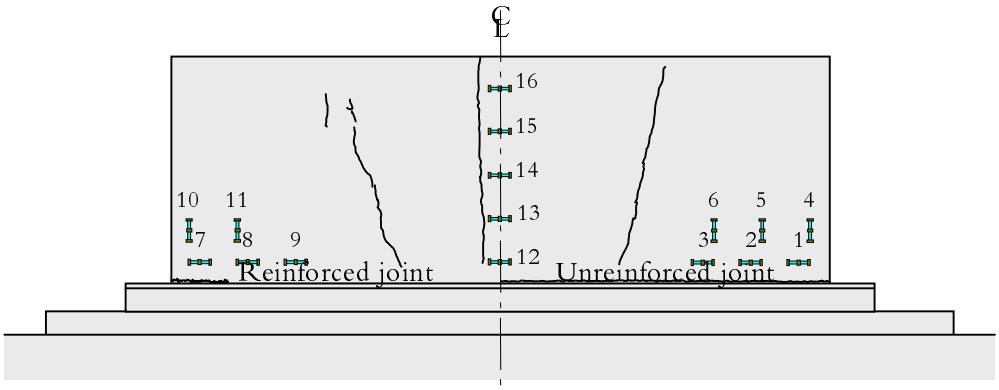

Figure 4.19 *Location of vibrating strain gages in relation to formed through cracks in the wall and in the casting joint in Test I and Test II.*

The strain variations in Test III are small, at maximum about $200 \cdot 10^{-6}$, see Appendix G, Figures G.13 to G.16. The strains at the thirds of the wall, VSG1 through VSG3 and VSG8 through VSG10 are very similar both in magnitude and in variation. The strains in the mid-section are smaller than in the thirds, which is unlogical and contradictory to what is expected. Further, as can be seen in Figure 4.20, one of the through cracks goes within the active gage length of VSG11 and VSG12. The effect is very apparent in the strain values from theses gages, see Appendix G, Figure G.16, showing momentary increased values at about 110hours after casting.

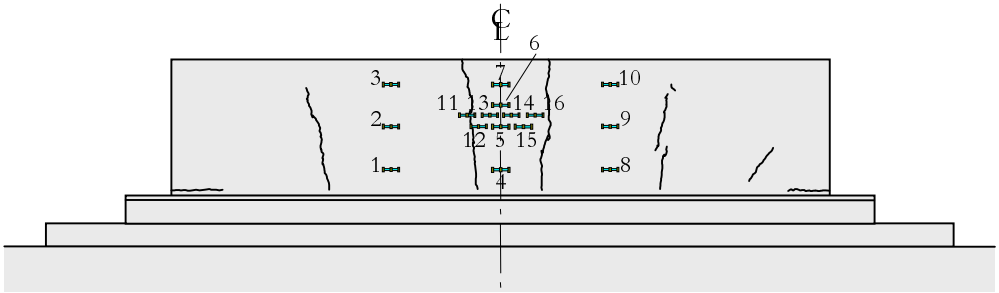

Figure 4.20 *Location of vibrating strain gages in relation to formed through cracks in the wall and in the casting joint in Test III.*

In Test IV, the variation of the strains is a little smaller than in Test III. This is the effect of the boundary restraint condition. In a structure subjected to severe boundary restraint, Test III, the strains are higher than in a structure sub-

jected to mild restraint conditions, Test IV. In the same context, the strains are smaller at the free top of the wall than at the bottom. See Appendix G, Figure G.18 through Figure G.21. The single through crack arisen in Test IV has not effected the VSG:s as what can be seen from the results. VSG4 and VSG12 are the closest gages to the crack, see Figure 4.21. As in Test III, the strains in the thirds are larger than in the middle of the wall, which again is unlogical.

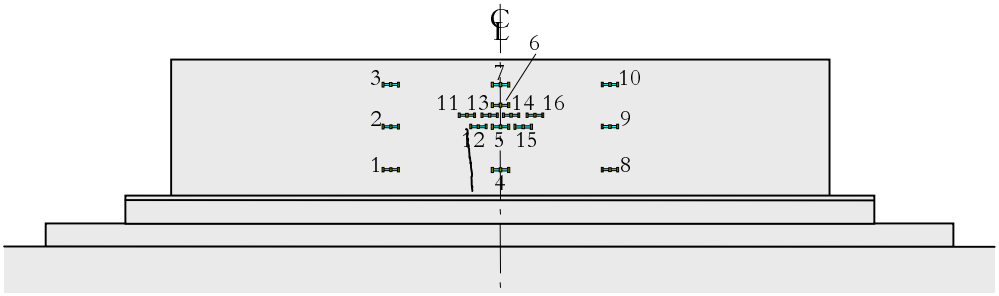

Figure 4.21 *Location of vibrating strain gages in relation to formed through cracks in the wall and in the casting joint in Test IV.*

Malfunction of strain measurements

As been indicated in the previously description of the strain measuring in the four tests, the results are suspected not being reliable. The stress related strains in the middle of the walls in Test III and IV were smaller than in the thirds.

As described above, the strains are measured through the frequency in the wire in the VSG:s. The strain in the wires depends on the tension of the wire as well as the temperature within the wire. Since the VSG:s were attached at the surface of the walls through steel bolts, see Figure 4.13, it can be suspected that the higher temperature of the concrete is transferred through the bolts into the end blocks of the VSG:s and then to the wires. Then the question is arisen about how the frequency of the wire is dependent on the different temperature within the wire? Since the temperature and the frequency are measured at the middle of the VSG:s, there is a risk that the wrong strain values are obtained in the evaluation.

Therefore, a thorough investigation of the VSG:s was done in addition to the wall tests to study the behaviour of the VSG:s as such. The investigation was performed through thermal dilation tests, a test of temperature variations within the gages, and a test with cast in gages and gages on the surface of a small reference wall.

Firstly, two thermal dilation tests were performed of the actual concrete. On a concrete specimen, 0.3m high, 0.07m in diameter and placed under sealed conditions in a sarcophagus, the strain variation is measured trough a temperature cycle simulating the hydration phase. Ordinarily, in these tests, the strain variation is measured through a type of graphite gages, which have been used for several years with reliable results. Theses measures were enhanced with measuring with VSG:s for a comparison of the results to check the strains. From these thermal dilation tests, the thermal dilation coefficients were determined, $\alpha_{\Delta T,c}$. In this connection, the shrinkage of the concrete was also determined, $\varepsilon_{sh}(t)$. The results of the two thermal dilation tests are shown in Figure 4.22. In the first test, Test1, the strains measured with the VSG:s were larger than the strains measured with the graphite gages. It might have been possible to find a correction factor for the VSG:s, but anyhow, the strains would have differed at the end of the test. In Test2, the strains differ even more than in Test1. The strains are not close to be parallel and could not have been corrected by any factor.

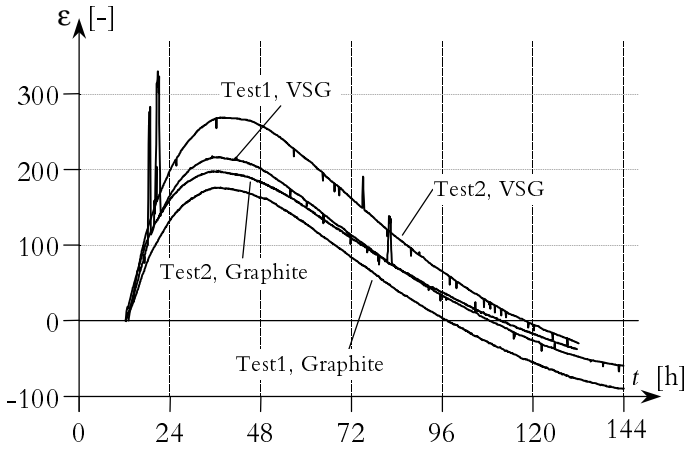

Figure 4.22 *Strains from tests of VSG behaviour as such.*

Secondly, a tests of the temperature differences in the VSG:s were performed. On one VSG with end blocks and bolts, the temperature was measured on the bolts, the end blocks and the protective steel tube during a temperature time development, see Figure 4.23. It was found that the temperature differs in the parts of the VSG. The VSG was mounted with its bolts in water, the same water that is used to change the temperature in the thermal dilation test. The temperature was found being highest in the bolts, a bit lower in the end blocks and at the ends of the steel tube, even lower on the steel tubes and lowest at the

middle, Figure 4.23. At the middle the coil and thermistor housing is attached, which is the point where the temperature that is corrected for is measured. If these higher temperatures are transferred through the protective steel tube in to the wire is not sure at present writing. But if the temperature is higher in the ends of the wire, then, how is that effecting the frequency and thereby the strain measured with the VSG:s?

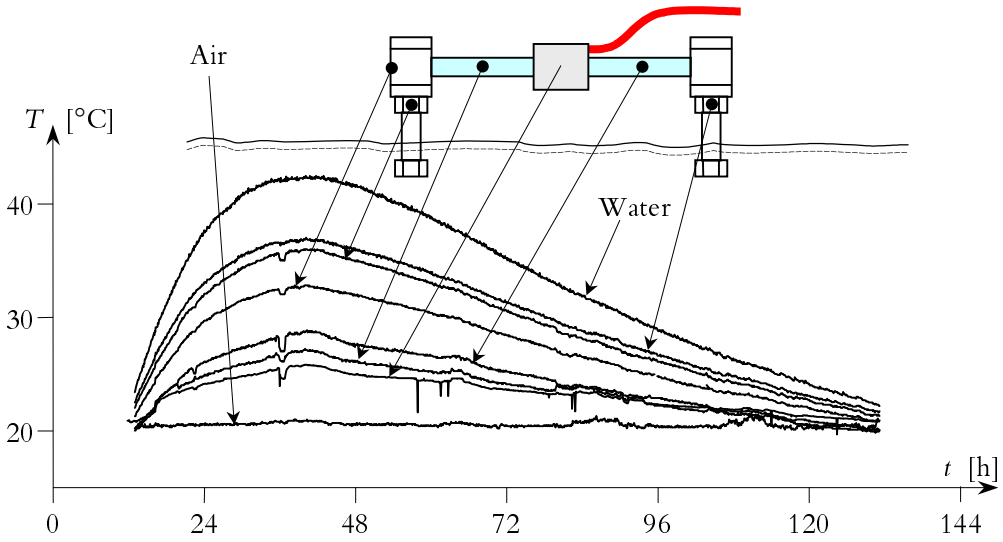

Figure 4.23 *Results from testing of temperature variation in VSG:s.*

Thirdly, a test with a small reference wall was performed. The test was designed to be the original wall-on-slab tests as like as possible. On a slab, 0.45m wide, 0.15m high and 0.9m long, a wall was cast, 0.15m thick, 0.3m high and 0.9m long, see Figure 4.24. The form was made of 12mm thick plywood, which was only loosened and then left in place during the whole test. In the wall, steel pipes for water were cast. At two places in the wall, two VSG:s were cast in. At the same positions, two VSG:s were attached on the surface of the concrete in the same way as in the real tests, see Section 4.5.3. The strains were then measured during the whole hydration phase of the concrete, which lasted until about 24hours after casting. Additionally, during a continuation of the test when the water pipes were used to load the structure with additional thermal stresses the strain variation was also measured.

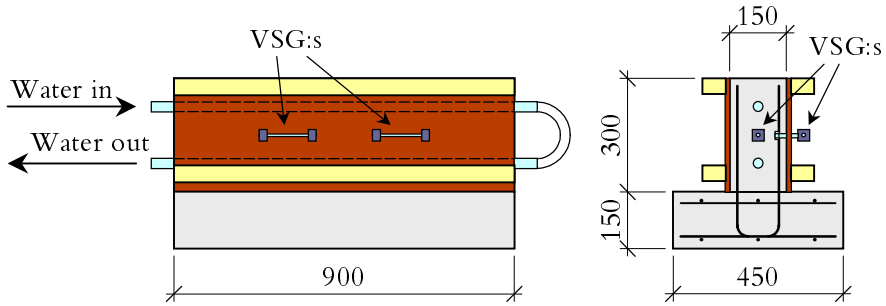

Figure 4.24 *Description of reference wall for test of VSG:s.*

From the test with the reference wall it was found that the VSG:s attached to the surface did not give the same values as the two VSG:s that were cast in the wall, see Figure 4.25. Firstly, during the heating phase, until 24hours after casting, the values followed one another quit well except for one of the gages at the surface that started to contract earlier than the others. During the contraction phase, the strains measured with the outer gages were parallel but not equal whereas the strains measured within the wall were parallel and almost equal. Nevertheless, the strains measured at the surface were not equal to the strains measured within the wall. During the continuation of the test, the strains measured on the surface of the wall were always larger in relation to the strains measured within the wall. That is, during the expansion, the compressive strains were larger and during the contraction, the tensile strains were larger on the surface relatively within the wall. No correlation has been found between the strains measured on the surface and the strains measured within the wall.

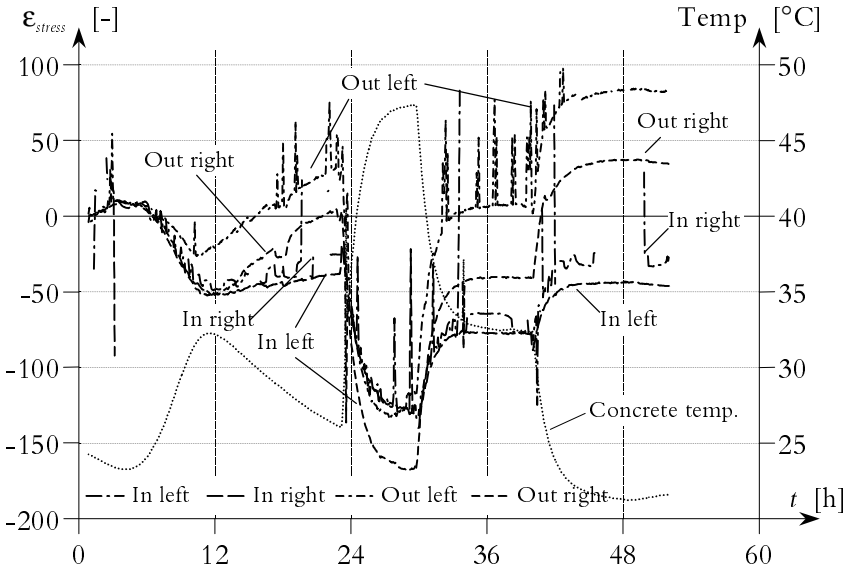

Figure 4.25 *Strains in test of cast in VSG:s and VSG:s attached at the surface of reference wall.*

Unfortunately, one severe conclusion is drawn from these tests of strain measures with VSG:s attached on the surface of a concrete structure with changing temperature. The strains measured in Test I through Test IV are not representative for the real strain cases and can therefore not be used to calculate the restraint development in the structures.

Restraint variation

The variation of restraint over time can be determined by a Relaxation Integral Method (RIM) presented in Larson (2000) as

$$\gamma_R(x,y,t) = \frac{\int_t R(t,t_0)d\varepsilon_{stress}(t)}{\int_t R(t,t_0)d\varepsilon^0(t)} \tag{4.11}$$

where

$R(t,t_0)$ is the relaxation function, [MPa]
$\varepsilon_{stress}(t)$ is the development of the strains induced by load changes (i.e. measured or calculated strains), [-]
$\varepsilon^0(t)$ is the inelastic strain development, [-]
t_0 is the time of loading, [h]

The relaxation function $R(t,t_0)$ is determined as

$$R(t,t_0) = E_c(t_0)\left(1 - \frac{\varphi(t,t_0)}{1+\chi(t,t_0)\varphi(t,t_0)}\right) \tag{4.12}$$

where

$E_c(t_0)$ is the modulus of elasticity, [MPa]
$\varphi(t,t_0)$ is the creep function or creep coefficient at time t for loading at t_0, [-]
$\chi(t,t_0)$ is the ageing coefficient, $0 < \chi(t,t_0) \leq 1$, [-]

The modulus of elasticity at the time of loading is calculated as, Larson (2000)

$$E_c(t_0) = E_{ref}\sqrt{\exp\left\{0.19\left(1 - \sqrt{\frac{28}{t_0 - t_s}}\right)\right\}} \tag{4.13}$$

with the reference value of the modulus of elasticity E_{ref} chosen as the value at the age of 28 days.

The creep function $\varphi(t,t_0)$ is calculated as

$$\varphi = \varphi_{ref}(\Delta t_{load}, t_0)\frac{E_c(t_0)}{E_{ref}} \tag{4.14}$$

where

$$\varphi_{ref}(\Delta t_{load}, t_0) = \phi_0 \beta_c(\Delta t_{load})\beta_\phi(t_0) \tag{4.15}$$

Δt_{load} is the time span after loading expressed as t-t_0, [days]
ϕ_0 is a reference creep coefficient, 1.5 for the reference concrete, [-]
$\beta_c(\Delta t_{load})$ is a time development function for the creep deformations, [-]
$\beta_\phi(t_0)$ is a coefficient considering relative creep at loading ages less than 28days, [-]

The time development function $\beta_c(\Delta t_{load})$ is modelled by

$$\beta_c(\Delta t_{load}) = \left(\frac{\Delta t_{load}}{1000 + \Delta t_{load}}\right)^{0.3} \tag{4.16}$$

and the coefficient considering relative creep at loading ages less than 28 days as

$$\beta_\phi(t_0) = \begin{cases} \dfrac{\exp\left(\sqrt{\dfrac{5}{t_0}}\right)}{1.5} & \text{for } 0.60 \le t_0 \le 28\text{days} \\ 1 & \text{for } t_0 > 28\text{days} \end{cases} \tag{4.17}$$

The ageing coefficient $\chi(t,t_0)$ is calculated as, Larson (2000),

$$\chi(\Delta t_{load}, \alpha) = \begin{cases} 0.45 & \text{for } \alpha < 0.2 \\ 0.45 + \exp\left\{\left(\dfrac{1}{\Delta t_{load}}\right)^{0.2}\right\}\dfrac{\alpha - 0.2}{3} & \text{for } 0.2 \le \alpha \le 0.8 \\ 1.00 & \text{for } \alpha > 0.8 \end{cases} \tag{4.18}$$

with α denoting the degree of hydration/maturity at the time of loading. α can be determined as

$$\alpha = \alpha^\star \alpha_{\max} \tag{4.19}$$

where $\alpha_{\max}$ ($\le$1) is the final degree of hydration in practice, see for instance Jonasson (1994) and Ekefors (1995). $\alpha^\star$ is the portion of the final degree of hydration in practice, $\alpha_{\max}$, and may according to Jonasson (1984) be expressed as

$$\alpha^\star = \exp\left\{-\lambda_1\left[\ln\left(1 + \frac{t_e}{t_q}\right)\right]^{-\kappa_1}\right\} \tag{4.20}$$

where λ_1, t_q and κ_1 are coefficients to be defined from tests for the specific concrete. t_e is the equivalent age and can be determined as

$$t_e = \int_0^t \beta_T dt \tag{4.21}$$

where β_T is the temperature rate factor describing the difference in hydration rate depending on the actual temperature. β_T can be described by the Arrhenius equation for thermal activation, assuming a linear relationship between the compressive strength and the degree of hydration, Byfors (1980),

$$\beta_T = \begin{cases} 0 & \text{for } T \le -10^\circ\text{C} \\ \exp\left(\theta\left(\dfrac{1}{T_{ref}} - \dfrac{1}{T + 273}\right)\right) & \text{for } T > -10^\circ\text{C} \end{cases} \tag{4.22}$$

where

T_{ref} is the chosen reference temperature, here +20°C, [°C]
θ is the activation temperature, here $\theta = \theta_{ref}$ = 4400K, Hedlund (2000), [K]

4.7 Concluding Remarks

The first aim regarding the verification of the phenomenon of slip failure in casting joint loaded by restraint stresses has been achieved through Test I, Test II and Test III. In Test IV, the boundary restraint condition, free translation and rotation, implied the stresses in the structure being to low resulting in no slip failures in the casting joint.

The formed slip failures in the reinforced casting joints in Test II and Test III are distinct and the phenomenon has been shown. However, the influence of the casting joint properties has not been verified. That is, the structure in the two joints in the tests is the same, sand of fraction 0.212 - 1mm, but the amounts of through reinforcements are different, 1% (2×∅12 *s*150) in Test II and 0.6% (2×∅8 *s*110) in Test III. The only conclusions that can be drawn from these two tests regarding the slip failures are the following. Firstly, the failures start at the ends of the joints, secondly, they propagate from reinforcement bars to reinforcement bars inwards along the joints. Thirdly, the amounts of reinforcement used here have minor influence on the slip. No difference has been found between Test II and Test III, which were subjected to the same boundary restraint conditions but different amounts of through reinforcement in the casting joints.

From the measuring of the strains, it is possible to determine the time after casting when though cracks arise. The slip failures in the casting joints are also traceable from the strain measuring. Further, from the development of the strains, the development of the restraint can be determined. Unfortunately, in the tests performed within this thesis, the values of the measured strains were not reliable, wherefore no restraints were calculated.

The idea of performing two tests on one structure was purely of economic reasons and due to limited available space in the laboratory. The doubts against this technique are, first, the effects of the two yokes loading the walls. Where is the assumed centre of dilatation located exactly? Do the yokes really prevent the loaded half of the wall from moving? Although these questions were answered positively, doubts will remain about a second test performed on the same structure, as the concrete is no longer young when a second test is conducted.

4.8 Continuation and Future Work

Further experiments are needed to find, if any, the influence of the amounts of through reinforcement in the joints on the slip failure propagation and on the risk of through cracking of the walls.

The conditions of the joints regarding the texture of the surfaces have to be further investigated. In the performed tests only one, but very well defined, texture of the surfaces was used. In future tests, perhaps the joint conditions shall be as authentic as possible meaning if footings are used, they shall not be cast upside-down, but letting the joint conditions be what they become from the casting of the old parts. Maybe the cohesion in the joint shall be reduced allowing the slip failures, which in turn reduce the restraint stresses causing through cracks in the walls.

The use of the same slab in all four tests is in some respects not appropriate. After the Test III, when the slab was loosened, it was lifted and several transverse cracks were found. When the slab was put back down on the floor, remaining deformations from the lifting and previous tests were present. In future tests, new slabs will be used in every test being performed.

In future tests such as these performed here, no vibrating strain gages attached at the surface of the concrete will be used. Instead, a type of vibrating strain gage that is designed to be cast into the concrete is preferable to avoid the risk of thermal differences within the gages.

5 Summary and Conclusions

5.1 Partial Coefficients for Thermal Cracking

Partial coefficients for thermal-cracking problems of young concrete have been calculate by a probabilistic method. The values presented in this thesis coincide well with crack safety values stated in the Swedish Building Code for Bridges, BRO94 (1999). However, the calculated values of the partial coefficient are based on many assumptions and simplifications and they shall not be seen as what are right, further judgements are necessary.

In the calculations of the partial coefficients, coefficients of variation of the thermal changes and of the shrinkage are needed. The values are roughly taken from Jonasson et al. (1994) and are only assumed values that are not being well verified and therefore need further investigations. Other assumptions and material data may lead to other values of the partial coefficients.

The crack safety values in BRO94 (1999) are all based on experience, meaning these values are a bit vague. The calculated partial coefficient presented here can be seen as an attempt of verification of the values in BRO94 (1999). However, all estimations of the risks of thermal cracking of young concrete have to be based on more judgements and analyses of the problems as whole rather than on the crack safety values given in BRO94 (1999).

Effects of environmental classes on differences in partial coefficients for thermal cracking problems need further investigations. The values that are stated in BRO94 (1999) are only based on logical arguments, meaning that higher environmental class needs higher partial coefficients.

5.2 Coefficients of Restraint

The restraint in representative points in structures assuming plane sections remaining plane can be determined by the introduced model. The model is based on a formulation for prestressed concrete beams, Collins & Mitchel (1991), that here is modified for problems of hydrating concrete structures. The model depends on the translational and rotational boundary restraint from foundation materials and on the height, area and modulus of elasticity ratios of adjoining and young parts of structures as well as the volume changes of the different parts.

Graphical application tools for simple structures are given for determination of the plane-section restraint in decisive points. The tools are valid for rectangular young concrete parts cast on rectangular older parts. The modulus of elasticity in the young part is 95% of the modulus of elasticity in the older and adjoining part. The volume changes in the adjoining part are equal to zero. The model is dependent on the translational and rotational boundary restraint from adjoining foundation materials. For the case of total rotational boundary restraint, the plane-section restraint in a decisive point is determined from one diagram depending on the translational boundary restraint and the area ratio of the old and young parts. For all other cases, the plane-section restraint in decisive points is given in twenty-five diagrams. The restraint is depending on the height and the area ratios of the old and young parts and on the amounts of translational and rotational boundary restraints from adjoining foundation materials.

For shorter structures, that is, with length to height ratios smaller than about five, plane sections do not remain plane when deforming, which here is expressed by resilience functions. A method is presented for the determination of resilience factors for the cases of walls cast on a slabs. The method is based on finite element calculations of stresses and strains, plane-section analysis of curvature and geometrical properties. The requirement for the model is that the curvature obtained by plane-section analysis has to be equal to the curvature in reality (e.g. found in the FE-analysis). Therefore, an effective width is introduced in the analytical model for the condition that the curvature equals the curvature obtained in FE-calculations. From the calculated stresses through the FE-calculation, the curvature and geometrical properties through the plane-section analysis, the resilience factors are evaluated as a function of the vertical coordinate in the wall.

In many cases, the young part of a structure is not located symmetrically on the adjoining older part. The effects on the resilience factor as well as the effective width have been studied in an example for the structure wall on slab. It has

been shown that for more unsymmetrical structures, larger resilience factors are needed then for symmetric structures. On the other hand, for the effective width, the location of the young part has great influence. Young parts located at the edges of older parts need smaller effective widths than young parts located at the centre of the old part.

Analytical models have been derived and presented for determination of the rotational boundary restraint from elastic materials on deforming concrete structures during the hydration phase. The models are valid both for structures that are totally resting on the foundation and for structures with lifting ends. The models depends on the stiffness and compaction of the ground material and the bending stiffness and geometric properties of the structures.

The effect of the age of the young concrete on the rotational boundary restraint has been studied and introduced in the models of rotational boundary restraint. The influence is introduced by the time dependent modulus of elasticity and bending stiffness. The modulus of elasticity is temperature dependent. However, the stiffness growth of structures is generally very rapid implying the influence of time on the rotational boundary restraint being negligible.

For the models of plane-section restraint coefficient, resilience factors and effective areas, further calculations and studies are needed before any more general conclusions can be drawn.

5.3 Medium Scale Experiments of Walls Cast on Slabs and Loaded by Restraint Stresses

The verification of the phenomenon of slip failure in casting joints loaded by restraint stresses has been achieved through Test I, Test II and Test III. In Test IV, the boundary restraint condition, free translation and rotation, implied the stresses in the structure being to low resulting in no slip failures in the casting joint.

The formed slip failures in the reinforced casting joints in Test II and Test III are distinct and the phenomenon has been shown. However, the influence of the casting joint properties has not been verified. That is, the structure in the two joints in the tests is the same, sand of fraction 0.212 - 1mm, but the amounts of through reinforcements are different, 1% (2×∅12 *s*150) in Test II and 0.6% (2×∅8 *s*110) in Test III. The only conclusions that can be drawn from these two tests regarding the slip failures are the following. Firstly, the failures start at the ends of the joints, secondly, they propagate from reinforcement bars to reinforcement bars inwards along the joints. Thirdly, the amounts of reinforcement used here have minor influence on the slip. No difference has been found between Test II and Test III, which were subjected to the same bound-

ary restraint conditions but different amounts of through reinforcement in the casting joints.

Further experiments are needed to find, if any, the influence of the amounts of through reinforcement in the joints on the slip failure propagation and on the risk of through cracking of the walls.

The conditions of the joints regarding the texture of the surfaces have to be further investigated. In the performed tests only one, but very well defined, texture of the surfaces was used. In future tests, perhaps the joint conditions shall be as authentic as possible meaning if footings are used, they shall not be cast upside-down, but letting the joint conditions be what they become from the casting of the old parts. Maybe the cohesion in the joint shall be reduced allowing the slip failures, which in turn reduce the restraint stresses causing through cracks in the walls.

From the measuring of the strains, it is possible to determine the time after casting when though cracks arise. The slip failures in the casting joints are also traceable from the strain measuring. Further, from the development of the strains, the development of the restraint can be determined. Unfortunately, in the tests performed within this thesis, the values of the measured strains were not reliable, wherefore no restraints have been calculated.

In future tests such as these performed here, no vibrating strain gages attached at the surface of the concrete will be used. Instead, a type of vibrating strain gage designed to be cast into the concrete is preferable to avoid the risk of thermal differences within the gages.

The idea of performing two tests on one structure was purely of economic reasons and due to limited available space in the laboratory. The doubts against this technique are, first, the effects of the two yokes loading the walls. Where is the assumed centre of dilatation located exactly? Do the yokes really prevent the loaded half of the wall from moving? Although these questions were answered positively, doubts will remain about a second test performed on the same structure, as the concrete is no longer young when a second test is conducted.

The use of the same slab in all four tests is in some respects not appropriate. After Test III, when the slab was loosened, it was lifted and several transverse cracks were found. When the slab was put back down on the floor, remaining deformations from the lifting and previous tests were present. In future tests, new slabs will be used in every test being performed.

References

AK79/81 (1982). *Allmänna regler för bärande konstruktioner. Principer, rekommendationer och kommentarer samt exempel på tillämpning* (1982). (General Regulations for Structures. Principles, Recomendations, Comments and Examples of Application). Stockholm, Sweden: Statens Planverk, Rapport nr 50, Liber 1982, pp. 159. ISBN 91-38-07090-1. (In Swedish).

BBK94 (1994). *Boverkets handbok om betongkonstruktioner* (1994). (The Swedish Building Administrations Handbook on Concrete Structures). Part 2 - Material, Performance and Control. Stockholm, Sweden: The Swedish Building Administration, Division of Buildings. pp. 116. ISBN 91-7332-687-9. (In Swedish).

BBK94 (1995). *Boverkets handbok om betongkonstruktioner* (1995). (The Swedish Building Administrations Handbook on Concrete Structures). Part 1 - Design. Stockholm, Sweden: The Swedish Building Administration, Division of Buildings. pp. 185. ISBN 91-7147-235-5. (In Swedish).

Bernander, S (1973). Cooling by Means of Embedded Cooling Pipes. Applications in Connection with the Construction of the Tingstad Tunnel, Gothenburg. *Nordisk Betong, n:o 2-73*. pp. 21-31. (In Swedish).

Bernander, S (1982). Temperature Stresses in Early Age Concrete Due to Hydration. In: *Proceedings from International Conference on Concrete at Early Ages, RILEM, held in Paris, France on 6-8 April 1982*. Vol II. pp. 218-221.

Bernander, S (1993). *Balk på elastiskt underlag åverkad av ändmoment M_1* (Beam on Resilient Ground Loaded by Bending Moments M_1 at its Ends). Gothenburg, Sweden: ConGeo AB. Notes and calculations with diagrams. (In Swedish).

Bernander, S (1998). Practical Measures to Avoiding Early Age Thermal Cracking in Concrete Structures. In: *Prevention of Thermal Cracking in Concrete at Early Ages*. Ed. by Springenschmidt, R. London, UK: E & FN Spon. RILEM Report 15. pp. 255-314. ISBN 0-419-22310-X.

BRO94 (1999). *BRO94 Allmän teknisk beskrivning för broar, 9. Förteckning* (1999). (General Technical Description for Bridges, BRO94, 9. Catalogue). Borlänge, Sweden: Swedish National Road Administration. Publ 1999:20. pp. 139. ISSN 1401-9612. (In Swedish).

Byfors, J (1980). *Plain Concrete at Early Ages*. Stockholm, Sweden: Swedish Cement and Concrete Research Institute. Fo/Research 3:80.

CEB-FIP Model Code 90 (1993). Comité Euro-International du Beton, Bulletin D information No. 213/214. London, UK: Thomas Telford Publishing. pp. 473.

Collins, M, P & Mitchell, D (1991). *Prestressed Concrete Structures*. Englewood Cliffs, New Jersey, U.S.A.: Prentice-Hall Inc. pp. 766. ISBN 0-13-691635-X.

ConTeSt Pro (1999). *Användarhandbok - ConTeSt Pro* (Users manual - Program for Temperature and Stress Calculations in Concrete). Developed by JEJMS Concrete AB in co-operation with Luleå University of Technology, Cementa AB and Peab Öst AB. Danderyd, Sweden: Cementa AB. pp. 207. (In Swedish)

Degerman, T (1981). *Dimensionering av Betongkonstruktioner enligt sannolikhetsteoretiska metoder* (Design of Concrete Structures with Probabilistic Methods). Lund, Sweden: Department of Building Technology, Lund Institute of Technology. Report TVBK-1003. 353 pp. (In Swedish).

Ekerfors, K (1995). *Mognadsutveckling i ung betong. Temperaturkänslighet, hållfasthet och värmeutveckling*. (Maturity Development in Young Concrete. Temperature Sensitivity, Strength and Heat Development). Luleå, Sweden: Division of Structural Engineering, Luleå University of Technology. Licentiate Thesis 1995:34L. pp. 136.

Emborg, M & Bernander, S (1994). Assesment of the Risk of Thermal Cracking in Hardening Concrete. In: *Jounal of Structural Engineering (ASCE), Vol 120, No 10, October 1994*. New York, U.S.A. pp. 2893-2912.

Emborg, M (1989). Thermal Stresses in Concrete Structures at Early Ages. Luleå, Sweden: Division of Structural Engineering, Luleå University of Technology. Doctoral Thesis 1989:73D. pp. 285.

Emborg, M, Bernander, S, Ekefors, K, Groth, P & Hedlund, H (1997). *Temperatursprickor i betongkonstruktioner - Beräkningsmetoder för hydratationsspänningar och diagram för några vanliga typfall* (Temperature Cracks in Concrete Structures - Calculation Methods for Hydration Stresses and Diagrams for some Common Typical Examples). Luleå, Sweden: Luleå University of Technology. Technical Report 1997:02. 100 pp. ISSN 1402-1536. (In Swedish).

Geokon (1996). *Instruction Manual Models VCE-4200/4202/4210 Vibrating Wire Strain Gages*. Lebanon, U.S.A.: Geokon, Inc., Geotechnical Instrumentation. pp. 18.

JCI (1992). *A Proposal of a Method of Calculating Crack Width due to Thermal Stress* (1992). Tokyo, Japan: Japan Concrete Institute, Committee on Thermal Stress of Massive Concrete Structures. JCI Committee Report. pp. 106.

Jonasson, J-E (1994). Krympning hos hårdnad betong (Shrinkage in Hardened Concrete). In: *Betonghandbok - Material*. (Concrete Handbook - Material). Edition 2. Stockholm, Sweden: AB Svensk Byggtjänst and Cementa AB. pp. 524-545. ISBN 91-7332-709-3. (In Swedish).

Jonasson, J-E, Emborg, M & Bernander, S (1994). Temperatur, mognadsutveckling och egenspänningar i ung betong (Temperature, Maturity Growth and Eigenstresses in Young Concrete). In: *Betonghandbok - Material*. (Concrete Handbook - Material). Edition 2. Stockholm, Sweden: AB Svensk Byggtjänst and Cementa AB. pp. 547-607. ISBN 91-7332-709-3. (In Swedish).

Larson, M (1999). Evaluation of Restraint from Adjoining Structures. In: *Midterm Assessment of Improved Production of Advanced Concrete Structures - IPACS*. Malmö, Sweden: NCC Teknik AB. pp. 23. (Confidential).

Larson, M (2000). *Estimation of Crack Risk in Early Age Concrete*. Luleå, Sweden: Division of Structural Engineering, Luleå University of Technology. Licentiate Thesis 2000:10. pp. 170.

Löfling, P (1993). *Bestämning av jords hållfasthets- och deformationsegenskaper* (Determination of Strength and Deformation Properties of Soils). Borlänge, Sweden: Swedish Road Administration, Publication 1993:6. pp. 30. (In Swedish).

Löfquist, B (1946). *Temperatureffekter i hårdnande betong* (Temperature Effects in Hardening Concrete). Stockholm, Sweden: Royal Hydro Power Administration. Technical Bulletins, Serie B, No 22. pp. 195. (In Swedish).

Nilsson, M (1998). *Inverkan av tvång i gjutfogar och i betongkonstruktioner på elastiskt underlag* (Influence of Restraint in Casting Joints and in Concrete Structures on

Elastic Foundation). Luleå, Sweden: Division of Structural Engineering, Luleå University of Technology. Master Thesis 1998:090 CIV. pp. 61. (In Swedish).

Nilsson, M (1999). Coefficients of Rotational Restraint. In: *Midterm Assessment of Improved Production of Advanced Concrete Structures - IPACS*. Report T4.7. Luleå, Sweden: Division of Structural Engineering, Luleå University of Technology. pp. 17. (Confidential).

Nilsson, M, Jonasson, J-E, Wallin, K, Emborg, M, Bernander, S & Elfgren, L (1999). Crack Prevention in Walls and Slabs - The Influence of Restraint. In: *Innovation in Concrete Structures, Design and Construction. Proceedings of the International Conference held at the University of Dundee, Scotland, UK on 8-10 September 1999*. Ed. by R. K. Dhir & M. R. Jones. London, UK: Thomas Telford Publishing. pp. 461-471. ISBN: 0 7277 2824 5.

Nilsson, M, Ohlsson, U & Elfgren, L (2000). *Partailkoefficienter för betongbroar längs Malmbanan* (Partial Coefficients for Concrete Bridges along Malmbanan). Luleå, Sweden: Luleå University of Technology. Technical report 1999:03. 66 pp. ISSN 1402-1536. (In Swedish).

NKB 78 (1978). *Retningslinier for last- og sikkerhetsbestemmelser for baerende konstruktioner* (Guiding Rules for Loads and Safety Regulations for Structures). NKB-rapport nr. 35. 146 pp. ISBN 87-503-2951-0. (In Swedish).

NKB 87 (1987). *Retningslinier for last- og sikkerhetsbestemmelser for baerende konstruktioner* (Guiding Rules for Loads and Safety Regulations for Structures). NKB-rapport nr. 55. 107+55 pp. ISBN 87-503-6991-1, ISSN 0359-9981. (In Swedish).

Pettersson, D (1996). *Restraint Stresses Due to Uniform Thermal Action in Walls and Floors of Concrete on a Frictional Surface*. Lund, Sweden: Department of Structural Engineering, Lund Institute of Technology. Report TVBK-7051. pp. 45.

Pettersson, D (1998). *Stresses in Concrete Structures from Ground Restraint*. Lund, Sweden: Department of Structural Engineering, Lund Institute of Technology. Report TVBK-1014. pp. 112.

Rostásy, F, S, Gutsch, A-W & Krauß, M (1999). Engineering models for the assessment of restraint of slabs by soil and in piles in the early age of concrete. In: *Midterm Assessment of Improved Production of Advanced Concrete Structures - IPACS*. Report T4.1. Braunschweig, Germany: Institute for Building Materials, Concrete Construction and Fire Protection, Technical University of Braunschweig. pp. 100. (Confidential).

Schneider, J (1997). Introduction to Safety and Reliability of Structures. In: *Structural Engineering Documents, 5*. Zürich: IABSE, International Association for Bridges and Structural Engineering. 138 pp.

Timoshenko, S (1958). Beams on Elastic Foundation. In: *Strength of Materials*. Part II: Advanced Theory and Problems. New York, U.S.A.: Van Nostrand Reinold Company. pp. 565.

Wallin, K, Emborg, M & Jonasson, J-E (1997). *Värme ett alternativ till kyla* (Heat an alternative to cold). Luleå, Sweden: Division of Structural Engineering, Luleå University of Technology. Technical Report 1997:15. pp. 168. (In Swedish).

Vännman, K (1990). *Matematisk statistik* (Mathematical Statistic). Lund, Sweden: Studentlitteratur. 314 pp. ISBN 91-44-32181-3. (In Swedish).

Östlund, L (1997). *Studium av erforderligt värde på partialkoefficienten för tåglast vid dimensionering av järnvägsbroar* (Study of Necessary Value of the Partial Coefficient for Load of Trains at Design of Railway Bridges). Borlänge, Sweden: Swedish Railroad Administration. Investigation on behalf of the Swedish Railroad Administration. pp. 19. (In Swedish).

Appendix A

Statistics and Equations for Derivation of Partial Coefficients

The derivations of equations are quoted from or based on AK79/81 (1982), NKB78 (1978), NKB87 (1987), Schneider (1997), Vännman (1990), Östlund (1997) and Nilsson et al. (2000).

A.1 Statistics for the Resistance and Stress Parameters

A.1.1 Resistance parameter

$$r = Ca\rho\varepsilon \tag{A.1}$$

Mean value

$$\mu_r = \mu_C \mu_a \mu_\rho \mu_\varepsilon \tag{A.2}$$

Coefficient of variation

For the product of two stochastic and independent variables

$$V_{12}^2 = \frac{\sigma_{12}^2}{\mu_{12}^2} = \frac{\mu_1^2\sigma_2^2 + \mu_2^2\sigma_1^2 + \sigma_1^2\sigma_2^2}{\mu_1^2\mu_2^2} = \frac{\sigma_2^2}{\mu_2^2} + \frac{\sigma_1^2}{\mu_1^2} + \frac{\sigma_1^2\sigma_2^2}{\mu_1^2\mu_2^2} = V_1^2 + V_2^2 + V_1^2V_2^2$$

Then for the resistance parameter, the coefficient of variation can be divided into two parts as

$$\begin{cases} V_{Ca}^2 = V_C^2 + V_a^2 + V_C^2V_a^2 \\ V_{\rho\varepsilon}^2 = V_\rho^2 + V_\varepsilon^2 + V_\rho^2V_\varepsilon^2 \end{cases}$$

giving

$$
\begin{aligned}
V_{Ca\rho\varepsilon}^2 &= V_{Ca}^2 + V_{\rho\varepsilon}^2 + V_{Ca}^2 V_{\rho\varepsilon}^2 = \\
&= V_C^2 + V_a^2 + V_C^2 V_a^2 + V_\rho^2 + V_\varepsilon^2 + V_\rho^2 V_\varepsilon^2 + \\
&\qquad \left(V_C^2 + V_a^2 + V_C^2 V_a^2\right)\left(V_\rho^2 + V_\varepsilon^2 + V_\rho^2 V_\varepsilon^2\right) = \\
&= V_C^2 + V_a^2 + V_\rho^2 + V_\varepsilon^2 + V_C^2 V_a^2 + V_\rho^2 V_\varepsilon^2 + \\
&\qquad V_C^2 V_\rho^2 + V_C^2 V_\varepsilon^2 + V_C^2 V_\rho^2 V_\varepsilon^2 + V_a^2 V_\rho^2 + V_a^2 V_\varepsilon^2 + V_a^2 V_\rho^2 V_\varepsilon^2 + \\
&\qquad\qquad V_C^2 V_a^2 V_\rho^2 + V_C^2 V_a^2 V_\varepsilon^2 + V_C^2 V_a^2 V_\rho^2 V_\varepsilon^2
\end{aligned}
$$

If terms of higher order are neglected, the coefficient of variation is

$$V_r \approx \sqrt{V_C^2 + V_a^2 + V_\rho^2 + V_\varepsilon^2} \tag{A.3}$$

A.1.1 Stress parameter

$$s = \gamma_R \left(b\varepsilon_T + c\varepsilon_{sh}\right) \tag{A.4}$$

Mean value

$$\mu_s = \gamma_R \left(b\mu_T + c\mu_{sh}\right) \tag{A.5}$$

Coefficient of variation

$$V_s = \frac{\sigma_s}{\mu_s} = \frac{\sqrt{b^2\sigma_T^2 + c^2\sigma_{sh}^2}}{b\mu_T + c\mu_{sh}} \tag{A.6}$$

A.2 Design Values for the Limit State Condition

For the limit state condition, design values can be derived as

$$\mu_r - \mu_s \geq \beta\sigma_\Theta$$

$$\mu_r - \mu_s \geq \beta\sqrt{\sigma_r^2 + \sigma_s^2} = \beta\frac{\sigma_r^2 + \sigma_s^2}{\sqrt{\sigma_r^2 + \sigma_s^2}}$$

$$\mu_r - \gamma_R\left(b\mu_T + c\mu_{sh}\right) \geq \beta\frac{\sigma_r^2 + \gamma_R^2\left(b^2\sigma_T^2 + c^2\sigma_{sh}^2\right)}{\sqrt{\sigma_r^2 + \gamma_R^2\left(b^2\sigma_T^2 + c^2\sigma_{sh}^2\right)}}$$

$$\mu_r - \gamma_R \left(b\mu_T + c\mu_{sh} \right) \geq \beta \frac{\sigma_r}{\sqrt{\sigma_r^2 + \gamma_R^2 \left(b^2\sigma_T^2 + c^2\sigma_{sh}^2 \right)}} \sigma_r +$$

$$\beta \frac{b\gamma_R\sigma_T}{\sqrt{\sigma_r^2 + \gamma_R^2 \left(b^2\sigma_T^2 + c^2\sigma_{sh}^2 \right)}} b\gamma_R\sigma_T + \beta \frac{c\gamma_R\sigma_{sh}}{\sqrt{\sigma_r^2 + \gamma_R^2 \left(b^2\sigma_T^2 + c^2\sigma_{sh}^2 \right)}} c\gamma_R\sigma_{sh}$$

Introduction of so called sensitivity factors

$$\begin{cases} \alpha_r = \dfrac{\sigma_r}{\sqrt{\sigma_r^2 + \gamma_R^2 \left(b^2\sigma_T^2 + c^2\sigma_{sh}^2 \right)}} \\ \alpha_T = \dfrac{\gamma_R b\sigma_{\Delta T}}{\sqrt{\sigma_r^2 + \gamma_R^2 \left(b^2\sigma_T^2 + c^2\sigma_{sh}^2 \right)}} \\ \alpha_{sh} = \dfrac{\gamma_R c\sigma_{sh}}{\sqrt{\sigma_r^2 + \gamma_R^2 \left(b^2\sigma_T^2 + c^2\sigma_{sh}^2 \right)}} \end{cases} \tag{A.7}$$

give

$$\mu_r - \gamma_R \left(b\mu_T + c\mu_{sh} \right) \geq \beta\alpha_r\sigma_r + b\gamma_R\beta\alpha_T\sigma_T + c\gamma_R\beta\alpha_{sh}\sigma_{sh}$$

Ordering the terms by r, T and sh leads to:

$$\mu_r - \beta\alpha_r\sigma_r \geq b\gamma_R\mu_T + b\gamma_R\beta\alpha_T\sigma_{\Delta T} + c\gamma_R\mu_{sh} + c\gamma_R\beta\alpha_{sh}\sigma_{sh}$$

$$\mu_r \left(1 - \beta\alpha_r V_r \right) \geq b\gamma_R\mu_T \left(1 + \beta\alpha_T V_T \right) + c\gamma_R\mu_{sh} \left(1 + \beta\alpha_{sh} V_{sh} \right) \tag{A.8}$$

A.3 Help Values κ_i for Design Values in the Limit State Condition

Design values $x_{i,d}$ and their help values κ_i are defined as follows.

If X_i are normally distributed

$$x_{i,d} = \mu_i \left(1 - \alpha_i \beta V_i \right) \quad \kappa_i = \mu_i V_i \left. \frac{\partial \Theta}{\partial X_i} \right|_{X_i = x_{i,d}} \tag{A.9}$$

and if X_i is logarithmic normally distributed:

$$x_{i,d} = \mu_i e^{-\alpha_i \beta V_i} \quad \kappa_i = x_{i,d} V_i \left. \frac{\partial \Theta}{\partial X_i} \right|_{X_i = x_{i,d}} \tag{A.10}$$

These expressions are valid for $V_i < 0.25$. If V_i is larger, μ_i and V_i in Equations (A.9) and (A.10) are replaced with $\mu_i \Big/ \sqrt{1+V_i^2}$ and $\sqrt{\ln\left(1+V_i^2\right)}$ respectively.

For the thermal cracking problem the help values are

$$\kappa_r = r_d V_r \left.\frac{\partial \Theta}{\partial r}\right|_{r=r_d} = r_d V_r \tag{A.11}$$

$$\kappa_T = \sigma_T \left.\frac{\partial \Theta}{\partial (T)}\right|_{T=T_d} = -b\gamma_R \sigma_T = -b\gamma_R \mu_T V_T \tag{A.12}$$

$$\kappa_{sh} = \sigma_{sh} \left.\frac{\partial \Theta}{\partial (sh)}\right|_{sh=sh_d} = -c\gamma_R \sigma_{sh} = -c\gamma_R \mu_{sh} V_{sh} \tag{A.13}$$

A.6 Calculating Resistance Parameter

The resistance parameter

$$r_c = C_c a_c \rho_c \varepsilon_c \tag{A.14}$$

with mean value

$$\mu_r = \mu_C \mu_a \mu_\rho \mu_\varepsilon \tag{A.15}$$

Equation (A.15) divided by Equation (A.14) gives

$$\frac{\mu_r}{r_c} = \frac{\mu_C}{C_c}\frac{\mu_a}{a_c}\frac{\mu_\rho}{\rho_c}\frac{\mu_\varepsilon}{\varepsilon_c} \tag{A.16}$$

where, see Equation (A.10)

$$\frac{\mu_i}{x_{i,c}} = e^{-\alpha_i \beta V_i} = e^{-k_i V_i} \tag{A.17}$$

k_i depends on what fractile value that is chosen according to Table A.1 and can be found in any table for the normal distribution.

Table A.1 *Coefficient k as function of actual fractile.*

Fractile	45%	40%	35%	30%	25%	20%	15%	10%	5%
k	0.13	0.25	0.39	0.52	0.67	0.84	1.04	1.28	1.65

Equation (A.17) in Equation (A.16) gives

$$\frac{\mu_r}{r_c} = e^{-k_C V_C} e^{-k_a V_a} e^{-k_\rho V_\rho} e^{-k_f V_\varepsilon} \tag{A.18}$$

which is used when calculating partial coefficients.

A.5 Steps for Calculating Partial Coefficients

1. A value of α'_{sh} is assumed
2. Calculate

$$\alpha'_T = \frac{\kappa_T \alpha'_{sh}}{\kappa_{sh}} = \frac{-b\gamma_R \mu_T V_T \alpha'_{sh}}{-c\gamma_R \mu_{sh} V_{sh}} = \frac{V_T \alpha'_{sh}}{\nu_{sh} V_{sh}}$$

3. Calculate ψ_1 with Equation (2.32)

$$\psi_1 = \left(1 - \alpha'_T \beta V_T\right) + \nu_{sh}\left(1 - \alpha'_{sh} \beta V_{sh}\right)$$

4. Calculate $\kappa_r = r_d V_r = b\gamma_R \mu_T \psi V_r$
5. Calculate N

$$\begin{aligned}
\sqrt{\Sigma \kappa_i^2} &= \sqrt{\kappa_r^2 + \kappa_T^2 + \kappa_{sh}^2} = \\
&= \sqrt{\left(r_d V_r\right)^2 + \left(-b\gamma_R \mu_T V_T\right)^2 + \left(-c\gamma_R \mu_{sh} V_{sh}\right)^2} = \\
&= b\gamma_R \mu_T \sqrt{\left(\frac{r_d V_r}{b\gamma_R \mu_T}\right)^2 + \left(-V_T\right)^2 + \left(\frac{-c\gamma_R \mu_{sh}}{b\gamma_R \mu_T} V_{sh}\right)^2} = \\
&= b\gamma_R \mu_T \sqrt{\left(\psi V_r\right)^2 + \left(-V_T\right)^2 + \left(\nu_{sh} V_{sh}\right)^2} \quad \Rightarrow \\
N &= \frac{\sqrt{\Sigma \kappa_i^2}}{b\gamma_R \mu_T} = \sqrt{\left(\psi V_r\right)^2 + \left(-V_T\right)^2 + \left(\nu_{sh} V_{sh}\right)^2}
\end{aligned}$$

6. Calculate α_{sh} and compare with α'_{sh}

$$\alpha_{sh} = \frac{\kappa_{sh}}{\sqrt{\Sigma \kappa_i^2}} = \frac{-c\gamma_R \mu_{sh} V_{sh}}{\sqrt{\Sigma \kappa_i^2}} = \frac{-c\gamma_R \mu_{sh} V_{sh}}{b\gamma_R \mu_T N} = \frac{-\nu_{sh} V_{sh}}{N}$$

7. When $\alpha_{sh} \approx \alpha'_{sh}$, calculate α_T and α_r

$$\alpha_T = \frac{\kappa_T}{\sqrt{\Sigma\kappa_i^2}} = \frac{-b\gamma_R\mu_T V_T}{\sqrt{\Sigma\kappa_i^2}} = \frac{-b\gamma_R\mu_T V_T}{b\gamma_R\mu_T N} = \frac{-V_T}{N}$$

$$\alpha_{r,ber} = \frac{\kappa_r}{\sqrt{\Sigma\kappa_i^2}} = \frac{r_d V_r}{\sqrt{\Sigma\kappa_i^2}} = \frac{b\gamma_R\mu_T\psi V_r}{b\gamma_R\mu_T N} = \frac{\psi V_{sh}}{N}$$

8. Check $\Sigma\alpha_i^2 = 1$

9. Calculate $Z = \psi_1 e^{\alpha_r \beta V_r}$

10. Calculate the partial coefficients as $\gamma_r\gamma_s = \frac{Z}{\psi_2}\frac{\mu_r}{r_c}$ with $\frac{\mu_r}{r_c}$ according to Equation (A.18) and $\psi_2 = (1+k_T V_T)+\nu_{sh}(1+k_{sh}V_{sh})$ where k_T and k_{sh} are taken from Table A.1 for the chosen fractile values.

Appendix B

Calculations of Partial Coefficients for Thermal Cracking Problems

B.1 Tables of Calculation of Partial Coefficients

Table B.1 through Table B.10:

The partial coefficients as functions of the safety index β, the coefficients b and c, and the coefficient of variations of the calculation method and the concrete strength, V_C and V_ε, respectively.

Table B.11a-B11e through Table B.15a-B.15e:

Thorough presentation of the results of the calculations of partial coefficients for the case of $\beta = 3.72$, $b = c = 1$, $V_C = 0.05, 0.10, 0.15, 0.20$ and 0.25, and $V_\varepsilon = 0.05, 0.10, 0.15, 0.20$ and 0.25.

Table B.1 *Partial coefficients for* $\beta = 3.72$, $b = 1$, $c = 1$, $V_C = 0.05 - 0.25$, $V_\varepsilon = 0.05 - 0.25$ *and* $k_T = k_{sh} = 1.65$.

β	b	c	V_C	V_ε	$\gamma_r\gamma_s$
3.72	1	1	0.05	0.05	1.15
3.72	1	1	0.05	0.10	1.29
3.72	1	1	0.05	0.15	1.48
3.72	1	1	0.05	0.20	1.73
3.72	1	1	0.05	0.25	2.04
3.72	1	1	0.10	0.05	1.19
3.72	1	1	0.10	0.10	1.30
3.72	1	1	0.10	0.15	1.47
3.72	1	1	0.10	0.20	1.70
3.72	1	1	0.10	0.25	1.98
3.72	1	1	0.15	0.05	1.27
3.72	1	1	0.15	0.10	1.36
3.72	1	1	0.15	0.15	1.51
3.72	1	1	0.15	0.20	1.71
3.72	1	1	0.15	0.25	1.97
3.72	1	1	0.20	0.05	1.38
3.72	1	1	0.20	0.10	1.46
3.72	1	1	0.20	0.15	1.59
3.72	1	1	0.20	0.20	1.77
3.72	1	1	0.20	0.25	2.01
3.72	1	1	0.25	0.05	1.51
3.72	1	1	0.25	0.10	1.57
3.72	1	1	0.25	0.15	1.69
3.72	1	1	0.25	0.20	1.86
3.72	1	1	0.25	0.25	2.09

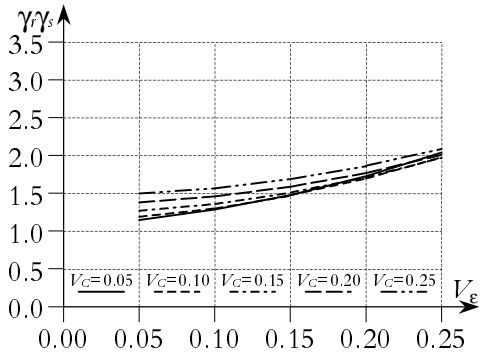

Table B.2 *Partial coefficients for* $\beta = 4.75$, $b = 1$, $c = 1$, $V_C = 0.05 - 0.25$, $V_\varepsilon = 0.05 - 0.25$ *and* $k_T = k_{sh} = 1.65$.

β	b	c	V_C	V_ε	$\gamma_r\gamma_s$
4.75	1	1	0.05	0.05	1.28
4.75	1	1	0.05	0.10	1.48
4.75	1	1	0.05	0.15	1.78
4.75	1	1	0.05	0.20	2.18
4.75	1	1	0.05	0.25	2.69
4.75	1	1	0.10	0.05	1.37
4.75	1	1	0.10	0.10	1.54
4.75	1	1	0.10	0.15	1.80
4.75	1	1	0.10	0.20	2.17
4.75	1	1	0.10	0.25	2.65
4.75	1	1	0.15	0.05	1.53
4.75	1	1	0.15	0.10	1.67
4.75	1	1	0.15	0.15	1.91
4.75	1	1	0.15	0.20	2.25
4.75	1	1	0.15	0.25	2.70
4.75	1	1	0.20	0.05	1.74
4.75	1	1	0.20	0.10	1.86
4.75	1	1	0.20	0.15	2.08
4.75	1	1	0.20	0.20	2.40
4.75	1	1	0.20	0.25	2.83
4.75	1	1	0.25	0.05	1.99
4.75	1	1	0.25	0.10	2.11
4.75	1	1	0.25	0.15	2.32
4.75	1	1	0.25	0.20	2.62
4.75	1	1	0.25	0.25	3.04

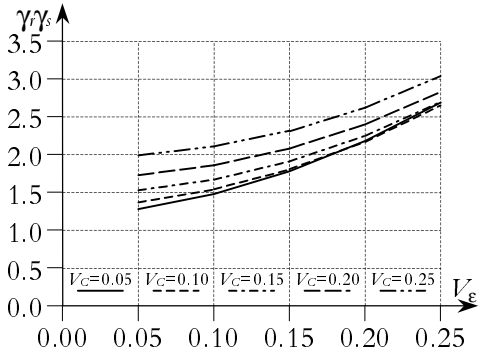

Table B.3 *Partial coefficients for* $\beta = 3.72$, $b = 1$, $c = 0.333$, $V_C = 0.05 - 0.25$, $V_\varepsilon = 0.05 - 0.25$ *and* $k_T = k_{sh} = 1.65$.

β	b	c	V_C	V_ε	$\gamma_r\gamma_s$
3.72	1	0.333	0.05	0.05	1.15
3.72	1	0.333	0.05	0.10	1.29
3.72	1	0.333	0.05	0.15	1.49
3.72	1	0.333	0.05	0.20	1.74
3.72	1	0.333	0.05	0.25	2.06
3.72	1	0.333	0.10	0.05	1.19
3.72	1	0.333	0.10	0.10	1.30
3.72	1	0.333	0.10	0.15	1.48
3.72	1	0.333	0.10	0.20	1.71
3.72	1	0.333	0.10	0.25	2.00
3.72	1	0.333	0.15	0.05	1.28
3.72	1	0.333	0.15	0.10	1.37
3.72	1	0.333	0.15	0.15	1.52
3.72	1	0.333	0.15	0.20	1.73
3.72	1	0.333	0.15	0.25	1.99
3.72	1	0.333	0.20	0.05	1.39
3.72	1	0.333	0.20	0.10	1.47
3.72	1	0.333	0.20	0.15	1.60
3.72	1	0.333	0.20	0.20	1.79
3.72	1	0.333	0.20	0.25	2.03
3.72	1	0.333	0.25	0.05	1.52
3.72	1	0.333	0.25	0.10	1.59
3.72	1	0.333	0.25	0.15	1.71
3.72	1	0.333	0.25	0.20	1.89
3.72	1	0.333	0.25	0.25	2.11

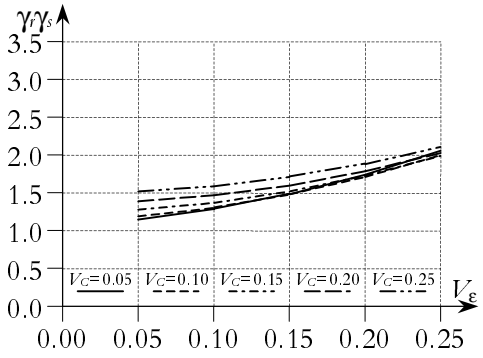

Table B.4 *Partial coefficients for* $\beta = 4.75$, $b = 1$, $c = 0.333$, $V_C = 0.05 - 0.25$, $V_\varepsilon = 0.05 - 0.25$ *and* $k_T = k_{sh} = 1.65$.

β	b	c	V_C	V_ε	$\gamma_r\gamma_s$
4.75	1	0.333	0.05	0.05	1.26
4.75	1	0.333	0.05	0.10	1.47
4.75	1	0.333	0.05	0.15	1.78
4.75	1	0.333	0.05	0.20	2.18
4.75	1	0.333	0.05	0.25	2.71
4.75	1	0.333	0.10	0.05	1.36
4.75	1	0.333	0.10	0.10	1.53
4.75	1	0.333	0.10	0.15	1.80
4.75	1	0.333	0.10	0.20	2.18
4.75	1	0.333	0.10	0.25	2.66
4.75	1	0.333	0.15	0.05	1.53
4.75	1	0.333	0.15	0.10	1.67
4.75	1	0.333	0.15	0.15	1.92
4.75	1	0.333	0.15	0.20	2.26
4.75	1	0.333	0.15	0.25	2.72
4.75	1	0.333	0.20	0.05	1.74
4.75	1	0.333	0.20	0.10	1.87
4.75	1	0.333	0.20	0.15	2.09
4.75	1	0.333	0.20	0.20	2.42
4.75	1	0.333	0.20	0.25	2.85
4.75	1	0.333	0.25	0.05	2.00
4.75	1	0.333	0.25	0.10	2.12
4.75	1	0.333	0.25	0.15	2.33
4.75	1	0.333	0.25	0.20	2.64
4.75	1	0.333	0.25	0.25	3.07

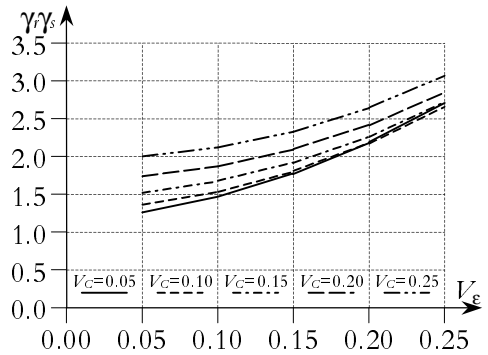

Table B.5 *Partial coefficients for* $\beta = 3.72$, $b = 1$, $c = 3$, $V_C = 0.05 - 0.25$, $V_\varepsilon = 0.05 - 0.25$ *and* $k_T = k_{sh} = 1.65$.

β	b	c	V_C	V_ε	$\gamma_r\gamma_s$
3.72	1	3	0.05	0.05	1.19
3.72	1	3	0.05	0.10	1.31
3.72	1	3	0.05	0.15	1.50
3.72	1	3	0.05	0.20	1.74
3.72	1	3	0.05	0.25	2.04
3.72	1	3	0.10	0.05	1.22
3.72	1	3	0.10	0.10	1.32
3.72	1	3	0.10	0.15	1.48
3.72	1	3	0.10	0.20	1.70
3.72	1	3	0.10	0.25	1.98
3.72	1	3	0.15	0.05	1.29
3.72	1	3	0.15	0.10	1.38
3.72	1	3	0.15	0.15	1.52
3.72	1	3	0.15	0.20	1.72
3.72	1	3	0.15	0.25	1.97
3.72	1	3	0.20	0.05	1.39
3.72	1	3	0.20	0.10	1.46
3.72	1	3	0.20	0.15	1.59
3.72	1	3	0.20	0.20	1.77
3.72	1	3	0.20	0.25	2.00
3.72	1	3	0.25	0.05	1.51
3.72	1	3	0.25	0.10	1.57
3.72	1	3	0.25	0.15	1.69
3.72	1	3	0.25	0.20	1.86
3.72	1	3	0.25	0.25	2.08

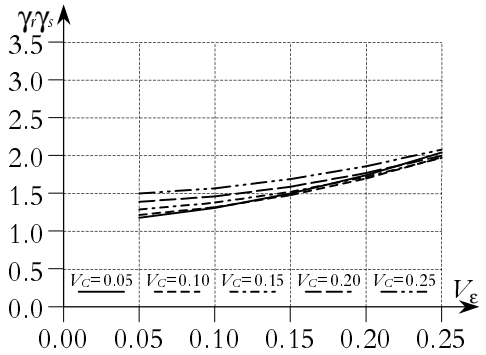

Table B.6 *Partial coefficients for* $\beta = 4.75$, $b = 1$, $c = 3$, $V_C = 0.05 - 0.25$, $V_\varepsilon = 0.05 - 0.25$ *and* $k_T = k_{sh} = 1.65$.

β	b	c	V_C	V_ε	$\gamma_r\gamma_s$
4.75	1	3	0.05	0.05	1.33
4.75	1	3	0.05	0.10	1.52
4.75	1	3	0.05	0.15	1.82
4.75	1	3	0.05	0.20	2.21
4.75	1	3	0.05	0.25	2.71
4.75	1	3	0.10	0.05	1.41
4.75	1	3	0.10	0.10	1.57
4.75	1	3	0.10	0.15	1.83
4.75	1	3	0.10	0.20	2.19
4.75	1	3	0.10	0.25	2.66
4.75	1	3	0.15	0.05	1.56
4.75	1	3	0.15	0.10	1.70
4.75	1	3	0.15	0.15	1.93
4.75	1	3	0.15	0.20	2.27
4.75	1	3	0.15	0.25	2.71
4.75	1	3	0.20	0.05	1.76
4.75	1	3	0.20	0.10	1.88
4.75	1	3	0.20	0.15	2.10
4.75	1	3	0.20	0.20	2.41
4.75	1	3	0.20	0.25	2.84
4.75	1	3	0.25	0.05	2.00
4.75	1	3	0.25	0.10	2.12
4.75	1	3	0.25	0.15	2.33
4.75	1	3	0.25	0.20	2.63
4.75	1	3	0.25	0.25	3.04

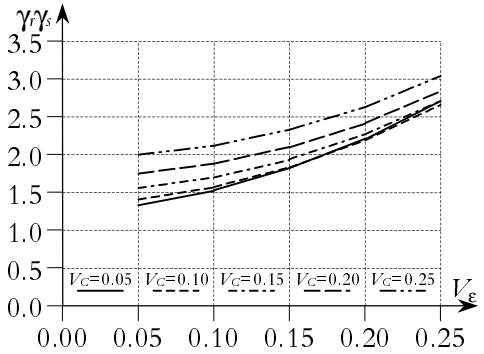

Table B.7 *Partial coefficients for* $\beta = 3.72$, $b = 0.333$, $c = 1$, $V_C = 0.05 - 0.25$, $V_\varepsilon = 0.05 - 0.25$ *and* $k_T = k_{sh} = 1.65$.

β	b	c	V_C	V_ε	$\gamma_r\gamma_s$
3.72	0.333	1	0.05	0.05	1.15
3.72	0.333	1	0.05	0.10	1.24
3.72	0.333	1	0.05	0.15	1.38
3.72	0.333	1	0.05	0.20	1.59
3.72	0.333	1	0.05	0.25	1.85
3.72	0.333	1	0.10	0.05	1.15
3.72	0.333	1	0.10	0.10	1.23
3.72	0.333	1	0.10	0.15	1.36
3.72	0.333	1	0.10	0.20	1.55
3.72	0.333	1	0.10	0.25	1.79
3.72	0.333	1	0.15	0.05	1.19
3.72	0.333	1	0.15	0.10	1.26
3.72	0.333	1	0.15	0.15	1.38
3.72	0.333	1	0.15	0.20	1.55
3.72	0.333	1	0.15	0.25	1.78
3.72	0.333	1	0.20	0.05	1.26
3.72	0.333	1	0.20	0.10	1.33
3.72	0.333	1	0.20	0.15	1.44
3.72	0.333	1	0.20	0.20	1.60
3.72	0.333	1	0.20	0.25	1.81
3.72	0.333	1	0.25	0.05	1.37
3.72	0.333	1	0.25	0.10	1.42
3.72	0.333	1	0.25	0.15	1.53
3.72	0.333	1	0.25	0.20	1.68
3.72	0.333	1	0.25	0.25	1.87

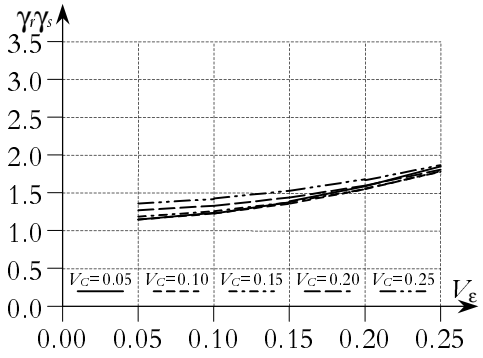

Table B.8 *Partial coefficients for* $\beta = 4.75$, $b = 0.333$, $c = 1$, $V_C = 0.05 - 0.25$, $V_\varepsilon = 0.05 - 0.25$ *and* $k_T = k_{sh} = 1.65$.

β	b	c	V_C	V_ε	$\gamma_r\gamma_s$
4.75	0.333	1	0.05	0.05	1.27
4.75	0.333	1	0.05	0.10	1.41
4.75	0.333	1	0.05	0.15	1.64
4.75	0.333	1	0.05	0.20	1.97
4.75	0.333	1	0.05	0.25	2.41
4.75	0.333	1	0.10	0.05	1.31
4.75	0.333	1	0.10	0.10	1.44
4.75	0.333	1	0.10	0.15	1.65
4.75	0.333	1	0.10	0.20	1.95
4.75	0.333	1	0.10	0.25	2.36
4.75	0.333	1	0.15	0.05	1.41
4.75	0.333	1	0.15	0.10	1.53
4.75	0.333	1	0.15	0.15	1.73
4.75	0.333	1	0.15	0.20	2.01
4.75	0.333	1	0.15	0.25	2.40
4.75	0.333	1	0.20	0.05	1.57
4.75	0.333	1	0.20	0.10	1.68
4.75	0.333	1	0.20	0.15	1.86
4.75	0.333	1	0.20	0.20	2.14
4.75	0.333	1	0.20	0.25	2.51
4.75	0.333	1	0.25	0.05	1.78
4.75	0.333	1	0.25	0.10	1.88
4.75	0.333	1	0.25	0.15	2.06
4.75	0.333	1	0.25	0.20	2.33
4.75	0.333	1	0.25	0.25	2.69

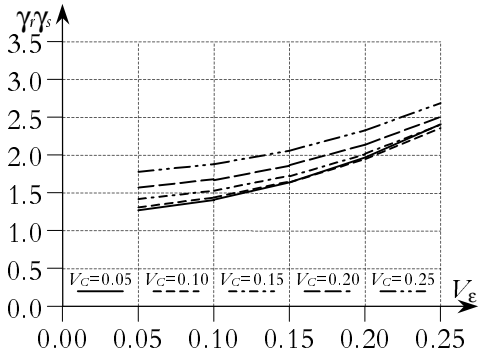

Table B.9 *Partial coefficients for* $\beta = 3.72$, $b = 3$, $c = 1$, $V_C = 0.05 - 0.25$, $V_\varepsilon = 0.05 - 0.25$ *and* $k_T = k_{sh} = 1.65$.

β	b	c	V_C	V_ε	$\gamma_r\gamma_s$
3.72	3	1	0.05	0.05	1.10
3.72	3	1	0.05	0.10	1.25
3.72	3	1	0.05	0.15	1.45
3.72	3	1	0.05	0.20	1.71
3.72	3	1	0.05	0.25	2.02
3.72	3	1	0.10	0.05	1.16
3.72	3	1	0.10	0.10	1.27
3.72	3	1	0.10	0.15	1.44
3.72	3	1	0.10	0.20	1.68
3.72	3	1	0.10	0.25	1.96
3.72	3	1	0.15	0.05	1.25
3.72	3	1	0.15	0.10	1.34
3.72	3	1	0.15	0.15	1.49
3.72	3	1	0.15	0.20	1.70
3.72	3	1	0.15	0.25	1.96
3.72	3	1	0.20	0.05	1.36
3.72	3	1	0.20	0.10	1.44
3.72	3	1	0.20	0.15	1.57
3.72	3	1	0.20	0.20	1.76
3.72	3	1	0.20	0.25	2.00
3.72	3	1	0.25	0.05	1.49
3.72	3	1	0.25	0.10	1.56
3.72	3	1	0.25	0.15	1.68
3.72	3	1	0.25	0.20	1.86
3.72	3	1	0.25	0.25	2.09

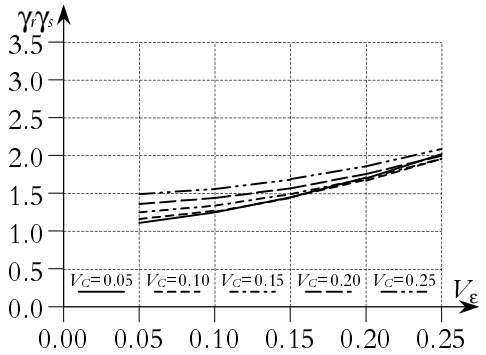

Table B.10 *Partial coefficients for* $\beta = 4.75$, $b = 3$, $c = 1$, $V_C = 0.05 - 0.25$, $V_\varepsilon = 0.05 - 0.25$ *and* $k_T = k_{sh} = 1.65$.

β	b	c	V_C	V_ε	$\gamma_r\gamma_s$
4.75	3	1	0.05	0.05	1.21
4.75	3	1	0.05	0.10	1.42
4.75	3	1	0.05	0.15	1.72
4.75	3	1	0.05	0.20	2.13
4.75	3	1	0.05	0.25	2.65
4.75	3	1	0.10	0.05	1.31
4.75	3	1	0.10	0.10	1.48
4.75	3	1	0.10	0.15	1.75
4.75	3	1	0.10	0.20	2.13
4.75	3	1	0.10	0.25	2.61
4.75	3	1	0.15	0.05	1.48
4.75	3	1	0.15	0.10	1.63
4.75	3	1	0.15	0.15	1.87
4.75	3	1	0.15	0.20	2.21
4.75	3	1	0.15	0.25	2.66
4.75	3	1	0.20	0.05	1.70
4.75	3	1	0.20	0.10	1.83
4.75	3	1	0.20	0.15	2.05
4.75	3	1	0.20	0.20	2.37
4.75	3	1	0.20	0.25	2.80
4.75	3	1	0.25	0.05	1.96
4.75	3	1	0.25	0.10	2.08
4.75	3	1	0.25	0.15	2.29
4.75	3	1	0.25	0.20	2.60
4.75	3	1	0.25	0.25	3.02

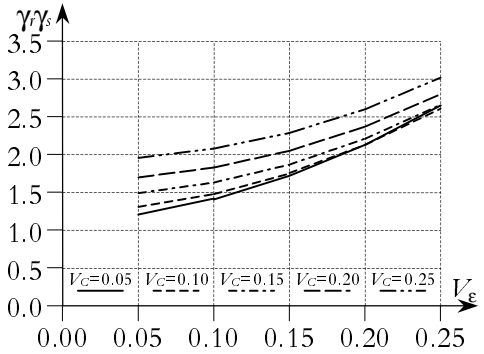

Table B.11a *b = 1, c = 1, V_C = 0.05 and V_ε = 0.05.*

Load values

ν_{sh}	0.01	0.20	0.50	1.00	2.00	
b	1	1	1	1	1	
c	1	1	1	1	1	
V_T	0.08	0.08	0.08	0.08	0.08	
V_{sh}	0.20	0.20	0.20	0.20	0.20	
k_T	1.65	1.65	1.65	1.65	1.65	
k_{sh}	1.65	1.65	1.65	1.65	1.65	

Resistance values

V_f	0.05	0.05	0.05	0.05	0.05	
V_C	0.05	0.05	0.05	0.05	0.05	
V_a	0	0	0	0	0	
V_ρ	0	0	0	0	0	
V_r	0.0707	0.0707	0.0707	0.0707	0.0707	
k_f	0.13	0.13	0.13	0.13	0.13	
f_c/μ_f	0.9935	0.9935	0.9935	0.9935	0.9935	
k_C	1.65	1.65	1.65	1.65	1.65	
C_c/μ_C	0.9208	0.9208	0.9208	0.9208	0.9208	
k_a	1.65	1.65	1.65	1.65	1.65	
a_c/μ_a	1	1	1	1	1	
k_ρ	1.65	1.65	1.65	1.65	1.65	
ρ_c/μ_ρ	1.0000	1.0000	1.0000	1.0000	1.0000	
r_c/μ_r	0.9148	0.9148	0.9148	0.9148	0.9148	

Calculation of partial coefficients

β	3.72	3.72	3.72	3.72	3.72	
α'_{sh}	-0.0170	-0.2973	-0.5486	-0.7052	-0.7911	
α'_T	-0.6820	-0.5946	-0.4389	-0.2821	-0.1582	
ψ	1.2131	1.5212	1.8347	2.6086	4.2243	
κ_r	0.0858	0.1005	0.1297	0.1845	0.2987	
N	0.1173	0.1345	0.1823	0.2836	0.5056	
α_{sh}	-0.0170	-0.2973	-0.5486	-0.7052	-0.7911	
α_T	-0.6820	-0.5946	-0.4389	-0.2821	-0.1582	
α_r	0.7312	0.7470	0.7117	0.6504	0.5908	
$\Sigma\alpha_i^2$	1.0000	1.0000	1.0000	1.0000	1.0000	
Z	1.4703	1.7298	2.2124	3.0954	4.9346	
$\gamma_r\gamma_s$	1.1745	1.1320	1.1263	1.1502	1.3187	1.15

Table B.11b *b = 1, c = 1, V_C = 0.05 and V_ε = 0.10.*

Load values

ν_{sh}	0.01	0.20	0.50	1.00	2.00	
b	1	1	1	1	1	
c	1	1	1	1	1	
V_T	0.08	0.08	0.08	0.08	0.08	
V_{sh}	0.20	0.20	0.20	0.20	0.20	
k_T	1.65	1.65	1.65	1.65	1.65	
k_{sh}	1.65	1.65	1.65	1.65	1.65	

Resistance values

V_f	0.10	0.10	0.10	0.10	0.10	
V_C	0.05	0.05	0.05	0.05	0.05	
V_a	0	0	0	0	0	
V_ρ	0	0	0	0	0	
V_r	0.1118	0.1118	0.1118	0.1118	0.1118	
k_f	0.13	0.13	0.13	0.13	0.13	
f_c/μ_f	0.9871	0.9871	0.9871	0.9871	0.9871	
k_C	1.65	1.65	1.65	1.65	1.65	
C_c/μ_C	0.9208	0.9208	0.9208	0.9208	0.9208	
k_a	1.65	1.65	1.65	1.65	1.65	
a_c/μ_a	1	1	1	1	1	
k_ρ	1.65	1.65	1.65	1.65	1.65	
ρ_c/μ_ρ	1.0000	1.0000	1.0000	1.0000	1.0000	
r_c/μ_r	0.9089	0.9089	0.9089	0.9089	0.9089	

Calculation of partial coefficients

β	3.72	3.72	3.72	3.72	3.72	
α'_{sh}	-0.0131	-0.2258	-0.4260	-0.5681	-0.6590	
α'_T	-0.5231	-0.4515	-0.3408	-0.2273	-0.1318	
ψ	1.1658	1.3680	1.7599	2.4903	4.0199	
κ_r	0.1303	0.1529	0.1968	0.2784	0.4494	
N	0.1529	0.1772	0.2348	0.3520	0.6070	
α_{sh}	-0.0131	-0.2258	-0.4260	-0.5681	-0.6590	
α_T	-0.5231	-0.4515	-0.3408	-0.2273	-0.1318	
α_r	0.8522	0.8632	0.8381	0.7909	0.7405	
$\Sigma\alpha_i^2$	1.0000	1.0000	1.0000	1.0000	1.0000	
Z	1.6616	1.9588	2.4938	3.4603	5.4697	
$\gamma_r\gamma_s$	1.3187	1.2735	1.2614	1.2775	1.3110	1.29

Table B.11c *b = 1, c = 1, V_C = 0.05 and V_ε = 0.15.*

Load values

ν_{sh}	0.01	0.20	0.50	1.00	2.00	
b	1	1	1	1	1	
c	1	1	1	1	1	
V_T	0.08	0.08	0.08	0.08	0.08	
V_{sh}	0.20	0.20	0.20	0.20	0.20	
k_T	1.65	1.65	1.65	1.65	1.65	
k_{sh}	1.65	1.65	1.65	1.65	1.65	

Resistance values

V_f	0.15	0.15	0.15	0.15	0.15	
V_C	0.05	0.05	0.05	0.05	0.05	
V_a	0	0	0	0	0	
V_ρ	0	0	0	0	0	
V_r	0.1581	0.1581	0.1581	0.1581	0.1581	
k_f	0.13	0.13	0.13	0.13	0.13	
f_c/μ_f	0.9807	0.9807	0.9807	0.9807	0.9807	
k_C	1.65	1.65	1.65	1.65	1.65	
C_c/μ_C	0.9208	0.9208	0.9208	0.9208	0.9208	
k_a	1.65	1.65	1.65	1.65	1.65	
a_c/μ_a	1	1	1	1	1	
k_ρ	1.65	1.65	1.65	1.65	1.65	
ρ_c/μ_ρ	1.0000	1.0000	1.0000	1.0000	1.0000	
r_c/μ_r	0.9030	0.9030	0.9030	0.9030	0.9030	

Calculation of partial coefficients

β	3.72	3.72	3.72	3.72	3.72	
α'_{sh}	-0.0102	-0.1750	-0.3351	-0.4589	-0.5463	
α'_T	-0.4082	-0.3500	-0.2681	-0.1836	-0.1093	
ψ	1.1315	1.3302	1.7045	2.3961	3.8454	
κ_r	0.1789	0.2103	0.2695	0.3789	0.6080	
N	0.1960	0.2286	0.2984	0.4358	0.7322	
α_{sh}	-0.0102	-0.1750	-0.3351	-0.4589	-0.5463	
α_T	-0.4082	-0.3500	-0.2681	-0.1836	-0.1093	
α_r	0.9128	0.9202	0.9032	0.8693	0.8304	
$\Sigma\alpha_i^2$	1.0000	1.0000	1.0000	1.0000	1.0000	
Z	1.9358	2.2856	2.8994	3.9954	6.2672	
$\gamma_r\gamma_s$	1.5263	1.4763	1.4570	1.4655	1.4925	1.48

Table B.11d *b = 1, c = 1, V_C = 0.05 and V_ε = 0.20.*

Load values

ν_{sh}	0.01	0.20	0.50	1.00	2.00	
b	1	1	1	1	1	
c	1	1	1	1	1	
V_T	0.08	0.08	0.08	0.08	0.08	
V_{sh}	0.20	0.20	0.20	0.20	0.20	
k_T	1.65	1.65	1.65	1.65	1.65	
k_{sh}	1.65	1.65	1.65	1.65	1.65	

Resistance values

V_f	0.20	0.20	0.20	0.20	0.20	
V_C	0.05	0.05	0.05	0.05	0.05	
V_a	0	0	0	0	0	
V_ρ	0	0	0	0	0	
V_r	0.2062	0.2062	0.2062	0.2062	0.2062	
k_f	0.13	0.13	0.13	0.13	0.13	
f_c/μ_f	0.9743	0.9743	0.9743	0.9743	0.9743	
k_C	1.65	1.65	1.65	1.65	1.65	
C_c/μ_C	0.9208	0.9208	0.9208	0.9208	0.9208	
k_a	1.65	1.65	1.65	1.65	1.65	
a_c/μ_a	1	1	1	1	1	
k_ρ	1.65	1.65	1.65	1.65	1.65	
ρ_c/μ_ρ	1.0000	1.0000	1.0000	1.0000	1.0000	
r_c/μ_r	0.8972	0.8972	0.8972	0.8972	0.8972	

Calculation of partial coefficients

β	3.72	3.72	3.72	3.72	3.72	
α'_{sh}	-0.0083	-0.1411	-0.2728	-0.3802	-0.4611	
α'_T	-0.3304	-0.2822	-0.2182	-0.1521	-0.0922	
ψ	1.1084	1.3050	1.6664	2.3281	3.7136	
κ_r	0.2285	0.2690	0.3435	0.4800	0.7656	
N	0.2421	0.2835	0.3666	0.5261	0.8675	
α_{sh}	-0.0083	-0.1411	-0.2728	-0.3802	-0.4611	
α_T	-0.3304	-0.2822	-0.2182	-0.1521	-0.0922	
α_r	0.9438	0.9489	0.9370	0.9123	0.8825	
$\Sigma\alpha_i^2$	1.0000	1.0000	1.0000	1.0000	1.0000	
Z	2.2858	2.7018	3.4187	4.6866	7.3068	
$\gamma_r\gamma_s$	1.7906	1.7339	1.7068	1.7079	1.7288	1.73

Table B.11e *b = 1, c = 1, V_C = 0.05 and V_ε = 0.25.*

Load values

ν_{sh}	0.01	0.20	0.50	1.00	2.00	
b	1	1	1	1	1	
c	1	1	1	1	1	
V_T	0.08	0.08	0.08	0.08	0.08	
V_{sh}	0.20	0.20	0.20	0.20	0.20	
k_T	1.65	1.65	1.65	1.65	1.65	
k_{sh}	1.65	1.65	1.65	1.65	1.65	

Resistance values

V_f	0.25	0.25	0.25	0.25	0.25	
V_C	0.05	0.05	0.05	0.05	0.05	
V_a	0	0	0	0	0	
V_ρ	0	0	0	0	0	
V_r	0.2550	0.2550	0.2550	0.2550	0.2550	
k_f	0.13	0.13	0.13	0.13	0.13	
f_c/μ_f	0.9680	0.9680	0.9680	0.9680	0.9680	
k_C	1.65	1.65	1.65	1.65	1.65	
C_c/μ_C	0.9208	0.9208	0.9208	0.9208	0.9208	
k_a	1.65	1.65	1.65	1.65	1.65	
a_c/μ_a	1	1	1	1	1	
k_ρ	1.65	1.65	1.65	1.65	1.65	
ρ_c/μ_ρ	1.0000	1.0000	1.0000	1.0000	1.0000	
r_c/μ_r	0.8914	0.8914	0.8914	0.8914	0.8914	

Calculation of partial coefficients

β	3.72	3.72	3.72	3.72	3.72	
α'_{sh}	-0.0069	-0.1176	-0.2287	-0.3228	-0.3969	
α'_T	-0.2761	-0.2351	-0.1830	-0.1291	-0.0794	
ψ	1.0922	1.2875	1.6395	2.2786	3.6143	
κ_r	0.2785	0.3282	0.4180	0.5809	0.9215	
N	0.2897	0.3402	0.4372	0.6196	1.0077	
α_{sh}	-0.0069	-0.1176	-0.2287	-0.3228	-0.3969	
α_T	-0.2761	-0.2351	-0.1830	-0.1291	-0.0794	
α_r	0.9611	0.9648	0.9561	0.9376	0.9144	
$\Sigma\alpha_i^2$	1.0000	1.0000	1.0000	1.0000	1.0000	
Z	2.7176	3.2147	4.0602	5.5445	8.6031	
$\gamma_r\gamma_s$	2.1150	2.0497	2.0140	2.0074	2.0223	2.04

Table B.12a *b = 1, c = 1, V_C = 0.10 and V_ε = 0.05.*

Load values

ν_{sh}	0.01	0.20	0.50	1.00	2.00	
b	1	1	1	1	1	
c	1	1	1	1	1	
V_T	0.08	0.08	0.08	0.08	0.08	
V_{sh}	0.20	0.20	0.20	0.20	0.20	
k_T	1.65	1.65	1.65	1.65	1.65	
k_{sh}	1.65	1.65	1.65	1.65	1.65	

Resistance values

V_f	0.05	0.05	0.05	0.05	0.05	
V_C	0.10	0.10	0.10	0.10	0.10	
V_a	0	0	0	0	0	
V_ρ	0	0	0	0	0	
V_r	0.1118	0.1118	0.1118	0.1118	0.1118	
k_f	0.13	0.13	0.13	0.13	0.13	
f_c/μ_f	0.9935	0.9935	0.9935	0.9935	0.9935	
k_C	1.65	1.65	1.65	1.65	1.65	
C_c/μ_C	0.8479	0.8479	0.8479	0.8479	0.8479	
k_a	1.65	1.65	1.65	1.65	1.65	
a_c/μ_a	1	1	1	1	1	
k_ρ	1.65	1.65	1.65	1.65	1.65	
ρ_c/μ_ρ	1.0000	1.0000	1.0000	1.0000	1.0000	
r_c/μ_r	0.8424	0.8424	0.8424	0.8424	0.8424	

Calculation of partial coefficients

β	3.72	3.72	3.72	3.72	3.72	
α'_{sh}	-0.0131	-0.2258	-0.4260	-0.5681	-0.6590	
α'_T	-0.5231	-0.4515	-0.3408	-0.2273	-0.1318	
ψ	1.1658	1.3680	1.7599	2.4903	4.0199	
κ_r	0.1303	0.1529	0.1968	0.2784	0.4494	
N	0.1529	0.1772	0.2348	0.3520	0.6070	
α_{sh}	-0.0131	-0.2258	-0.4260	-0.5681	-0.6590	
α_T	-0.5231	-0.4515	-0.3408	-0.2273	-0.1318	
α_r	0.8522	0.8632	0.8381	0.7909	0.7405	
$\Sigma\alpha_i^2$	1.0000	1.0000	1.0000	1.0000	1.0000	
Z	1.6616	1.9588	2.4938	3.4603	5.4697	
$\gamma_r\gamma_s$	1.2222	1.1803	1.1691	1.1840	1.2151	1.19

Table B.12b *b = 1, c = 1, V_C = 0.10 and V_ε = 0.10.*

Load values

ν_{sh}	0.01	0.20	0.50	1.00	2.00	
b	1	1	1	1	1	
c	1	1	1	1	1	
V_T	0.08	0.08	0.08	0.08	0.08	
V_{sh}	0.20	0.20	0.20	0.20	0.20	
k_T	1.65	1.65	1.65	1.65	1.65	
k_{sh}	1.65	1.65	1.65	1.65	1.65	

Resistance values

V_f	0.10	0.10	0.10	0.10	0.10	
V_C	0.10	0.10	0.10	0.10	0.10	
V_a	0	0	0	0	0	
V_ρ	0	0	0	0	0	
V_r	0.1414	0.1414	0.1414	0.1414	0.1414	
k_f	0.13	0.13	0.13	0.13	0.13	
f_c/μ_f	0.9871	0.9871	0.9871	0.9871	0.9871	
k_C	1.65	1.65	1.65	1.65	1.65	
C_c/μ_C	0.8479	0.8479	0.8479	0.8479	0.8479	
k_a	1.65	1.65	1.65	1.65	1.65	
a_c/μ_a	1	1	1	1	1	
k_ρ	1.65	1.65	1.65	1.65	1.65	
ρ_c/μ_ρ	1.0000	1.0000	1.0000	1.0000	1.0000	
r_c/μ_r	0.8369	0.8369	0.8369	0.8369	0.8369	

Calculation of partial coefficients

β	3.72	3.72	3.72	3.72	3.72	
α'_{sh}	-0.0111	-0.1907	-0.3635	-0.4937	-0.5829	
α'_T	-0.4438	-0.3813	-0.2908	-0.1975	-0.1166	
ψ	1.1422	1.3419	1.7218	2.4261	3.9020	
κ_r	0.1615	0.1898	0.2435	0.3431	0.5518	
N	0.1803	0.2098	0.2751	0.4051	0.6862	
α_{sh}	-0.0111	-0.1907	-0.3635	-0.4937	-0.5829	
α_T	-0.4438	-0.3813	-0.2908	-0.1975	-0.1166	
α_r	0.8961	0.9046	0.8851	0.8469	0.8041	
$\Sigma\alpha_i^2$	1.0000	1.0000	1.0000	1.0000	1.0000	
Z	1.8300	2.1596	2.7427	3.7880	5.9569	
$\gamma_r\gamma_s$	1.3373	1.2929	1.2774	1.2877	1.3148	1.30

Table B.12c *b = 1, c = 1, V_C = 0.10 and V_ε = 0.15.*

Load values

ν_{sh}	0.01	0.20	0.50	1.00	2.00	
b	1	1	1	1	1	
c	1	1	1	1	1	
V_T	0.08	0.08	0.08	0.08	0.08	
V_{sh}	0.20	0.20	0.20	0.20	0.20	
k_T	1.65	1.65	1.65	1.65	1.65	
k_{sh}	1.65	1.65	1.65	1.65	1.65	

Resistance values

V_f	0.15	0.15	0.15	0.15	0.15	
V_C	0.10	0.10	0.10	0.10	0.10	
V_a	0	0	0	0	0	
V_ρ	0	0	0	0	0	
V_r	0.1803	0.1803	0.1803	0.1803	0.1803	
k_f	0.13	0.13	0.13	0.13	0.13	
f_c/μ_f	0.9807	0.9807	0.9807	0.9807	0.9807	
k_C	1.65	1.65	1.65	1.65	1.65	
C_c/μ_C	0.8479	0.8479	0.8479	0.8479	0.8479	
k_a	1.65	1.65	1.65	1.65	1.65	
a_c/μ_a	1	1	1	1	1	
k_ρ	1.65	1.65	1.65	1.65	1.65	
ρ_c/μ_ρ	1.0000	1.0000	1.0000	1.0000	1.0000	
r_c/μ_r	0.8315	0.8315	0.8315	0.8315	0.8315	

Calculation of partial coefficients

β	3.72	3.72	3.72	3.72	3.72	
α'_{sh}	-0.0092	-0.1576	-0.3033	-0.4191	-0.5037	
α'_T	-0.3684	-0.3153	-0.2427	-0.1677	-0.1007	
ψ	1.1197	1.3173	1.6851	2.3617	3.7795	
κ_r	0.2019	0.2375	0.3038	0.4258	0.6814	
N	0.2171	0.2538	0.3297	0.4772	0.7941	
α_{sh}	-0.0092	-0.1576	-0.3033	-0.4191	-0.5037	
α_T	-0.3684	-0.3153	-0.2427	-0.1677	-0.1007	
α_r	0.9296	0.9358	0.9215	0.8923	0.8580	
$\Sigma\alpha_i^2$	1.0000	1.0000	1.0000	1.0000	1.0000	
Z	2.0886	2.4674	3.1260	4.2965	6.7193	
$\gamma_r\gamma_s$	1.5164	1.4676	1.4465	1.4511	1.4734	1.47

Table B.12d *b = 1, c = 1, V_C = 0.10 and V_ε = 0.20.*

Load values

ν_{sh}	0.01	0.20	0.50	1.00	2.00	
b	1	1	1	1	1	
c	1	1	1	1	1	
V_T	0.08	0.08	0.08	0.08	0.08	
V_{sh}	0.20	0.20	0.20	0.20	0.20	
k_T	1.65	1.65	1.65	1.65	1.65	
k_{sh}	1.65	1.65	1.65	1.65	1.65	

Resistance values

V_f	0.20	0.20	0.20	0.20	0.20	
V_C	0.10	0.10	0.10	0.10	0.10	
V_a	0	0	0	0	0	
V_ρ	0	0	0	0	0	
V_r	0.2236	0.2236	0.2236	0.2236	0.2236	
k_f	0.13	0.13	0.13	0.13	0.13	
f_c/μ_f	0.9743	0.9743	0.9743	0.9743	0.9743	
k_C	1.65	1.65	1.65	1.65	1.65	
C_c/μ_C	0.8479	0.8479	0.8479	0.8479	0.8479	
k_a	1.65	1.65	1.65	1.65	1.65	
a_c/μ_a	1	1	1	1	1	
k_ρ	1.65	1.65	1.65	1.65	1.65	
ρ_c/μ_ρ	1.0000	1.0000	1.0000	1.0000	1.0000	
r_c/μ_r	0.8261	0.8261	0.8261	0.8261	0.8261	

Calculation of partial coefficients

β	3.72	3.72	3.72	3.72	3.72	
α'_{sh}	-0.0077	-0.1317	-0.2553	-0.3576	-0.4360	
α'_T	-0.3088	-0.2634	-0.2042	-0.1430	-0.0872	
ψ	1.1020	1.2980	1.6557	2.3086	3.6748	
κ_r	0.2464	0.2902	0.3702	0.5162	0.8217	
N	0.2591	0.3037	0.3918	0.5594	0.9174	
α_{sh}	-0.0077	-0.1317	-0.2553	-0.3576	-0.4360	
α_T	-0.3088	-0.2634	-0.2042	-0.1430	-0.0872	
α_r	0.9511	0.9557	0.9451	0.9229	0.8957	
$\Sigma\alpha_i^2$	1.0000	1.0000	1.0000	1.0000	1.0000	
Z	2.4308	2.8741	3.6341	4.9744	7.7411	
$\gamma_r\gamma_s$	1.7534	1.6984	1.6707	1.6692	1.6865	1.70

Table B.12e *b = 1, c = 1, V_C = 0.10 and V_ε = 0.25.*

Load values

ν_{sh}	0.01	0.20	0.50	1.00	2.00
b	1	1	1	1	1
c	1	1	1	1	1
V_T	0.08	0.08	0.08	0.08	0.08
V_{sh}	0.20	0.20	0.20	0.20	0.20
k_T	1.65	1.65	1.65	1.65	1.65
k_{sh}	1.65	1.65	1.65	1.65	1.65

Resistance values

V_f	0.25	0.25	0.25	0.25	0.25
V_C	0.10	0.10	0.10	0.10	0.10
V_a	0	0	0	0	0
V_ρ	0	0	0	0	0
V_r	0.2693	0.2693	0.2693	0.2693	0.2693
k_f	0.13	0.13	0.13	0.13	0.13
f_c/μ_f	0.9680	0.9680	0.9680	0.9680	0.9680
k_C	1.65	1.65	1.65	1.65	1.65
C_c/μ_C	0.8479	0.8479	0.8479	0.8479	0.8479
k_a	1.65	1.65	1.65	1.65	1.65
a_c/μ_a	1	1	1	1	1
k_ρ	1.65	1.65	1.65	1.65	1.65
ρ_c/μ_ρ	1.0000	1.0000	1.0000	1.0000	1.0000
r_c/μ_r	0.8208	0.8208	0.8208	0.8208	0.8208

Calculation of partial coefficients

β	3.72	3.72	3.72	3.72	3.72	
α'_{sh}	-0.0066	-0.1121	-0.2183	-0.3090	-0.3812	
α'_T	-0.2633	-0.2241	-0.1747	-0.1236	-0.0762	
ψ	1.0884	1.2834	1.6332	2.2667	3.5900	
κ_r	0.2931	0.3456	0.4398	0.6103	0.9666	
N	0.3038	0.3569	0.4580	0.6472	1.0492	
α_{sh}	-0.0066	-0.1121	-0.2183	-0.3090	-0.3812	
α_T	-0.2633	-0.2241	-0.1747	-0.1236	-0.0762	
α_r	0.9647	0.9681	0.9601	0.9430	0.9213	
$\Sigma\alpha_i^2$	1.0000	1.0000	1.0000	1.0000	1.0000	
Z	2.8605	3.3844	4.2726	5.8291	9.0339	
$\gamma_r\gamma_s$	2.0500	1.9870	1.9515	1.9433	1.9554	1.98

Table B.13a *b = 1, c = 1, V_C = 0.15 and V_ε = 0.05.*

Load values

ν_{sh}	0.01	0.20	0.50	1.00	2.00	
b	1	1	1	1	1	
c	1	1	1	1	1	
V_T	0.08	0.08	0.08	0.08	0.08	
V_{sh}	0.20	0.20	0.20	0.20	0.20	
k_T	1.65	1.65	1.65	1.65	1.65	
k_{sh}	1.65	1.65	1.65	1.65	1.65	

Resistance values

V_f	0.05	0.05	0.05	0.05	0.05	
V_C	0.15	0.15	0.15	0.15	0.15	
V_a	0	0	0	0	0	
V_ρ	0	0	0	0	0	
V_r	0.1581	0.1581	0.1581	0.1581	0.1581	
k_f	0.13	0.13	0.13	0.13	0.13	
f_c/μ_f	0.9935	0.9935	0.9935	0.9935	0.9935	
k_C	1.65	1.65	1.65	1.65	1.65	
C_c/μ_C	0.7808	0.7808	0.7808	0.7808	0.7808	
k_a	1.65	1.65	1.65	1.65	1.65	
a_c/μ_a	1	1	1	1	1	
k_ρ	1.65	1.65	1.65	1.65	1.65	
ρ_c/μ_ρ	1.0000	1.0000	1.0000	1.0000	1.0000	
r_c/μ_r	0.7757	0.7757	0.7757	0.7757	0.7757	

Calculation of partial coefficients

β	3.72	3.72	3.72	3.72	3.72	
α'_{sh}	-0.0102	-0.1750	-0.3351	-0.4589	-0.5463	
α'_T	-0.4082	-0.3500	-0.2681	-0.1836	-0.1093	
ψ	1.1315	1.3302	1.7045	2.3961	3.8454	
κ_r	0.1789	0.2103	0.2695	0.3789	0.6080	
N	0.1960	0.2286	0.2684	0.4358	0.7322	
α_{sh}	-0.0102	-0.1750	-0.3351	-0.4589	-0.5463	
α_T	-0.4082	-0.3500	-0.2681	-0.1836	-0.1093	
α_r	0.9128	0.9202	0.9032	0.8693	0.8304	
$\Sigma\alpha_i^2$	1.0000	1.0000	1.0000	1.0000	1.0000	
Z	1.9358	2.2856	2.8994	3.9954	6.2672	
$\gamma_r\gamma_s$	1.3111	1.2682	1.2516	1.2588	1.2820	1.27

Table B.13b *b = 1, c = 1, V_C = 0.15 and V_ε = 0.10.*

Load values

ν_{sh}	0.01	0.20	0.50	1.00	2.00	
b	1	1	1	1	1	
c	1	1	1	1	1	
V_T	0.08	0.08	0.08	0.08	0.08	
V_{sh}	0.20	0.20	0.20	0.20	0.20	
k_T	1.65	1.65	1.65	1.65	1.65	
k_{sh}	1.65	1.65	1.65	1.65	1.65	

Resistance values

V_f	0.10	0.10	0.10	0.10	0.10	
V_C	0.15	0.15	0.15	0.15	0.15	
V_a	0	0	0	0	0	
V_ρ	0	0	0	0	0	
V_r	0.1803	0.1803	0.1803	0.1803	0.1803	
k_f	0.13	0.13	0.13	0.13	0.13	
f_c/μ_f	0.9871	0.9871	0.9871	0.9871	0.9871	
k_C	1.65	1.65	1.65	1.65	1.65	
C_c/μ_C	0.7808	0.7808	0.7808	0.7808	0.7808	
k_a	1.65	1.65	1.65	1.65	1.65	
a_c/μ_a	1	1	1	1	1	
k_ρ	1.65	1.65	1.65	1.65	1.65	
ρ_c/μ_ρ	1.0000	1.0000	1.0000	1.0000	1.0000	
r_c/μ_r	0.7707	0.7707	0.7707	0.7707	0.7707	

Calculation of partial coefficients

β	3.72	3.72	3.72	3.72	3.72	
α'_{sh}	-0.0092	-0.1576	-0.3033	-0.4191	-0.5037	
α'_T	-0.3684	-0.3153	-0.2427	-0.1677	-0.1007	
ψ	1.1197	1.3173	1.6851	2.3617	3.7795	
κ_r	0.2019	0.2375	0.3038	0.4258	0.6814	
N	0.2171	0.2538	0.3297	0.4772	0.7941	
α_{sh}	-0.0092	-0.1576	-0.3033	-0.4191	-0.5037	
α_T	-0.3684	-0.3153	-0.2427	-0.1677	-0.1007	
α_r	0.9296	0.9358	0.9215	0.8923	0.8580	
$\Sigma\alpha_i^2$	1.0000	1.0000	1.0000	1.0000	1.0000	
Z	2.0886	2.4674	3.1260	4.2965	6.7193	
$\gamma_r\gamma_s$	1.4054	1.3602	1.3406	1.3449	1.3656	1.36

Table B.13c *b = 1, c = 1, V_C = 0.15 and V_ε = 0.15.*

Load values

ν_{sh}	0.01	0.20	0.50	1.00	2.00	
b	1	1	1	1	1	
c	1	1	1	1	1	
V_T	0.08	0.08	0.08	0.08	0.08	
V_{sh}	0.20	0.20	0.20	0.20	0.20	
k_T	1.65	1.65	1.65	1.65	1.65	
k_{sh}	1.65	1.65	1.65	1.65	1.65	

Resistance values

V_f	0.15	0.15	0.15	0.15	0.15	
V_C	0.15	0.15	0.15	0.15	0.15	
V_a	0	0	0	0	0	
V_ρ	0	0	0	0	0	
V_r	0.2121	0.2121	0.2121	0.2121	0.2121	
k_f	0.13	0.13	0.13	0.13	0.13	
f_c/μ_f	0.9807	0.9807	0.9807	0.9807	0.9807	
k_C	1.65	1.65	1.65	1.65	1.65	
C_c/μ_C	0.7808	0.7808	0.7808	0.7808	0.7808	
k_a	1.65	1.65	1.65	1.65	1.65	
a_c/μ_a	1	1	1	1	1	
k_ρ	1.65	1.65	1.65	1.65	1.65	
ρ_c/μ_ρ	1.0000	1.0000	1.0000	1.0000	1.0000	
r_c/μ_r	0.7657	0.7657	0.7657	0.7657	0.7657	

Calculation of partial coefficients

β	3.72	3.72	3.72	3.72	3.72	
α'_{sh}	-0.0081	-0.1377	-0.2665	-0.3721	-0.4522	
α'_T	-0.3227	-0.2755	-0.2132	-0.1489	-0.0904	
ψ	1.1061	1.3025	1.6626	2.3212	3.6998	
κ_r	0.2346	0.2763	0.3527	0.4924	0.7848	
N	0.2479	0.2904	0.3752	0.5374	0.8845	
α_{sh}	-0.0081	-0.1377	-0.2665	-0.3721	-0.4522	
α_T	-0.3227	-0.2755	-0.2132	-0.1489	-0.0904	
α_r	0.9465	0.9514	0.9400	0.9162	0.8873	
$\Sigma\alpha_i^2$	1.0000	1.0000	1.0000	1.0000	1.0000	
Z	2.3343	2.7595	3.4908	4.7829	7.4520	
$\gamma_r\gamma_s$	1.5606	1.5113	1.4874	1.4875	1.5047	1.51

Table B.13d *b = 1, c = 1, V_C = 0.15 and V_ε = 0.20.*

Load values

ν_{sh}	0.01	0.20	0.50	1.00	2.00	
b	1	1	1	1	1	
c	1	1	1	1	1	
V_T	0.08	0.08	0.08	0.08	0.08	
V_{sh}	0.20	0.20	0.20	0.20	0.20	
k_T	1.65	1.65	1.65	1.65	1.65	
k_{sh}	1.65	1.65	1.65	1.65	1.65	

Resistance values

V_f	0.20	0.20	0.20	0.20	0.20	
V_C	0.15	0.15	0.15	0.15	0.15	
V_a	0	0	0	0	0	
V_ρ	0	0	0	0	0	
V_r	0.2500	0.2500	0.2500	0.2500	0.2500	
k_f	0.13	0.13	0.13	0.13	0.13	
f_c/μ_f	0.9743	0.9743	0.9743	0.9743	0.9743	
k_C	1.65	1.65	1.65	1.65	1.65	
C_c/μ_C	0.7808	0.7808	0.7808	0.7808	0.7808	
k_a	1.65	1.65	1.65	1.65	1.65	
a_c/μ_a	1	1	1	1	1	
k_ρ	1.65	1.65	1.65	1.65	1.65	
ρ_c/μ_ρ	1.0000	1.0000	1.0000	1.0000	1.0000	
r_c/μ_r	0.7607	0.7607	0.7607	0.7607	0.7607	

Calculation of partial coefficients

β	3.72	3.72	3.72	3.72	3.72	
α'_{sh}	-0.0070	-0.1196	-0.2326	-0.3279	-0.4027	
α'_T	-0.2808	-0.2392	-0.1861	-0.1311	-0.0805	
ψ	1.0936	1.2890	1.6419	2.2829	3.6231	
κ_r	0.2734	0.3222	0.4105	0.5707	0.9058	
N	0.2849	0.3344	0.4300	0.6100	0.9934	
α_{sh}	-0.0070	-0.1196	-0.2326	-0.3279	-0.4027	
α_T	-0.2808	-0.2392	-0.1861	-0.1311	-0.0805	
α_r	0.9597	0.9636	0.9546	0.9356	0.9118	
$\Sigma\alpha_i^2$	1.0000	1.0000	1.0000	1.0000	1.0000	
Z	2.6699	3.1581	3.9894	5.4497	8.4597	
$\gamma_r\gamma_s$	1.7734	1.7185	1.6888	1.6839	1.6971	1.71

Table B.13e *b = 1, c = 1, V_C = 0.15 and V_ε = 0.25.*

Load values

ν_{sh}	0.01	0.20	0.50	1.00	2.00	
b	1	1	1	1	1	
c	1	1	1	1	1	
V_T	0.08	0.08	0.08	0.08	0.08	
V_{sh}	0.20	0.20	0.20	0.20	0.20	
k_T	1.65	1.65	1.65	1.65	1.65	
k_{sh}	1.65	1.65	1.65	1.65	1.65	

Resistance values

V_f	0.25	0.25	0.25	0.25	0.25	
V_C	0.15	0.15	0.15	0.15	0.15	
V_a	0	0	0	0	0	
V_ρ	0	0	0	0	0	
V_r	0.2915	0.2915	0.2915	0.2915	0.2915	
k_f	0.13	0.13	0.13	0.13	0.13	
f_c/μ_f	0.9680	0.9680	0.9680	0.9680	0.9680	
k_C	1.65	1.65	1.65	1.65	1.65	
C_c/μ_C	0.7808	0.7808	0.7808	0.7808	0.7808	
k_a	1.65	1.65	1.65	1.65	1.65	
a_c/μ_a	1	1	1	1	1	
k_ρ	1.65	1.65	1.65	1.65	1.65	
ρ_c/μ_ρ	1.0000	1.0000	1.0000	1.0000	1.0000	
r_c/μ_r	0.7558	0.7558	0.7558	0.7558	0.7558	

Calculation of partial coefficients

β	3.72	3.72	3.72	3.72	3.72	
α'_{sh}	-0.0061	-0.1044	-0.2038	-0.2897	-0.3591	
α'_T	-0.2456	-0.2088	-0.1631	-0.1159	-0.0718	
ψ	1.0831	1.2777	1.6244	2.2500	3.5557	
κ_r	0.3158	0.3725	0.4736	0.6560	1.0366	
N	0.3258	0.3831	0.4906	0.6904	1.1140	
α_{sh}	-0.0061	-0.1044	-0.2038	-0.2897	-0.3591	
α_T	-0.2456	-0.2088	-0.1631	-0.1159	-0.0718	
α_r	0.9694	0.9724	0.9653	0.9501	0.9305	
$\Sigma\alpha_i^2$	1.0000	1.0000	1.0000	1.0000	1.0000	
Z	3.0993	3.6679	4.6277	6.3051	9.7549	
$\gamma_r\gamma_s$	2.0452	1.9830	1.9463	1.9355	1.9443	1.97

Table B.14a *b = 1, c = 1, V_C = 0.20 and V_ε = 0.05.*

Load values

ν_{sh}	0.01	0.20	0.50	1.00	2.00	
b	1	1	1	1	1	
c	1	1	1	1	1	
V_T	0.08	0.08	0.08	0.08	0.08	
V_{sh}	0.20	0.20	0.20	0.20	0.20	
k_T	1.65	1.65	1.65	1.65	1.65	
k_{sh}	1.65	1.65	1.65	1.65	1.65	

Resistance values

V_f	0.05	0.05	0.05	0.05	0.05	
V_C	0.20	0.20	0.20	0.20	0.20	
V_a	0	0	0	0	0	
V_ρ	0	0	0	0	0	
V_r	0.2062	0.2062	0.2062	0.2062	0.2062	
k_f	0.13	0.13	0.13	0.13	0.13	
f_c/μ_f	0.9935	0.9935	0.9935	0.9935	0.9935	
k_C	1.65	1.65	1.65	1.65	1.65	
C_c/μ_C	0.7189	0.7189	0.7189	0.7189	0.7189	
k_a	1.65	1.65	1.65	1.65	1.65	
a_c/μ_a	1	1	1	1	1	
k_ρ	1.65	1.65	1.65	1.65	1.65	
ρ_c/μ_ρ	1.0000	1.0000	1.0000	1.0000	1.0000	
r_c/μ_r	0.7143	0.7143	0.7143	0.7143	0.7143	

Calculation of partial coefficients

β	3.72	3.72	3.72	3.72	3.72	
α'_{sh}	-0.0083	-0.1411	-0.2728	-0.3802	-0.4611	
α'_T	-0.3304	-0.2822	-0.2182	-0.1521	-0.0922	
ψ	1.1084	1.3050	1.6664	2.3281	3.7136	
κ_r	0.2285	0.2690	0.3435	0.4800	0.7656	
N	0.2421	0.2835	0.3666	0.5261	0.8675	
α_{sh}	-0.0083	-0.1411	-0.2728	-0.3802	-0.4611	
α_T	-0.3304	-0.2822	-0.2182	-0.1521	-0.0922	
α_r	0.9438	0.9489	0.9370	0.9123	0.8825	
$\Sigma\alpha_i^2$	1.0000	1.0000	1.0000	1.0000	1.0000	
Z	2.2858	2.7018	3.4187	4.6866	7.3068	
$\gamma_r\gamma_s$	1.4255	1.3804	1.3589	1.3597	1.3763	1.38

Table B.14b *b = 1, c = 1, V_C = 0.20 and V_ε = 0.10.*

Load values

ν_{sh}	0.01	0.20	0.50	1.00	2.00	
b	1	1	1	1	1	
c	1	1	1	1	1	
V_T	0.08	0.08	0.08	0.08	0.08	
V_{sh}	0.20	0.20	0.20	0.20	0.20	
k_T	1.65	1.65	1.65	1.65	1.65	
k_{sh}	1.65	1.65	1.65	1.65	1.65	

Resistance values

V_f	0.10	0.10	0.10	0.10	0.10	
V_C	0.20	0.20	0.20	0.20	0.20	
V_a	0	0	0	0	0	
V_ρ	0	0	0	0	0	
V_r	0.2236	0.2236	0.2236	0.2236	0.2236	
k_f	0.13	0.13	0.13	0.13	0.13	
f_c/μ_f	0.9871	0.9871	0.9871	0.9871	0.9871	
k_C	1.65	1.65	1.65	1.65	1.65	
C_c/μ_C	0.7189	0.7189	0.7189	0.7189	0.7189	
k_a	1.65	1.65	1.65	1.65	1.65	
a_c/μ_a	1	1	1	1	1	
k_ρ	1.65	1.65	1.65	1.65	1.65	
ρ_c/μ_ρ	1.0000	1.0000	1.0000	1.0000	1.0000	
r_c/μ_r	0.7096	0.7096	0.7096	0.7096	0.7096	

Calculation of partial coefficients

β	3.72	3.72	3.72	3.72	3.72	
α'_{sh}	-0.0077	-0.1317	-0.2553	-0.3576	-0.4360	
α'_T	-0.3088	-0.2634	-0.2042	-0.1430	-0.0872	
ψ	1.1020	1.2980	1.6557	2.3086	3.6748	
κ_r	0.2464	0.2902	0.3702	0.5162	0.8217	
N	0.2591	0.3037	0.3918	0.5594	0.9174	
α_{sh}	-0.0077	-0.1317	-0.2553	-0.3576	-0.4360	
α_T	-0.3088	-0.2634	-0.2042	-0.1430	-0.0872	
α_r	0.9511	0.9557	0.9451	0.9229	0.8957	
$\Sigma\alpha_i^2$	1.0000	1.0000	1.0000	1.0000	1.0000	
Z	2.4308	2.8741	3.6341	4.9744	7.7411	
$\gamma_r\gamma_s$	1.5062	1.4589	1.4351	1.4338	1.4487	1.46

Table B.14c *b = 1, c = 1, V_C = 0.20 and V_ε = 0.15.*

Load values

ν_{sh}	0.01	0.20	0.50	1.00	2.00	
b	1	1	1	1	1	
c	1	1	1	1	1	
V_T	0.08	0.08	0.08	0.08	0.08	
V_{sh}	0.20	0.20	0.20	0.20	0.20	
k_T	1.65	1.65	1.65	1.65	1.65	
k_{sh}	1.65	1.65	1.65	1.65	1.65	

Resistance values

V_f	0.15	0.15	0.15	0.15	0.15	
V_C	0.20	0.20	0.20	0.20	0.20	
V_a	0	0	0	0	0	
V_ρ	0	0	0	0	0	
V_r	0.2500	0.2500	0.2500	0.2500	0.2500	
k_f	0.13	0.13	0.13	0.13	0.13	
f_c/μ_f	0.9807	0.9807	0.9807	0.9807	0.9807	
k_C	1.65	1.65	1.65	1.65	1.65	
C_c/μ_C	0.7189	0.7189	0.7189	0.7189	0.7189	
k_a	1.65	1.65	1.65	1.65	1.65	
a_c/μ_a	1	1	1	1	1	
k_ρ	1.65	1.65	1.65	1.65	1.65	
ρ_c/μ_ρ	1.0000	1.0000	1.0000	1.0000	1.0000	
r_c/μ_r	0.7050	0.7050	0.7050	0.7050	0.7050	

Calculation of partial coefficients

β	3.72	3.72	3.72	3.72	3.72	
α'_{sh}	-0.0070	-0.1196	-0.2326	-0.3279	-0.4027	
α'_T	-0.2808	-0.2392	-0.1861	-0.1311	-0.0805	
ψ	1.0936	1.2890	1.6419	2.2829	3.6231	
κ_r	0.2734	0.3222	0.4105	0.5707	0.9058	
N	0.2849	0.3344	0.4300	0.6100	0.9934	
α_{sh}	-0.0070	-0.1196	-0.2326	-0.3279	-0.4027	
α_T	-0.2808	-0.2392	-0.1861	-0.1311	-0.0805	
α_r	0.9597	0.9636	0.9546	0.9356	0.9118	
$\Sigma\alpha_i^2$	1.0000	1.0000	1.0000	1.0000	1.0000	
Z	2.6699	3.1581	3.9894	5.4497	8.4597	
$\gamma_r\gamma_s$	1.6436	1.5927	1.5652	1.5606	1.5729	1.59

Table B.14d *b = 1, c = 1, V_C = 0.20 and V_ε = 0.20.*

Load values

ν_{sh}	0.01	0.20	0.50	1.00	2.00	
b	1	1	1	1	1	
c	1	1	1	1	1	
V_T	0.08	0.08	0.08	0.08	0.08	
V_{sh}	0.20	0.20	0.20	0.20	0.20	
k_T	1.65	1.65	1.65	1.65	1.65	
k_{sh}	1.65	1.65	1.65	1.65	1.65	

Resistance values

V_f	0.20	0.20	0.20	0.20	0.20	
V_C	0.20	0.20	0.20	0.20	0.20	
V_a	0	0	0	0	0	
V_ρ	0	0	0	0	0	
V_r	0.2828	0.2828	0.2828	0.2828	0.2828	
k_f	0.13	0.13	0.13	0.13	0.13	
f_c/μ_f	0.9743	0.9743	0.9743	0.9743	0.9743	
k_C	1.65	1.65	1.65	1.65	1.65	
C_c/μ_C	0.7189	0.7189	0.7189	0.7189	0.7189	
k_a	1.65	1.65	1.65	1.65	1.65	
a_c/μ_a	1	1	1	1	1	
k_ρ	1.65	1.65	1.65	1.65	1.65	
ρ_c/μ_ρ	1.0000	1.0000	1.0000	1.0000	1.0000	
r_c/μ_r	0.7005	0.7005	0.7005	0.7005	0.7005	

Calculation of partial coefficients

β	3.72	3.72	3.72	3.72	3.72	
α'_{sh}	-0.0063	-0.1073	-0.2093	-0.2969	-0.3674	
α'_T	-0.2522	-0.2146	-0.1674	-0.1188	-0.0735	
ψ	1.0851	1.2798	1.6277	2.2563	3.5686	
κ_r	0.3069	0.3620	0.4604	0.6382	1.0094	
N	0.3172	0.3729	0.4779	0.6735	1.0887	
α_{sh}	-0.0063	-0.1073	-0.2093	-0.2969	-0.3674	
α_T	-0.2522	-0.2146	-0.1674	-0.1188	-0.0735	
α_r	0.9679	0.9708	0.9634	0.9475	0.9271	
$\Sigma\alpha_i^2$	1.0000	1.0000	1.0000	1.0000	1.0000	
Z	3.0036	3.5543	4.4854	6.1143	9.4659	
$\gamma_r\gamma_s$	1.8370	1.7809	1.7484	1.7396	1.7486	1.77

Table B.14e *b = 1, c = 1, V_C = 0.20 and V_ε = 0.25.*

Load values

ν_{sh}	0.01	0.20	0.50	1.00	2.00	
b	1	1	1	1	1	
c	1	1	1	1	1	
V_T	0.08	0.08	0.08	0.08	0.08	
V_{sh}	0.20	0.20	0.20	0.20	0.20	
k_T	1.65	1.65	1.65	1.65	1.65	
k_{sh}	1.65	1.65	1.65	1.65	1.65	

Resistance values

V_f	0.25	0.25	0.25	0.25	0.25	
V_C	0.20	0.20	0.20	0.20	0.20	
V_a	0	0	0	0	0	
V_ρ	0	0	0	0	0	
V_r	0.3202	0.3202	0.3202	0.3202	0.3202	
k_f	0.13	0.13	0.13	0.13	0.13	
f_c/μ_f	0.9680	0.9680	0.9680	0.9680	0.9680	
k_C	1.65	1.65	1.65	1.65	1.65	
C_c/μ_C	0.7189	0.7189	0.7189	0.7189	0.7189	
k_a	1.65	1.65	1.65	1.65	1.65	
a_c/μ_a	1	1	1	1	1	
k_ρ	1.65	1.65	1.65	1.65	1.65	
ρ_c/μ_ρ	1.0000	1.0000	1.0000	1.0000	1.0000	
r_c/μ_r	0.6959	0.6959	0.6959	0.6959	0.6959	

Calculation of partial coefficients

β	3.72	3.72	3.72	3.72	3.72	
α'_{sh}	-0.0056	-0.0960	-0.1878	-0.2680	-0.3340	
α'_T	-0.2259	-0.1920	-0.1502	-0.1072	-0.0668	
ψ	1.0773	1.2714	1.6146	2.2313	3.5169	
κ_r	0.3449	0.4070	0.5169	0.7144	1.1260	
N	0.3541	0.4168	0.5325	0.7461	1.1976	
α_{sh}	-0.0056	-0.0960	-0.1878	-0.2680	-0.3340	
α_T	-0.2259	-0.1920	-0.1502	-0.1072	-0.0668	
α_r	0.9741	0.9767	0.9707	0.9574	0.9402	
$\Sigma\alpha_i^2$	1.0000	1.0000	1.0000	1.0000	1.0000	
Z	3.4370	4.0688	5.1299	6.9788	10.7762	
$\gamma_r\gamma_s$	2.0885	2.0255	1.9867	1.9727	1.9777	2.01

Table B.15a *b = 1, c = 1, V_C = 0.25 and V_ε = 0.05.*

Load values

ν_{sh}	0.01	0.20	0.50	1.00	2.00	
b	1	1	1	1	1	
c	1	1	1	1	1	
V_T	0.08	0.08	0.08	0.08	0.08	
V_{sh}	0.20	0.20	0.20	0.20	0.20	
k_T	1.65	1.65	1.65	1.65	1.65	
k_{sh}	1.65	1.65	1.65	1.65	1.65	

Resistance values

V_f	0.05	0.05	0.05	0.05	0.05	
V_C	0.25	0.25	0.25	0.25	0.25	
V_a	0	0	0	0	0	
V_ρ	0	0	0	0	0	
V_r	0.2550	0.2550	0.2550	0.2550	0.2550	
k_f	0.13	0.13	0.13	0.13	0.13	
f_c/μ_f	0.9935	0.9935	0.9935	0.9935	0.9935	
k_C	1.65	1.65	1.65	1.65	1.65	
C_c/μ_C	0.6620	0.6620	0.6620	0.6620	0.6620	
k_a	1.65	1.65	1.65	1.65	1.65	
a_c/μ_a	1	1	1	1	1	
k_ρ	1.65	1.65	1.65	1.65	1.65	
ρ_c/μ_ρ	1.0000	1.0000	1.0000	1.0000	1.0000	
r_c/μ_r	0.6577	0.6577	0.6577	0.6577	0.6577	

Calculation of partial coefficients

β	3.72	3.72	3.72	3.72	3.72	
α'_{sh}	-0.0069	-0.1176	-0.2287	-0.3228	-0.3969	
α'_T	-0.2761	-0.2351	-0.1830	-0.1291	-0.0794	
ψ	1.0922	1.2875	1.6395	2.2786	3.6143	
κ_r	0.2785	0.3282	0.4180	0.8509	0.9215	
N	0.2897	0.3402	0.4372	0.6196	1.0077	
α_{sh}	-0.0069	-0.1176	-0.2287	-0.3228	-0.3969	
α_T	-0.2761	-0.2351	-0.1830	-0.1291	-0.0794	
α_r	0.9611	0.9648	0.9561	0.9376	0.9144	
$\Sigma\alpha_i^2$	1.0000	1.0000	1.0000	1.0000	1.0000	
Z	2.7176	3.2147	4.0602	5.5445	8.6031	
$\gamma_r\gamma_s$	1.5606	1.5124	1.4860	1.4812	1.4922	1.51

Table B.15b *b = 1, c = 1, V_C = 0.25 and V_ε = 0.10.*

Load values

ν_{sh}	0.01	0.20	0.50	1.00	2.00	
b	1	1	1	1	1	
c	1	1	1	1	1	
V_T	0.08	0.08	0.08	0.08	0.08	
V_{sh}	0.20	0.20	0.20	0.20	0.20	
k_T	1.65	1.65	1.65	1.65	1.65	
k_{sh}	1.65	1.65	1.65	1.65	1.65	

Resistance values

V_f	0.10	0.10	0.10	0.10	0.10	
V_C	0.25	0.25	0.25	0.25	0.25	
V_a	0	0	0	0	0	
V_ρ	0	0	0	0	0	
V_r	0.2693	0.2693	0.2693	0.2693	0.2693	
k_f	0.13	0.13	0.13	0.13	0.13	
f_c/μ_f	0.9871	0.9871	0.9871	0.9871	0.9871	
k_C	1.65	1.65	1.65	1.65	1.65	
C_c/μ_C	0.6620	0.6620	0.6620	0.6620	0.6620	
k_a	1.65	1.65	1.65	1.65	1.65	
a_c/μ_a	1	1	1	1	1	
k_ρ	1.65	1.65	1.65	1.65	1.65	
ρ_c/μ_ρ	1.0000	1.0000	1.0000	1.0000	1.0000	
r_c/μ_r	0.6534	0.6534	0.6534	0.6534	0.6534	

Calculation of partial coefficients

β	3.72	3.72	3.72	3.72	3.72	
α'_{sh}	-0.0066	-0.1121	-0.2183	-0.3090	-0.3812	
α'_T	-0.2633	-0.2241	-0.1747	-0.1236	-0.0762	
ψ	1.0884	1.2834	1.6332	2.2667	3.5900	
κ_r	0.2931	0.3456	0.4398	0.6103	0.9666	
N	0.3038	0.3569	0.4580	0.6472	1.0492	
α_{sh}	-0.0066	-0.1121	-0.2183	-0.3090	-0.3812	
α_T	-0.2633	-0.2241	-0.1747	-0.1236	-0.0762	
α_r	0.9647	0.9681	0.9601	0.9430	0.9213	
$\Sigma\alpha_i^2$	1.0000	1.0000	1.0000	1.0000	1.0000	
Z	2.8605	3.3844	4.2726	5.8291	9.0339	
$\gamma_r\gamma_s$	1.6320	1.5819	1.5537	1.5471	1.5567	1.57

Table B.15c *b = 1, c = 1, V_C = 0.25 and V_ε = 0.15.*

Load values

ν_{sh}	0.01	0.20	0.50	1.00	2.00	
b	1	1	1	1	1	
c	1	1	1	1	1	
V_T	0.08	0.08	0.08	0.08	0.08	
V_{sh}	0.20	0.20	0.20	0.20	0.20	
k_T	1.65	1.65	1.65	1.65	1.65	
k_{sh}	1.65	1.65	1.65	1.65	1.65	

Resistance values

V_f	0.15	0.15	0.15	0.15	0.15	
V_C	0.25	0.25	0.25	0.25	0.25	
V_a	0	0	0	0	0	
V_ρ	0	0	0	0	0	
V_r	0.2915	0.2915	0.2915	0.2915	0.2915	
k_f	0.13	0.13	0.13	0.13	0.13	
f_c/μ_f	0.9807	0.9807	0.9807	0.9807	0.9807	
k_C	1.65	1.65	1.65	1.65	1.65	
C_c/μ_C	0.6620	0.6620	0.6620	0.6620	0.6620	
k_a	1.65	1.65	1.65	1.65	1.65	
a_c/μ_a	1	1	1	1	1	
k_ρ	1.65	1.65	1.65	1.65	1.65	
ρ_c/μ_ρ	1.0000	1.0000	1.0000	1.0000	1.0000	
r_c/μ_r	0.6492	0.6492	0.6492	0.6492	0.6492	

Calculation of partial coefficients

β	3.72	3.72	3.72	3.72	3.72	
α'_{sh}	-0.0061	-0.1044	-0.2038	-0.2897	-0.3591	
α'_T	-0.2456	-0.2088	-0.1631	-0.1159	-0.0718	
ψ	1.0831	1.2777	1.6244	2.2500	3.5557	
κ_r	0.3158	0.3725	0.4736	0.6560	1.0366	
N	0.3258	0.3831	0.4906	0.6904	1.1140	
α_{sh}	-0.0061	-0.1044	-0.2038	-0.2897	-0.3591	
α_T	-0.2456	-0.2088	-0.1631	-0.1159	-0.0718	
α_r	0.9694	0.9724	0.9653	0.9501	0.9305	
$\Sigma\alpha_i^2$	1.0000	1.0000	1.0000	1.0000	1.0000	
Z	3.0993	3.6679	4.6277	6.3051	9.7549	
$\gamma_r\gamma_s$	1.7568	1.7033	1.6719	1.6626	1.6701	1.69

Table B.15d *b = 1, c = 1, V_C = 0.25 and V_ε = 0.20.*

Load values

ν_{sh}	0.01	0.20	0.50	1.00	2.00	
b	1	1	1	1	1	
c	1	1	1	1	1	
V_T	0.08	0.08	0.08	0.08	0.08	
V_{sh}	0.20	0.20	0.20	0.20	0.20	
k_T	1.65	1.65	1.65	1.65	1.65	
k_{sh}	1.65	1.65	1.65	1.65	1.65	

Resistance values

V_f	0.20	0.20	0.20	0.20	0.20	
V_C	0.25	0.25	0.25	0.25	0.25	
V_a	0	0	0	0	0	
V_ρ	0	0	0	0	0	
V_r	0.3202	0.3202	0.3202	0.3202	0.3202	
k_f	0.13	0.13	0.13	0.13	0.13	
f_c/μ_f	0.9743	0.9743	0.9743	0.9743	0.9743	
k_C	1.65	1.65	1.65	1.65	1.65	
C_c/μ_C	0.6620	0.6620	0.6620	0.6620	0.6620	
k_a	1.65	1.65	1.65	1.65	1.65	
a_c/μ_a	1	1	1	1	1	
k_ρ	1.65	1.65	1.65	1.65	1.65	
ρ_c/μ_ρ	1.0000	1.0000	1.0000	1.0000	1.0000	
r_c/μ_r	0.6450	0.6450	0.6450	0.6450	0.6450	

Calculation of partial coefficients

β	3.72	3.72	3.72	3.72	3.72	
α'_{sh}	-0.0056	-0.0960	-0.1878	-0.2680	-0.3340	
α'_T	-0.2259	-0.1920	-0.1502	-0.1072	-0.0668	
ψ	1.0773	1.2714	1.6146	2.2313	3.5169	
κ_r	0.3449	0.4070	0.5169	0.7144	1.1260	
N	0.3541	0.4168	0.5325	0.7461	1.1976	
α_{sh}	-0.0056	-0.0960	-0.1878	-0.2680	-0.3340	
α_T	-0.2259	-0.1920	-0.1502	-0.1072	-0.0668	
α_r	0.9741	0.9767	0.9707	0.9574	0.9402	
$\Sigma\alpha_i^2$	1.0000	1.0000	1.0000	1.0000	1.0000	
Z	3.4370	4.0688	5.1299	6.9788	10.7762	
$\gamma_r\gamma_s$	1.9356	1.8773	1.8413	1.8283	1.8330	1.86

Table B.15e *b = 1, c = 1, V_C = 0.25 and V_ε = 0.25.*

Load values

ν_{sh}	0.01	0.20	0.50	1.00	2.00	
b	1	1	1	1	1	
c	1	1	1	1	1	
V_T	0.08	0.08	0.08	0.08	0.08	
V_{sh}	0.20	0.20	0.20	0.20	0.20	
k_T	1.65	1.65	1.65	1.65	1.65	
k_{sh}	1.65	1.65	1.65	1.65	1.65	

Resistance values

V_f	0.25	0.25	0.25	0.25	0.25	
V_C	0.25	0.25	0.25	0.25	0.25	
V_a	0	0	0	0	0	
V_ρ	0	0	0	0	0	
V_r	0.3536	0.3536	0.3536	0.3536	0.3536	
k_f	0.13	0.13	0.13	0.13	0.13	
f_c/μ_f	0.9680	0.9680	0.9680	0.9680	0.9680	
k_C	1.65	1.65	1.65	1.65	1.65	
C_c/μ_C	0.6620	0.6620	0.6620	0.6620	0.6620	
k_a	1.65	1.65	1.65	1.65	1.65	
a_c/μ_a	1	1	1	1	1	
k_ρ	1.65	1.65	1.65	1.65	1.65	
ρ_c/μ_ρ	1.0000	1.0000	1.0000	1.0000	1.0000	
r_c/μ_r	0.6408	0.6408	0.6408	0.6408	0.6408	

Calculation of partial coefficients

β	3.72	3.72	3.72	3.72	3.72	
α'_{sh}	-0.0052	-0.0877	-0.1719	-0.2465	-0.3088	
α'_T	-0.2066	-0.1754	-0.1375	-0.0986	-0.0618	
ψ	1.0715	1.2652	1.6049	2.2127	3.4778	
κ_r	0.3788	0.4473	0.5674	0.7823	1.2296	
N	0.3872	0.4562	0.5817	0.8114	1.2955	
α_{sh}	-0.0052	-0.0877	-0.1719	-0.2465	-0.3088	
α_T	-0.2066	-0.1754	-0.1375	-0.0986	-0.0618	
α_r	0.9784	0.9806	0.9755	0.9641	0.9491	
$\Sigma\alpha_i^2$	1.0000	1.0000	1.0000	1.0000	1.0000	
Z	3.8803	4.5949	5.7892	7.8637	12.1184	
$\gamma_r\gamma_s$	2.1711	2.1062	2.0645	2.0468	2.0479	2.09

Table B.16 *Partial coefficients for* $\beta = 3.72$, $b = 1$, $c = 1$, $V_C = 0.05 - 0.25$, $V_\varepsilon = 0.05 - 0.25$ *and* $k_T = k_{sh} = 0.13$.

β	b	c	V_C	V_ε	$\gamma_r\gamma_s$
3.72	1	1	0.05	0.05	1.36
3.72	1	1	0.05	0.10	1.52
3.72	1	1	0.05	0.15	1.75
3.72	1	1	0.05	0.20	2.04
3.72	1	1	0.05	0.25	2.41
3.72	1	1	0.10	0.05	1.41
3.72	1	1	0.10	0.10	1.54
3.72	1	1	0.10	0.15	1.73
3.72	1	1	0.10	0.20	2.00
3.72	1	1	0.10	0.25	2.33
3.72	1	1	0.15	0.05	1.50
3.72	1	1	0.15	0.10	1.61
3.72	1	1	0.15	0.15	1.78
3.72	1	1	0.15	0.20	2.02
3.72	1	1	0.15	0.25	2.32
3.72	1	1	0.20	0.05	1.63
3.72	1	1	0.20	0.10	1.72
3.72	1	1	0.20	0.15	1.87
3.72	1	1	0.20	0.20	2.09
3.72	1	1	0.20	0.25	2.37
3.72	1	1	0.25	0.05	1.78
3.72	1	1	0.25	0.10	1.86
3.72	1	1	0.25	0.15	2.00
3.72	1	1	0.25	0.20	2.20
3.72	1	1	0.25	0.25	2.46

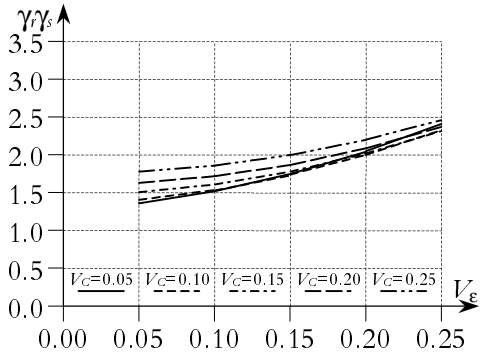

Appendix C

Deflection, Ground Pressure and Bending Moments in Structures on Elastic Foundations

C.1 Structures on Elastic Foundations

Consider a prismatic beam of finite length supported along its whole length by an elastic material, see Figure C.1. The deflection in every single point along the beam is proportional to the intensity of the uniform ground pressure.

The total deflexion $w_{tot}(x)$ from the surface of the unloaded ground, is the sum of two components; one rigid body deformation, w_0, and one deformation, w, originating from the actual loading case. The following derivations of the deflexion are valid for the second component.

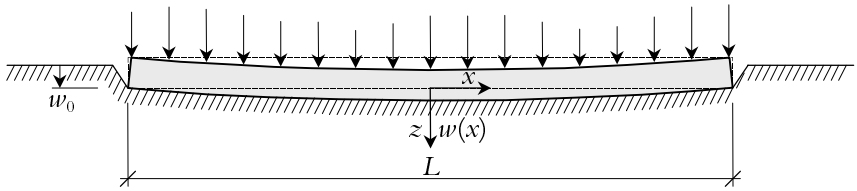

Figure C.1 *Prismatic beam of finite length on elastic foundation.*

The ground pressure $p(x)$ along the beam is

$$p = q + kw \tag{C.1}$$

$q = q(x)$ [N/m] is the distributed dead weight of the beam and $w = w(x)$ is the sought deflexion. k is the modulus of stiffness of the ground, which can be expressed as

$$k = \frac{2K_j}{\kappa} \tag{C.2}$$

where K_j [N/m^2] is the modulus of compression of the elastic material and κ [-] is a factor depending on the shape of the surface of the beam resting on the ground, here the width divided by the length.

The elastic curve equation derived twice

$$EI_y \frac{d^4w}{dx^4} = q - p \tag{C.3}$$

Equation (C.1) in Equation (C.3) give

$$EI_y \frac{d^4w}{dx^4} = q - q - kw = -kw$$

$$w^{IV} + \frac{k}{EI_y} w = 0 \tag{C.4}$$

If the so-called elastic length is introduced

$$L_e = \sqrt[4]{\frac{4EI_y}{k}}$$

the differential equation of forth order can be written as

$$w^{IV} + 4\frac{1}{L_e^4} w = 0 \tag{C.5}$$

C.1.1 General solution

The solution to Equation (C.5) is obtained as the sum of a particular solution and a solution of a homogeneous equation

$$w = w_p + w_h \tag{C.6}$$

Particular solution

The particular solution is obtained by letting

$$w_p = a$$

that in Equation (C.5) gives

$$4\frac{1}{L_e^4}a = 0 \quad \Rightarrow$$

$$a = 0$$

which gives the particular solution

$$w_p = 0 \tag{C.7}$$

Solution of homogeneous equation

The general solution of the homogeneous equation is obtained through the characteristic equation

$$s^4 + 4\frac{1}{L_e^4} = 0$$

$$s^4 = -4\frac{1}{L_e^4} \tag{C.8}$$

Now, for complex numbers is

$$e^{i\pi} = -1$$

The left part of Equation (C.8) can then be written as

$$s^4 = \left(re^{i\varphi}\right)^4 = r^4 e^{i4\varphi} \tag{C.9}$$

In the same way for the right part

$$-4\frac{1}{L_e^4} = 4\frac{1}{L_e^4}e^{i\pi} \tag{C.10}$$

Equation (C.9) and Equation (C.10) in Equation (C.8) then give

$$r^4 e^{i4\varphi} = 4\frac{1}{L_e^4}e^{i\pi}$$

Identification of the constants r and φ give

Real part:

$$r^4 = 4\frac{1}{L_e^4} \quad \Rightarrow$$

$$r = \sqrt[4]{4\frac{1}{L_e^4}} = \sqrt{2}\frac{1}{L_e}$$

Imaginary part:

$$4\varphi = \pi + 2n\pi \quad \Rightarrow$$

$$\varphi = \frac{\pi}{4} + n\frac{\pi}{2}; \quad n = 0,1,2...$$

These constants in Equation (C.10) give

$$s^4 = 4\frac{1}{L_e^4}e^{i4\left(\frac{\pi}{4}+n\frac{\pi}{2}\right)}; \quad n = 0,1,2...$$

whose four solutions are

$$s_1 = \frac{1}{L_e}\sqrt{2}e^{i\frac{\pi}{4}} = \sqrt{2}\frac{1}{L_e}\left(\cos\frac{\pi}{4} + i\sin\frac{\pi}{4}\right) = \frac{1}{L_e}(1+i)$$

$$s_2 = \frac{1}{L_e}\sqrt{2}e^{i\frac{3\pi}{4}} = \sqrt{2}\frac{1}{L_e}\left(\cos\frac{3\pi}{4} + i\sin\frac{3\pi}{4}\right) = \frac{1}{L_e}(-1+i)$$

$$s_3 = \overline{s_2} = \frac{1}{L_e}(-1-i)$$

$$s_4 = \overline{s_1} = \frac{1}{L_e}(1-i)$$

These give the solution of the homogeneous equation to

$$w_h = e^{\frac{x}{L_e}}\left(A_1\cos\frac{x}{L_e} + A_2\sin\frac{x}{L_e}\right) + e^{\frac{-x}{L_e}}\left(A_3\cos\frac{x}{L_e} + A_4\sin\frac{x}{L_e}\right) \quad \text{(C.11)}$$

Finally, the general solution of the differential equation (C.5) is obtained with Equations (C.7) and (C.11) in Equation (C.6)

$$w = e^{\frac{x}{L_e}}\left(A_1\cos\frac{x}{L_e} + A_2\sin\frac{x}{L_e}\right) + e^{\frac{-x}{L_e}}\left(A_3\cos\frac{x}{L_e} + A_4\sin\frac{x}{L_e}\right) \quad \text{(C.12)}$$

C.1.3 Symmetry

The solution of the differential equation (C.12) is expressed in terms of hyperbolic functions as

$$w = C_1 \sin\frac{x}{L_e}\sinh\frac{x}{L_e} + C_2 \sin\frac{x}{L_e}\cosh\frac{x}{L_e} + C_3 \cos\frac{x}{L_e}\sinh\frac{x}{L_e} + C_4 \cos\frac{x}{L_e}\cosh\frac{x}{L_e} \tag{C.13}$$

To fulfil the symmetry around the mid-section of the beam ($x = 0$), the constants C_2 and C_3 must be equal to zero ($C_2 = C_3 = 0$), see Figure C.2.

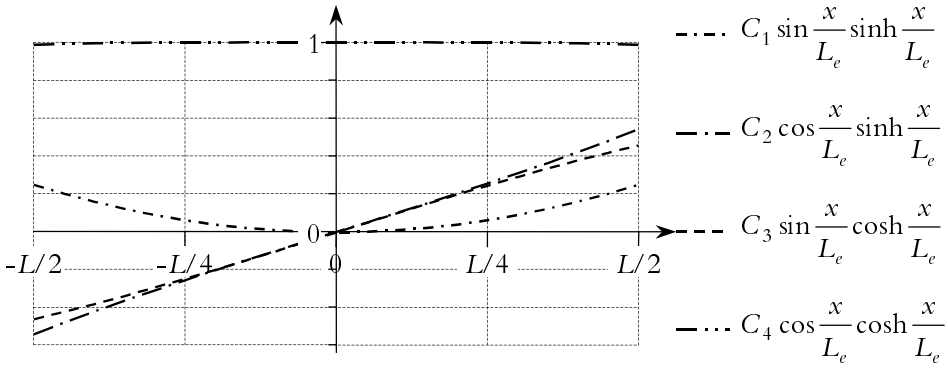

Figure C.2 *Graphical presentation of the symmetry of the four parts of Equation (C.13) depending on the constants C_1 to C_4.*

In Equation (C.13) this gives

$$w = C_1 \sin\frac{x}{L_e}\sinh\frac{x}{L_e} + C_4 \cos\frac{x}{L_e}\cosh\frac{x}{L_e} \tag{C.14}$$

Derivation of Equation (C.14)

$$\frac{dw}{dx} = \frac{1}{L_e}C_1\left(\cos\frac{x}{L_e}\sinh\frac{x}{L_e} + \sin\frac{x}{L_e}\cosh\frac{x}{L_e}\right) + \frac{1}{L_e}C_4\left(\cos\frac{x}{L_e}\sinh\frac{x}{L_e} - \sin\frac{x}{L_e}\cosh\frac{x}{L_e}\right) \tag{C.15}$$

$$\frac{d^2w}{dx^2} = \frac{2}{L_e^2} C_1 \cos\frac{x}{L_e}\cosh\frac{x}{L_e} - \frac{2}{L_e^2} C_4 \sin\frac{x}{L_e}\sinh\frac{x}{L_e} \tag{C.16}$$

$$\begin{aligned}\frac{d^3w}{dx^3} = \frac{2}{L_e^3} C_1 \left(\cos\frac{x}{L_e}\sinh\frac{x}{L_e} - \sin\frac{x}{L_e}\cosh\frac{x}{L_e} \right) - \\ \frac{2}{L_e^3} C_4 \left(\cos\frac{x}{L_e}\sinh\frac{x}{L_e} + \sin\frac{x}{L_e}\cosh\frac{x}{L_e} \right)\end{aligned} \tag{C.17}$$

C.2 Structures Loaded by Equals and Opposite Bending Moments at the Ends

For a case with a finite beam loaded by two equals and opposite bending moments at its ends, see Figure C.3, the following boundary conditions are valid

$$\left.\frac{d^2w}{dx^2}\right|_{x=\frac{-L}{2}} = \left.\frac{d^2w}{dx^2}\right|_{x=\frac{L}{2}} = -\frac{M_{RI}}{EI_y} \tag{C.18}$$

$$\left.\frac{d^3w}{dx^3}\right|_{x=\frac{-L}{2}} = \left.\frac{d^3w}{dx^3}\right|_{x=\frac{L}{2}} = 0 \tag{C.19}$$

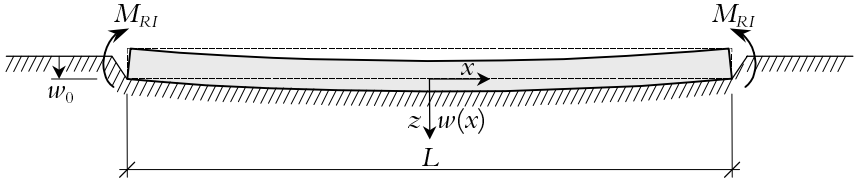

Figure C.3 *Prismatic beam of finite length on elastic foundation loaded by two equals and opposite bending moments at its ends.*

Equation (C.16) with boundary condition (C.18)

$$\frac{2}{L_e^2} C_1 \cos\frac{L}{2L_e}\cosh\frac{L}{2L_e} - \frac{2}{L_e^2} C_4 \sin\frac{L}{2L_e}\sinh\frac{L}{2L_e} = -\frac{M_{RI}}{EI_y}$$

$$C_1 - C_4 \frac{\sin\frac{L}{2L_e}\sinh\frac{L}{2L_e}}{\cos\frac{L}{2L_e}\cosh\frac{L}{2L_e}} = -\frac{M_{RI}L_e^2}{2EI_y}\frac{1}{\cos\frac{L}{2L_e}\cosh\frac{L}{2L_e}} \qquad \text{(C.20)}$$

Equation (C.17) with boundary condition (C.19)

$$\frac{2}{L_e^3}C_1\left\{\cos\left(-\frac{L}{2L_e}\right)\sinh\left(-\frac{L}{2L_e}\right)-\sin\left(-\frac{L}{2L_e}\right)\cosh\left(-\frac{L}{2L_e}\right)\right\}-$$
$$\frac{2}{L_e^3}C_4\left\{\cos\left(-\frac{L}{2L_e}\right)\sinh\left(-\frac{L}{2L_e}\right)+\sin\left(-\frac{L}{2L_e}\right)\cosh\left(-\frac{L}{2L_e}\right)\right\}=0$$

$$C_1 = C_4\frac{\cos\frac{L}{2L_e}\sinh\frac{L}{2L_e}+\sin\frac{L}{2L_e}\cosh\frac{L}{2L_e}}{\cos\frac{L}{2L_e}\sinh\frac{L}{2L_e}-\sin\frac{L}{2L_e}\cosh\frac{L}{2L_e}} \qquad \text{(C.21)}$$

Equation (C.21) in Equation (C.20) give

$$C_4\frac{\cos\frac{L}{2L_e}\sinh\frac{L}{2L_e}+\sin\frac{L}{2L_e}\cosh\frac{L}{2L_e}}{\cos\frac{L}{2L_e}\sinh\frac{L}{2L_e}-\sin\frac{L}{2L_e}\cosh\frac{L}{2L_e}} - C_4\frac{\sin\frac{L}{2L_e}\sinh\frac{L}{2L_e}}{\cos\frac{L}{2L_e}\cosh\frac{L}{2L_e}} =$$
$$= -\frac{M_{RI}L_e^2}{2EI_y}\frac{1}{\cos\frac{L}{2L_e}\cosh\frac{L}{2L_e}}$$

$$C_4\left\{\frac{\cos^2\frac{L}{2L_e}\cosh\frac{L}{2L_e}\sinh\frac{L}{2L_e}+\cos\frac{L}{2L_e}\sin\frac{L}{2L_e}\cosh^2\frac{L}{2L_e}}{\cos\frac{L}{2L_e}\cosh\frac{L}{2L_e}\left(\cos\frac{L}{2L_e}\sinh\frac{L}{2L_e}-\sin\frac{L}{2L_e}\cosh\frac{L}{2L_e}\right)}-\right.$$

$$\left.\frac{\cos\frac{L}{2L_e}\sin\frac{L}{2L_e}\sinh^2\frac{L}{2L_e}+\sin^2\frac{L}{2L_e}\cosh\frac{L}{2L_e}\sinh\frac{L}{2L_e}}{\cos\frac{L}{2L_e}\cosh\frac{L}{2L_e}\left(\cos\frac{L}{2L_e}\sinh\frac{L}{2L_e}-\sin\frac{L}{2L_e}\cosh\frac{L}{2L_e}\right)}\right\}=$$

$$=-\frac{M_{RI}L_e^2}{2EI_y}\frac{1}{\cos\frac{L}{2L_e}\cosh\frac{L}{2L_e}}$$

$$C_4\frac{\left(\cos^2\frac{L}{2L_e}+\sin^2\frac{L}{2L_e}\right)\cosh\frac{L}{2L_e}\sinh\frac{L}{2L_e}}{\cos\frac{L}{2L_e}\cosh\frac{L}{2L_e}\left(\cos\frac{L}{2L_e}\sinh\frac{L}{2L_e}-\sin\frac{L}{2L_e}\cosh\frac{L}{2L_e}\right)}+$$

$$\frac{\left(\cosh^2\frac{L}{2L_e}-\sinh^2\frac{L}{2L_e}\right)\cos\frac{L}{2L_e}\sin\frac{L}{2L_e}}{\cos\frac{L}{2L_e}\cosh\frac{L}{2L_e}\left(\cos\frac{L}{2L_e}\sinh\frac{L}{2L_e}-\sin\frac{L}{2L_e}\cosh\frac{L}{2L_e}\right)}=$$

$$=-\frac{M_{RI}L_e^2}{2EI_y}\frac{1}{\cos\frac{L}{2L_e}\cosh\frac{L}{2L_e}}$$

$$C_4\frac{\cosh\frac{L}{2L_e}\sinh\frac{L}{2L_e}+\cos\frac{L}{2L_e}\sin\frac{L}{2L_e}}{\cos\frac{L}{2L_e}\sinh\frac{L}{2L_e}-\sin\frac{L}{2L_e}\cosh\frac{L}{2L_e}}=-\frac{M_{RI}L_e^2}{2EI_y}$$

$$C_4 \frac{\sinh\frac{L}{L_e}+\sin\frac{L}{L_e}}{\cos\frac{L}{2L_e}\sinh\frac{L}{2L_e}-\sin\frac{L}{2L_e}\cosh\frac{L}{2L_e}} = -\frac{M_{RI}L_e^2}{EI_y}$$

$$C_4 = -\frac{M_{RI}L_e^2}{EI_y}\frac{\cos\frac{L}{2L_e}\sinh\frac{L}{2L_e}-\sin\frac{L}{2L_e}\cosh\frac{L}{2L_e}}{\sinh\frac{L}{L_e}+\sin\frac{L}{L_e}} \tag{C.22}$$

With Equation (C.22) in Equation (C.21) C_1 is determined as

$$C_1 = -\frac{M_{RI}L_e^2}{EI_y}\frac{\cos\frac{L}{2L_e}\sinh\frac{L}{2L_e}-\sin\frac{L}{2L_e}\cosh\frac{L}{2L_e}}{\sinh\frac{L}{L_e}+\sin\frac{L}{L_e}}\cdot$$

$$\cdot\frac{\cos\frac{L}{2L_e}\sinh\frac{L}{2L_e}+\sin\frac{L}{2L_e}\cosh\frac{L}{2L_e}}{\cos\frac{L}{2L_e}\sinh\frac{L}{2L_e}-\sin\frac{L}{2L_e}\cosh\frac{L}{2L_e}}$$

$$C_1 = -\frac{M_{RI}L_e^2}{EI_y}\frac{\cos\frac{L}{2L_e}\sinh\frac{L}{2L_e}+\sin\frac{L}{2L_e}\cosh\frac{L}{2L_e}}{\sinh\frac{L}{L_e}+\sin\frac{L}{L_e}} \tag{C.23}$$

Final solution

Equations (C.22) and (C.23) will give the final equation for the deflexion

$$w(x) = -\frac{4M_{RI}}{kL_e^2\left(\sin\frac{L}{L_e}+\sinh\frac{L}{L_e}\right)}\cdot \left\{\left(\cos\frac{L}{2L_e}\sinh\frac{L}{2L_e}+\sin\frac{L}{2L_e}\cosh\frac{L}{2L_e}\right)\sin\frac{x}{L_e}\sinh\frac{x}{L_e}+ \right. \left. +\left(\cos\frac{L}{2L_e}\sinh\frac{L}{2L_e}-\sin\frac{L}{2L_e}\cosh\frac{L}{2L_e}\right)\cos\frac{x}{L_e}\cosh\frac{x}{L_e}\right\} \quad \text{(C.24)}$$

With the deflexion known, the equations for the ground pressure and the moment distribution along the beam can be determined.

The ground pressure is obtained according to Equation (C.1) with Equation (C.24)

$$p(x) = q - \frac{4M_{RI}}{L_e^2\left(\sin\frac{L}{L_e}+\sinh\frac{L}{L_e}\right)}\cdot \left\{\left(\cos\frac{L}{2L_e}\sinh\frac{L}{2L_e}+\sin\frac{L}{2L_e}\cosh\frac{L}{2L_e}\right)\sin\frac{x}{L_e}\sinh\frac{x}{L_e}+ \right. \left. +\left(\cos\frac{L}{2L_e}\sinh\frac{L}{2L_e}-\sin\frac{L}{2L_e}\cosh\frac{L}{2L_e}\right)\cos\frac{x}{L_e}\cosh\frac{x}{L_e}\right\} \quad \text{(C.25)}$$

The moment distribution is obtained from the elastic line equation

$$M(x) = -EI_y\frac{d^2w}{dx^2}$$

$$M(x)=\frac{2M_{RI}}{\left(\sin\frac{L}{L_e}+\sinh\frac{L}{L_e}\right)}\cdot$$
$$\cdot\left\{\left(\cos\frac{L}{2L_e}\sinh\frac{L}{2L_e}+\sin\frac{L}{2L_e}\cosh\frac{L}{2L_e}\right)\cos\frac{x}{L_e}\cosh\frac{x}{L_e}-\right. \tag{C.26}$$
$$\left.-\left(\cos\frac{L}{2L_e}\sinh\frac{L}{2L_e}-\sin\frac{L}{2L_e}\cosh\frac{L}{2L_e}\right)\sin\frac{x}{L_e}\sinh\frac{x}{L_e}\right\}$$

The bending moment in the mid span of the beam is obtained by equation (C.26) with x=0:

$$M_{mid}=\frac{2M_{RI}}{\left(\sin\frac{L}{L_e}+\sinh\frac{L}{L_e}\right)}\left(\cos\frac{L}{2L_e}\sinh\frac{L}{2L_e}+\sin\frac{L}{2L_e}\cosh\frac{L}{2L_e}\right) \tag{C.27}$$

C.3 Structures Loaded by Equals and Opposite Bending Moments and Equals and Vertical Forces at the Ends

For a case with a finite beam loaded by two equals and opposite bending moments and two equals and vertical forces at its ends, see Figure C.7, the following boundary conditions are valid

$$\left.\frac{d^2w}{dx^2}\right|_{x=\frac{-L_\delta}{2}}=\left.\frac{d^2w}{dx^2}\right|_{x=\frac{L_\delta}{2}}=-\frac{M_\delta}{EI_\gamma} \tag{C.28}$$

$$\left.\frac{d^3w}{dx^3}\right|_{x=\frac{-L_\delta}{2}}=\left.\frac{d^3w}{dx^3}\right|_{x=\frac{L_\delta}{2}}=-\frac{V_\delta}{EI_\gamma} \tag{C.29}$$

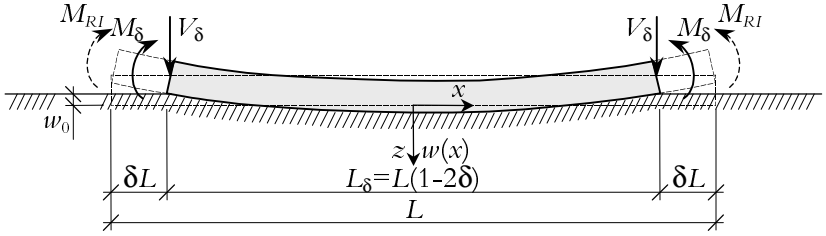

Figure C.4 *Prismatic beam of finite length on elastic foundation loaded by two equal and opposite equivalent bending moments and vertical and equal shear forces at its ends.*

Equation (C.16) with boundary condition (C.28) give

$$\frac{2}{L_e^2}C_1\cos\frac{L_\delta}{2L_e}\cosh\frac{L_\delta}{2L_e}-\frac{2}{L_e^2}C_4\sin\frac{L_\delta}{2L_e}\sinh\frac{L_\delta}{2L_e}=-\frac{M_\delta}{EI_\gamma}$$

$$C_1=C_4\frac{\sin\frac{L_\delta}{2L_e}\sinh\frac{L_\delta}{2L_e}}{\cos\frac{L_\delta}{2L_e}\cosh\frac{L_\delta}{2L_e}}-\frac{M_\delta L_e^2}{2EI_\gamma}\frac{1}{\cos\frac{L_\delta}{2L_e}\cosh\frac{L_\delta}{2L_e}} \qquad \text{(C.30a)}$$

or

$$C_4=C_1\frac{\cos\frac{L_\delta}{2L_e}\cosh\frac{L_\delta}{2L_e}}{\sin\frac{L_\delta}{2L_e}\sinh\frac{L_\delta}{2L_e}}+\frac{M_\delta L_e^2}{2EI_\gamma}\frac{1}{\sin\frac{L_\delta}{2L_e}\sinh\frac{L_\delta}{2L_e}} \qquad \text{(C.30b)}$$

Equation (C.17) with boundary condition (C.29) give

$$\frac{2}{L_e^3}C_1\left(\cos\frac{L_\delta}{2L_e}\sinh\frac{L_\delta}{2L_e}-\sin\frac{L_\delta}{2L_e}\cosh\frac{L_\delta}{2L_e}\right)-$$
$$-\frac{2}{L_e^3}C_4\left(\cos\frac{L_\delta}{2L_e}\sinh\frac{L_\delta}{2L_e}+\sin\frac{L_\delta}{2L_e}\cosh\frac{L_\delta}{2L_e}\right)=-\frac{V_\delta}{EI_\gamma}$$

$$C_1=C_4\frac{\cos\frac{L_\delta}{2L_e}\sinh\frac{L_\delta}{2L_e}+\sin\frac{L_\delta}{2L_e}\cosh\frac{L_\delta}{2L_e}}{\cos\frac{L_\delta}{2L_e}\sinh\frac{L_\delta}{2L_e}-\sin\frac{L_\delta}{2L_e}\cosh\frac{L_\delta}{2L_e}}-$$
$$-\frac{V_\delta L_e^3}{2EI_\gamma}\frac{1}{\cos\frac{L_\delta}{2L_e}\sinh\frac{L_\delta}{2L_e}-\sin\frac{L_\delta}{2L_e}\cosh\frac{L_\delta}{2L_e}} \qquad \text{(C.31a)}$$

or

$$C_4 = C_1 \frac{\cos\frac{L_\delta}{2L_e}\sinh\frac{L_\delta}{2L_e} - \sin\frac{L_\delta}{2L_e}\cosh\frac{L_\delta}{2L_e}}{\cos\frac{L_\delta}{2L_e}\sinh\frac{L_\delta}{2L_e} + \sin\frac{L_\delta}{2L_e}\cosh\frac{L_\delta}{2L_e}} + \\ + \frac{V_\delta L_e^3}{2EI_\gamma}\frac{1}{\cos\frac{L_\delta}{2L_e}\sinh\frac{L_\delta}{2L_e} + \sin\frac{L_\delta}{2L_e}\cosh\frac{L_\delta}{2L_e}} \tag{C.31b}$$

Equation (C.30a) and Equation (C.31a) give

$$C_4 \frac{\sin\frac{L_\delta}{2L_e}\sinh\frac{L_\delta}{2L_e}}{\cos\frac{L_\delta}{2L_e}\cosh\frac{L_\delta}{2L_e}} - \frac{M_\delta L_e^2}{2EI_\gamma}\frac{1}{\cos\frac{L_\delta}{2L_e}\cosh\frac{L_\delta}{2L_e}} = \\ C_4 \frac{\cos\frac{L_\delta}{2L_e}\sinh\frac{L_\delta}{2L_e} + \sin\frac{L_\delta}{2L_e}\cosh\frac{L_\delta}{2L_e}}{\cos\frac{L_\delta}{2L_e}\sinh\frac{L_\delta}{2L_e} - \sin\frac{L_\delta}{2L_e}\cosh\frac{L_\delta}{2L_e}} - \\ - \frac{V_\delta L_e^3}{2EI_\gamma}\frac{1}{\cos\frac{L_\delta}{2L_e}\sinh\frac{L_\delta}{2L_e} - \sin\frac{L_\delta}{2L_e}\cosh\frac{L_\delta}{2L_e}}$$

$$C_4 \frac{\cos\frac{L_\delta}{2L_e}\sinh\frac{L_\delta}{2L_e} + \sin\frac{L_\delta}{2L_e}\cosh\frac{L_\delta}{2L_e}}{\cos\frac{L_\delta}{2L_e}\sinh\frac{L_\delta}{2L_e} - \sin\frac{L_\delta}{2L_e}\cosh\frac{L_\delta}{2L_e}} - C_4 \frac{\sin\frac{L_\delta}{2L_e}\sinh\frac{L_\delta}{2L_e}}{\cos\frac{L_\delta}{2L_e}\cosh\frac{L_\delta}{2L_e}} = \\ = \frac{V_\delta L_e^3}{2EI_\gamma}\frac{1}{\cos\frac{L_\delta}{2L_e}\sinh\frac{L_\delta}{2L_e} - \sin\frac{L_\delta}{2L_e}\cosh\frac{L_\delta}{2L_e}} - \frac{M_\delta L_e^2}{2EI_\gamma}\frac{1}{\cos\frac{L_\delta}{2L_e}\cosh\frac{L_\delta}{2L_e}}$$

$$C_4\left\{\frac{\cos^2\frac{L_\delta}{2L_e}\cosh\frac{L_\delta}{2L_e}\sinh\frac{L_\delta}{2L_e}+\cos\frac{L_\delta}{2L_e}\sin\frac{L_\delta}{2L_e}\cosh^2\frac{L_\delta}{2L_e}}{\cos\frac{L_\delta}{2L_e}\cosh\frac{L_\delta}{2L_e}\left(\cos\frac{L_\delta}{2L_e}\sinh\frac{L_\delta}{2L_e}-\sin\frac{L_\delta}{2L_e}\cosh\frac{L_\delta}{2L_e}\right)}-\right.$$

$$\left.-\frac{\cos\frac{L_\delta}{2L_e}\sin\frac{L_\delta}{2L_e}\sinh^2\frac{L_\delta}{2L_e}-\sin^2\frac{L_\delta}{2L_e}\cosh\frac{L_\delta}{2L_e}\sinh\frac{L_\delta}{2L_e}}{\cos\frac{L_\delta}{2L_e}\cosh\frac{L_\delta}{2L_e}\left(\cos\frac{L_\delta}{2L_e}\sinh\frac{L_\delta}{2L_e}-\sin\frac{L_\delta}{2L_e}\cosh\frac{L_\delta}{2L_e}\right)}\right\}=$$

$$=\frac{V_\delta L_e^3}{2EI_\gamma}\frac{1}{\cos\frac{L_\delta}{2L_e}\sinh\frac{L_\delta}{2L_e}-\sin\frac{L_\delta}{2L_e}\cosh\frac{L_\delta}{2L_e}}-\frac{M_\delta L_e^2}{2EI_\gamma}\frac{1}{\cos\frac{L_\delta}{2L_e}\cosh\frac{L_\delta}{2L_e}}$$

$$C_4\left\{\frac{\left(\cos^2\frac{L_\delta}{2L_e}+\sin^2\frac{L_\delta}{2L_e}\right)\cosh\frac{L_\delta}{2L_e}\sinh\frac{L_\delta}{2L_e}}{\cos\frac{L_\delta}{2L_e}\cosh\frac{L_\delta}{2L_e}\left(\cos\frac{L_\delta}{2L_e}\sinh\frac{L_\delta}{2L_e}-\sin\frac{L_\delta}{2L_e}\cosh\frac{L_\delta}{2L_e}\right)}+\right.$$

$$\left.+\frac{\left(\cosh^2\frac{L_\delta}{2L_e}-\sinh^2\frac{L_\delta}{2L_e}\right)\cos\frac{L_\delta}{2L_e}\sin\frac{L_\delta}{2L_e}}{\cos\frac{L_\delta}{2L_e}\cosh\frac{L_\delta}{2L_e}\left(\cos\frac{L_\delta}{2L_e}\sinh\frac{L_\delta}{2L_e}-\sin\frac{L_\delta}{2L_e}\cosh\frac{L_\delta}{2L_e}\right)}\right\}=$$

$$=\frac{V_\delta L_e^3}{2EI_\gamma}\frac{1}{\cos\frac{L_\delta}{2L_e}\sinh\frac{L_\delta}{2L_e}-\sin\frac{L_\delta}{2L_e}\cosh\frac{L_\delta}{2L_e}}-\frac{M_\delta L_e^2}{2EI_\gamma}\frac{1}{\cos\frac{L_\delta}{2L_e}\cosh\frac{L_\delta}{2L_e}}$$

$$C_4 \frac{\cosh\frac{L_\delta}{2L_e}\sinh\frac{L_\delta}{2L_e}+\cos\frac{L_\delta}{2L_e}\sin\frac{L_\delta}{2L_e}}{\cos\frac{L_\delta}{2L_e}\cosh\frac{L_\delta}{2L_e}\left(\cos\frac{L_\delta}{2L_e}\sinh\frac{L_\delta}{2L_e}-\sin\frac{L_\delta}{2L_e}\cosh\frac{L_\delta}{2L_e}\right)}=$$

$$=\frac{V_\delta L_e^3}{2EI_y}\frac{1}{\cos\frac{L_\delta}{2L_e}\sinh\frac{L_\delta}{2L_e}-\sin\frac{L_\delta}{2L_e}\cosh\frac{L_\delta}{2L_e}}-\frac{M_\delta L_e^2}{2EI_y}\frac{1}{\cos\frac{L_\delta}{2L_e}\cosh\frac{L_\delta}{2L_e}}$$

$$C_4=\frac{V_\delta L_e^3}{2EI_y}\frac{\cos\frac{L_\delta}{2L_e}\cosh\frac{L_\delta}{2L_e}}{\cosh\frac{L_\delta}{2L_e}\sinh\frac{L_\delta}{2L_e}+\cos\frac{L_\delta}{2L_e}\sin\frac{L_\delta}{2L_e}}-$$

$$-\frac{M_\delta L_e^2}{2EI_y}\frac{\cos\frac{L_\delta}{2L_e}\sinh\frac{L_\delta}{2L_e}-\sin\frac{L_\delta}{2L_e}\cosh\frac{L_\delta}{2L_e}}{\cosh\frac{L_\delta}{2L_e}\sinh\frac{L_\delta}{2L_e}+\cos\frac{L_\delta}{2L_e}\sin\frac{L_\delta}{2L_e}}$$

$$C_4=\frac{V_\delta L_e^3}{EI_y}\frac{\cos\frac{L_\delta}{2L_e}\cosh\frac{L_\delta}{2L_e}}{\sin\frac{L_\delta}{L_e}+\sinh\frac{L_\delta}{L_e}}-\frac{M_\delta L_e^2}{EI_y}\frac{\cos\frac{L_\delta}{2L_e}\sinh\frac{L_\delta}{2L_e}-\sin\frac{L_\delta}{2L_e}\cosh\frac{L_\delta}{2L_e}}{\sin\frac{L_\delta}{L_e}+\sinh\frac{L_\delta}{L_e}} \quad \text{(C.32)}$$

Equation (C.30b) and Equation (C.31b) give C_1

$$C_1 \frac{\cos\frac{L_\delta}{2L_e}\cosh\frac{L_\delta}{2L_e}}{\sin\frac{L_\delta}{2L_e}\sinh\frac{L_\delta}{2L_e}} + \frac{M_\delta L_e^2}{2EI_y}\frac{1}{\sin\frac{L_\delta}{2L_e}\sinh\frac{L_\delta}{2L_e}} =$$

$$C_1 \frac{\cos\frac{L_\delta}{2L_e}\sinh\frac{L_\delta}{2L_e} - \sin\frac{L_\delta}{2L_e}\cosh\frac{L_\delta}{2L_e}}{\cos\frac{L_\delta}{2L_e}\sinh\frac{L_\delta}{2L_e} + \sin\frac{L_\delta}{2L_e}\cosh\frac{L_\delta}{2L_e}} +$$

$$+ \frac{V_\delta L_e^3}{2EI_y}\frac{1}{\cos\frac{L_\delta}{2L_e}\sinh\frac{L_\delta}{2L_e} + \sin\frac{L_\delta}{2L_e}\cosh\frac{L_\delta}{2L_e}}$$

$$C_1 \frac{\cos\frac{L_\delta}{2L_e}\sinh\frac{L_\delta}{2L_e} - \sin\frac{L_\delta}{2L_e}\cosh\frac{L_\delta}{2L_e}}{\cos\frac{L_\delta}{2L_e}\sinh\frac{L_\delta}{2L_e} + \sin\frac{L_\delta}{2L_e}\cosh\frac{L_\delta}{2L_e}} - C_1 \frac{\cos\frac{L_\delta}{2L_e}\cosh\frac{L_\delta}{2L_e}}{\sin\frac{L_\delta}{2L_e}\sinh\frac{L_\delta}{2L_e}} =$$

$$= -\frac{V_\delta L_e^3}{2EI_y}\frac{1}{\cos\frac{L_\delta}{2L_e}\sinh\frac{L_\delta}{2L_e} + \sin\frac{L_\delta}{2L_e}\cosh\frac{L_\delta}{2L_e}} + \frac{M_\delta L_e^2}{2EI_y}\frac{1}{\sin\frac{L_\delta}{2L_e}\sinh\frac{L_\delta}{2L_e}}$$

$$C_1\left\{\frac{\cos\frac{L_\delta}{2L_e}\sin\frac{L_\delta}{2L_e}\sinh^2\frac{L_\delta}{2L_e}-\sin^2\frac{L_\delta}{2L_e}\cosh\frac{L_\delta}{2L_e}\sinh\frac{L_\delta}{2L_e}}{\sin\frac{L_\delta}{2L_e}\sinh\frac{L_\delta}{2L_e}\left(\cos\frac{L_\delta}{2L_e}\sinh\frac{L_\delta}{2L_e}+\sin\frac{L_\delta}{2L_e}\cosh\frac{L_\delta}{2L_e}\right)}-\right.$$

$$\left.-\frac{\cos^2\frac{L_\delta}{2L_e}\cosh\frac{L_\delta}{2L_e}\sinh\frac{L_\delta}{2L_e}+\cos\frac{L_\delta}{2L_e}\sin\frac{L_\delta}{2L_e}\cosh^2\frac{L_\delta}{2L_e}}{\sin\frac{L_\delta}{2L_e}\sinh\frac{L_\delta}{2L_e}\left(\cos\frac{L_\delta}{2L_e}\sinh\frac{L_\delta}{2L_e}+\sin\frac{L_\delta}{2L_e}\cosh\frac{L_\delta}{2L_e}\right)}\right\}=$$

$$=-\frac{V_\delta L_e^3}{2EI_\gamma}\frac{1}{\cos\frac{L_\delta}{2L_e}\sinh\frac{L_\delta}{2L_e}+\sin\frac{L_\delta}{2L_e}\cosh\frac{L_\delta}{2L_e}}+\frac{M_\delta L_e^2}{2EI_\gamma}\frac{1}{\sin\frac{L_\delta}{2L_e}\sinh\frac{L_\delta}{2L_e}}$$

$$C_1\left\{\frac{-\left(\cos^2\frac{L_\delta}{2L_e}+\sin^2\frac{L_\delta}{2L_e}\right)\cosh\frac{L_\delta}{2L_e}\sinh\frac{L_\delta}{2L_e}}{\sin\frac{L_\delta}{2L_e}\sinh\frac{L_\delta}{2L_e}\left(\cos\frac{L_\delta}{2L_e}\sinh\frac{L_\delta}{2L_e}+\sin\frac{L_\delta}{2L_e}\cosh\frac{L_\delta}{2L_e}\right)}+\right.$$

$$\left.+\frac{-\left(\cosh^2\frac{L_\delta}{2L_e}-\sinh^2\frac{L_\delta}{2L_e}\right)\cos\frac{L_\delta}{2L_e}\sin\frac{L_\delta}{2L_e}}{\sin\frac{L_\delta}{2L_e}\sinh\frac{L_\delta}{2L_e}\left(\cos\frac{L_\delta}{2L_e}\sinh\frac{L_\delta}{2L_e}+\sin\frac{L_\delta}{2L_e}\cosh\frac{L_\delta}{2L_e}\right)}\right\}=$$

$$=-\frac{V_\delta L_e^3}{2EI_\gamma}\frac{1}{\cos\frac{L_\delta}{2L_e}\sinh\frac{L_\delta}{2L_e}+\sin\frac{L_\delta}{2L_e}\cosh\frac{L_\delta}{2L_e}}+\frac{M_\delta L_e^2}{2EI_\gamma}\frac{1}{\sin\frac{L_\delta}{2L_e}\sinh\frac{L_\delta}{2L_e}}$$

$$-C_1 \frac{\cosh\frac{L_\delta}{2L_e}\sinh\frac{L_\delta}{2L_e}+\cos\frac{L_\delta}{2L_e}\sin\frac{L_\delta}{2L_e}}{\sin\frac{L_\delta}{2L_e}\sinh\frac{L_\delta}{2L_e}\left(\cos\frac{L_\delta}{2L_e}\sinh\frac{L_\delta}{2L_e}+\sin\frac{L_\delta}{2L_e}\cosh\frac{L_\delta}{2L_e}\right)}=$$

$$=-\frac{V_\delta L_e^3}{2EI_\gamma}\frac{1}{\cos\frac{L_\delta}{2L_e}\sinh\frac{L_\delta}{2L_e}+\sin\frac{L_\delta}{2L_e}\cosh\frac{L_\delta}{2L_e}}+\frac{M_\delta L_e^2}{2EI_\gamma}\frac{1}{\sin\frac{L_\delta}{2L_e}\sinh\frac{L_\delta}{2L_e}}$$

$$C_1=\frac{V_\delta L_e^3}{2EI_\gamma}\frac{\sin\frac{L_\delta}{2L_e}\sinh\frac{L_\delta}{2L_e}}{\cosh\frac{L_\delta}{2L_e}\sinh\frac{L_\delta}{2L_e}+\cos\frac{L_\delta}{2L_e}\sin\frac{L_\delta}{2L_e}}-$$

$$-\frac{M_\delta L_e^2}{2EI_\gamma}\frac{\cos\frac{L_\delta}{2L_e}\sinh\frac{L_\delta}{2L_e}+\sin\frac{L_\delta}{2L_e}\cosh\frac{L_\delta}{2L_e}}{\cosh\frac{L_\delta}{2L_e}\sinh\frac{L_\delta}{2L_e}+\cos\frac{L_\delta}{2L_e}\sin\frac{L_\delta}{2L_e}}$$

$$C_1=\frac{V_\delta L_e^3}{EI_\gamma}\frac{\sin\frac{L_\delta}{2L_e}\sinh\frac{L_\delta}{2L_e}}{\sin\frac{L_\delta}{L_e}+\sinh\frac{L_\delta}{L_e}}-\frac{M_\delta L_e^2}{EI_\gamma}\frac{\cos\frac{L_\delta}{2L_e}\sinh\frac{L_\delta}{2L_e}+\sin\frac{L_\delta}{2L_e}\cosh\frac{L_\delta}{2L_e}}{\sin\frac{L_\delta}{L_e}+\sinh\frac{L_\delta}{L_e}} \quad \text{(C.33)}$$

Final solution

Equations (C.32) and (C.33) in Equation (C.14) give the final equation for the deflexion

$$w(x)=\left\{\frac{V_\delta L_e^3}{EI_y}\frac{\sin\frac{L_\delta}{2L_e}\sinh\frac{L_\delta}{2L_e}}{\sin\frac{L_\delta}{L_e}+\sinh\frac{L_\delta}{L_e}}-\frac{M_\delta L_e^2}{EI_y}\frac{\cos\frac{L_\delta}{2L_e}\sinh\frac{L_\delta}{2L_e}+\sin\frac{L_\delta}{2L_e}\cosh\frac{L_\delta}{2L_e}}{\sin\frac{L_\delta}{L_e}+\sinh\frac{L_\delta}{L_e}}\right\}\cdot$$

$$\cdot\sin\frac{x}{L_e}\sinh\frac{x}{L_e}+\left\{\frac{V_\delta L_e^3}{EI_y}\frac{\cos\frac{L_\delta}{2L_e}\cosh\frac{L_\delta}{2L_e}}{\sin\frac{L_\delta}{L_e}+\sinh\frac{L_\delta}{L_e}}-\right.$$

$$\left.\frac{M_\delta L_e^2}{EI_y}\frac{\cos\frac{L_\delta}{2L_e}\sinh\frac{L_\delta}{2L_e}-\sin\frac{L_\delta}{2L_e}\cosh\frac{L_\delta}{2L_e}}{\sin\frac{L_\delta}{L_e}+\sinh\frac{L_\delta}{L_e}}\right\}\cdot\cos\frac{x}{L_e}\cosh\frac{x}{L_e}$$

$$w(x)=\frac{V_\delta L_e^3}{EI_y}\frac{\sin\frac{L_\delta}{2L_e}\sinh\frac{L_\delta}{2L_e}}{\sin\frac{L_\delta}{L_e}+\sinh\frac{L_\delta}{L_e}}\sin\frac{x}{L_e}\sinh\frac{x}{L_e}+$$

$$+\frac{V_\delta L_e^3}{EI_y}\frac{\cos\frac{L_\delta}{2L_e}\cosh\frac{L_\delta}{2L_e}}{\sin\frac{L_\delta}{L_e}+\sinh\frac{L_\delta}{L_e}}\cos\frac{x}{L_e}\cosh\frac{x}{L_e}-$$

$$-\frac{M_\delta L_e^2}{EI_y}\frac{\cos\frac{L_\delta}{2L_e}\sinh\frac{L_\delta}{2L_e}+\sin\frac{L_\delta}{2L_e}\cosh\frac{L_\delta}{2L_e}}{\sin\frac{L_\delta}{L_e}+\sinh\frac{L_\delta}{L_e}}\sin\frac{x}{L_e}\sinh\frac{x}{L_e}-$$

$$-\frac{M_\delta L_e^2}{EI_y}\frac{\cos\frac{L_\delta}{2L_e}\sinh\frac{L_\delta}{2L_e}-\sin\frac{L_\delta}{2L_e}\cosh\frac{L_\delta}{2L_e}}{\sin\frac{L_\delta}{L_e}+\sinh\frac{L_\delta}{L_e}}\cos\frac{x}{L_e}\cosh\frac{x}{L_e}$$

$$w(x) = \frac{4}{kL_e^2\left(\sin\frac{L_\delta}{L_e} + \sinh\frac{L_\delta}{L_e}\right)} \cdot \left\{ V_\delta L_e \left(\sin\frac{L_\delta}{2L_e}\sinh\frac{L_\delta}{2L_e}\sin\frac{x}{L_e}\sinh\frac{x}{L_e} + \right.\right.$$
$$\left. \cos\frac{L_\delta}{2L_e}\cosh\frac{L_\delta}{2L_e}\cos\frac{x}{L_e}\cosh\frac{x}{L_e} \right) -$$
$$- M_\delta \left(\left(\cos\frac{L_\delta}{2L_e}\sinh\frac{L_\delta}{2L_e} + \sin\frac{L_\delta}{2L_e}\cosh\frac{L_\delta}{2L_e} \right)\sin\frac{x}{L_e}\sinh\frac{x}{L_e} - \right.$$
$$\left.\left. \left(\cos\frac{L_\delta}{2L_e}\sinh\frac{L_\delta}{2L_e} - \sin\frac{L_\delta}{2L_e}\cosh\frac{L_\delta}{2L_e} \right)\cos\frac{x}{L_e}\cosh\frac{x}{L_e} \right) \right\} \tag{C.34}$$

With the deflexion known, the equations for the ground pressure and the moment distribution along the beam can be determined.

The ground pressure is obtained according to Equation (C.1) with Equation (C.34)

$$p(x) = q + \frac{4}{L_e^2\left(\sin\frac{L_\delta}{L_e} + \sinh\frac{L_\delta}{L_e}\right)} \left\{ V_\delta L_e \left(\sin\frac{L_\delta}{2L_e}\sinh\frac{L_\delta}{2L_e}\sin\frac{x}{L_e}\sinh\frac{x}{L_e} + \right.\right.$$
$$\left. + \cos\frac{L_\delta}{2L_e}\cosh\frac{L_\delta}{2L_e}\cos\frac{x}{L_e}\cosh\frac{x}{L_e} \right)$$
$$- M_\delta \left(\left(\cos\frac{L_\delta}{2L_e}\sinh\frac{L_\delta}{2L_e} + \sin\frac{L_\delta}{2L_e}\cosh\frac{L_\delta}{2L_e} \right)\sin\frac{x}{L_e}\sinh\frac{x}{L_e} - \right.$$
$$\left.\left. - \left(\cos\frac{L_\delta}{2L_e}\sinh\frac{L_\delta}{2L_e} - \sin\frac{L_\delta}{2L_e}\cosh\frac{L_\delta}{2L_e} \right)\cos\frac{x}{L_e}\cosh\frac{x}{L_e} \right) \right\} \tag{C.35}$$

The moment distribution is obtained from the elastic line equation

$$M(x) = -EI_\gamma \frac{d^2 w}{dx^2}$$

implying

$$\begin{aligned} M(x) = &-\frac{2V_\delta L_e}{\sin\frac{L_\delta}{L_e} + \sinh\frac{L_\delta}{L_e}}\left(\sin\frac{L_\delta}{2L_e}\sinh\frac{L_\delta}{2L_e}\cos\frac{x}{L_e}\cosh\frac{x}{L_e} - \right. \\ &\left. -\cos\frac{L_\delta}{2L_e}\cosh\frac{L_\delta}{2L_e}\sin\frac{x}{L_e}\sinh\frac{x}{L_e}\right) + \frac{2M_\delta}{\sin\frac{L}{L_e} + \sinh\frac{L}{L_e}} \cdot \\ &\cdot\left\{\left(\cos\frac{L}{2L_e}\sinh\frac{L}{2L_e} + \sin\frac{L}{2L_e}\cosh\frac{L}{2L_e}\right)\cos\frac{x}{L_e}\cosh\frac{x}{L_e} - \right. \\ &\left. -\left(\cos\frac{L}{2L_e}\sinh\frac{L}{2L_e} - \sin\frac{L}{2L_e}\cosh\frac{L}{2L_e}\right)\sin\frac{x}{L_e}\sinh\frac{x}{L_e}\right\} \end{aligned} \tag{C.36}$$

The bending moment in the mid span of the beam is obtained by equation (C.36) with $x = 0$:

$$\begin{aligned} M(x=0) = &-\frac{2V_\delta L_e}{\sin\frac{L_\delta}{L_e} + \sinh\frac{L_\delta}{L_e}}\sin\frac{L_\delta}{2L_e}\sinh\frac{L_\delta}{2L_e} \\ &+\frac{2M_\delta}{\sin\frac{L_\delta}{L_e} + \sinh\frac{L_\delta}{L_e}}\left(\cos\frac{L_\delta}{2L_e}\sinh\frac{L_\delta}{2L_e} + \sin\frac{L_\delta}{2L_e}\cosh\frac{L_\delta}{2L_e}\right) \end{aligned} \tag{C.37}$$

Appendix D

Derivation of Formulas for Application Tools for the Determination of Plane-Section Restraint Coefficients

D.1 Restraint in Decisive Points

In the following, one young structural member (subscript *y*) cast on an older one (subscript *a*) is studied. The present derivation is based on formulas for prestressed concrete beams, Collins & Mitchell (1991), and a proposed method for calculation of crack widths due to thermal stresses, JCI (1992). Plane sections are assumed remaining plane implying the strains over the height of the structures varying linearly. No slip failure between the members is assumed.

Under the assumption of plane sections remaining plane, the restraint coefficient is in the following being refereed to as plane-section restraint coefficient, γ^0_R. The plane-section restraint coefficient in a point in a young concrete part is generally defined as the ratio between actual stresses in the point σ_1 and stresses at fixation ($\varepsilon \equiv 0$) of the volume changes of the young concrete, $\zeta E_{28y}\Delta\varepsilon_y{}^0$ (shrinkage strains and thermal strains). That is

$$\gamma^0_R(x,z) = \frac{\sigma_1(x,z)}{-\Delta\varepsilon^0_y \zeta E_{28y}} \tag{D.1}$$

The actual stresses in a point is found as

$$\sigma_1(x,z) = \zeta E_{28y}(\varepsilon^0_{cen}(x) + \varepsilon^0_\varphi(x,z) - \Delta\varepsilon^0_y) \tag{D.2}$$

where $\varepsilon^0{}_{cen}$ is the translational strains and $\varepsilon^0{}_\varphi$ is the rotational strains giving

$$\gamma_R^0(x,z) = \frac{\varepsilon_{cen}^0(x) + \varepsilon_\varphi^0(x,z) - \Delta\varepsilon_\gamma^0}{-\Delta\varepsilon_\gamma^0} \tag{D.3}$$

The plane-section restraint coefficient can be separated in one translational part $\gamma_R{}^{0T}$, and one rotational part $\gamma_R{}^{0\varphi}$, that is

$$\gamma_R^0(x,z) = \frac{\varepsilon_{cen}^0(x)}{-\Delta\varepsilon_\gamma^0} + \frac{\varepsilon_\varphi^0(x,z)}{-\Delta\varepsilon_\gamma^0} - \frac{\Delta\varepsilon_\gamma^0}{-\Delta\varepsilon_\gamma^0} = 1 - \gamma_R^{0T}(x) - \gamma_R^{0\varphi}(x,z) \tag{D.4}$$

The translational strain in the decisive point, $\varepsilon^0{}_{cen}$, is determined from the requirement of translational equilibrium in the section. The integral of stresses over the area implies

$$\int_{A_\gamma} \sigma_\gamma dA_\gamma + \int_{A_{a,eff}} \sigma_a dA_{a,eff} = 0$$

$$\int_{A_\gamma} \zeta E_{28\gamma}(\varepsilon_{cen}^0 - \Delta\varepsilon_\gamma^0) dA_\gamma + \int_{A_{a,eff}} E_{28a}(\varepsilon_{cen}^0 - \Delta\varepsilon_a^0) dA_{a,eff} = 0$$

The imposed volume changes in the adjoining concrete is expressed as a factor λ times the imposed volume changes in the young concrete, $\Delta\varepsilon_a{}^0 = \lambda\Delta\varepsilon_\gamma{}^0$, giving

$$\int_{A_\gamma} \zeta E_{28\gamma}(\varepsilon_{cen}^0 - \Delta\varepsilon_\gamma^0) dA_\gamma + \int_{A_{a,eff}} E_{28a}(\varepsilon_{cen}^0 - \lambda\Delta\varepsilon_\gamma^0) dA_{a,eff} = 0$$

Collection of terms gives

$$\zeta E_{28\gamma}\varepsilon_{cen}^0 \left(\int_{A_\gamma} dA_\gamma + \frac{E_{28a}}{\zeta E_{28\gamma}} \int_{A_{a,eff}} dA_{a,eff} \right) - \\ - \Delta\varepsilon_\gamma^0 \left(\int_{A_\gamma} \zeta E_{28\gamma} dA_\gamma + \int_{A_{a,eff}} E_{28a}\lambda dA_{a,eff} \right) = 0$$

where from the normal strain is solved

$$\varepsilon_{cen}^0 = \frac{N_{RI}}{\zeta E_{28\gamma} A_{trans}} \tag{D.5}$$

A_{trans} is the transformed area

$$A_{trans} = \int_{A_\gamma} dA_\gamma + \frac{E_{28a}}{\zeta E_{28\gamma}} \int_{A_{a,eff}} dA_{a,eff} \tag{D.6}$$

and N_{RI} is the force required to produce zero strain in the concrete, that is the normal force of internal loading

$$N_{RI} = \Delta\varepsilon_{\gamma}^{0}\left(\int_{A_{\gamma}} \zeta E_{28\gamma} dA_{\gamma} + \int_{A_{a,eff}} E_{28a}\lambda dA_{a,eff}\right) \tag{D.7}$$

The rotational strain is determined from the requirement of rotational equilibrium in the section. The integral of the stresses times the distance from the centroidal axis over the area imply

$$\int_{A_{\gamma}} \zeta E_{28\gamma}(\varphi^{0} z - \Delta\varepsilon_{\gamma}^{0}) z dA_{\gamma} + \int_{A_{a,eff}} E_{28a}(\varphi^{0} z - \lambda\Delta\varepsilon_{\gamma}^{0}) z dA_{a,eff} = 0$$

where once again the volume changes of the adjoining structure are expressed in relation to the volume changes of the young part.

Collection of terms gives

$$\zeta E_{28\gamma}\varphi^{0}\left(\int_{A_{\gamma}} z^{2} dA_{\gamma} + \frac{E_{28a}}{\zeta E_{28\gamma}}\int_{A_{a,eff}} z^{2} dA_{a,eff}\right) -$$
$$-\Delta\varepsilon_{\gamma}^{0}\left(\int_{A_{\gamma}} \zeta E_{28\gamma} z dA_{\gamma} + \int_{A_{a,eff}} E_{28a}\lambda z dA_{a,eff}\right) = 0$$

where from the rotation is solved as

$$\varphi^{0} = \frac{M_{RI}}{\zeta E_{28\gamma} I_{trans}} \tag{D.8}$$

I_{trans} is the transformed moment of inertia

$$I_{trans} = \int_{A_{\gamma}} z^{2} dA_{\gamma} + \frac{E_{28a}}{\zeta E_{28\gamma}}\int_{A_{a,eff}} z^{2} dA_{a,eff} \tag{D.9}$$

and M_0 is the moment required to produce zero strain in the concrete

$$M_{RI} = \Delta\varepsilon_{\gamma}^{0}\left(\int_{A_{\gamma}} \zeta E_{28\gamma} z dA_{\gamma} + \int_{A_{a,eff}} E_{28a}\lambda z dA_{a,eff}\right) \tag{D.10}$$

D.1.1 Translational plane-section restraint coefficient

The translational plane-section restraint coefficient is generally defined as

$$\gamma_{R}^{0T}(x) = \frac{\varepsilon_{cen}^{0}(1 - \gamma_{RT}(x))}{\Delta\varepsilon_{\gamma}^{0}}$$

By including the expression for the translational strain, the normal force of internal loading and the transformed area of the section, the translational plane-section restraint coefficients is

$$\gamma_R^{0T}(x) = \frac{N_{RI}}{\zeta E_{28\gamma} A_{trans}} \frac{(1-\gamma_{RT}(x))}{\Delta\varepsilon_\gamma^0}$$

$$\gamma_R^{0T}(x) = \frac{\Delta\varepsilon_\gamma^0 \left(\int_{A_\gamma} \zeta E_{28\gamma} dA_\gamma + \int_{A_{a,eff}} E_{28a} \lambda dA_{a,eff} \right)}{\zeta E_{28\gamma} \left(\int_{A_\gamma} dA_\gamma + \frac{E_{28a}}{\zeta E_{28\gamma}} \int_{A_{a,eff}} dA_{a,eff} \right)} \frac{(1-\gamma_{RT}(x))}{\Delta\varepsilon_\gamma^0}$$

$$\gamma_R^{0T}(x) = \frac{\int_{A_\gamma} dA_\gamma + \frac{E_{28a}}{\zeta E_{28\gamma}} \int_{A_{a,eff}} \lambda dA_{a,eff}}{\int_{A_\gamma} dA_\gamma + \frac{E_{28a}}{\zeta E_{28\gamma}} \int_{A_{a,eff}} dA_{a,eff}} (1-\gamma_{RT}(x)) \tag{D.11}$$

D.1.1 Rotational plane-section restraint coefficient

The rotational plane-section restraint coefficient is generally defined as

$$\gamma_R^{0\varphi}(x,z) = \frac{\varphi^0 (1-\gamma_{RR}(x))z}{\Delta\varepsilon_\gamma^0} \tag{D.12}$$

By including the expression for the curvature, the moment of internal loading and the moment of inertia of the transformed cross section, the rotational plane-section restraint coefficients is

$$\gamma_R^{0\varphi}(x,z) = \frac{M_{RI}}{\zeta E_{28\gamma} I_{trans}} \frac{(1-\gamma_{RR}(x))z}{\Delta\varepsilon_\gamma^0}$$

$$\gamma_R^{0\varphi}(x,z) = \frac{\Delta\varepsilon_\gamma^0 \left(\int_{A_\gamma} \zeta E_{28\gamma} z_\gamma dA_\gamma + \int_{A_{a,eff}} E_{28a} \lambda z_a dA_{a,eff} \right)}{\zeta E_{28\gamma} \left(\int_{A_\gamma} z^2 dA_\gamma + \frac{E_{28a}}{\zeta E_{28\gamma}} \int_{A_{a,eff}} z^2 dA_{a,eff} \right)} \frac{(1-\gamma_{RR}(x))z}{\Delta\varepsilon_\gamma^0}$$

$$\gamma_R^{0\varphi}(x,z) = \frac{z_\gamma \int_{A_\gamma} dA_\gamma + \frac{E_{28a}}{\zeta E_{28\gamma}} \lambda z_a \int_{A_{a,eff}} dA_{a,eff}}{\int_{A_\gamma} z_\gamma^2 dA_\gamma + \frac{E_{28a}}{\zeta E_{28\gamma}} \int_{A_{a,eff}} z_a^2 dA_{a,eff}} (1-\gamma_{RR}(x))z$$

D.2 Formulas for Application Tools

For simple structures, analytical formulas can be derived for the rotational plane-section restraint coefficient in the young concrete parts in terms of the translational and the rotational boundary restraint conditions. Both the young and the old concrete parts are here assumed rectangular shaped. The modulus of elasticity as well as the temperature is presumed being equal over the area of the young part and of the old one, respectively, see Figure D.1.

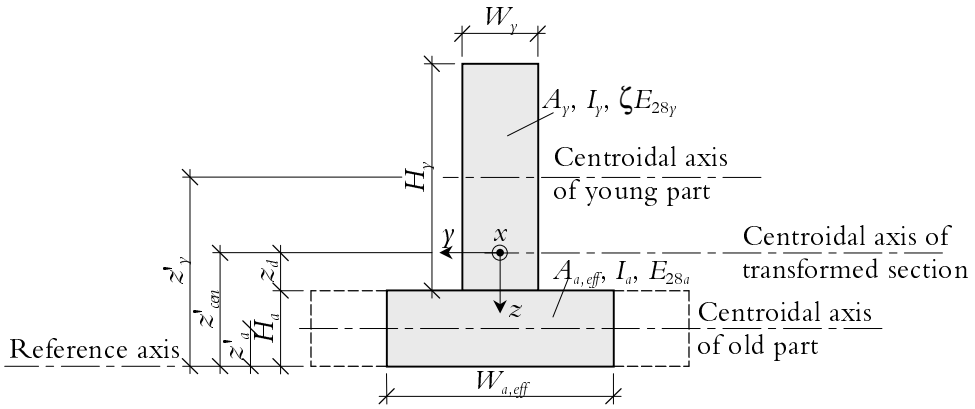

Figure D.1 *Section properties of a structure containing of a young concrete part cast on an older one assuming rectangular shapes and equal properties over the areas of each part.*

For defined areas of rectangular shaped surfaces with a reference axis at the bottom of the structure, the translational plane-section restraint coefficients is

$$\gamma_R^{0T}(x) = \frac{1 + \dfrac{E_{28a}}{\zeta E_{28y}} \lambda \dfrac{A_{a,eff}}{A_y}}{1 + \dfrac{E_{28a}}{\zeta E_{28y}} \dfrac{A_{a,eff}}{A_y}} (1 - \gamma_{RT}(x)) \tag{D.13}$$

For defined areas of rectangular shaped surfaces with a reference axis at the bottom of the structure, the rotational plane-section restraint coefficients is

$$\gamma_R^{0\varphi}(x,z) = \frac{\left(A_y(z'_{cen} - z_y) + \dfrac{E_{28a}}{\zeta E_{28y}} \lambda A_{a,eff}(z'_{cen} - z_a) \right) z}{I_{trans}} (1 - \gamma_{RR}(x)) \tag{D.14}$$

Under the stated assumptions, the transformed section properties will be as follows if the modulus of elasticity of the young part is set as reference.

The centroid of the transformed section, from a reference axis at the bottom of the structure is

$$z'_{cen} = \frac{z'_y + \frac{E_{28a}}{\zeta E_{28y}} \frac{A_{a,eff}}{A_y} z'_a}{1 + \frac{E_{28a}}{\zeta E_{28y}} \frac{A_{a,eff}}{A_y}}$$

that with the distances from the bottom of the structure to the centroidal axes of the young and the old parts respectively is

$$z'_{cen} = \frac{H_a + \frac{H_y}{2} + \frac{E_{28a}}{\zeta E_{28y}} \frac{A_{a,eff}}{A_y} \frac{H_a}{2}}{1 + \frac{E_{28a}}{\zeta E_{28y}} \frac{A_{a,eff}}{A_y}} \tag{D.15}$$

The moment of inertia of the transformed section is

$$I_{trans} = I_{0y} + A_y (z'_{trans} - z'_y)^2 + \frac{E_{28a}}{\zeta E_{28y}} \left(I_{0a} + A_{a,eff} (z'_{trans} - z'_a)^2 \right) \tag{D.16}$$

Equation (D.15), the moment of inertia of rectangular shaped surfaces around their own centroidal axes and the distances to the centroidal axes of the young and of the old parts, from the bottom of the structure, together in Equation (D.16) give

$$I_{trans} = \frac{W_y H_y^3}{12} + W_y H_y \left(\frac{H_a + \frac{H_y}{2} + \frac{E_{28a}}{\zeta E_{28y}} \frac{A_{a,eff}}{A_y} \frac{H_a}{2}}{1 + \frac{E_{28a}}{\zeta E_{28y}} \frac{A_{a,eff}}{A_y}} - \left(H_a + \frac{H_y}{2} \right) \right)^2 +$$

$$\frac{E_{28a}}{\zeta E_{28y}} \frac{W_{a,eff} H_a^3}{12} + \frac{E_{28a}}{\zeta E_{28y}} W_{a,eff} H_a \left(\frac{H_a + \frac{H_y}{2} + \frac{E_{28a}}{\zeta E_{28y}} \frac{A_{a,eff}}{A_y} \frac{H_a}{2}}{1 + \frac{E_{28a}}{\zeta E_{28y}} \frac{A_{a,eff}}{A_y}} - \frac{H_a}{2} \right)^2$$

$$I_{trans} = \frac{A_\gamma H_\gamma^2}{12} + A_\gamma \left(\frac{\frac{E_{28a}}{\zeta E_{28\gamma}} \frac{A_{a,eff}}{A_\gamma} \left(\frac{H_a}{2} + \frac{H_\gamma}{2} \right)}{1 + \frac{E_{28a}}{\zeta E_{28\gamma}} \frac{A_{a,eff}}{A_\gamma}} \right)^2 +$$

$$+ \frac{E_{28a}}{\zeta E_{28\gamma}} \frac{A_{a,eff} H_a^2}{12} + \frac{E_{28a}}{\zeta E_{28\gamma}} A_{a,eff} \left(\frac{\frac{H_a}{2} + \frac{H_\gamma}{2}}{1 + \frac{E_{28a}}{\zeta E_{28\gamma}} \frac{A_{a,eff}}{A_\gamma}} \right)^2$$

$$I_{trans} = \frac{A_\gamma H_\gamma^2}{12} + A_\gamma \frac{H_\gamma^2}{4} \left(- \frac{\frac{E_{28a}}{\zeta E_{28\gamma}} \frac{A_{a,eff}}{A_\gamma} \left(1 + \frac{H_a}{H_\gamma} \right)}{1 + \frac{E_{28a}}{\zeta E_{28\gamma}} \frac{A_{a,eff}}{A_\gamma}} \right)^2 +$$

$$+ \frac{E_{28a}}{\zeta E_{28\gamma}} \frac{A_{a,eff} H_a^2}{12} + \frac{E_{28a}}{\zeta E_{28\gamma}} A_{a,eff} \frac{H_\gamma^2}{4} \left(\frac{1 + \frac{H_a}{H_\gamma}}{1 + \frac{E_{28a}}{\zeta E_{28\gamma}} \frac{A_{a,eff}}{A_\gamma}} \right)^2$$

$$I_{trans} = \frac{A_\gamma H_\gamma^2}{4} \left\{ \frac{1}{3} + \frac{\left(\frac{E_{28a}}{\zeta E_{28\gamma}} \frac{A_{a,eff}}{A_\gamma} \left(1 + \frac{H_a}{H_\gamma} \right) \right)^2}{\left(1 + \frac{E_{28a}}{\zeta E_{28\gamma}} \frac{A_{a,eff}}{A_\gamma} \right)^2} + \right.$$

$$\left. + \frac{1}{3} \frac{E_{28a}}{\zeta E_{28\gamma}} \frac{A_{a,eff}}{A_\gamma} \left(\frac{H_a}{H_\gamma} \right)^2 + \frac{E_{28a}}{\zeta E_{28\gamma}} \frac{A_{a,eff}}{A_\gamma} \frac{\left(1 + \frac{H_a}{H_\gamma} \right)^2}{\left(1 + \frac{E_{28a}}{\zeta E_{28\gamma}} \frac{A_{a,eff}}{A_\gamma} \right)^2} \right\}$$

$$I_{trans} = \frac{A_y H_y^2}{4\left(1+\frac{E_{28a}}{\zeta E_{28y}}\frac{A_{a,eff}}{A_y}\right)^2}\left\{\frac{1}{3}\left(1+\frac{E_{28a}}{\zeta E_{28y}}\frac{A_{a,eff}}{A_y}\right)^2 + \right.$$
$$+\left(\frac{E_{28a}}{\zeta E_{28y}}\frac{A_{a,eff}}{A_y}\right)^2\left(1+\frac{H_a}{H_y}\right)^2 + \frac{1}{3}\frac{E_{28a}}{\zeta E_{28y}}\frac{A_{a,eff}}{A_y}\left(\frac{H_a}{H_y}\right)^2\left(1+\frac{E_{28a}}{\zeta E_{28y}}\frac{A_{a,eff}}{A_y}\right)^2$$
$$\left.+\frac{E_{28a}}{\zeta E_{28y}}\frac{A_{a,eff}}{A_y}\left(1+\frac{H_a}{H_y}\right)^2\right\}$$

$$I_{trans} = \frac{A_y H_y^2}{4\left(1+\frac{E_{28a}}{\zeta E_{28y}}\frac{A_{a,eff}}{A_y}\right)^2}\left\{\frac{1}{3}\left(1+\frac{E_{28a}}{\zeta E_{28y}}\frac{A_{a,eff}}{A_y}\right)^2\left(1+\frac{E_{28a}}{\zeta E_{28y}}\frac{A_{a,eff}}{A_y}\left(\frac{H_a}{H_y}\right)^2\right)+\right.$$
$$\left.+\frac{E_{28a}}{\zeta E_{28y}}\frac{A_{a,eff}}{A_y}\left(1+\frac{H_a}{H_y}\right)^2\left(1+\frac{E_{28a}}{\zeta E_{28y}}\frac{A_{a,eff}}{A_y}\right)\right\}$$

$$I_{trans} = \frac{A_y H_y^2}{4\left(1+\frac{E_{28a}}{\zeta E_{28y}}\frac{A_{a,eff}}{A_y}\right)^2}\cdot \tag{D.17}$$
$$\left(\frac{1}{3}\left(1+\frac{E_{28a}}{\zeta E_{28y}}\frac{A_{a,eff}}{A_y}\right)\left(1+\frac{E_{28a}}{\zeta E_{28y}}\frac{A_{a,eff}}{A_y}\left(\frac{H_a}{H_y}\right)^2\right)+\frac{E_{28a}}{\zeta E_{28y}}\frac{A_{a,eff}}{A_y}\left(1+\frac{H_a}{H_y}\right)^2\right)$$

Equation (D.15) into the numerator in Equation (D.14) gives

$$\text{Numerator} = \left\{ A_\gamma \left(\frac{H_a + \frac{H_\gamma}{2} + \frac{E_{28a}}{\zeta E_{28\gamma}} \frac{A_{a,eff}}{A_\gamma} \frac{H_a}{2}}{1 + \frac{E_{28a}}{\zeta E_{28\gamma}} \frac{A_{a,eff}}{A_\gamma}} - \left(H_a + \frac{H_\gamma}{2} \right) \right) + \right.$$

$$\left. + \frac{E_{28a}}{\zeta E_{28\gamma}} \lambda A_{a,eff} \left(\frac{H_a + \frac{H_\gamma}{2} + \frac{E_{28a}}{\zeta E_{28\gamma}} \frac{A_{a,eff}}{A_\gamma} \frac{H_a}{2}}{1 + \frac{E_{28a}}{\zeta E_{28\gamma}} \frac{A_{a,eff}}{A_\gamma}} - \frac{H_a}{2} \right) \right\} z =$$

$$= \left\{ A_\gamma \left(- \frac{\frac{E_{28a}}{\zeta E_{28\gamma}} \frac{A_{a,eff}}{A_\gamma} \left(\frac{H_a}{2} + \frac{H_\gamma}{2} \right)}{1 + \frac{E_{28a}}{\zeta E_{28\gamma}} \frac{A_{a,eff}}{A_\gamma}} \right) + \frac{E_{28a}}{\zeta E_{28\gamma}} \lambda A_{a,eff} \left(\frac{\frac{H_a}{2} + \frac{H_\gamma}{2}}{1 + \frac{E_{28a}}{\zeta E_{28\gamma}} \frac{A_{a,eff}}{A_\gamma}} \right) \right\} z =$$

$$= \left\{ \frac{A_\gamma H_\gamma}{2} \left(- \frac{\frac{E_{28a}}{\zeta E_{28\gamma}} \frac{A_{a,eff}}{A_\gamma} \left(1 + \frac{H_a}{H_\gamma} \right)}{1 + \frac{E_{28a}}{\zeta E_{28\gamma}} \frac{A_{a,eff}}{A_\gamma}} \right) + \frac{E_{28a}}{\zeta E_{28\gamma}} \lambda \frac{A_{a,eff} H_\gamma}{2} \left(\frac{1 + \frac{H_a}{2}}{1 + \frac{E_{28a}}{\zeta E_{28\gamma}} \frac{A_{a,eff}}{A_\gamma}} \right) \right\} z =$$

$$= \frac{A_\gamma H_\gamma}{2} \left(- \frac{\frac{E_{28a}}{\zeta E_{28\gamma}} \frac{A_{a,eff}}{A_\gamma} \left(1 + \frac{H_a}{H_\gamma} \right)}{1 + \frac{E_{28a}}{\zeta E_{28\gamma}} \frac{A_{a,eff}}{A_\gamma}} + \lambda \frac{\frac{E_{28a}}{\zeta E_{28\gamma}} \frac{A_{a,eff}}{A_\gamma} \left(1 + \frac{H_a}{2} \right)}{1 + \frac{E_{28a}}{\zeta E_{28\gamma}} \frac{A_{a,eff}}{A_\gamma}} \right) z =$$

$$= \frac{A_\gamma H_\gamma}{2} \frac{\frac{E_{28a}}{\zeta E_{28\gamma}} \frac{A_{a,\underline{eff}}}{A_\gamma} \left(1 + \frac{H_a}{H_\gamma}\right)}{1 + \frac{E_{28a}}{\zeta E_{28\gamma}} \frac{A_{a,\underline{eff}}}{A_\gamma}} (\lambda - 1) z =$$

$$= \frac{A_\gamma H_\gamma}{2\left(1 + \frac{E_{28a}}{\zeta E_{28\gamma}} \frac{A_{a,\underline{eff}}}{A_\gamma}\right)} \frac{E_{28a}}{\zeta E_{28\gamma}} \frac{A_{a,\underline{eff}}}{A_\gamma} \left(1 + \frac{H_a}{H_\gamma}\right) (\lambda - 1) z \qquad \text{(D.18)}$$

Equations (D.17) and (D.20) in Equation (D.14) give the rotational plane-section restraint coefficient

$$\gamma_R^{0\varphi}(x,z) = (1 - \gamma_{RR}(x))(\lambda - 1) z \cdot \frac{2}{H_\gamma}$$

$$\frac{\frac{E_{28a}}{\zeta E_{28\gamma}} \frac{A_{a,\underline{eff}}}{A_\gamma} \left(1 + \frac{H_a}{H_\gamma}\right)}{\left(\frac{1}{3}\left(1 + \frac{E_{28a}}{\zeta E_{28\gamma}} \frac{A_{a,\underline{eff}}}{A_\gamma}\right)\left(1 + \frac{E_{28a}}{\zeta E_{28\gamma}} \frac{A_{a,\underline{eff}}}{A_\gamma} \left(\frac{H_a}{H_\gamma}\right)^2\right) + \frac{E_{28a}}{\zeta E_{28\gamma}} \frac{A_{a,\underline{eff}}}{A_\gamma} \left(1 + \frac{H_a}{H_\gamma}\right)^2\right)} \qquad \text{(D.19)}$$

For one special case studying the lowest part of the wall, for instance $z_1 = z'_{cen} - H_a$, being at the joint between the young and the old parts of a structure, Equation (D.15) put into the numerator in Equation (D.14) give

$$\text{Numerator} = \left\{ A_\gamma \left(\frac{H_a + \frac{H_\gamma}{2} + \frac{E_{28a}}{\zeta E_{28\gamma}} \frac{A_{a,\underline{eff}}}{A_\gamma} \frac{H_a}{2}}{1 + \frac{E_{28a}}{\zeta E_{28\gamma}} \frac{A_{a,\underline{eff}}}{A_\gamma}} - \left(H_a + \frac{H_\gamma}{2} \right) \right) + \right.$$

$$\left. + \frac{E_{28a}}{\zeta E_{28\gamma}} \lambda A_{a,\underline{eff}} \left(\frac{H_a + \frac{H_\gamma}{2} + \frac{E_{28a}}{\zeta E_{28\gamma}} \frac{A_{a,\underline{eff}}}{A_\gamma} \frac{H_a}{2}}{1 + \frac{E_{28a}}{\zeta E_{28\gamma}} \frac{A_{a,\underline{eff}}}{A_\gamma}} - \frac{H_a}{2} \right) \right\} \cdot$$

$$\cdot \left(\frac{H_a + \frac{H_\gamma}{2} + \frac{E_{28a}}{\zeta E_{28\gamma}} \frac{A_{a,\underline{eff}}}{A_\gamma} \frac{H_a}{2}}{1 + \frac{E_{28a}}{\zeta E_{28\gamma}} \frac{A_{a,\underline{eff}}}{A_\gamma}} - H_a \right) =$$

$$= \left\{ A_\gamma \left(- \frac{\frac{E_{28a}}{\zeta E_{28\gamma}} \frac{A_{a,\underline{eff}}}{A_\gamma} \left(\frac{H_a}{2} + \frac{H_\gamma}{2} \right)}{1 + \frac{E_{28a}}{\zeta E_{28\gamma}} \frac{A_{a,\underline{eff}}}{A_\gamma}} \right) + \frac{E_{28a}}{\zeta E_{28\gamma}} \lambda A_{a,\underline{eff}} \left(\frac{\frac{H_a}{2} + \frac{H_\gamma}{2}}{1 + \frac{E_{28a}}{\zeta E_{28\gamma}} \frac{A_{a,\underline{eff}}}{A_\gamma}} \right) \right\} \cdot$$

$$\cdot \frac{\frac{H_\gamma}{2} - \frac{E_{28a}}{\zeta E_{28\gamma}} \frac{A_{a,\underline{eff}}}{A_\gamma} \frac{H_a}{2}}{1 + \frac{E_{28a}}{\zeta E_{28\gamma}} \frac{A_{a,\underline{eff}}}{A_\gamma}} =$$

$$= \left\{ \frac{A_\gamma H_\gamma}{2} \left(- \frac{\frac{E_{28a}}{\zeta E_{28\gamma}} \frac{A_{a,\mathit{eff}}}{A_\gamma} \left(1 + \frac{H_a}{H_\gamma} \right)}{1 + \frac{E_{28a}}{\zeta E_{28\gamma}} \frac{A_{a,\mathit{eff}}}{A_\gamma}} \right) + \frac{E_{28a}}{\zeta E_{28\gamma}} \lambda \frac{A_{a,\mathit{eff}} H_\gamma}{2} \left(\frac{1 + \frac{H_a}{2}}{1 + \frac{E_{28a}}{\zeta E_{28\gamma}} \frac{A_{a,\mathit{eff}}}{A_\gamma}} \right) \right\} \cdot$$

$$\cdot \frac{H_\gamma}{2} \left(\frac{1 - \frac{E_{28a}}{\zeta E_{28\gamma}} \frac{A_{a,\mathit{eff}}}{A_\gamma} \frac{H_a}{H_\gamma}}{1 + \frac{E_{28a}}{\zeta E_{28\gamma}} \frac{A_{a,\mathit{eff}}}{A_\gamma}} \right) =$$

$$= \frac{A_\gamma H_\gamma^2}{4} \left(- \frac{\frac{E_{28a}}{\zeta E_{28\gamma}} \frac{A_{a,\mathit{eff}}}{A_\gamma} \left(1 + \frac{H_a}{H_\gamma} \right)}{1 + \frac{E_{28a}}{\zeta E_{28\gamma}} \frac{A_{a,\mathit{eff}}}{A_\gamma}} + \lambda \frac{\frac{E_{28a}}{\zeta E_{28\gamma}} \frac{A_{a,\mathit{eff}}}{A_\gamma} \left(1 + \frac{H_a}{2} \right)}{1 + \frac{E_{28a}}{\zeta E_{28\gamma}} \frac{A_{a,\mathit{eff}}}{A_\gamma}} \right)$$

$$\cdot \left(\frac{1 - \frac{E_{28a}}{\zeta E_{28\gamma}} \frac{A_{a,\mathit{eff}}}{A_\gamma} \frac{H_a}{H_\gamma}}{1 + \frac{E_{28a}}{\zeta E_{28\gamma}} \frac{A_{a,\mathit{eff}}}{A_\gamma}} \right) =$$

$$= \frac{A_\gamma H_\gamma^2}{4} \frac{\frac{E_{28a}}{\zeta E_{28\gamma}} \frac{A_{a,\mathit{eff}}}{A_\gamma} \left(1 + \frac{H_a}{H_\gamma} \right)}{1 + \frac{E_{28a}}{\zeta E_{28\gamma}} \frac{A_{a,\mathit{eff}}}{A_\gamma}} \frac{1 - \frac{E_{28a}}{\zeta E_{28\gamma}} \frac{A_{a,\mathit{eff}}}{A_\gamma} \frac{H_a}{H_\gamma}}{1 + \frac{E_{28a}}{\zeta E_{28\gamma}} \frac{A_{a,\mathit{eff}}}{A_\gamma}} (\lambda - 1) =$$

$$= \frac{A_\gamma H_\gamma^2}{4 \left(1 + \frac{E_{28a}}{\zeta E_{28\gamma}} \frac{A_{a,\mathit{eff}}}{A_\gamma} \right)^2} \frac{E_{28a}}{\zeta E_{28\gamma}} \frac{A_{a,\mathit{eff}}}{A_\gamma} \left(1 + \frac{H_a}{H_\gamma} \right) \left(1 - \frac{E_{28a}}{\zeta E_{28\gamma}} \frac{A_{a,\mathit{eff}}}{A_\gamma} \frac{H_a}{H_\gamma} \right) (\lambda - 1) \tag{D.20}$$

Equations (D.17) and (D.20) in Equation (D.14) give the rotational plane-section restraint coefficient

$$\gamma_R^{0\varphi}(x,z_d)=(1-\gamma_{RR}(x))(\lambda-1)\cdot\frac{\dfrac{E_{28a}}{\zeta E_{28\gamma}}\dfrac{A_{a,\mathit{eff}}}{A_\gamma}}{\left(1+\dfrac{E_{28a}}{\zeta E_{28\gamma}}\dfrac{A_{a,\mathit{eff}}}{A_\gamma}\right)}\cdot \tag{D.21}$$
$$\frac{\left(1+\dfrac{H_a}{H_\gamma}\right)\left(1-\dfrac{E_{28a}}{\zeta E_{28\gamma}}\dfrac{A_{a,\mathit{eff}}}{A_\gamma}\dfrac{H_a}{H_\gamma}\right)}{\left(\dfrac{1}{3}\left(1+\dfrac{E_{28a}}{\zeta E_{28\gamma}}\dfrac{A_{a,\mathit{eff}}}{A_\gamma}\right)\left(1+\dfrac{E_{28a}}{\zeta E_{28\gamma}}\dfrac{A_{a,\mathit{eff}}}{A_\gamma}\left(\dfrac{H_a}{H_\gamma}\right)^2\right)+\dfrac{E_{28a}}{\zeta E_{28\gamma}}\dfrac{A_{a,\mathit{eff}}}{A_\gamma}\left(1+\dfrac{H_a}{H_\gamma}\right)^2\right)}$$

The plane-section restraint coefficient at three quarters of the width of the wall above the joint is determined by letting $z = z'_{cen}$-H_a-3/4W_γ in the numerator in Equation (D.14) giving

$$\text{Numerator}=\left\{A_\gamma\left(\frac{H_a+\dfrac{H_\gamma}{2}+\dfrac{E_{28a}}{\zeta E_{28\gamma}}\dfrac{A_{a,\mathit{eff}}}{A_\gamma}\dfrac{H_a}{2}}{1+\dfrac{E_{28a}}{\zeta E_{28\gamma}}\dfrac{A_{a,\mathit{eff}}}{A_\gamma}}-\left(H_a+\frac{H_\gamma}{2}\right)\right)+\right.$$
$$\left.+\frac{E_{28a}}{\zeta E_{28\gamma}}\lambda A_{a,\mathit{eff}}\left(\frac{H_a+\dfrac{H_\gamma}{2}+\dfrac{E_{28a}}{\zeta E_{28\gamma}}\dfrac{A_{a,\mathit{eff}}}{A_\gamma}\dfrac{H_a}{2}}{1+\dfrac{E_{28a}}{\zeta E_{28\gamma}}\dfrac{A_{a,\mathit{eff}}}{A_\gamma}}-\frac{H_a}{2}\right)\right\}\cdot$$
$$\cdot\left(\frac{H_a+\dfrac{H_\gamma}{2}+\dfrac{E_{28a}}{\zeta E_{28\gamma}}\dfrac{A_{a,\mathit{eff}}}{A_\gamma}\dfrac{H_a}{2}}{1+\dfrac{E_{28a}}{\zeta E_{28\gamma}}\dfrac{A_{a,\mathit{eff}}}{A_\gamma}}-H_a-\frac{3W_\gamma}{4}\right)=$$

$$= \left\{ A_\gamma \left(-\frac{\frac{E_{28a}}{\zeta E_{28\gamma}} \frac{A_{a,eff}}{A_\gamma} \left(\frac{H_a}{2} + \frac{H_\gamma}{2} \right)}{1 + \frac{E_{28a}}{\zeta E_{28\gamma}} \frac{A_{a,eff}}{A_\gamma}} \right) + \frac{E_{28a}}{\zeta E_{28\gamma}} \lambda A_a \left(\frac{\frac{H_a}{2} + \frac{H_\gamma}{2}}{1 + \frac{E_{28a}}{\zeta E_{28\gamma}} \frac{A_{a,eff}}{A_\gamma}} \right) \right\} \cdot$$

$$\cdot \frac{\frac{H_\gamma}{2} - \frac{E_{28a}}{\zeta E_{28\gamma}} \frac{A_{a,eff}}{A_\gamma} \frac{H_a}{2} - \frac{3W_\gamma}{4} \left(1 + \frac{E_{28a}}{\zeta E_{28\gamma}} \frac{A_{a,eff}}{A_\gamma} \right)}{1 + \frac{E_{28a}}{\zeta E_{28\gamma}} \frac{A_{a,eff}}{A_\gamma}} =$$

$$= \left\{ \frac{A_\gamma H_\gamma}{2} \left(-\frac{\frac{E_{28a}}{\zeta E_{28\gamma}} \frac{A_{a,eff}}{A_\gamma} \left(1 + \frac{H_a}{H_\gamma} \right)}{1 + \frac{E_{28a}}{\zeta E_{28\gamma}} \frac{A_{a,eff}}{A_\gamma}} \right) + \frac{E_{28a}}{\zeta E_{28\gamma}} \lambda \frac{A_{a,eff} H_\gamma}{2} \left(\frac{1 + \frac{H_a}{2}}{1 + \frac{E_{28a}}{\zeta E_{28\gamma}} \frac{A_{a,eff}}{A_\gamma}} \right) \right\} \cdot$$

$$\cdot \frac{H_\gamma}{2} \left(\frac{1 - \frac{E_{28a}}{\zeta E_{28\gamma}} \frac{A_{a,eff}}{A_\gamma} \frac{H_a}{H_\gamma} - \frac{3}{8} \frac{W_\gamma}{H_\gamma} \left(1 + \frac{E_{28a}}{\zeta E_{28\gamma}} \frac{A_{a,eff}}{A_\gamma} \right)}{1 + \frac{E_{28a}}{\zeta E_{28\gamma}} \frac{A_{a,eff}}{A_\gamma}} \right) =$$

$$= \frac{A_\gamma H_\gamma^2}{4} \left(-\frac{\frac{E_{28a}}{\zeta E_{28\gamma}} \frac{A_{a,eff}}{A_\gamma} \left(1 + \frac{H_a}{H_\gamma} \right)}{1 + \frac{E_{28a}}{\zeta E_{28\gamma}} \frac{A_{a,eff}}{A_\gamma}} + \lambda \frac{\frac{E_{28a}}{\zeta E_{28\gamma}} \frac{A_{a,eff}}{A_\gamma} \left(1 + \frac{H_a}{2} \right)}{1 + \frac{E_{28a}}{\zeta E_{28\gamma}} \frac{A_{a,eff}}{A_\gamma}} \right)$$

$$\cdot \left(\frac{1 - \frac{E_{28a}}{\zeta E_{28\gamma}} \frac{A_{a,eff}}{A_\gamma} \frac{H_a}{H_\gamma} - \frac{3}{8} \frac{W_\gamma}{H_\gamma} \left(1 + \frac{E_{28a}}{\zeta E_{28\gamma}} \frac{A_{a,eff}}{A_\gamma} \right)}{1 + \frac{E_{28a}}{\zeta E_{28\gamma}} \frac{A_{a,eff}}{A_\gamma}} \right) =$$

$$= \frac{A_\gamma H_\gamma^2}{4} \frac{\frac{E_{28a}}{\zeta E_{28\gamma}} \frac{A_{a,\underline{eff}}}{A_\gamma} \left(1 + \frac{H_a}{H_\gamma}\right)}{1 + \frac{E_{28a}}{\zeta E_{28\gamma}} \frac{A_{a,\underline{eff}}}{A_\gamma}} \cdot$$

$$\cdot \frac{1 - \frac{E_{28a}}{\zeta E_{28\gamma}} \frac{A_{a,\underline{eff}}}{A_\gamma} \frac{H_a}{H_\gamma} - \frac{3}{8} \frac{W_\gamma}{H_\gamma} \left(1 + \frac{E_{28a}}{\zeta E_{28\gamma}} \frac{A_{a,\underline{eff}}}{A_\gamma}\right)}{1 + \frac{E_{28a}}{\zeta E_{28\gamma}} \frac{A_{a,\underline{eff}}}{A_\gamma}} (\lambda - 1) =$$

$$= \frac{A_\gamma H_\gamma^2}{4\left(1 + \frac{E_{28a}}{\zeta E_{28\gamma}} \frac{A_{a,\underline{eff}}}{A_\gamma}\right)^2} \frac{E_{28a}}{\zeta E_{28\gamma}} \frac{A_{a,\underline{eff}}}{A_\gamma} \cdot$$

$$\cdot \left(1 + \frac{H_a}{H_\gamma}\right) \left(1 - \frac{E_{28a}}{\zeta E_{28\gamma}} \frac{A_{a,\underline{eff}}}{A_\gamma} \frac{H_a}{H_\gamma} - \frac{3}{8} \frac{W_\gamma}{H_\gamma} \left(1 + \frac{E_{28a}}{\zeta E_{28\gamma}} \frac{A_{a,\underline{eff}}}{A_\gamma}\right)\right) (\lambda - 1) \tag{D.22}$$

which in Equation (D.14) together with Equation (D.17) give the plane-section restraint coefficient at three quarter of the width of the wall above the joint as

$$\gamma_R^{0\varphi}(x, z_1) = (1 - \gamma_{RR}(x))(\lambda - 1) \cdot \frac{\frac{E_{28a}}{\zeta E_{28\gamma}} \frac{A_{a,\underline{eff}}}{A_\gamma}}{\left(1 + \frac{E_{28a}}{\zeta E_{28\gamma}} \frac{A_{a,\underline{eff}}}{A_\gamma}\right)} \cdot$$

$$\cdot \frac{\left(1 + \frac{H_a}{H_\gamma}\right)\left(1 - \frac{E_{28a}}{\zeta E_{28\gamma}} \frac{A_{a,\underline{eff}}}{A_\gamma} \frac{H_a}{H_\gamma} - \frac{3}{8} \frac{W_\gamma}{H_\gamma} \left(1 + \frac{E_{28a}}{\zeta E_{28\gamma}} \frac{A_{a,\underline{eff}}}{A_\gamma}\right)\right)}{\left(\frac{1}{3}\left(1 + \frac{E_{28a}}{\zeta E_{28\gamma}} \frac{A_{a,\underline{eff}}}{A_\gamma}\right)\left(1 + \frac{E_{28a}}{\zeta E_{28\gamma}} \frac{A_{a,\underline{eff}}}{A_\gamma} \left(\frac{H_a}{H_\gamma}\right)^2\right) + \frac{E_{28a}}{\zeta E_{28\gamma}} \frac{A_{a,\underline{eff}}}{A_\gamma} \left(1 + \frac{H_a}{H_\gamma}\right)^2\right)} \tag{D.23}$$

Appendix E

Diagrams of Plane-Section Restraint Coefficients in Young Parts of Concrete Structures

E.1 Diagrams for the Restraint at the Joint

In the present diagrams, the following presumptions and conditions are valid.

- The modulus of elasticity at 28 days is equal in both the young concrete and in the older one, $E_{28a}/E_{28y} = 1$.
- The modulus of elasticity in the young concrete is set 0.95 times the modulus of elasticity at 28 days, $\zeta = 0.95 \Rightarrow E_{28a}/0.95E_{28y} = 1.053E_{28a}/E_{28y}$.
- The cross sections of both young and old concrete are rectangular with heights H_y, H_a, and areas A_y and A_a.
- The imposed volume changes of the adjoining concrete are equal to zero, $\lambda = 0 \Rightarrow \Delta\varepsilon_a^{\,0} = \lambda\Delta\varepsilon_y^{\,0} = 0$.
- The ratio between the area of the adjoining concrete and the young concrete is varied between 0.05 and 10.
- The ratios between the heights of the adjoining concrete and the young concrete that have been used are $H_a/H_y = 0.1$, 0.25, 0.5, 0.75 and 1.
- The translational and rotational restraints from adjoining materials, $\gamma_{RT}(x)$ and $\gamma_{RR}(x)$, have been given the values 0, 0.25, 0.5, 0.75 and 1.

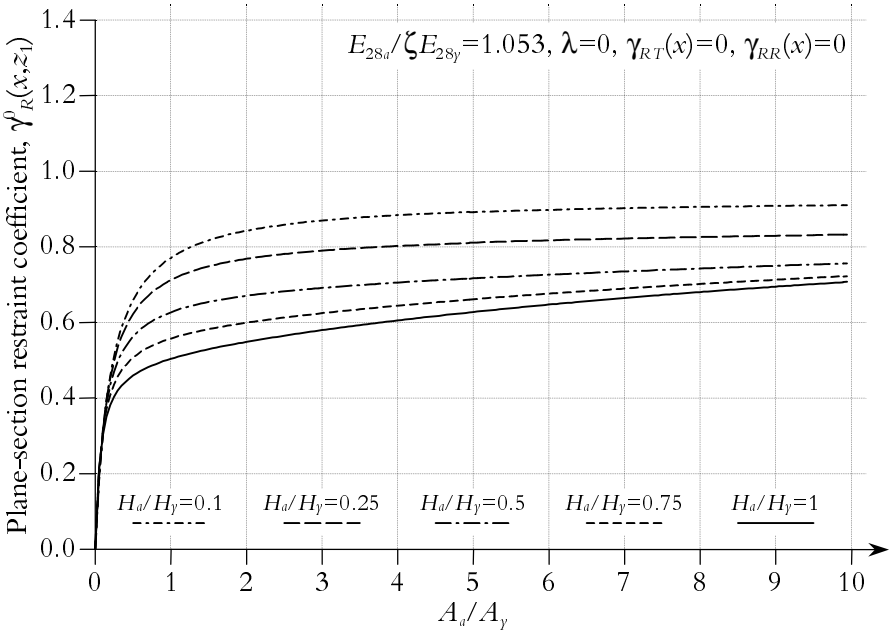

Figure E.1 *Restraint at the joint as function of A_a/A_y and H_a/H_y ratios. $E_{28a}/\zeta E_{28y}$ = 1.053, λ = 0, $\gamma_{RT}(x)$ = 0, $\gamma_{RR}(x)$ = 0.*

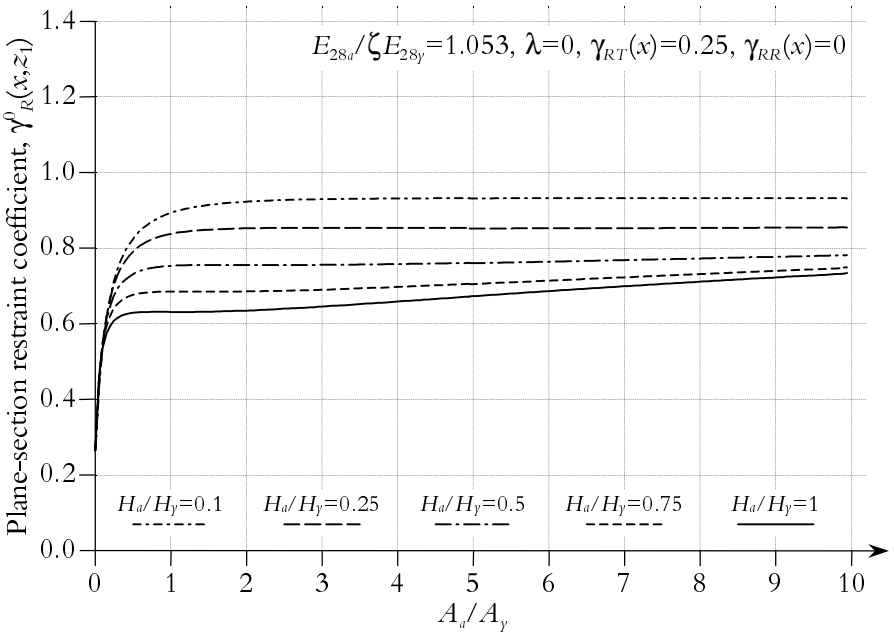

Figure E.2 *Restraint at the joint as function of A_a/A_y and H_a/H_y ratios. $E_{28a}/\zeta E_{28y}$ = 1.053, λ = 0, $\gamma_{RT}(x)$ = 0.25, $\gamma_{RR}(x)$ = 0.*

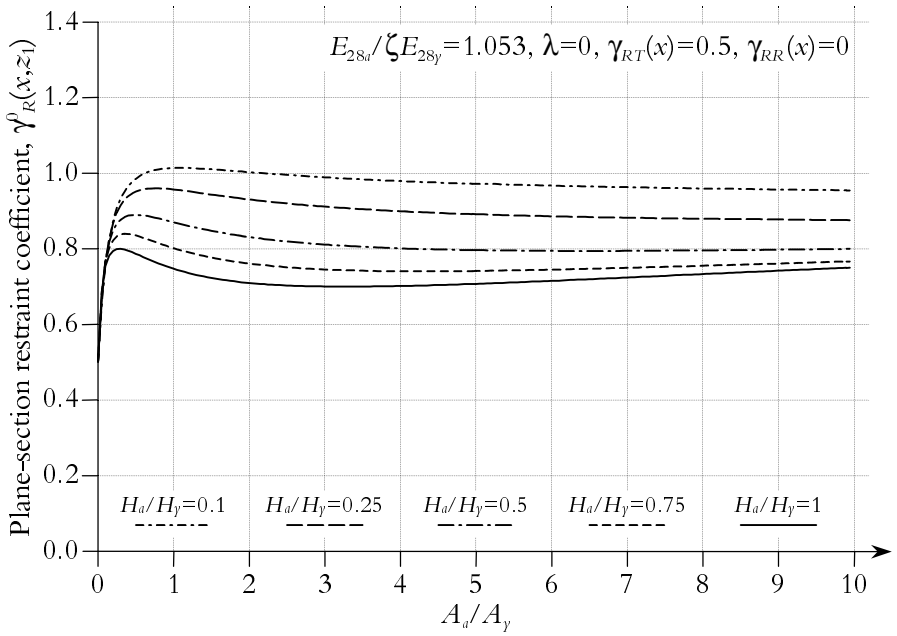

Figure E.3 *Restraint at the joint as function of A_a/A_y and H_a/H_y ratios. $E_{28a}/\zeta E_{28y}$ = 1.053, λ = 0, $\gamma_{RT}(x)$ = 0.5, $\gamma_{RR}(x)$ = 0.*

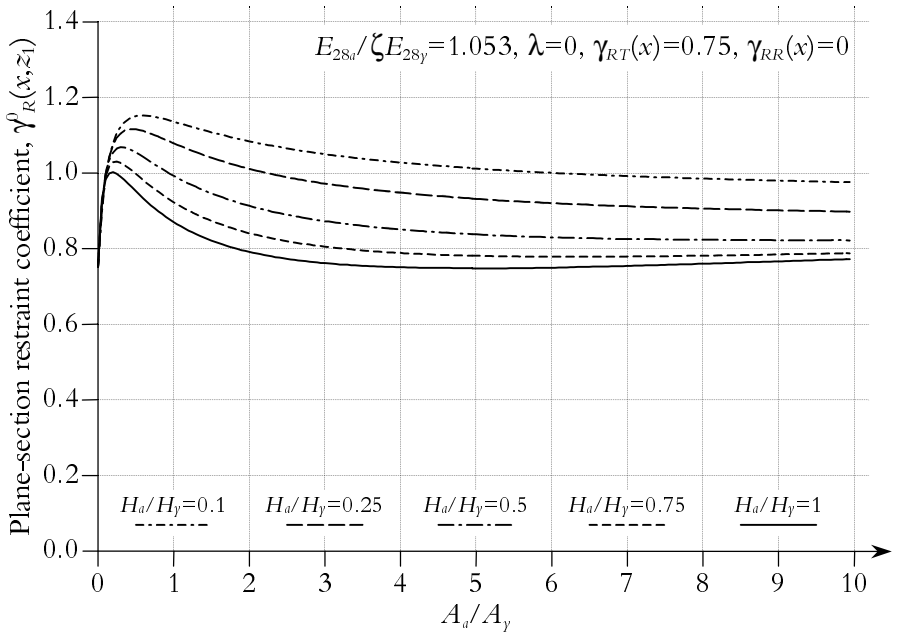

Figure E.4 *Restraint at the joint as function of A_a/A_y and H_a/H_y ratios. $E_{28a}/\zeta E_{28y}$ = 1.053, λ = 0, $\gamma_{RT}(x)$ = 0.75, $\gamma_{RR}(x)$ = 0.*

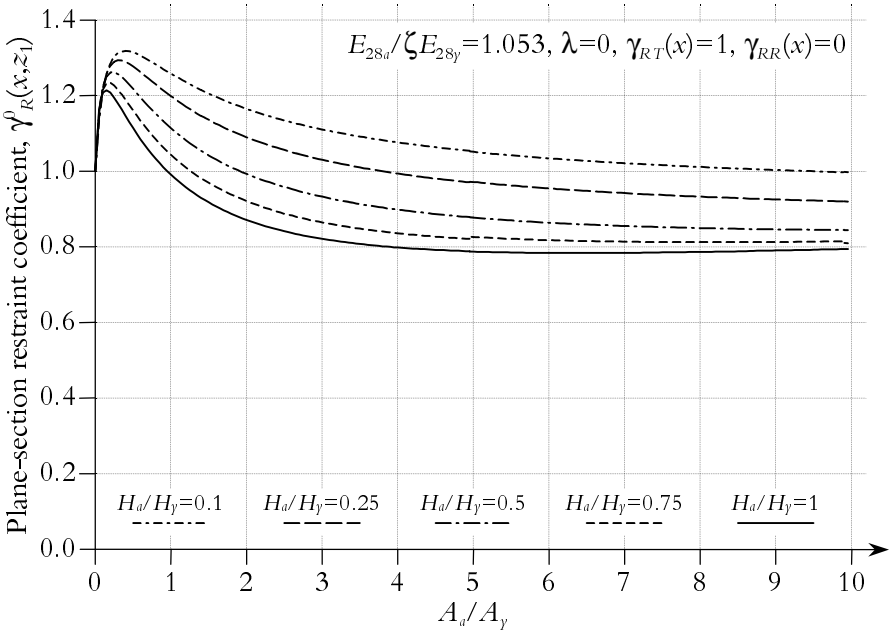

Figure E.5 *Restraint at the joint as function of A_a/A_y and H_a/H_y ratios. $E_{28a}/\zeta E_{28y}$ = 1.053, λ = 0, $\gamma_{RT}(x)$ = 1, $\gamma_{RR}(x)$ = 0.*

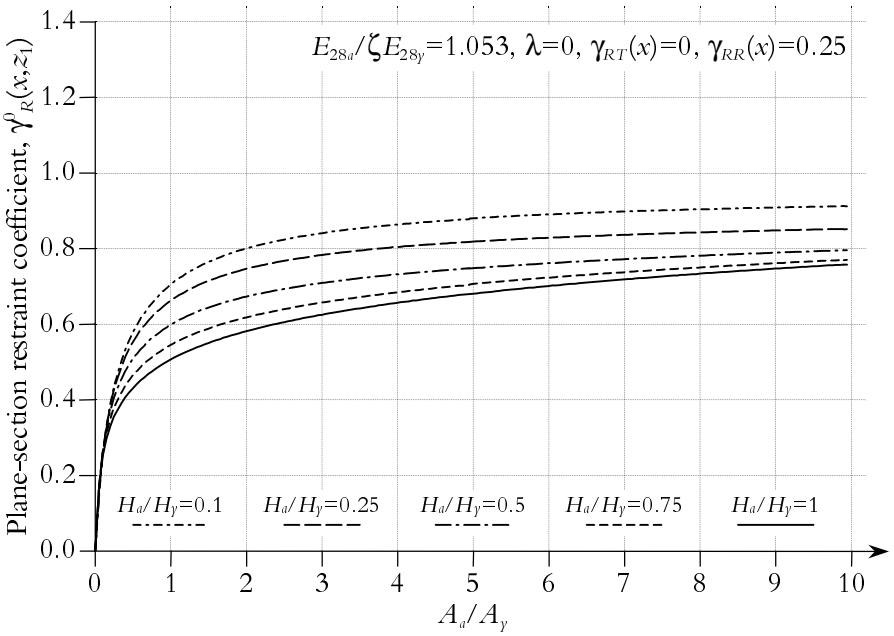

Figure E.6 *Restraint at the joint as function of A_a/A_y and H_a/H_y ratios. $E_{28a}/\zeta E_{28y}$ = 1.053, λ = 0, $\gamma_{RT}(x)$ = 0, $\gamma_{RR}(x)$ = 0.25.*

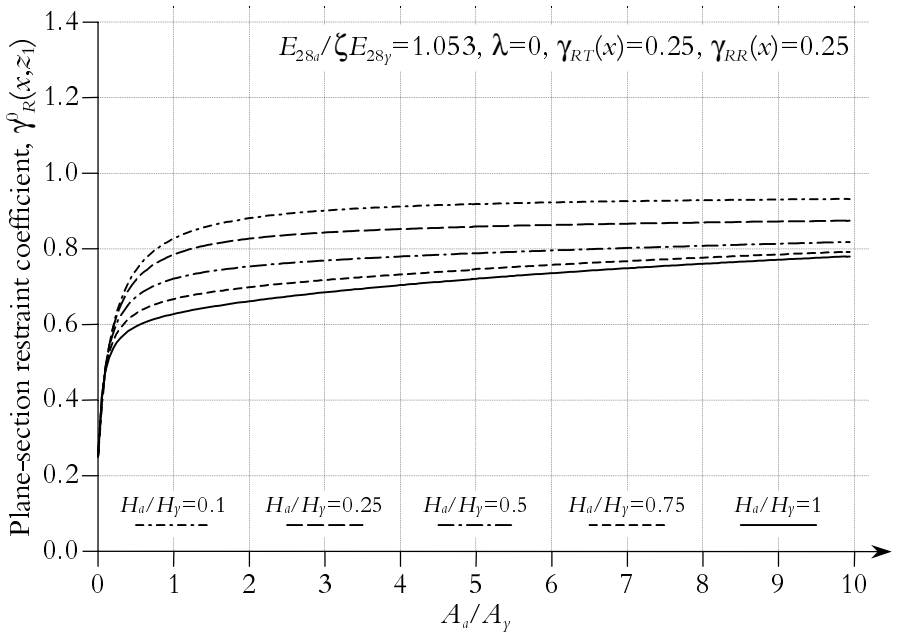

Figure E.7 *Restraint at the joint as function of A_a/A_y and H_a/H_y ratios. $E_{28a}/\zeta E_{28y}$ = 1.053, λ = 0, $\gamma_{RT}(x)$ = 0.25, $\gamma_{RR}(x)$ = 0.25.*

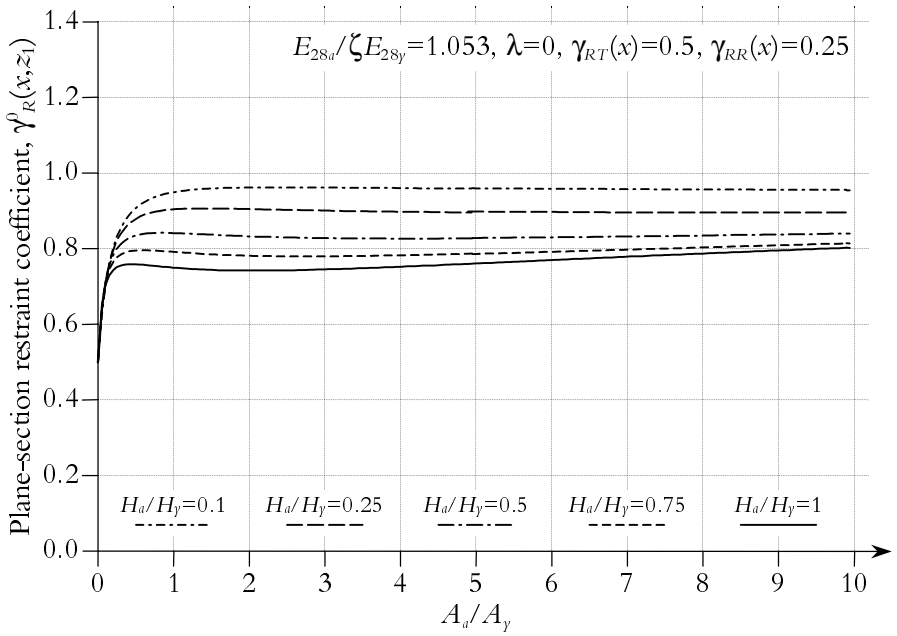

Figure E.8 *Restraint at the joint as function of A_a/A_y and H_a/H_y ratios. $E_{28a}/\zeta E_{28y}$ = 1.053, λ = 0, $\gamma_{RT}(x)$ = 0.5, $\gamma_{RR}(x)$ = 0.25.*

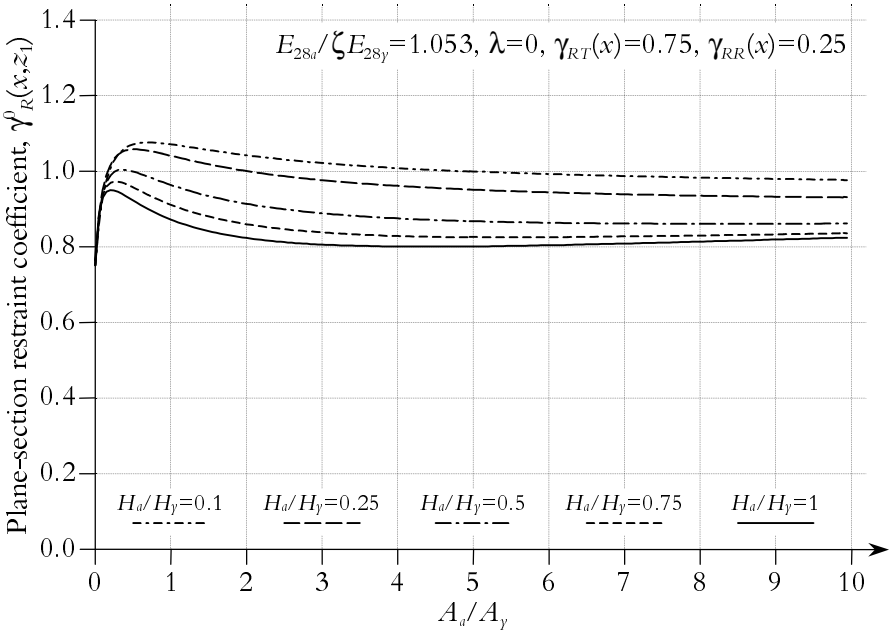

Figure E.9 *Restraint at the joint as function of A_a/A_y and H_a/H_y ratios. $E_{28a}/\zeta E_{28y}$ = 1.053, λ = 0, $\gamma_{RT}(x)$ = 0.75, $\gamma_{RR}(x)$ = 0.25.*

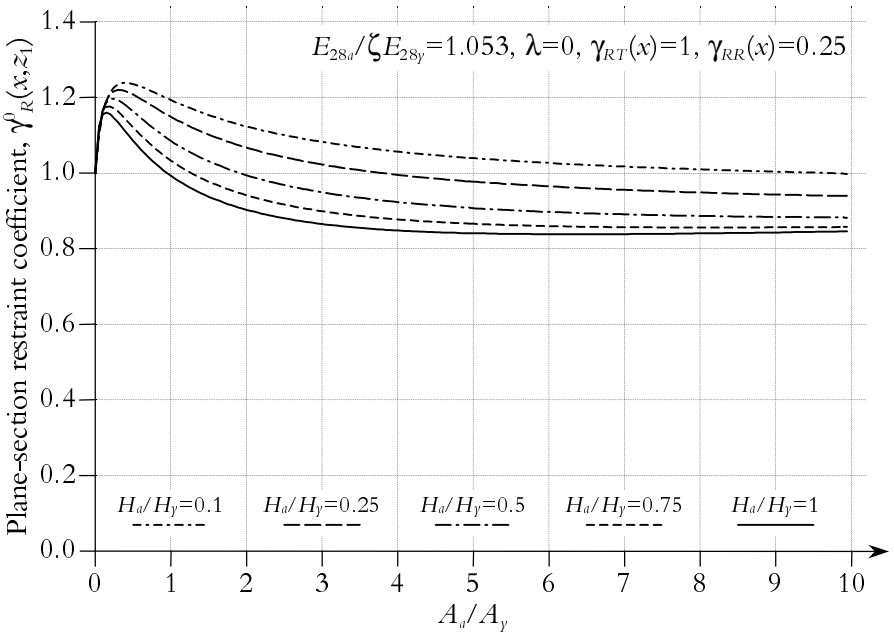

Figure E.10 *Restraint at the joint as function of A_a/A_y and H_a/H_y ratios. $E_{28a}/\zeta E_{28y}$ = 1.053, λ = 0, $\gamma_{RT}(x)$ = 1, $\gamma_{RR}(x)$ = 0.25.*

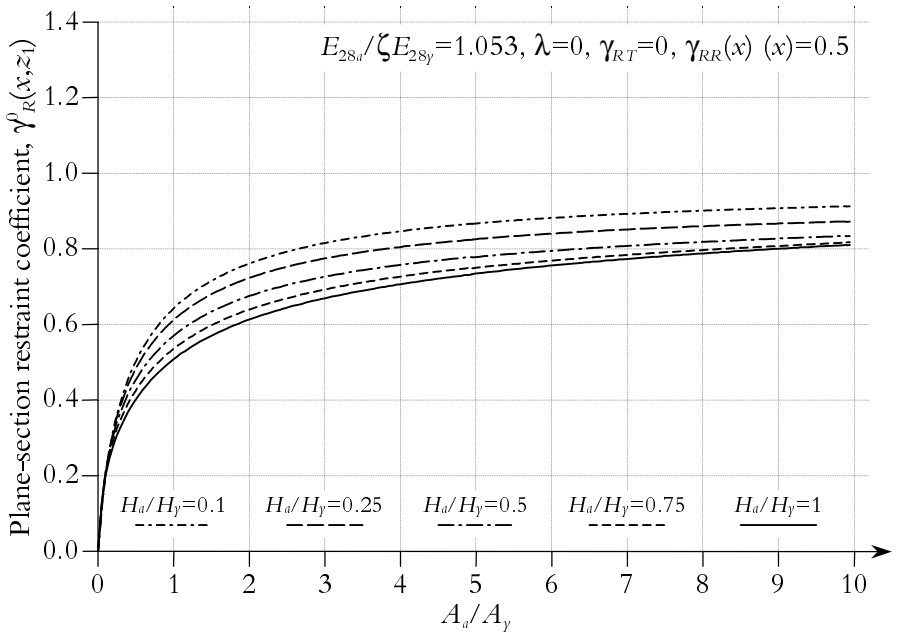

Figure E.11 *Restraint at the joint as function of A_a/A_y and H_a/H_y ratios. $E_{28a}/\zeta E_{28y}$ = 1.053, λ = 0, $\gamma_{RT}(x)$ = 0, $\gamma_{RR}(x)$ = 0.5.*

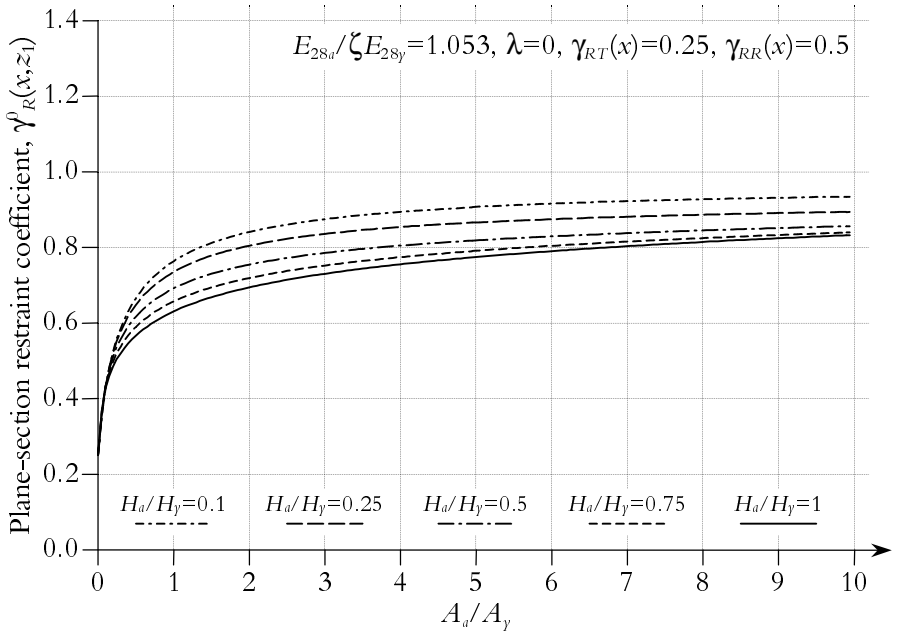

Figure E.12 *Restraint at the joint as function of A_a/A_y and H_a/H_y ratios. $E_{28a}/\zeta E_{28y}$ = 1.053, λ = 0, $\gamma_{RT}(x)$ = 0.25, $\gamma_{RR}(x)$ = 0.5.*

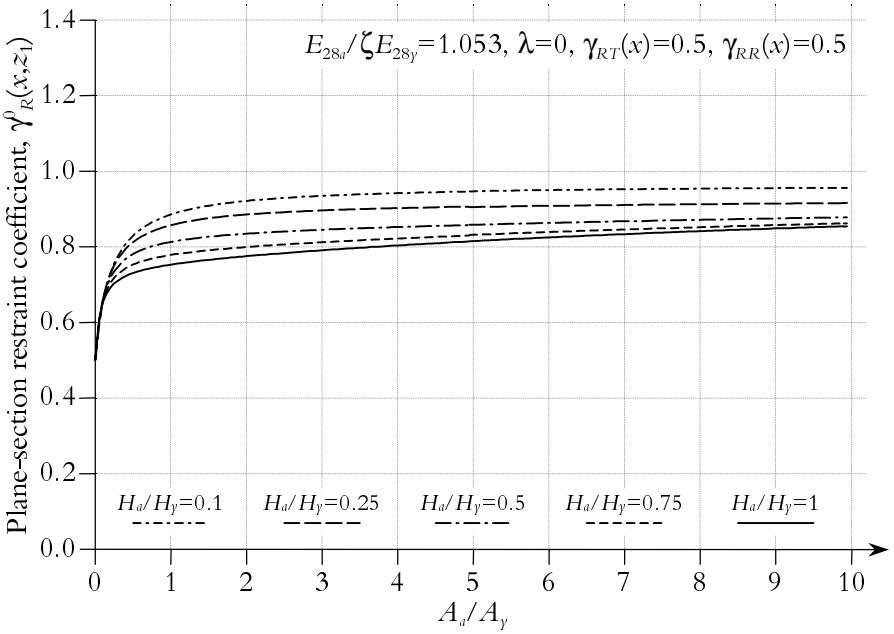

Figure E.13 *Restraint at the joint as function of A_a/A_y and H_a/H_y ratios. $E_{28a}/\zeta E_{28y}$ = 1.053, λ = 0, $\gamma_{RT}(x)$ = 0.5, $\gamma_{RR}(x)$ = 0.5.*

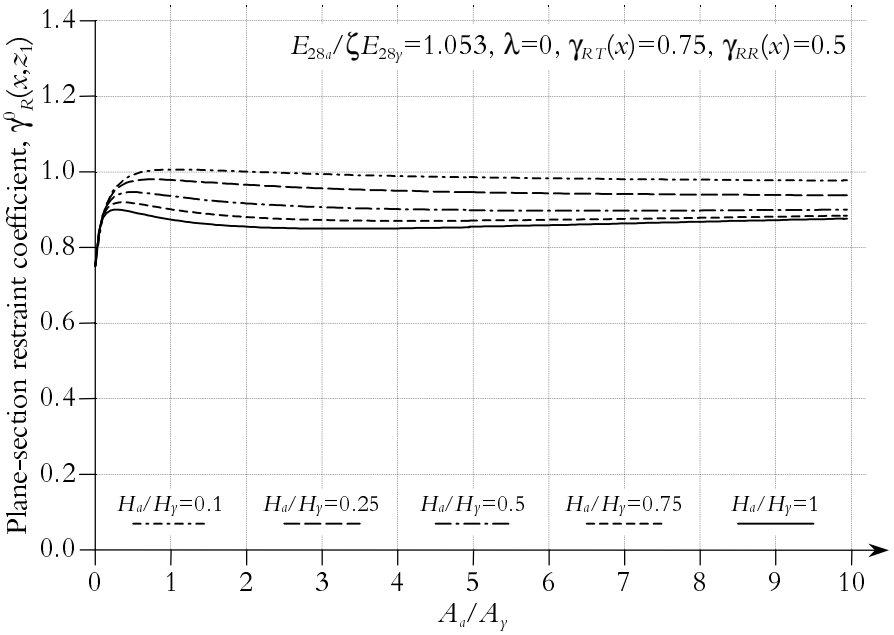

Figure E.14 *Restraint at the joint as function of A_a/A_y and H_a/H_y ratios. $E_{28a}/\zeta E_{28y}$ = 1.053, λ = 0, $\gamma_{RT}(x)$ = 0.75, $\gamma_{RR}(x)$ = 0.5.*

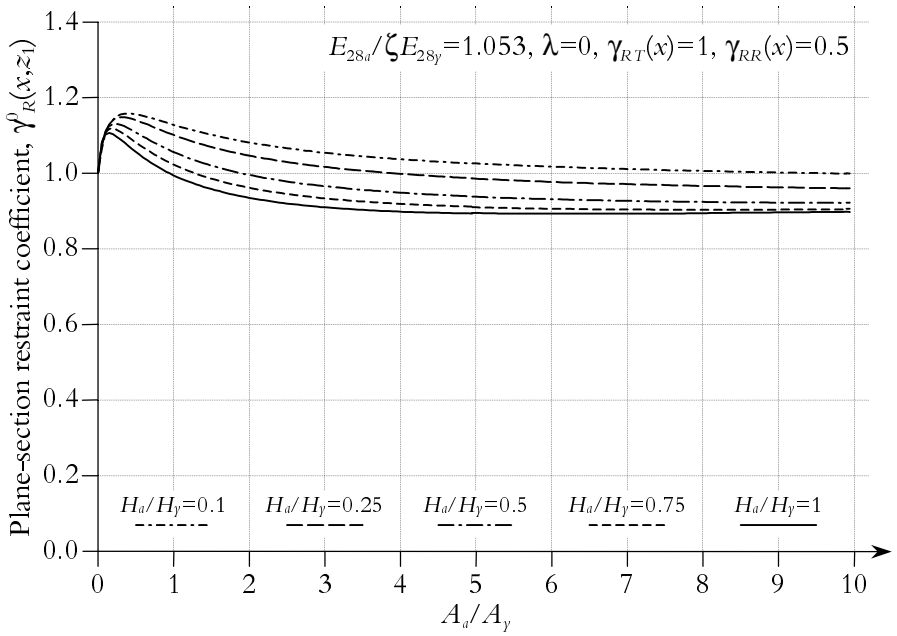

Figure E.15 *Restraint at the joint as function of A_a/A_y and H_a/H_y ratios. $E_{28a}/\zeta E_{28y}$ = 1.053, λ = 0, $\gamma_{RT}(x)$ = 1, $\gamma_{RR}(x)$ = 0.5.*

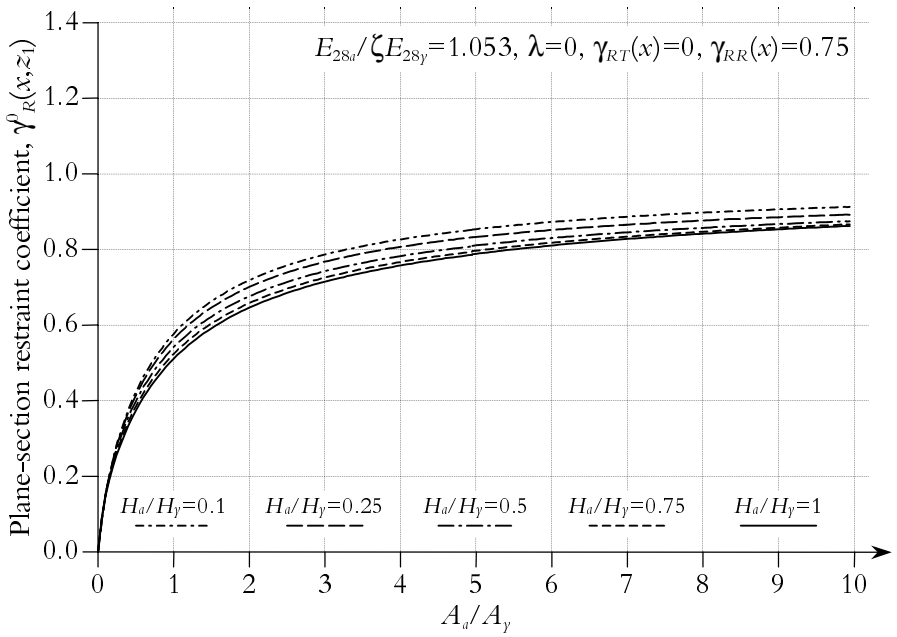

Figure E.16 *Restraint at the joint as function of A_a/A_y and H_a/H_y ratios. $E_{28a}/\zeta E_{28y}$ = 1.053, λ = 0, $\gamma_{RT}(x)$ = 0, $\gamma_{RR}(x)$ = 0.75.*

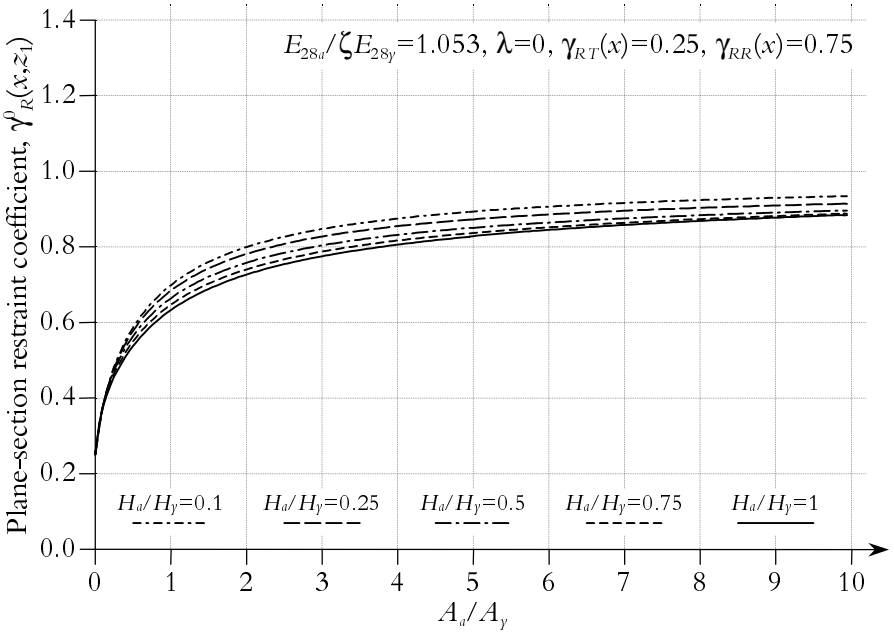

Figure E.17 *Restraint at the joint as function of A_a/A_y and H_a/H_y ratios. $E_{28a}/\zeta E_{28y}$ = 1.053, λ = 0, $\gamma_{RT}(x)$ = 0.25, $\gamma_{RR}(x)$ = 0.75.*

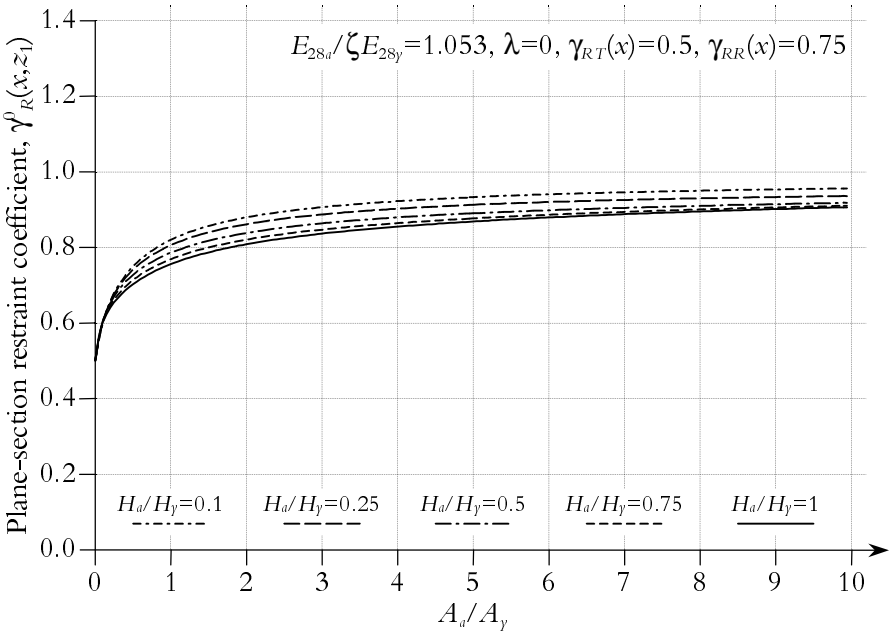

Figure E.18 *Restraint at the joint as function of A_a/A_y and H_a/H_y ratios. $E_{28a}/\zeta E_{28y}$ = 1.053, λ = 0, $\gamma_{RT}(x)$ = 0.5, $\gamma_{RR}(x)$ = 0.75.*

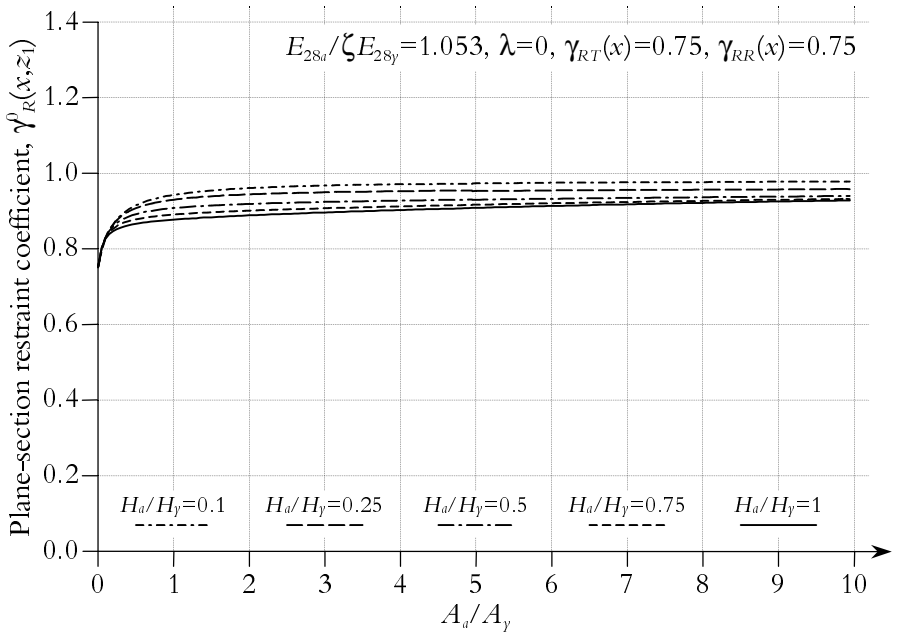

Figure E.19 *Restraint at the joint as function of A_a/A_y and H_a/H_y ratios. $E_{28a}/\zeta E_{28y}$ = 1.053, λ = 0, $\gamma_{RT}(x)$ = 0.75, $\gamma_{RR}(x)$ = 0.75.*

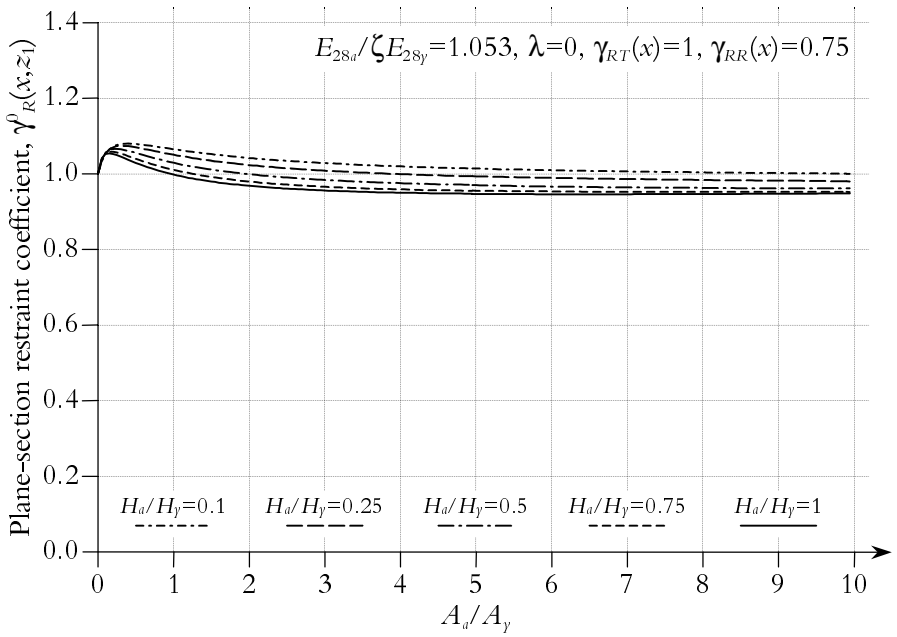

Figure E.20 *Restraint at the joint as function of A_a/A_y and H_a/H_y ratios. $E_{28a}/\zeta E_{28y}$ = 1.053, λ = 0, $\gamma_{RT}(x)$ = 1, $\gamma_{RR}(x)$ = 0.75.*

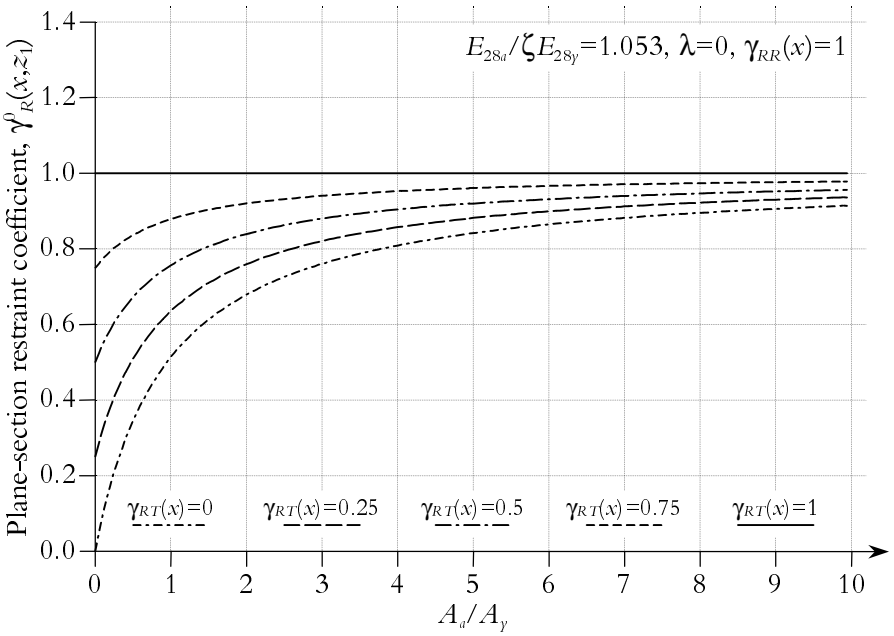

Figure E.21 *Restraint at the joint as function of A_a/A_y and γ_{RT}. $E_{28a}/\zeta E_{28y}$ = 1.053, λ = 0, $\gamma_{RR}(x)$ = 1.*

E.2 Diagrams for the Restraint at three quarters of the width of the wall above the Joint

In the present diagrams, the following presumptions and conditions are valid.

- The modulus of elasticity at 28 days is equal in both the young concrete and in the older one, $E_{28a}/E_{28y} = 1$.
- The modulus of elasticity in the young concrete is set 0.95 times the modulus of elasticity at 28 days, $\zeta = 0.95 \Rightarrow E_{28a}/0.95E_{28y} = 1.053E_{28a}/E_{28y}$.
- The cross sections of both young and old concrete are rectangular with heights H_y, H_a, and areas A_y and A_a.
- The imposed volume changes of the adjoining concrete are equal to zero, $\lambda = 0 \Rightarrow \Delta\varepsilon_a^{\,0} = \lambda\Delta\varepsilon_y^{\,0} = 0$.
- The ratio between the area of the adjoining concrete and the young concrete is varied between 0.05 and 10.
- The ratio between the heights of the adjoining concrete and the young concrete that has been used are $H_a/H_y = 0.1$, 0.25, 0.5, 0.75 and 1.
- The translational and rotational restraints from adjoining materials, $\gamma_{RT}(x)$ and $\gamma_{RR}(x)$, have been given the value 0.
- The ratio between the width and the height of the young concrete part is given the values $W_y/H_y = 0.1$, 0.25, 0.5, 0.75 and 1.

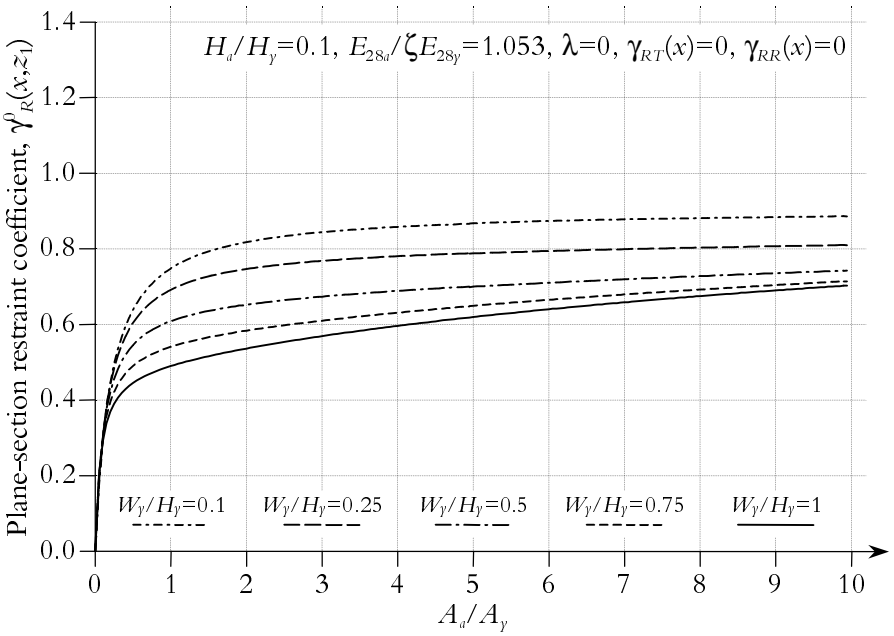

Figure E.22 *Restraint at 3/4W_y above the joint as function of A_a/A_y and W_y/H_y ratios. $E_{28a}/\zeta E_{28y}$ = 1.053, λ = 0, $\gamma_{RT}(x)$ = 0, $\gamma_{RR}(x)$ = 0, H_a/H_y = 0.1.*

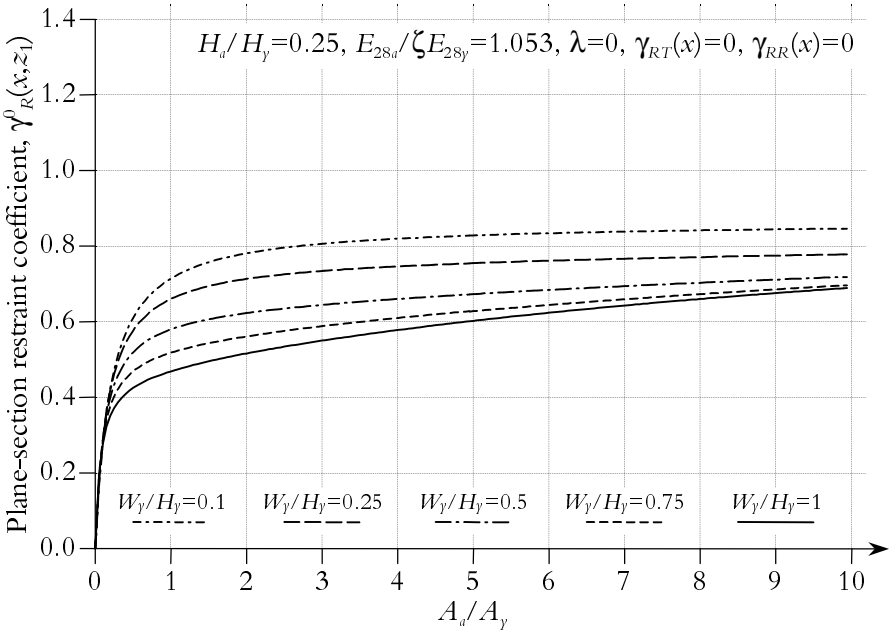

Figure E.23 *Restraint at 3/4W_y above the joint as function of A_a/A_y and W_y/H_y ratios. $E_{28a}/\zeta E_{28y}$ = 1.053, λ = 0, $\gamma_{RT}(x)$ = 0, $\gamma_{RR}(x)$ = 0, H_a/H_y = 0.25.*

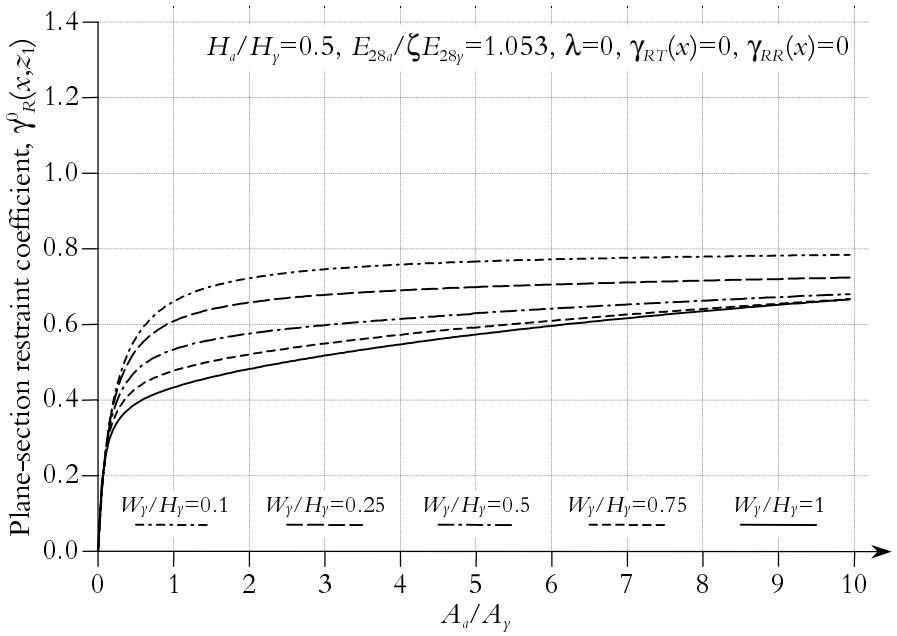

Figure E.24 *Restraint at 3/4W_y above the joint as function of A_a/A_y and W_y/H_y ratios. $E_{28a}/\zeta E_{28y}$ = 1.053, λ = 0, $\gamma_{RT}(x)$ = 0, $\gamma_{RR}(x)$ = 0, H_a/H_y = 0.5.*

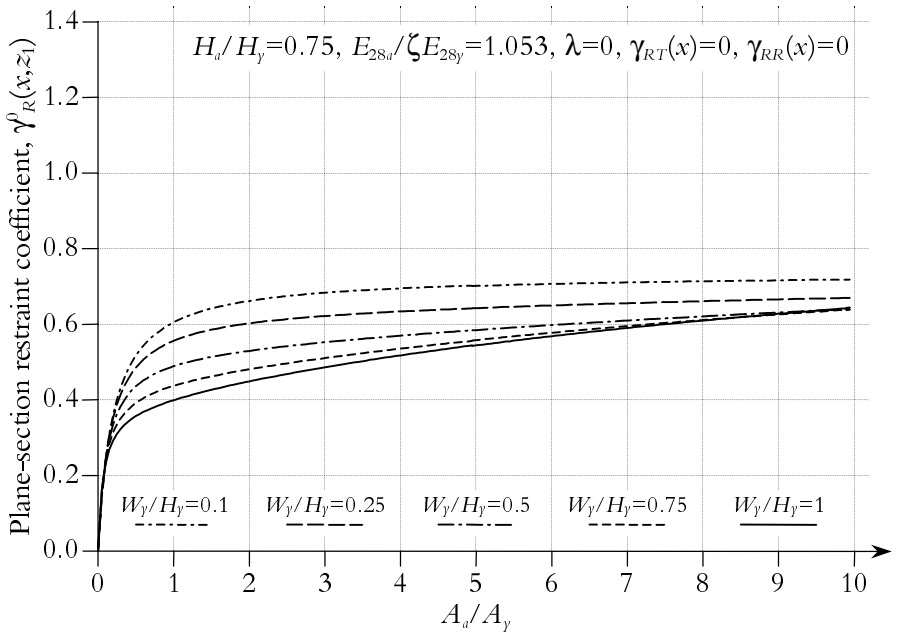

Figure E.25 *Restraint at 3/4W_y above the joint as function of A_a/A_y and W_y/H_y ratios. $E_{28a}/\zeta E_{28y}$ = 1.053, λ = 0, $\gamma_{RT}(x)$ = 0, $\gamma_{RR}(x)$ = 0, H_a/H_y = 0.75.*

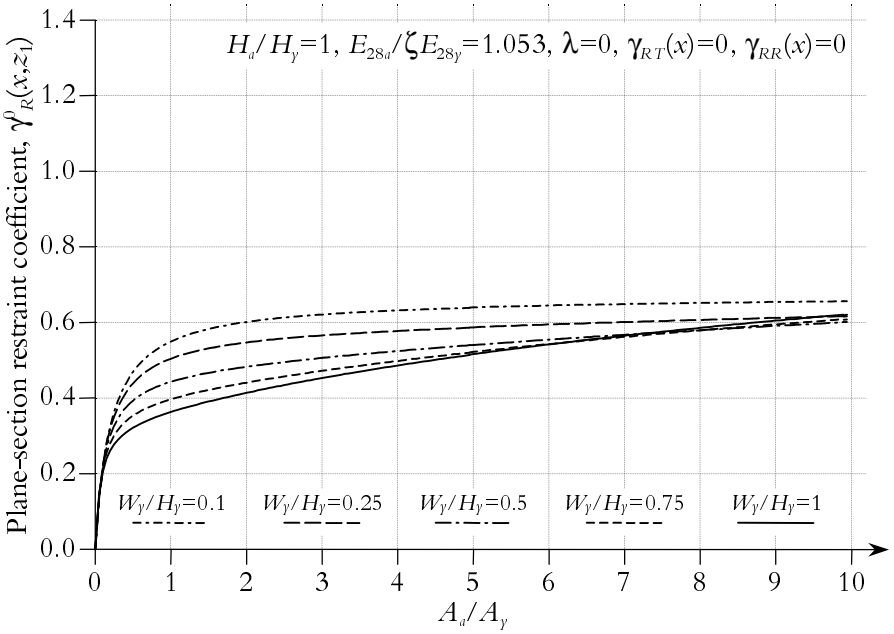

Figure E.26 *Restraint at 3/4W_y above the joint as function of A_a/A_y and W_y/H_y ratios. $E_{28a}/\zeta E_{28y}$ = 1.053, λ = 0, $\gamma_{RT}(x)$ = 0, $\gamma_{RR}(x)$ = 0, H_a/H_y = 1.*

Appendix F

Diagrams of Relative Displacements

The relative displacements between the parts of the structures have been measured with so-called Linear Displacement Transducers (LDT).

F.1 Relative Displacements Test I and Test II

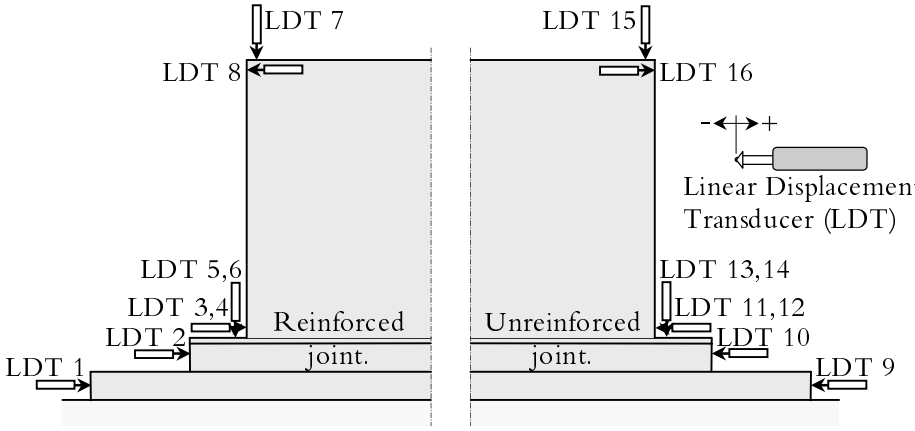

Figure F.1 *Location of Linear Displacement Transducers for measuring of relative movements between the different parts in Test I and Test II.*

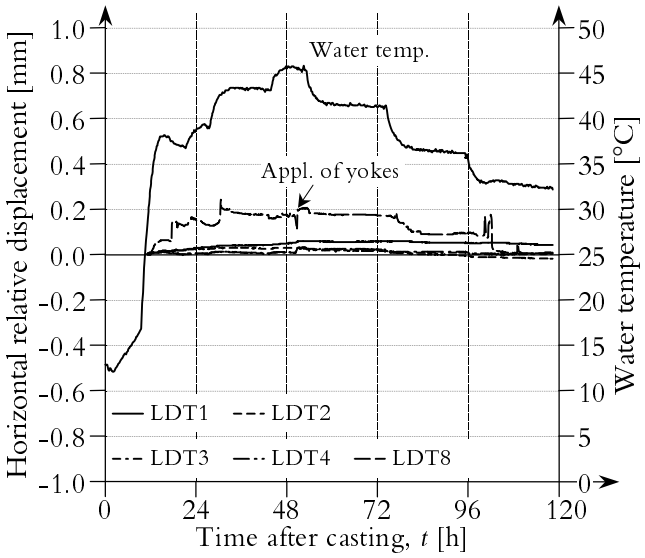

Figure F.2 *Horizontal relative displacements at the reinforced joint in Test I between the floor and the slab (LDT1), the slab and the footing (LDT2), the footing and the wall (LDT3 and LDT4), and the floor and top corner of the wall (LDT8).*

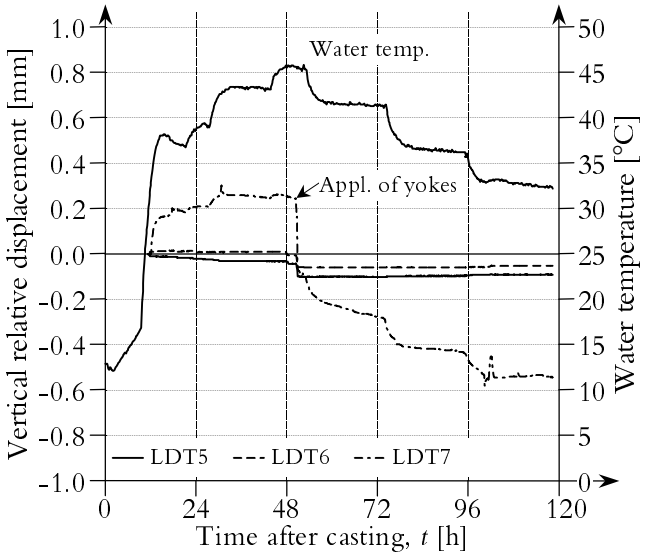

Figure F.3 *Vertical relative displacements at the reinforced joint in Test I between the footing and the wall (LDT5 and LDT6), and the floor and top corner of the wall (LDT7).*

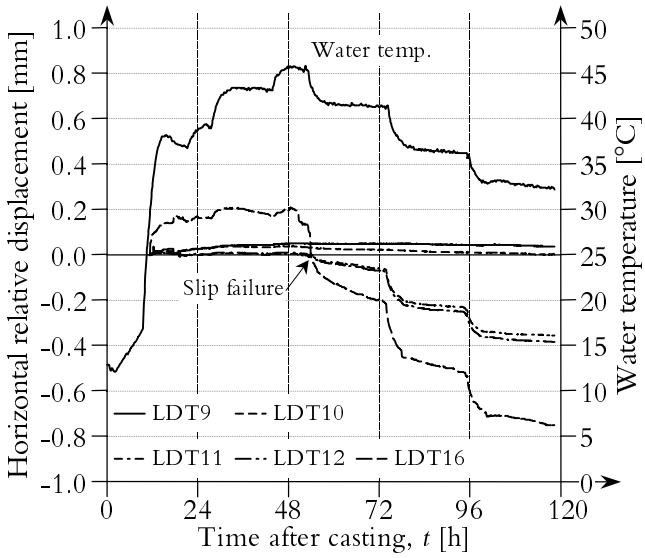

Figure F.4 *Horizontal relative displacements at the unreinforced joint in Test I between the floor and the slab (LDT9), the slab and the footing (LDT10), the footing and the wall (LDT11 and LDT12), and the floor and top corner of the wall (LDT16).*

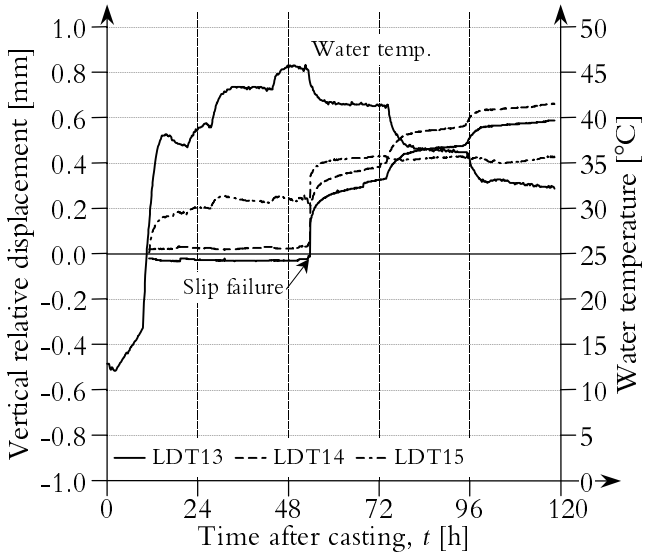

Figure F.5 *Vertical relative displacements at the unreinforced joint in Test I between the footing and the wall (LDT13 and LDT14), and the floor and top corner of the wall (LDT15).*

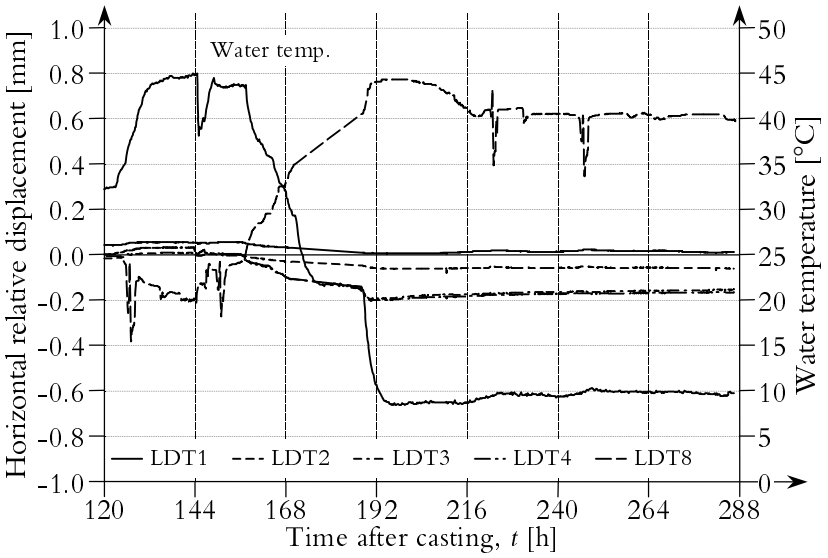

Figure F.6 *Horizontal relative displacements at the reinforced joint in Test II between the floor and the slab (LDT1), the slab and the footing (LDT2), the footing and the wall (LDT3 and LDT4), and the floor and top corner of the wall (LDT8).*

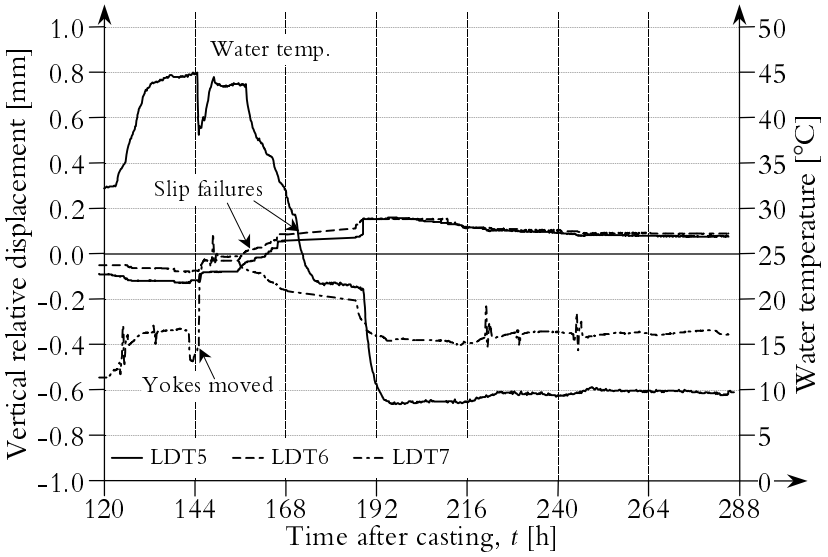

Figure F.7 *Vertical relative displacements at the reinforced joint in Test II between the footing and the wall (LDT5 and LDT6), and the floor and top corner of the wall (LDT7).*

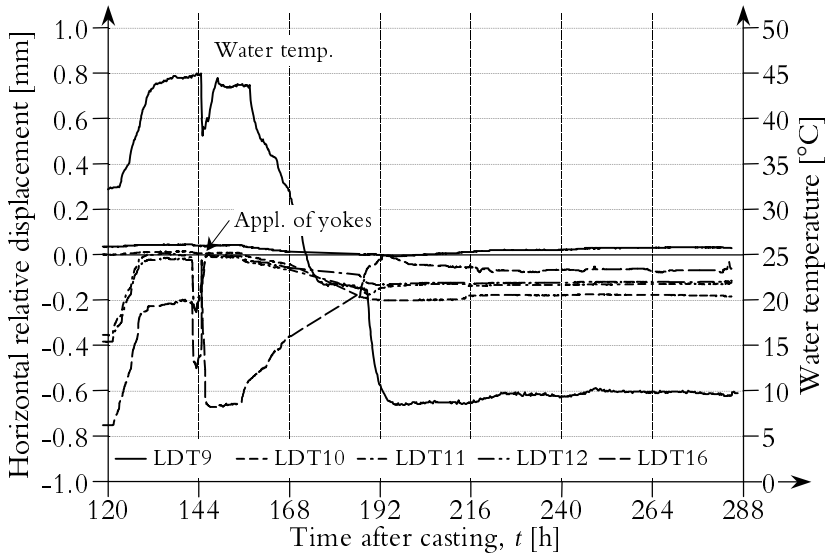

Figure F.8 *Horizontal relative displacements at the unreinforced joint in Test II between the floor and the slab (LDT9), the slab and the footing (LDT10), the footing and the wall (LDT11 and LDT12), and the floor and top corner of the wall (LDT16).*

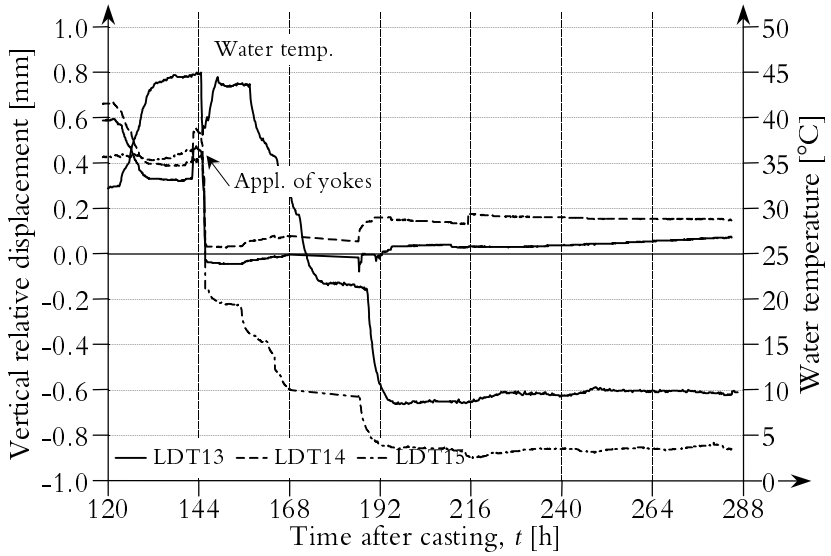

Figure F.9 *Vertical relative displacements at the unreinforced joint in Test II between the footing and the wall (LDT13 and LDT14), and the floor and top corner of the wall (LDT15).*

F.2 Relative Dsplacements Test III

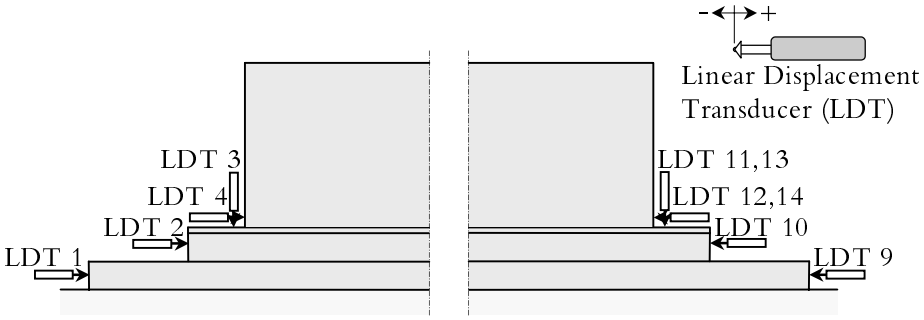

Figure F.10 *Location of Linear Displacement Transducers for measuring of relative movements between the different parts in Test III.*

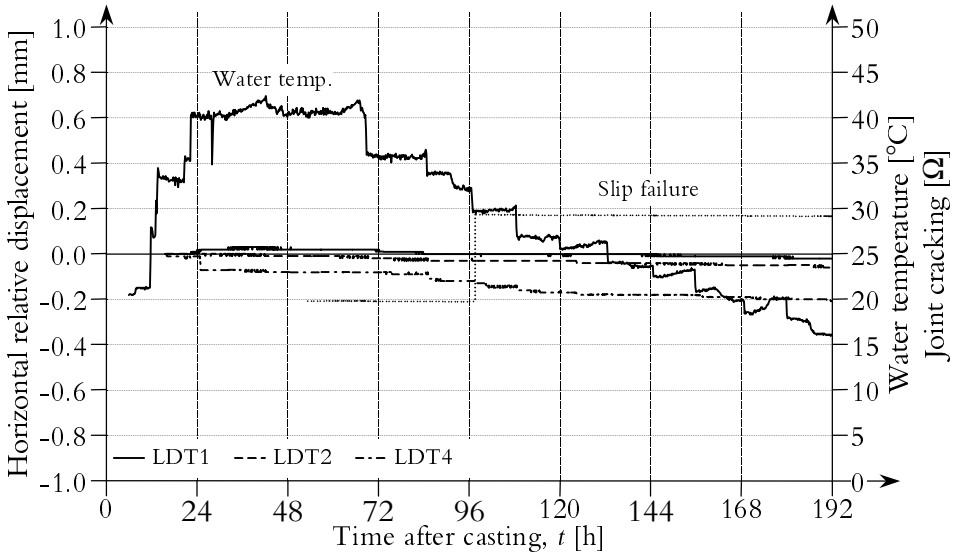

Figure F.11 *Horizontal relative displacements in Test III between the floor and the slab (LDT1), the slab and the footing (LDT2), and the footing and the wall (LDT4).*

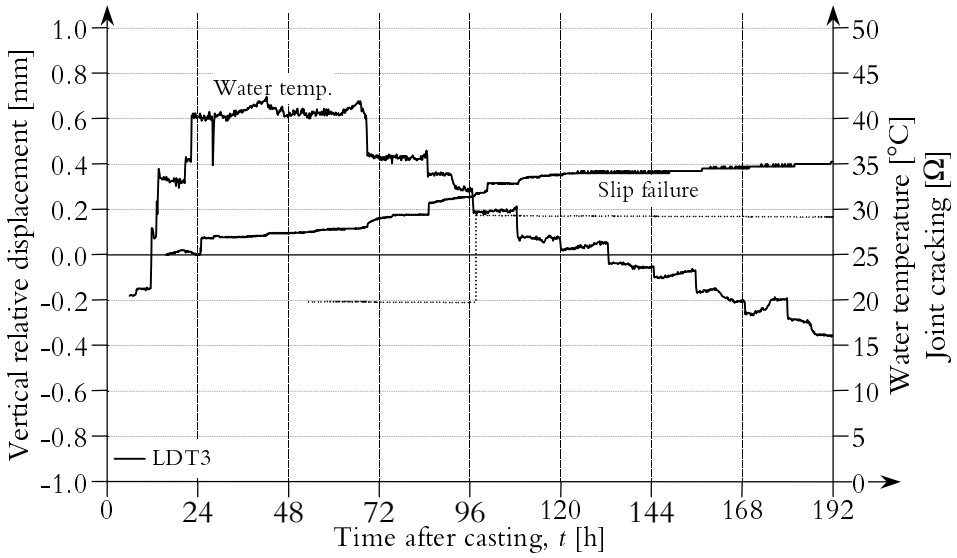

Figure F.12 *Vertical relative displacements in Test III between the footing and the wall (LDT3).*

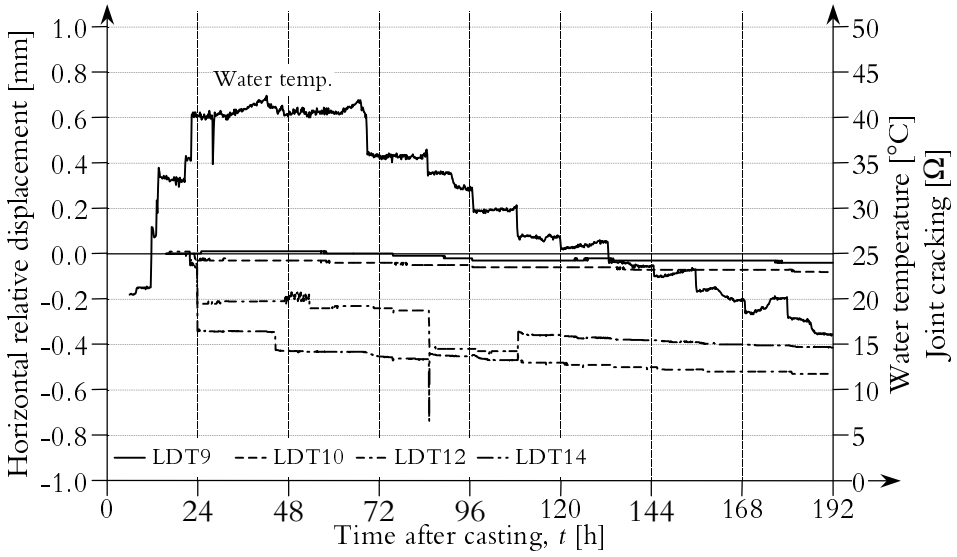

Figure F.13 *Horizontal relative displacements in Test III between the floor and the slab (LDT9), the slab and the footing (LDT10), and the footing and the wall (LDT12 and LDT14).*

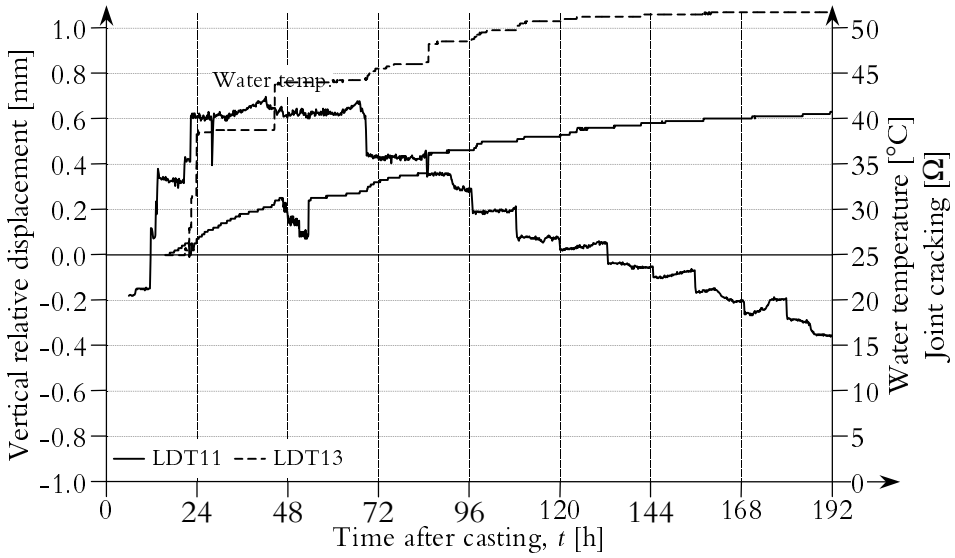

Figure F.14 *Vertical relative displacements in Test III between the footing and the wall (LDT11 and LDT13).*

F.3 Relative Dsplacements Test IV

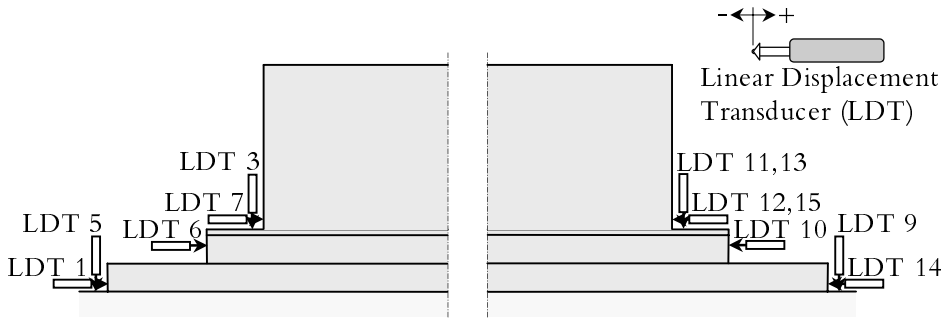

Figure F.15 *Location of Linear Displacement Transducers for measuring of relative movements between the different parts in Test IV.*

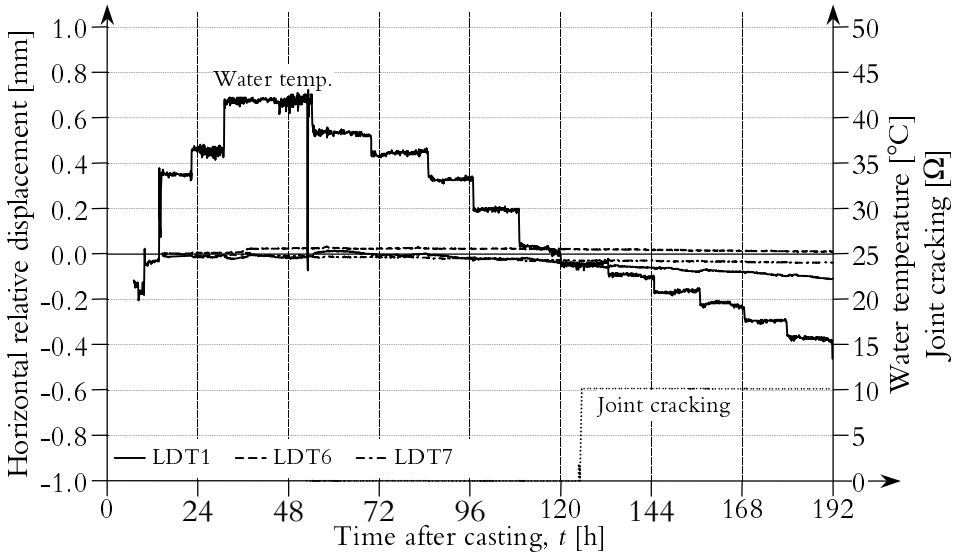

Figure F.16 *Horizontal relative displacements in Test IV between the floor and the slab (LDT1), the slab and the footing (LDT6), and the footing and the wall (LDT7).*

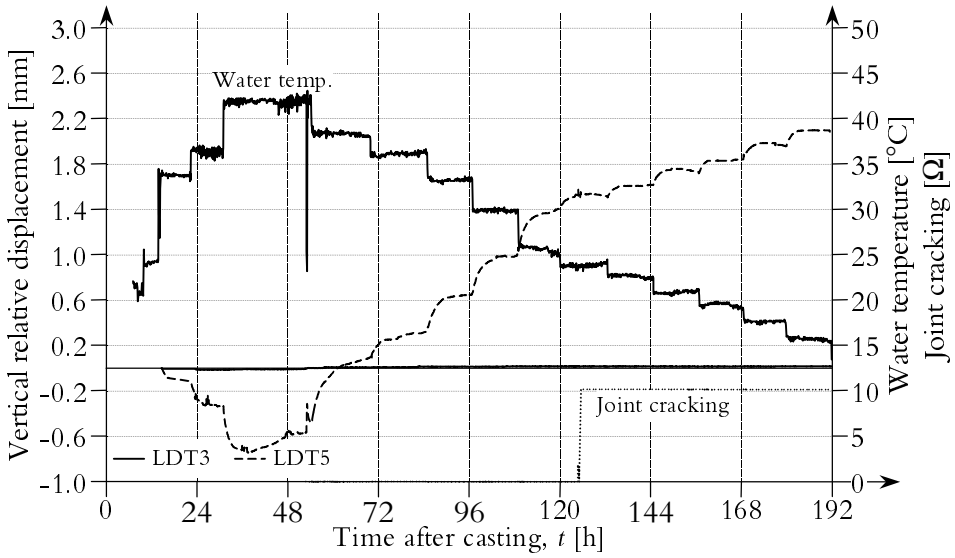

Figure F.17 *Vertical relative displacements in Test IV between the floor and the slab (LDT5), and the footing and the wall (LDT3). Observe the enhanced range on the axis of vertical relative displacements.*

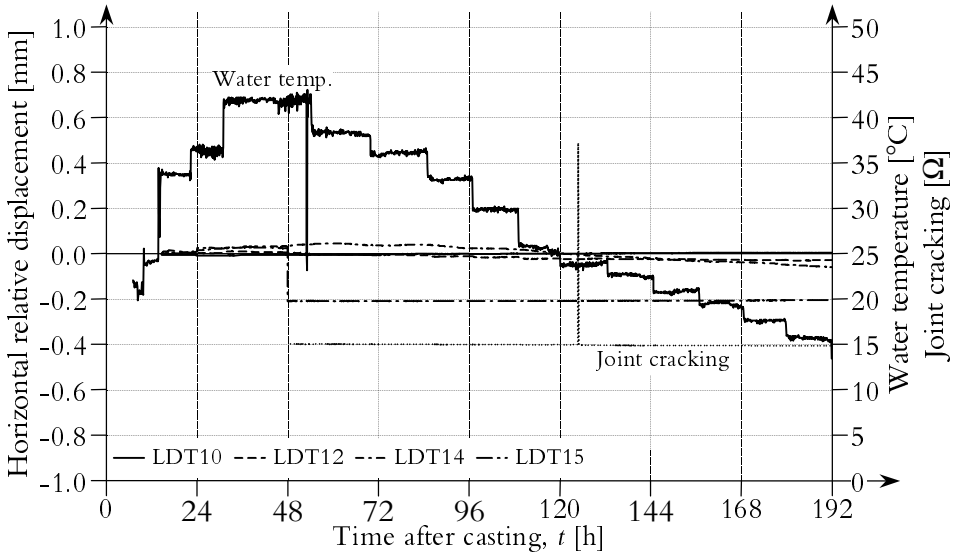

Figure F.18 *Horizontal relative displacements in Test IV between the floor and the slab (LDT14), the slab and the footing (LDT10), and the footing and the wall (LDT12 and LDT15).*

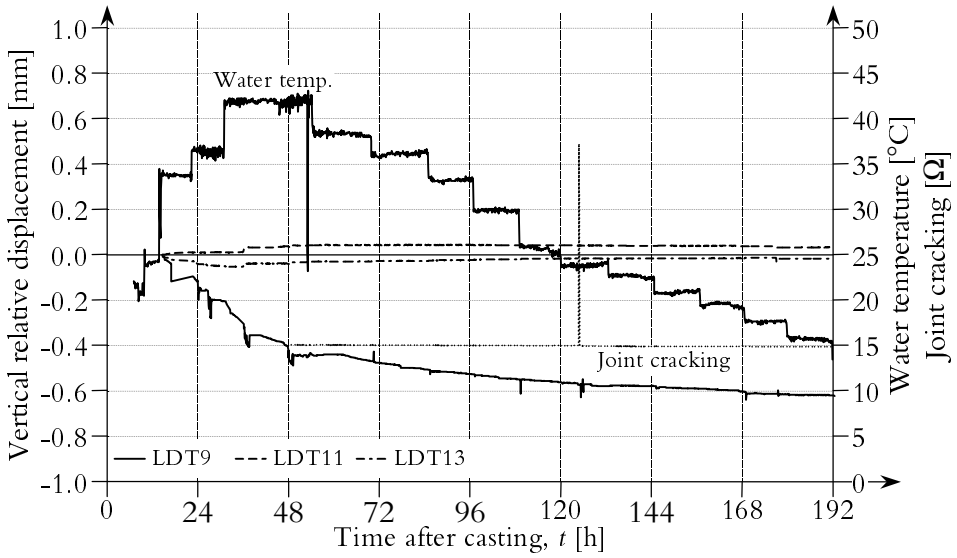

Figure F.19 *Vertical relative displacements in Test IV between the floor and the slab (LDT9), and the footing and the wall (LDT11 and LDT13).*

Appendix G

Diagrams of Strains

The strains at chosen points in the structures have been measured with so-called Vibrating Strain Gages (VSG).

G.1 Strains in Test I and Test II

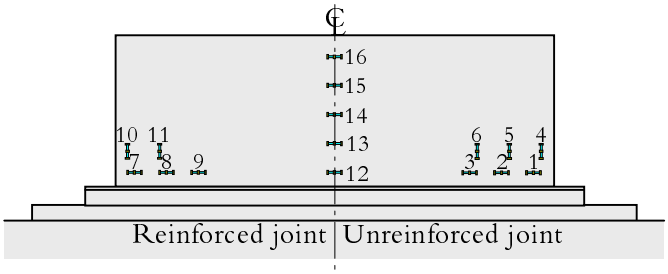

Figure G.1 *Location of Vibrating Strain Gages for measuring of strains in Test I and Test II.*

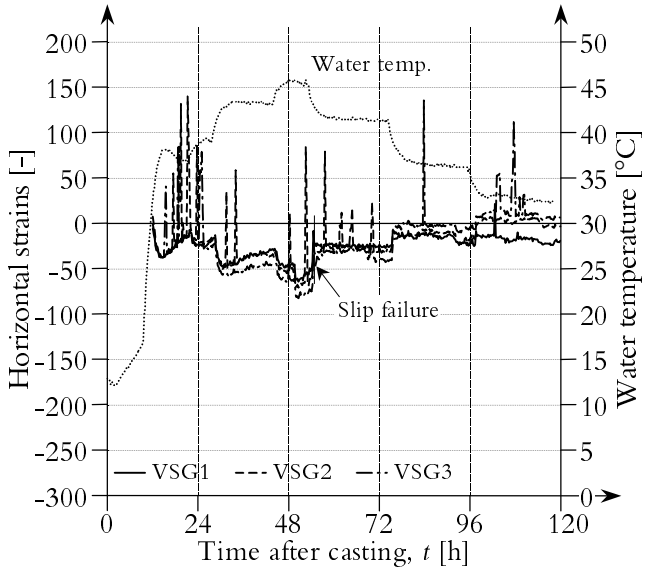

Figure G.2 *Horizontal strains at the end of the unreinforced joint in Test I. VSG1, VSG2 and VSG3.*

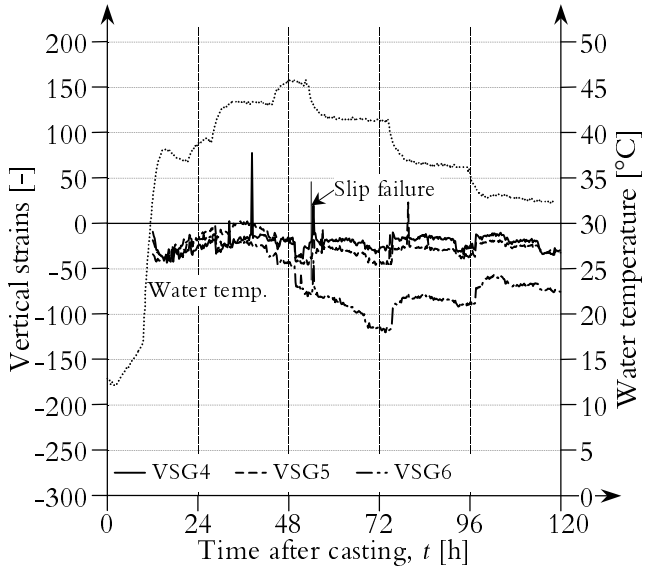

Figure G.3 *Vertical strains at the end of the unreinforced joint in Test I. VSG4, VSG5 and VSG6.*

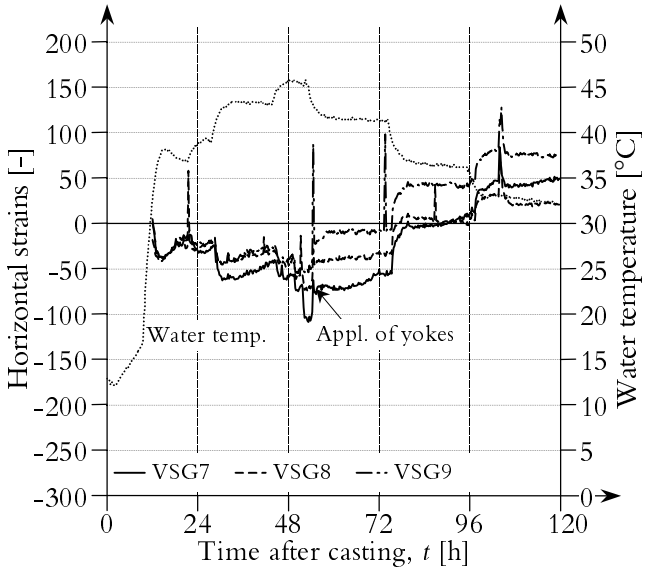

Figure G.4 *Horizontal strains at the end of the reinforced joint in Test I. VSG7, VSG8 and VSG9.*

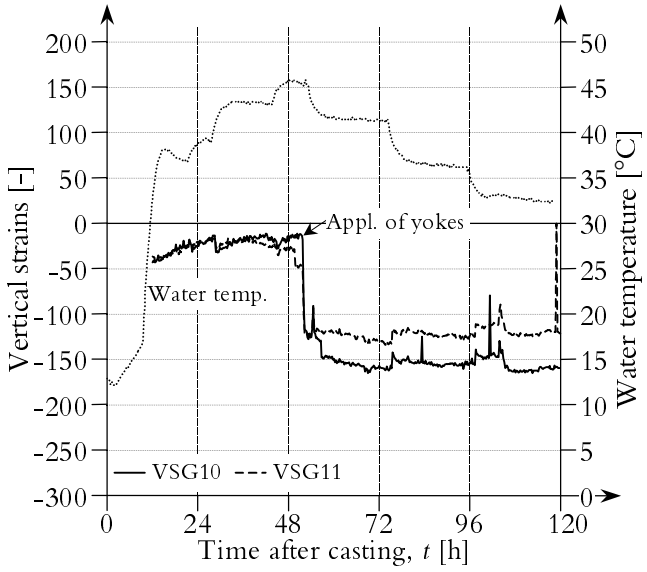

Figure G.5 *Vertical strains at the end of the reinforced joint in Test I. VSG10 and VSG11.*

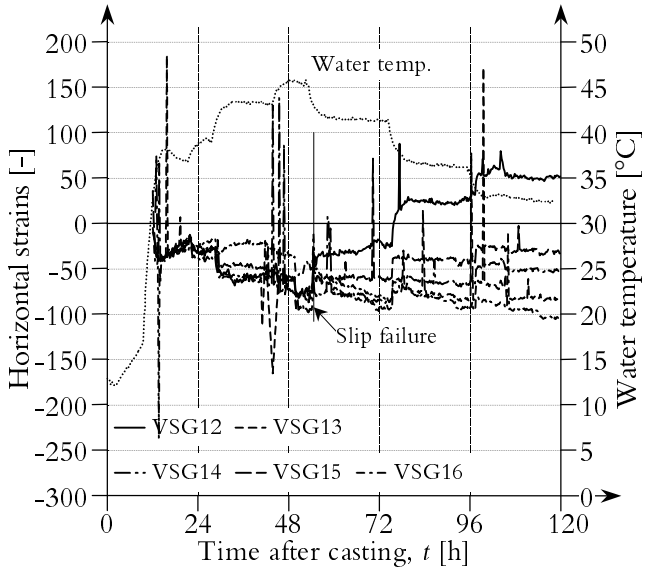

Figure G.6 *Vertical strains at the midsection of the wall in Test I. VSG12, VSG13, VSG14, VSG15 and VSG16.*

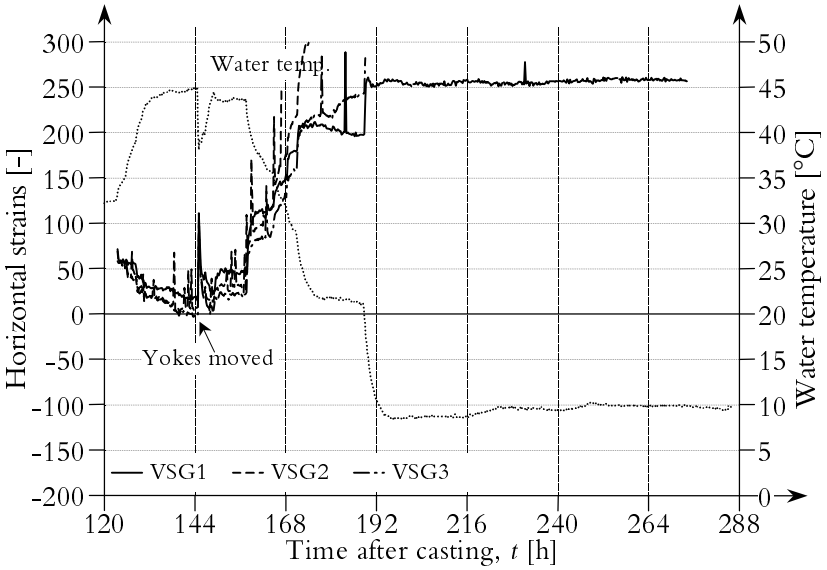

Figure G.7 *Horizontal strains at the unreinforced joint in Test II. VSG1, VSG2 and VSG3.*

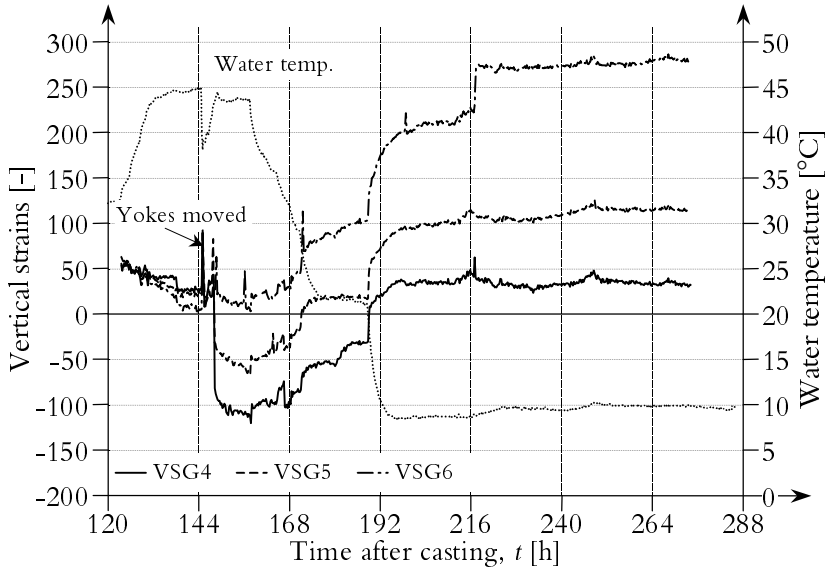

Figure G.8 *Vertical strains at the end of the unreinforced joint in Test II. VSG4, VSG5 and VSG6.*

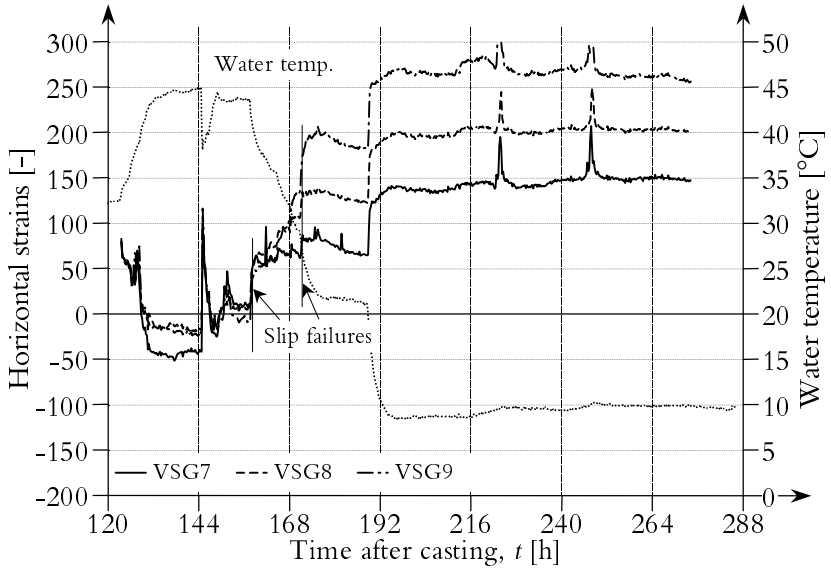

Figure G.9 *Horizontal strains at the end of the reinforced joint in Test II. VSG7, VSG8 and VSG9.*

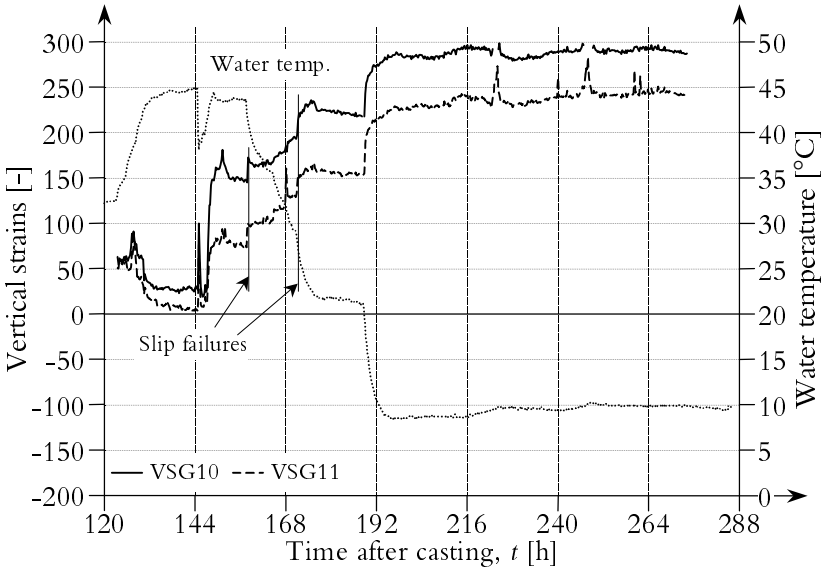

Figure G.10 *Vertical strains at the end of the reinforced joint in Test II. VSG10 and VSG11.*

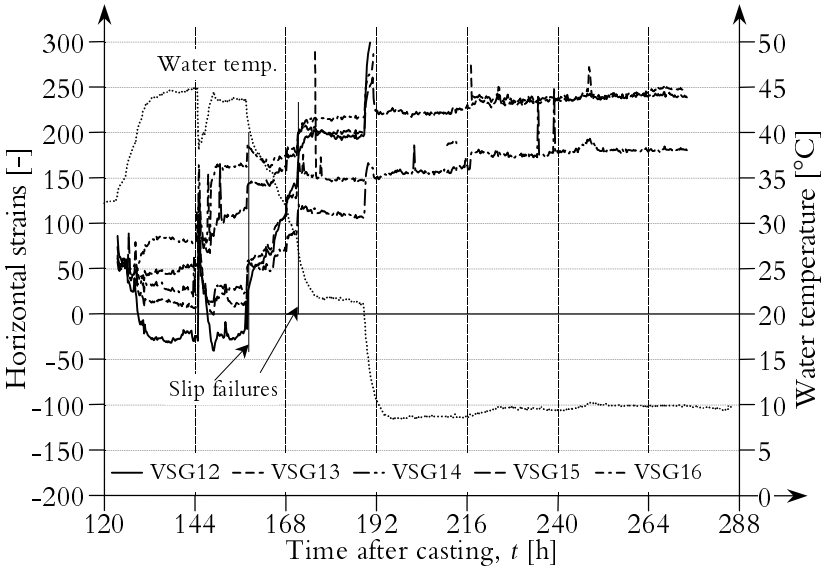

Figure G.11 *Horizontal strains at the midsection of the wall in Test II. VSG12, VSG13, VSG14, VSG15 and VSG16.*

G.2 Strains in Test III

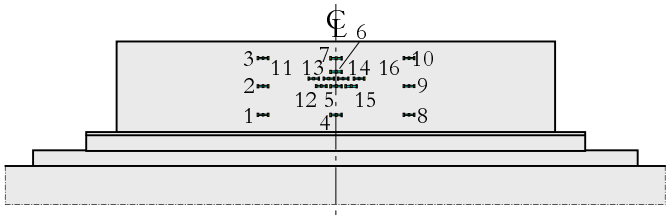

Figure G.12 *Location of Vibrating Strain Gages for measuring of strains in Test III.*

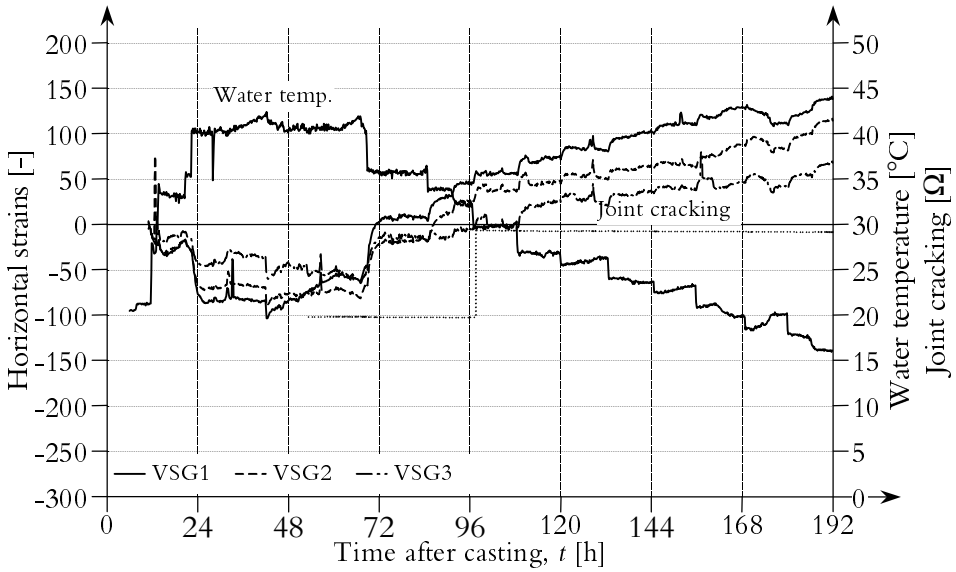

Figure G.13 *Horizontal strains in one third of the wall in Test III. VSG1, VSG2 and VSG3.*

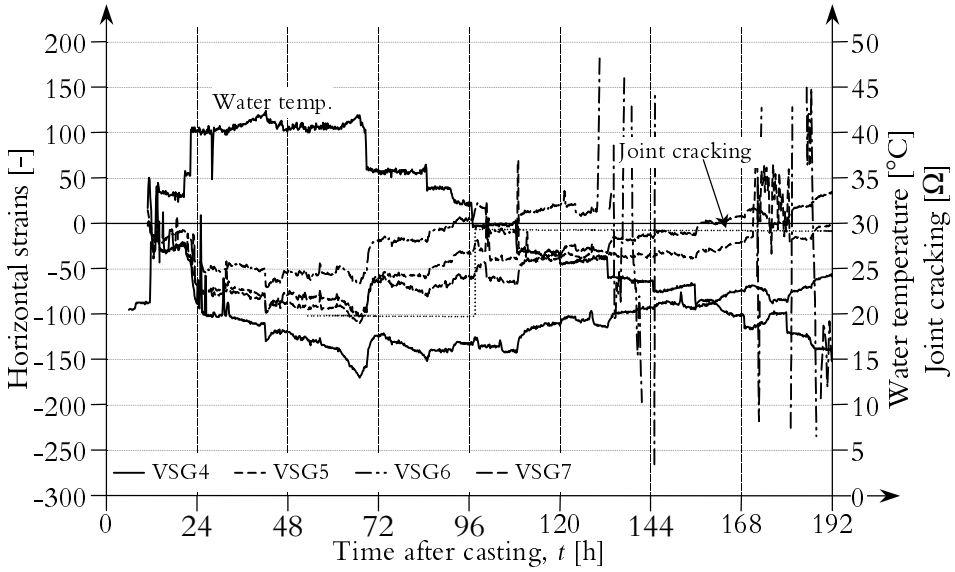

Figure G.14 *Horizontal strains in the midsection of the wall in Test III. VSG4, VSG5, VSG6 and VSG7.*

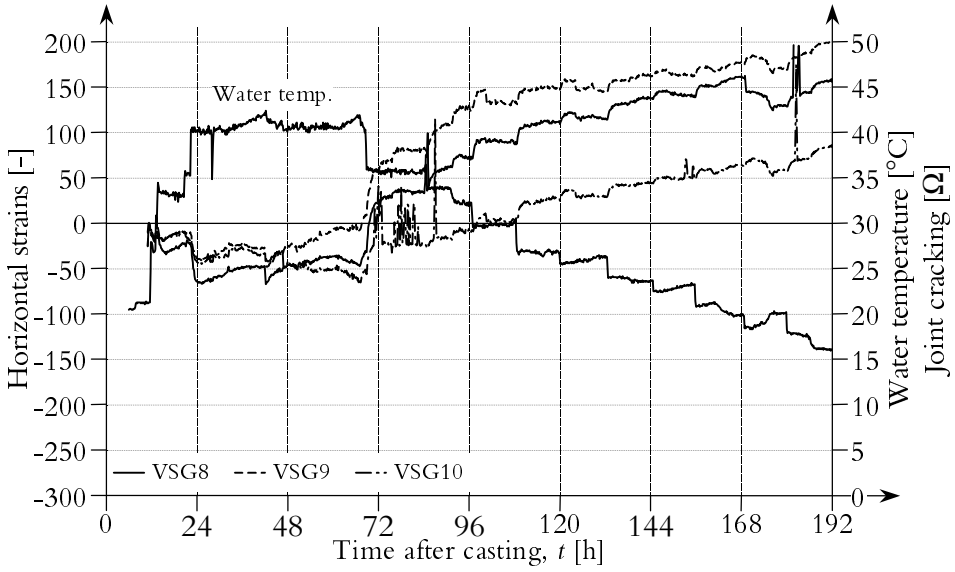

Figure G.15 *Horizontal strains at one third of the wall in Test III. VSG8, VSG9 and VSG10.*

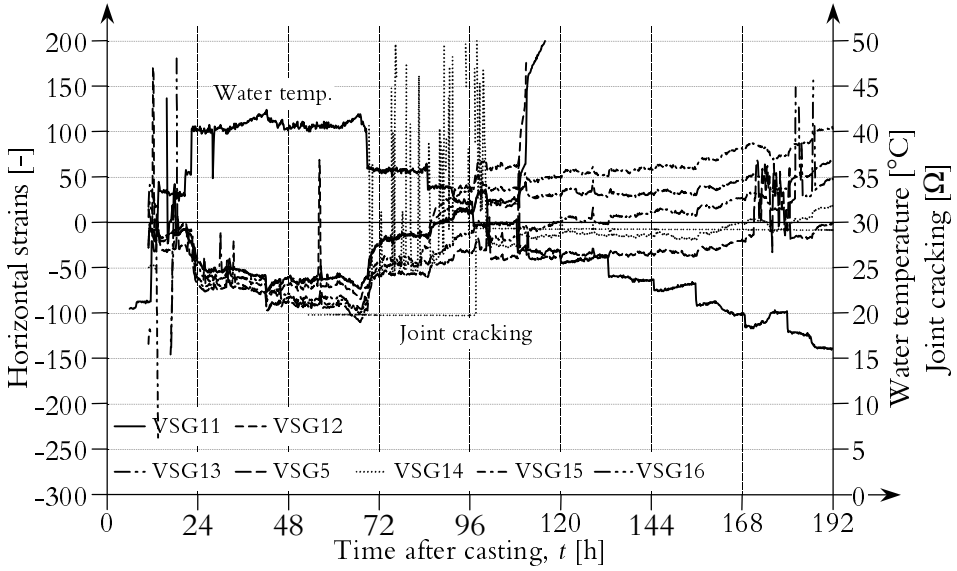

Figure G.16 *Horizontal strains at a line across the midsection of the wall in Test III. VSG11, VSG12, VSG13, VSG5, VSG14, VSG15 and VSG16. No values are registered for VSG14.*

G.3 Strains in Test IV

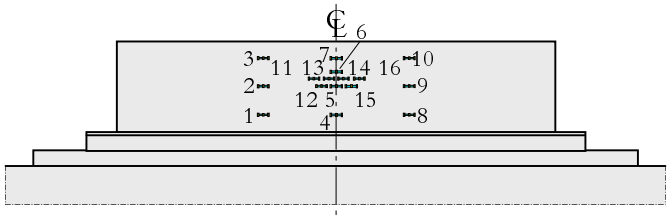

Figure G.17 *Location of Linear Displacement Transducers for measuring of relative movements between the different parts in Test IV.*

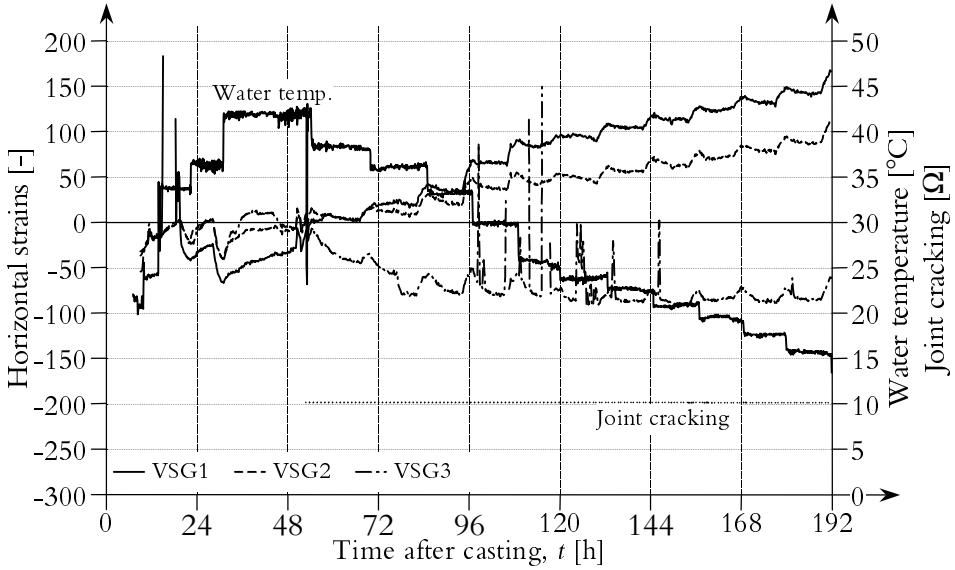

Figure G.18 *Horizontal strains in one third of the wall in Test IV. VSG1, VSG2 and VSG3.*

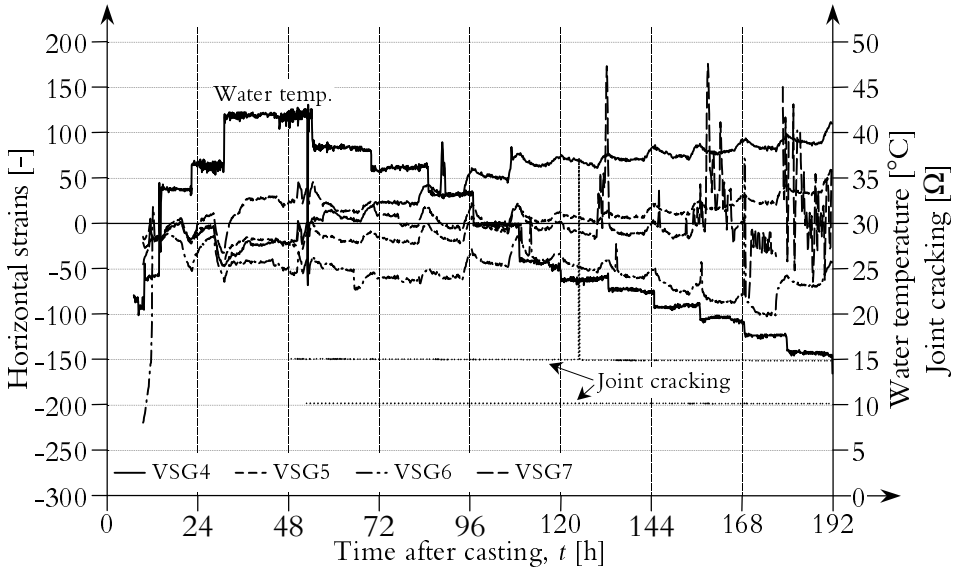

Figure G.19 *Horizontal strains in the midsection of the wall in Test IV. VSG4, VSG5, VSG6 and VSG7.*

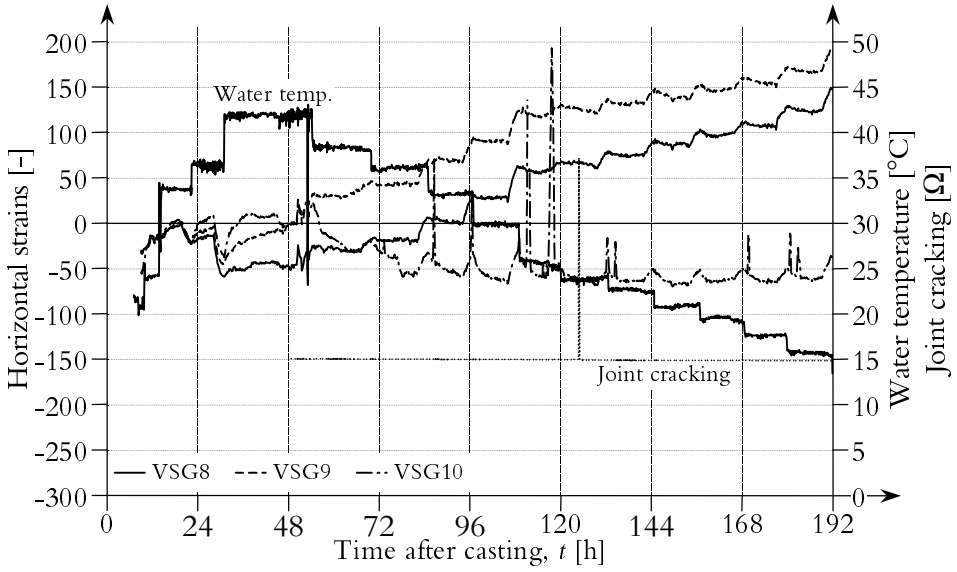

Figure G.20 *Horizontal strains at one third of the wall in Test IV. VSG8, VSG9 and VSG10.*

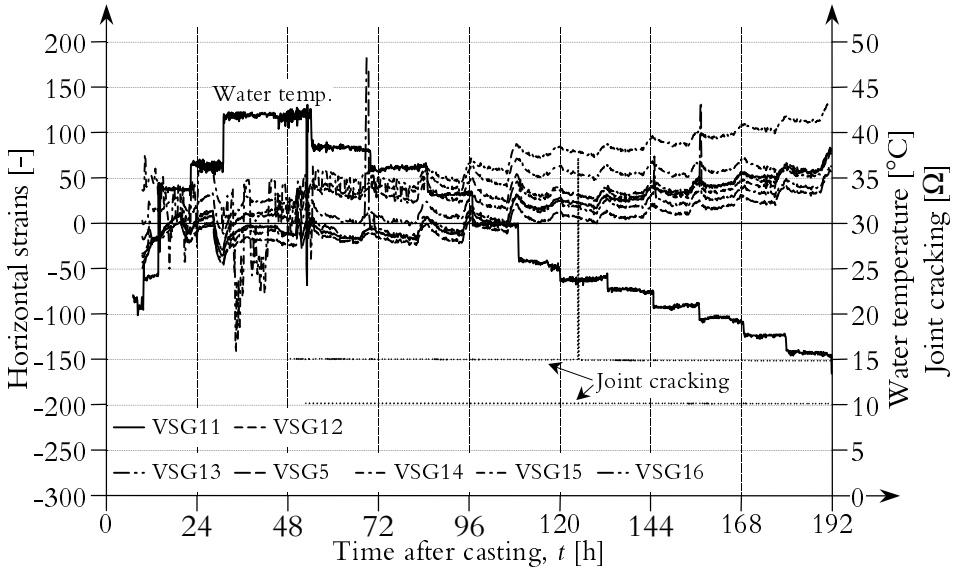

Figure G.21 *Horizontal strains at a line across the midsection of the wall in Test IV. VSG11, VSG12, VSG13, VSG5, VSG14, VSG15 and VSG16.*

Appendix H

List of Events from the Medium Scale Experiments

The following lists of events are copies of the diaries written during the tests.

H.1 Test I

Date and time	Time after casting, [h]	Events
1998-05-27 12:00	0.00	Casting of the wall started
13:30	1.50	Temperature measuring started
14:15	2.25	Casting of the wall finished
22:30	10.50	Water temperature +35°C
23:30	11.50	Strain measuring started
1998-05-28 02:00	14.00	Measuring of relative movements started
07:00	19.00	Stays of formwork loosened
08:30	20.50	VSG:s 7, 8 & 9 temporarily loosened
08:45	20.75	VSG:s 7, 8 & 9 reattached
10:30	22.50	Water temperature +40°C
15:00	27.00	CDG:s started
17:00	29.00	Water temperature +45°C
1998-05-29 09:30	45.50	Water temperature +55°C
15:45	51.75	First yoke applied, load 400kN
16:15	52.25	Second yoke applied, load 400kN

Continued →

17:15	53.25	Water temperature +60°C
17:30	53.50	Cracking in unreinforced joint
18:00	54.00	Water temperature +35°C
18:15	54.25	Water temperature +45°C
1998-05-30 15:30	75.50	Water temperature +38°C
15:45	75.75	Slip failure in the unreinforced joint
1998-05-31 13:30	97.50	Water temperature +33°C
1998-06-01 15:00	123.00	Test I is finished

H.2 Test II

Date and time	Time after casting, [h]	Events
1998-06-01 15:45	123.75	Start of Test II, water temperature +37°C
18:00	126.00	Water temperature +41°C
20:30	128.50	Water temperature +47°C
23:30	131.50	Water temperature +52°C
1998-06-02 13:30	145.50	Water temperature +10°C
14:30	146.50	Water temperature +52°C
15:00	147.00	Yokes removed from reinforced wall
15:30	147.50	First yoke reapplied, load 400kN
15:45	147.75	Second yoke reapplied, load 400kN
17:15	149.25	Water temperature +46°C
1998-06-03 02:00	158.00	Water temperature +38°C
02:30	158.50	1st CDG cracks
02:45	158.75	2nd CDG cracks
04:45	160.75	3rd CDG cracks
09:00	165.00	Water temperature +33°C
12:15	168.25	Water temperature +28°C
15:00	171.00	Water temperature +22°C
15:30	171.50	4th CDG cracks
15:45	171.75	5th CDG cracks
1998-06-04 00:15	180.25	Incoming water hose came loose
06:00	186.00	Possible through crack indicated in VSG12 through VSG16 in the middle of the wall
07:45	187.75	Water is turned off, incoming water hose remounted

Continued →

09:00	189.00	Water turned on again, only cold water used
10:30	190.50	A clicking sound is heard from the wall
1998-06-05 11:00	215.00	One side of the formwork is removed
15:00	219.00	Second side of the formwork is removed
1998-06-08 09:15	285.25	Test II is finished

H.3 Test III

Date and time	Time after casting, [h]	Events
1999-05-26 12:00	0.00	Casting of Wall III and Footing IV
13:00	1.00	Casting finished
23:00	11.00	Strain measuring started
199-05-27 01:00	13.00	Water temperature +35°C
03:00	15.00	Measuring of relative movements started
09:00	21.00	Water temperature +40°C
17:30	29.30	Stays of formwork loosened
18:00	30.00	Water temperature +45°C
1999-05-28 18:00	54.00	Water temperature +42°C
1999-05-29 09:00	69.00	Water temperature +38°C
15:00	75.00	3 CDG:s attached at one of the joint ends
17:30	77.50	CDG:s monitor possible slip failure
1999-05-30 00:45	84.75	Water temperature +34°C
01:00	85.00	LDT13 & 14 unfortunately dislodged
13:00	97.00	Water temperature +31°C
17:00	101.00	One CDG indicates slip failure in joint
1999-05-31 00:15	108.25	LDT11, 12, 13 & 14 unfortunately dislodged
00:30	108.50	Water temperature +27°C
00:45	108.75	Crack found on the coping
12:00	120.00	Water temperature +25°C
1999-06-01 00:30	132.50	Water temperature +23°C
12:30	144.50	Water temperature +21°C
23:45	155.75	Water temperature +19°C
1999-06-02 12:00	168.00	Water temperature +17°C
1999-06-03 00:00	180.00	Water temperature +15°C
13:30	193.50	Water is turned off
14:15	194.25	Test III is finished.

H.4 Test IV

Date and time	Time after casting, [h]	Events
1999-08-04 09:15	0.00	Casting is started
10:45	1.00	Casting is finished
16:00	6.75	Temperature measuring started
18:00	8.75	Strain measuring started
19:00	9.75	Stays of formwork loosened
23:30	14.25	Water temperature +35°C
23:30	14.25	Measuring of relative movements started
1999-08-05 07:30	22.25	Water temperature +40°C
15:45	30.50	Water temperature +45°C
22:30	37.25	1st set of CDG:s attached at one end of the joint
1999-08-06 09:45	48.50	1st set of CDG:s monitor possible slip failure
12:30	51.25	2nd set of CDG:s attached at the other end of the joint
15:30	54.25	Water temperature +42°C
1999-08-07 07:00	69.75	Water temperature +38°C
22:00	84.75	Water temperature +34°C
1999-08-08 10:00	96.75	Water temperature +31°C
22:00	108.75	Water temperature +27°C
1999-08-09 09:00	119.75	Water temperature +25°C
14:15	125.00	2nd set of CDG:s monitor possible slip failure
21:30	132.25	Water temperature +23°C
1999-08-10 09:45	144.50	Water temperature +21°C
21:45	156.50	Water temperature +19°C
1999-08-11 09:30	168.25	Water temperature +17°C
21:00	179.75	Water temperature +15°C
1999-08-12 10:00	192.75	Water temperature +10°C
18:00	200.75	Power failure due to thunder
1999-08-13 02:00	208.75	Power back again
1999-08-14 13:45	244.50	Water is turned off and Test IV is finished

Appendix I

Drawings of Medium Scale Experiments

I.1 List of Drawings

	Description	
Drawing K01	Slab	Measure, Reinforcement
Drawing K02	Footing	Measure, Reinforcement
Drawing K03	Wall 1, 2 & 3	Measure, Reinforcement
Drawing K04	Yokes	Measures

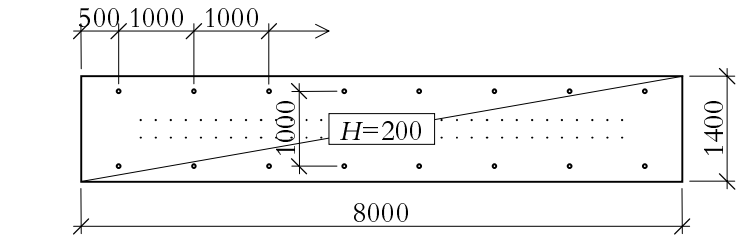

1 SLAB
MEASURES

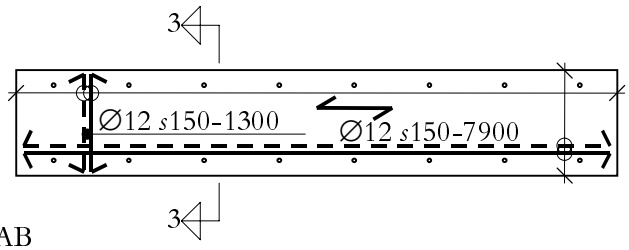

2 SLAB
REINFORCEMENT

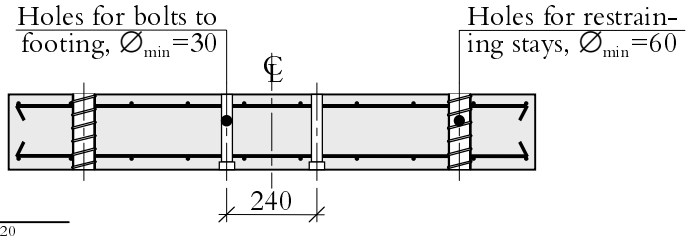

3 SLAB
DETAILS 1:20

MEDIUM SCALE EXPERIMENTS		
Slab: Measures and Reinforcement		
Drawn by MARTIN NILSSON		Date 00-01-28
Scale 1:100, 1:20	Drawing K01	Rev.

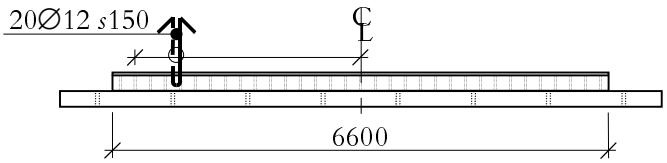

1 FOOTING 1
MEASURES, REINFORCEMENT

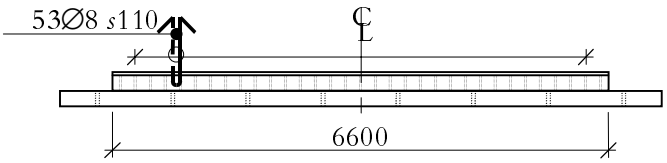

2 FOOTING 2&3
MEASURES, REINFORCEMENT

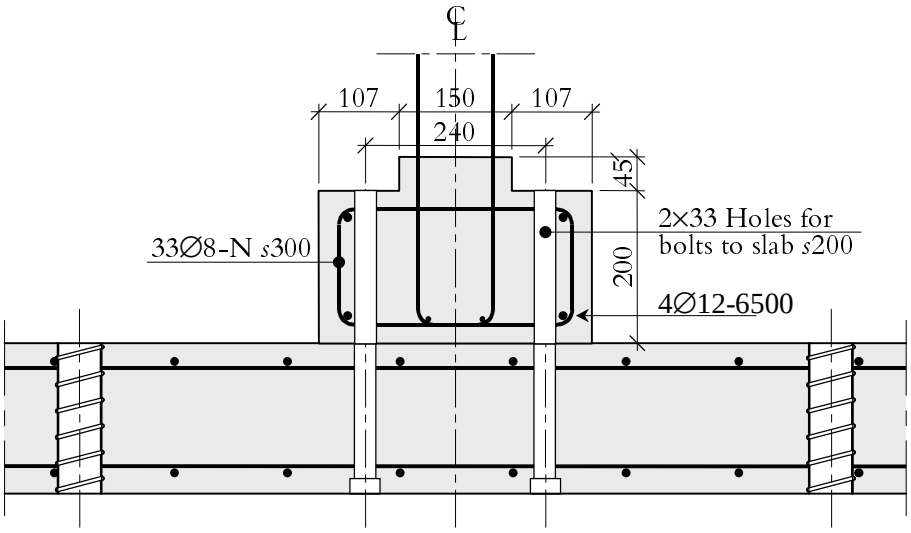

3 FOOTING
DETAILS 1:10

MEDIUM SCALE EXPERIMENTS		
Footing: Measures and Reinforcement		
Drawn by MARTIN NILSSON		Date 00-01-28
Scale 1:100, 1:10	Drawing K02	Rev.

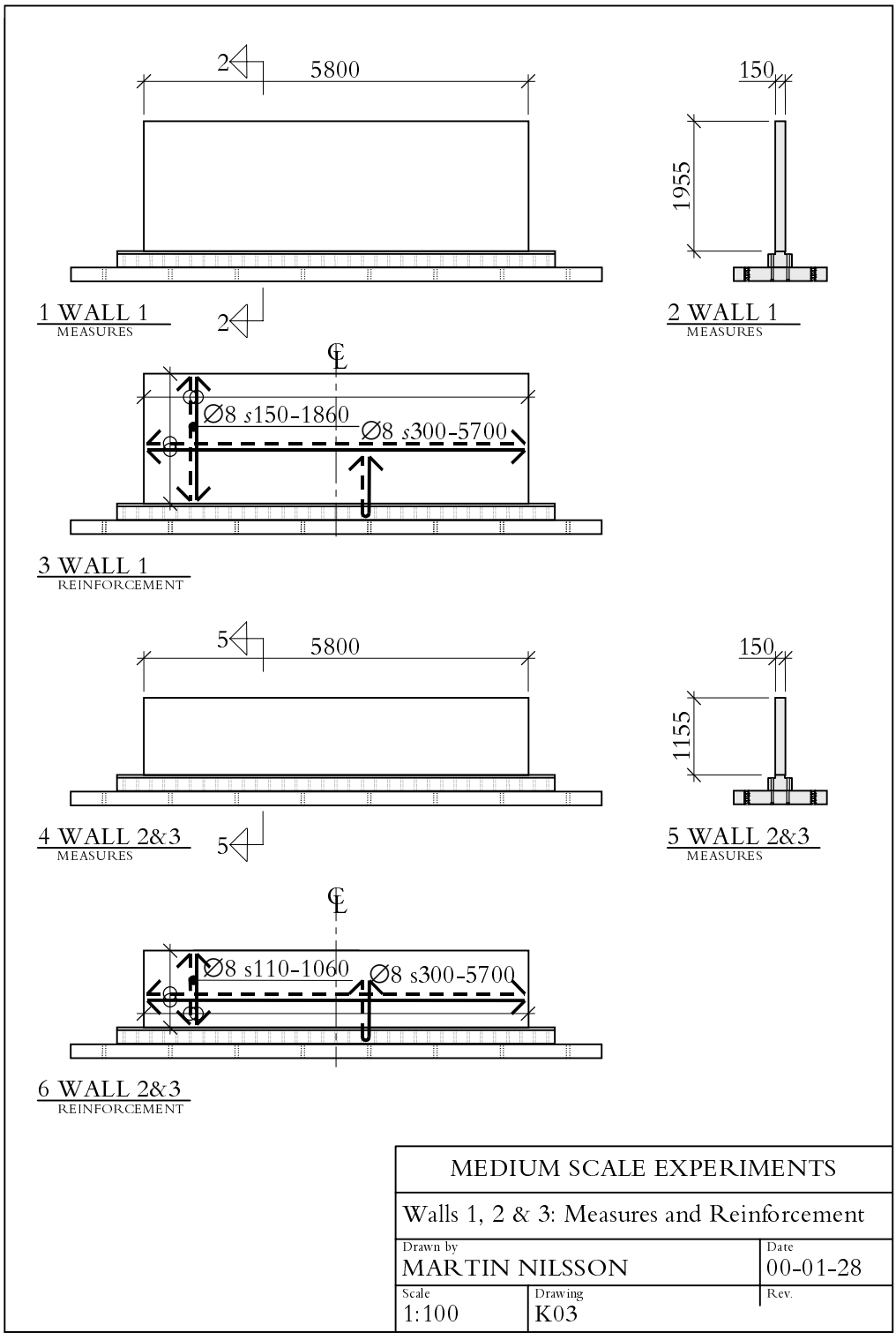
2
5800
150
1955
1 WALL 1
MEASURES
2
2 WALL 1
MEASURES
℄
Ø8 s150-1860
Ø8 s300-5700
3 WALL 1
REINFORCEMENT
5
5800
150
1155
4 WALL 2&3
MEASURES
5
5 WALL 2&3
MEASURES
℄
Ø8 s110-1060
Ø8 s300-5700
6 WALL 2&3
REINFORCEMENT
MEDIUM SCALE EXPERIMENTS
Walls 1, 2 & 3: Measures and Reinforcement
Drawn by
MARTIN NILSSON
Date
00-01-28
Scale
1:100
Drawing
K03
Rev.

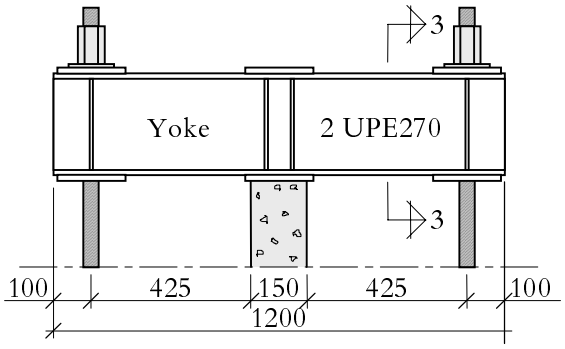

1 YOKE
ELEVATION

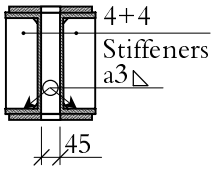

3 YOKE
SECTION

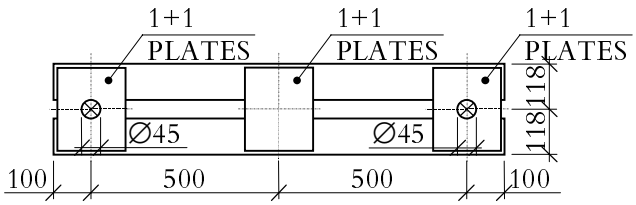

2 YOKE
PLANE

MEDIUM SCALE EXPERIMENTS		
Yokes: Measures		
Drawn by MARTIN NILSSON		Date 00-01-28
Scale 1:100	Drawing K04	Rev.

Doctoral and Licentiate Theses from the Division of Structural Engineering Luleå University of Technology

Doctoral Theses

1980 Ulf Arne Girhammar: Dynamic Fail-safe Behaviour of Steel Structures. Doctoral Thesis 1980:06D. pp. 309.

1983 Kent Gylltoft: Fracture Mechanics Models for Fatigue in Concrete Structures. Doctoral Thesis 1983:25D. pp. 210.

1988 Lennart Fransson: Thermal Ice Pressure on Structures in Ice Covers. Doctoral Thesis 1988:67D. pp. 161.

1989 Mats Emborg: Thermal Stresses in Concrete Structures at Early Ages. Doctoral Thesis 1989:73D, 2nd Edition, 1990. pp. 285.

1993 Lars Stehn: Tensile Fracture of Ice. Test Methods and Fracture Mechanics Analysis. Doctoral Thesis 1993:129D. pp. 136.

1994 Björn Täljsten: Plate Bonding. Strengthening of Existing Concrete Structures with Epoxy Bonded Plates of Steel or Fibre Reinforced Plastics. Doctoral Thesis 1994:152D, 2nd Edition 1994. pp. 308.

1994 Jan-Erik Jonasson: Modelling of Temperature, Moisture and Stresses in Young Concrete. Doctoral Thesis 1994:153D. pp. 225.

1995 Ulf Ohlsson: Fracture Mechanics Analysis of Concrete Structures. Doctoral Thesis 1995:179D. pp. 94.

1998 Keivan Noghabai: Effect of Tension Softening on the Performance of Concrete Structures. Experimental, Analytical and Computational Studies. Doctoral Thesis 1998:21. pp. 147.

1999 Gustaf Westman: Concrete Creep and Thermal Stresses. New creep models and their effects on stress developments. Doctoral Thesis 1999:10, May 1999. pp. 301.

1999 Henrik Gabrielsson: Ductility in High Performance Concrete Structures. An experimental investigation and a theoretical study of prestressed hollow core slabs and prestressed cylindrical pole elements. Doctoral Thesis 1999:15, May 1999. pp. 283.

2000 Patrik Groth: Fibre Reinforced Concrete. Fracture mechanics methods applied on self-compacting concrete and energetically modified binders. Doctoral Thesis 2000:04, January 2000. pp. 214.

Licentiate Theses

1984 Lennart Fransson: Bärförmåga hos ett flytande istäcke. Beräkningsmodeller och experimentella studier av naturlig is och av is förstärkt med armering. (Load-carrying Capacity of a Floating Ice Cover. Analytical Models and Experimental Studies of Natural Ice and of Ice Strengthened with Reinforcement) Licentiate Thesis 1984:012L, 2nd Edition, 1988. pp. 137.

1985 Mats Emborg: Temperature Stresses in Massive Concrete Structures. Viscoelastic Models and Laboratory Tests. Licentiate Thesis 1985:011L, 2nd Edition, 1988, pp. 163.

1987 Christer Hjalmarsson: Effektbehov i bostadshus. Experimentell bestämning av effektbehov i små- och flerbostadshus (Heating Demand in Single and Multi Family Houses. A comparison of Models for Calculation and Methods for Measurement). Licentiate Thesis 1987:009L. pp. 72.

1990 Björn Täljsten: Förstärkning av betongkonstruktioner genom pålimning av stålplåtar. (Concrete Structures Strengthened by Externally Bonded Steel Plates). Licentiate Thesis 1990:06L. pp. 205.

1990 Ulf Ohlsson: Fracture Mechanics Studies of Concrete Structures. Licentiate Thesis 1990:07L. pp. 66.

1990 Lars Stehn: Fracture Toughness of Sea Ice. Development of a Test System Based on Chevron Notched Specimens. Licentiate Thesis 1990:11L. pp. 88.

1992 Per Anders Daerga: Some Experimental Fracture Mechanics Studies in Mode I of Concrete and Wood Licentiate Thesis 1992:12L, 2nd Edition. pp. 76.

1993 Henrik Gabrielsson: Shear Capacity of Beams of Reinforced High Performance Concrete. Licentiate Thesis 1993:21L, 2nd Edition. pp. 111.

1995 Keivan Noghabai: Splitting of Concrete in the Anchoring Zone of Deformed Bars. A fracture mechanics approach to bond. Licentiate Thesis 1995:26L, 2nd Edition. pp. 131+46.

1995 Gustaf Westman: Thermal Cracking in High Performance Concrete. Viscoelastic Models and Laboratory Tests. Licentiate Thesis 1995:27L. pp. 123.

1995 Katarina Ekerfors: Mognadsutveckling i ung betong. Temperaturkänslighet, hållfasthet och värmeutveckling. (Maturity Development in

Young Concrete. Temperature Sensitivity, Strength and Heat Development). Licentiate Thesis 1995:34L. pp. 136.

1996 Patrik Groth: Cracking in Concrete. Crack Prevention with Air-Cooling and Crack Distribution with Steel Fibre Reinforcement. Licentiate Thesis 1996:37L. pp. 126.

1996 Hans Hedlund: Stresses in High Performance Concrete due to Temperature and Moisture Variations at Early Ages. Licentiate Thesis 1996:38L. pp. 240.

2000 Mårten Larsson: Estimation of Crack Risk in Early Age Concrete. Simplified methods for practical use. Licentiate Thesis 2000:10. pp. 171.

2000 Stig Bernander: Progressive Landslides in Long Natural Slopes. Formation, potential extension, and configuration of finished slides in strain-softening soils. Licentiate Thesis 2000:16. pp. 135.